THE FLOW OF SUSPENSIONS THROUGH TUBES - KARNIS 1966

THE FLOW OF SUSPENSIONS THROUGH TUBES

A Thesis

by

Alkibiadis Karnis, B.Eng., M.A. Sc.

Submitted to the Faculty of Graduate Studies and Research of McGill University in partial fulfilment of the requirements for the degree of Doctor of Philosophy

Department of Chemistry,
McGill University,
Montreal, Canada.

March, 1966

ACKNOWLEDGEMENTS

The author wishes to express his sincere thanks to

Dr. S.G. Mason

for his valuable guidance and encouragement in this work.

Grateful acknowledgement is also made to:

Dr. H. Brenner, Dr. H.L. Goldsmith and Dr. C.E. Chaffey for many useful discussions;

the Pulp and Paper Research Institute of Canada for laboratory accommodation and equipment, the help received from the technical service facilities and for financial assistance during the summers 1963, 1964 and 1965;

the Spruce Falls Power and Paper Company Ltd. for a fellowship during the session 1963-64;

the Canadian Industries Ltd. for a fellowship during the session 1964-65;

N. Wynn for his assistance in preparing some of the suspensions.

ABSTRACT

The flow mechanism of concentrated suspensions of rigid particles undergoing slow Poiseuille flow was studied. It was shown that the deviations from the parabolic velocity distribution arise from a wall effect of the type described by Vand. Particle accumulation behind an advancing meniscus is caused by the radial flow and particle-particle and particle-wall interactions. In many cases, the motions of particles were reversible when the direction of flow was reversed. In dilute suspensions, the statistical properties of the particle paths were in good agreement with a theory of collision doublets based on rectilinear paths of approach and recession.

At high Reynolds numbers rigid cylinders exhibited the tubular pinch effect previously found for spheres, and attained limiting rotational orbits corresponding to maximum energy dissipation. In concentrated suspensions, radial migration produced a plasmatic zone at the wall which changed the initial velocity profile and decreased the apparent viscosity.

The behaviour of rigid and deformable particles suspended in viscoelastic fluids differed in several important aspects from that in newtonian media.

FOREWORD

The investigation described in this thesis forms part of a series conducted in this laboratory with the purpose of arriving at a better understanding of the flow properties of liquid dispersions. The work deals mainly with the behaviour of particles flowing through cylindrical tubes over a wide range of particle concentrations from those in which particle interactions are negligible to those in which they become predominant.

The structure of the thesis requires some explanation. In Part I a review of the general background is given and the scope of the work is defined. The principal portions of the study are described in Parts II to V each of which has been written in a manner suitable for publication; each Part is complete with its own Abstract, Introduction, Experimental Section, Discussion, Bibliography and List of Symbols which, with minor exceptions, are used consistently throughout the thesis.

Certain details of the experimental apparatus, calculations, and preliminary experiments are presented as Appendices I to V. Finally, Part VI consists of a General Discussion and includes recommendations for further work.

TABLE OF CONTENTS

Page

PART III

INERTIAL EFFECTS

Page

PART IV

MENISCUS EFFECTS

Page

PART V

PART VI

PART VII

APPENDIX I

Page

APPENDIX II

WALL MIGRATION OF FLUID DROPS IN COUETTE FLOW

APPENDIX III

THE APPARENT VISCOSITY AND VELOCITY DISTRIBUTION IN CONCENTRATED SUSPENSIONS; A SEMI-EMPIRICAL MODEL OF FLOW

APPENDIX IV

THE BEHAVIOUR OF ISOLATED SPHERES IN CONTACT WITH A RIGID WALL

APPENDIX V

THE TUBE AND COUETTE APPARATUS

LIST OF TABLES

LIST OF FIGURES

Figure		Page

PART V (Cont'd.)

APPENDIX II

APPENDIX III

APPENDIX V

PART I

GENERAL INTRODUCTION

The rheology and stability of suspensions and emulsions have been widely studied because of their importance to Colloid Science and because of their interest in various technical and scientific fields. Two main approaches have been used: one based on the macroscopic rheological properties of the dispersions and the other based on microrheology i.e. the behaviour of the individual particles. Of the two methods, the second has been more extensively used in this laboratory and has dealt with the motion of isolated rigid[1-4)] and deformable[4-8)] particles and two-body collisions[9,10)] in newtonian liquid media undergoing slow Couette[1-5, 7-9)] and Poiseuille[6,10)] flows. This thesis describes an extension of these studies, i) to concentration ranges at which particle crowding effects become significant ii) to the flow regime where inertial effects start to become important and iii) to viscoelastic suspending media in which normal stress effects are present.

Particle crowding effects

In the creeping flow regime, small isolated and neutrally buoyant rigid particles in newtonian liquids rotate in accordance with a theory due to Jeffery[11)], and translate in linear paths with the velocity of the undisturbed flow at their centres[6)]. Flexible particles, which are deformed by the shear, migrate away from the walls bounding the suspending fluid[6, 8)].

At higher concentrations particle crowding effects become predominant. The composition of a suspension moving into an initially empty tube is not uniform along the tube; an accumulation of particles occurs near an advancing[12, 13] and a depletion near a receding[14] meniscus. When the suspension is allowed to flow in a tube until steady conditions are established it can continue to exhibit anomalous behaviour with the apparent viscosity coefficient decreasing with decreasing tube radius. This is known as the sigma effect and was first reported by Bingham[15] for paints and later observed in clays[16, 17], blood[18] and other concentrated suspensions[19].

Dix and Scott-Blair[20] used a summation rather an integration treatment of the Poiseuille equations of flow and derived an equation to explain the sigma effect. Maude and Whitmore[12,21,22] postulated an entrance effect which resulted in a decrease in the concentration of the suspension in the tube, which in turn produced a decrease in the apparent viscosity. Finally, Vand[23] suggested that the sigma phenomenon arises from a hydrodynamic interaction of the particles with the tube wall.

Inertial effects

At low but not zero Reynolds numbers isolated neutrally buoyant rigid spheres in Poiseuille flow exhibit the tubular pinch effect[24] in which the particles accumulate at a stable radial position about half-way between the tube axis and tube wall. These original observations on spheres[24] have been extended to rectangular ducts[25], and to non-neutrally buoyant systems[25-27]. In the latter case the direction of migration depended on the relative directions of sedimentation velocity and flow[25-27]. Furthermore, whereas rigid spheroids in the creeping flow regime rotate in a periodic manner as predicted by Jeffery[11] and in a constant orbit[6, 28], it has been predicted theoretically by Saffman[29] that inertial effects can cause a steady drift in the orbit to values corresponding to minimum energy dissipation in Couette flow[11].

Although the theoretical interpretations[29-30] of the lateral migration predict qualitatively some of the observed phenomena, especially in non-neutrally buoyant systems, they have failed, however, to provide an explanation of the two-way migration in the neutrally buoyant case. This is because these theories take into account only the inertial effects without considering the presence of the tube wall which, as has been pointed out[8,14,33], is of cardinal importance. Recently Cox and Brenner[34] have treated the problem of a neutrally buoyant sphere, which is freely rotating and translating parallel to the axis of a tube of finite radius. While the calculations are not yet complete there are reasons to believe[33] that it will provide the explanation for the tubular pinch effect.

Two-way migration of single rigid particles has been also observed in oscillatory and pulsatile flows[35, 36]; in concentrated suspension undergoing oscillatory flow a particle-free layer is formed near the wall as a result of radial migration[35], a phenomenon which has also been observed in pulp fibre suspension in steady flow[14].

Viscoelastic media

In a newtonian liquid, under steady state conditions, the normal components of stress are equal and the tangential stress is proportional to the rate of shear, the proportionality coefficient being the viscosity. Viscoelastic fluids behave differently in two respects: the viscosity is not constant but is a function of shear rate, and there are additional components of normal and tangential stresses[37]. The excess of normal stress over the classical value corresponding to a newtonian liquid implies that, besides a shearing force, additional normal forces must be applied to the fluid in order to maintain flow[38]. In the case of a liquid contained between concentric cylinders in relative motion, the existence of the excess stress produces a "strangulation" of the liquid (analogous to the pressure exerted by a rope pulled tight round a pole) and the liquid climbs up the inner cylinder thus demonstrating the Weissenberg effect[39].

When the steady flow is abruptly altered by making the stress zero, the viscoelastic liquid undergoes an elastic recovery generally involving a lateral expansion and a longitudinal contraction[38]. Thus, when a viscoelastic fluid issues from a tube it swells at the exit to a diameter greater than that of the tube[40].

Scope of the thesis

The three different aspects touched on above, have been studied and are reported upon in the succeeding Parts of the thesis. Most of the experiments were performed in Poiseuille flow but observations on particle motions were also made in Couette flow either for comparison purposes or to obtain additional information and evidence. The following is an outline of the objectives of the study and scope of the thesis.

i) To investigate the kinetics of concentrated suspensions of rigid particles in the creeping flow regime by carrying out a detailed study of the motion of individual particles and velocity distributions in tubes (Part II).

ii) To study the translational, radial, and rotational velocities of isolated rigid and deformable particles at high Reynolds numbers and to test Jeffery's[11] and Saffman's[30] theoretical equations. To investigate the effect of radial migration on the flow of concentrated suspensions (Part III).

iii) To study the accumulation of particles behind an advancing meniscus of a suspension flowing in a tube at low Reynolds numbers (Part IV).

iv) To investigate the motion of particles in viscoelastic media in which the presence of excess stress would be expected to influence their behaviour, and to compare the results with similar observations in newtonian liquids (Part V).

REFERENCES

1. TREVELYAN, B.J. and MASON, S.G. J. Colloid Sci. 6, 354 (1951)
2. MASON, S.G. and MANLEY, R.St.J. Proc. Roy. Soc. (London) A238, 117 (1956)
3. GOLDSMITH, H.L. and MASON, S.G. J. Fluid Mech. 12, 88 (1962)
4. BARTOK, W. and MASON, S.G. J. Colloid Sci. 12, 243 (1957)
5. RUMSCHEIDT, F.D. and MASON, S.G. J. Colloid Sci. 16, 238 (1961)
6. GOLDSMITH, H.L. and MASON, S.G. J. Colloid Sci. 17, 448 (1962)
7. BARTOK, W. and MASON, S.G. J. Colloid Sci. 13, 293 (1958)
8. CHAFFEY, C.H., BRENNER, H. and MASON, S.G. Rheol. Acta 4, 64 (1965)
9. MANLEY, R.St.J. and MASON, S.G. J. Colloid Sci. 7, 354 (1952)
10. GOLDSMITH, H.L. and MASON, S.G. Proc. Roy. Soc. (London) A282, 569 (1964)
11. JEFFERY, G.B. Proc. Roy. Soc. (London) A102, 161 (1922)
12. WHITMORE, R.L. Rheology of Disperse Systems Ed. C.C. Mill. Pergamon Press 49 (1959)
13. VEJLENS, G. Acta. Pathol. Microbiol. Scand. Suppl. No. 33 (1938)
14. FORGACS, G.L., ROBERTSON, A.A. and MASON, S.G. Fundamentals of Papermaking Fibres 447 (1958)
15. BINHAM, E.C. and GREEN, H. Proc. Amer. Soc. Test. Mater. 19, 640 (1919)
16. SCHOFIELD, R.K. and SCOTT-BLAIR, G.W. J. Phys. Chem. 34, 248 (1930)
17. SCHOFIELD, R.K. and SCOTT-BLAIR, G.W. J. Phys. Chem. 35, 1212 (1931)
18. FARHAEUS, R. and LINDQUIST, T. Amer. J. Physiol. 96, 562 (1931)
19. HIGGINBOTHAM, G.H., OLIVER, D.R. and WARD, S.G. Brit. J. Appl. Phys. 9, 372 (1958)
20. DIX, F.J. and SCOTT-BLAIR, G.W. J. Appl. Phys. 11, 514 (1940)
21. MAUDE, A.D. and WHITMORE, R.L. Brit. J. Appl. Phys. 7, 98 (1956)
22. MAUDE, A.D. Brit. J. Appl. Phys. 10, 371 (1959)

23. VAND, V. J. Phys. and Colloid Chem. 52, 277, 300 (1948)

24. SEGRE, G. and SILBERBERG, A. Nature 189, 209 (1961)

25. REPETTI, R.V. and LEONARD, E.F. Nature 203, 1346 (1964)

26. OLIVER, D.R. Nature 194, 1269 (1962)

27. JEFFREY, R.C. Ph.D. Thesis Cambridge University, Pembroke College (1964)

28. ANCZUROWSKI, E. and MASON, S.G. Forthcoming publication

29. SAFFMAN, P.G. J. Fluid Mech. 1, 540 (1956)

30. RUBINOW, S.I. and KELLER, J.B. J. Fluid Mech. 11, 447 (1961)

31. SAFFMAN, P.G. J. Fluid Mech. 22, 385 (1965)

32. SEGRE, G. and SILBERBERG, A. J. Fluid Mech. 14, 356 (1962)

33. BRENNER, H. Chapter prepared for inclusion in "Advances of Chemical Engineering" Volume 6, Academic Press (1965)

34. COX, R.G. and BRENNER, H. Forthcoming publication

35. SHIZGAL, B., GOLDSMITH, H.L. and MASON, S.G. Canad. J. Chem. Eng. 43, 97 (1965)

36. TAKANO, M. and MASON, S.G. Forthcoming publication

37. LODGE, A.S. Flow Properties of Blood Ed. A.L. Copley and G. Stainsby Pergamon Press 5 (1960)

38. ERINGEN, A.C. Nonlinear Theory of Continuous Media McGraw Hill (1962)

39. WEISSENBERG, K. Nature 159, 310 (1947)

40. MERRINGTON, A.C. Nature 152, 663 (1943)

PART II

CONCENTRATED SUSPENSIONS OF RIGID PARTICLES

ABSTRACT

In the viscous flow regime the velocity profiles of dilute suspensions of rigid spheres in Newtonian liquids undergoing Couette or Poiseuille flow were found to be identical with those predicted by the theory with no particles present. At concentrations low enough so that the formation of triplets and higher order multiplets could be neglected, a given sphere exhibited fluctuations about a fixed mean radial position. The measured distribution of lateral displacements agreed with a theory based on rectilinear approach and recession of colliding pairs, whereas the time average radial displacements were twice the predicted values.

On increasing the concentration partial plug flow developed in the tube with a central core in which the particles travelled with identical velocities without rotating and at fixed radial positions. Outside this central core the particles described irregular paths which, however, were reversible with respect to translation and rotation when the direction of flow was reversed. The concentration profiles were found to be uniform over prolonged periods of flow, and the suspensions showed Newtonian behaviour.

The phenomena, many of which were similar in suspensions of rods and discs, were shown to result from a wall effect predicted by Vand and were not manifestations of non-Newtonian behaviour.

INTRODUCTION

Earlier publications from this laboratory have dealt with the translation, rotation and interaction of small particles suspended at low concentrations in a Newtonian liquid of the same density undergoing Poiseuille flow at low Reynolds numbers ($< 10^{-3}$) [1,2]. Most of the phenomena observed were in agreement with theories based on Couette flow.

This part of the thesis represents an extension of the earlier studies of rigid spheres, rods and discs from very dilute suspensions to concentrations at which particle interaction effects would be expected to play an increasingly important and, ultimately, the dominant role. Starting with the simple theory of shear-induced collision doublets, equations describing the statistical nature of the paths of rigid spheres are derived in the Theoretical Part and these have been tested in both Poiseuille and Couette flows. Velocity profiles of spheres, rods and discs in tube flow have been measured and found to show a pronounced deviation from the parabolic distribution of velocities as the concentration is increased presumably because of a wall effect. Corresponding measurements were made in Couette flow. Finally, a series of experiments on reversibility in Poiseuille flow was conducted which indicate a surprising degree of order to what at first sight are exceedingly complicated and disordered phenomena.

The principles described, although not fully understood, are relevant to a number of problems of suspension rheology.

THEORETICAL PART

1. The path of a sphere in Couette flow

Consider an initially uniformly dispersed dilute suspension of rigid spheres of volume fraction c in Couette flow. An isolated sphere translates at the velocity of undisturbed flow of gradient G defined by

$$u = Gy \; ; \quad v, w = 0 \; , \tag{1}$$

where u, v and w are the respective fluid velocities along the X-, Y- and Z- axes, until it encounters another sphere and suffers a momentary but recoverable lateral displacement from the X- axis. The statistical properties of the path can be calculated from a consideration of the approximate theory of 2-body collisions [3].

If a "collision sphere" of radius 2b (Fig. 1a) is described about a reference sphere of radius b, all the particles whose centers are carried to the surface of the circumscribed sphere will collide with the reference sphere. We assume for simplicity [3] that (i) a particle moves in a rectilinear path parallel to the X- axis until its centre approaches within 2b of the reference sphere when a collision occurs at the polar angles θ_o and Φ_o, (ii) the doublet rotates as an ellipsoid of axis ratio $r_e = 1$, (iii) the collisions are symmetrical, with the angles of separation θ_o, $-\Phi_o$ the mirror images of those of approach and (iv) the mid-point between the two sphere centers is at the origin of the field. The path of the center of each sphere is an arc of a circle of radius b $\sin\theta_o$ (Fig. 1b), and the Y- displacement of each particle from its pre-collision path at any time during the collision process is

$$\Delta y = \pm\, b \sin\theta_o (\cos\Phi - \cos\Phi_o) \; , \tag{2}$$

the positive sign applying to one sphere and the negative to the other. Considering only magnitudes of displacement, without regard to sign, the time average absolute lateral displacement is given by

$$|\overline{\Delta y}_t| = \frac{1}{t}\int |\Delta y| dt \quad , \tag{3}$$

the integral being evaluated over unit time. For a particular collision Θ_o, Φ_o the contribution to the integral in (3) is readily evaluated by substituting for the angular velocity of the doublet [3)]

$$\frac{d\Phi}{dt} = \frac{G}{2} \quad , \tag{4}$$

which yields over the life of the doublet τ after substituting from (2)

$$\int_0^\tau |\Delta y| dt = 2\int_0^{\Phi_o} b \sin\Theta_o(\cos\Phi - \cos\Phi_o)\,\frac{2}{G}\,d\Phi_o$$

or $$|\Delta \bar{y}_\tau| . \tau = \frac{4b}{G}\sin\Theta_o(\sin\Phi_o - \Phi_o\cos\Phi_o) \ . \tag{5}$$

The total number of collisions per sphere in unit time is [3)]

$$f = \frac{8cG}{\pi} \quad , \tag{6}$$

and the fraction of collisions occurring in the interval $d\Theta_o$, $d\Phi_o$ at Θ_o, Φ_o is $p(\Theta_o, \Phi_o)d\Theta_o d\Phi_o$ where [3)]

$$p(\Theta_o, \Phi_o) = 3\sin^3\Theta_o \sin\Phi_o \cos\Phi_o \quad , \tag{7}$$

and the limits of Θ_o and Φ_o are taken between 0 and $\pi/2$.

Equation (3) can now be integrated over all possible collisions, giving

$$|\overline{\Delta y}_t| = \int_0^{\pi/2}\int_0^{\pi/2} \frac{4b}{G}\sin\Theta_o(\sin\Phi_o - \Phi_o\cos\Phi_o).f.\ p(\Theta_o, \Phi_o)d\Theta_o d\Phi_o \tag{8}$$

which after inserting (6) and (7) simplifies to

$$|\overline{\Delta y}_t| = 2bc \tag{9}$$

The distribution of displacements can be calculated in a similar way. The maximum displacement in a given collision occurs when $\Phi = 0$ and from (2) is

$$\Delta y_o = b \sin\theta_o(1 - \cos\Phi_o) . \tag{10}$$

Setting $\xi = \Delta y_o/\Delta y_{max}$, where $\Delta y_{max} = b$ is the maximum possible displacement, corresponding to a collision in which θ_o, $\Phi_o = \pi/2$, (10) may be written in the dimensionless form:

$$\xi = \sin\theta_o(1 - \cos\Phi_o) . \tag{11}$$

The fraction of collisions having displacements less than ξ is

$$P(\xi) = \iint p(\theta_o, \Phi_o)d\theta_o d\Phi_o \quad , \tag{12}$$

where $p(\theta_o, \Phi_o)$ is given by (7) and the integration is carried out over the two hatched areas marked A and B in Fig. 1a, namely

$$\begin{aligned} P(\xi) &= \int_0^{\theta_o'}\int_0^{\pi/2} p(\theta_o, \Phi_o)d\theta_o d\Phi_o + \int_{\theta_o'}^{\pi/2}\int_0^{\Phi_o(\theta_o)} p(\theta_o, \Phi_o)d\theta_o d\Phi_o \\ &= \frac{3}{2}\int_0^{\theta_o'} \sin^3\theta_o d\theta_o + \frac{3}{2}\int_0^{\pi/2} \sin^3\theta_o \sin^2\Phi_o \, d\theta_o . \end{aligned} \tag{13}$$

The locus of constant ξ (Fig. 1a) is found from (11)

$$\cos\Phi_o = 1 - \frac{\xi}{\sin\theta_o} \quad , \tag{14}$$

from which it follows that

$$\sin^2\Phi_o = \frac{2\xi}{\sin\theta_o} - \frac{\xi^2}{\sin^2\theta_o} \quad , \tag{15}$$

with a lower limit θ_o' (at $\Phi_o = \pi/2$) given by

$$\theta_o' = \sin^{-1}\xi . \tag{16}$$

Inserting (15) and (16) into (13) and integrating we obtain

$$P(\xi) = 1 - (1-\xi)^{1/2}\,(1 + \frac{\xi^2}{2}) + 3(\frac{\pi}{4} - \frac{1}{2}\sin^{-1}\xi).\xi\,. \qquad (17)$$

The differential distribution function of displacements is therefore

$$\begin{aligned} p(\xi) &= \frac{dP(\xi)}{d\xi} \\ &= 3(\frac{\pi}{4} - \frac{1}{2}\sin^{-1}\xi) - \frac{\xi}{2(1-\xi^2)^{1/2}}\,(7-\xi^2)\,. \end{aligned} \qquad (18)$$

The mean free path $\bar{l}$, i.e. the average distance in the X direction travelled by the reference sphere between collisions, is

$$\bar{l} = \frac{u(y)}{f}\,, \qquad (19)$$

where u(y) is the mean translational velocity of the sphere in the Couette field given by (1) and y is the distance of the particle center from the stationary layer. Substituting (1) and (6) into (19) we obtain

$$\bar{l} = \frac{\pi y}{8c} = \frac{3y}{32nb^3}\,. \qquad (20)$$

The fraction of time spent in collisions is $f\bar{\tau}$, where $\bar{\tau}$ is the mean doublet life given by [3] $\bar{\tau} = \pi/G$ and, therefore, $f\bar{\tau} = 8c$ by making use of (6). Hence the mean time between collisions is

$$\bar{t} = \frac{\pi(1-8c)}{8cG}\,. \qquad (21)$$

2. <u>Poiseuille Flow</u>

In Poiseuille flow the fluid translational velocity u(r) at distance r from the tube axis is

$$u(r) = u^*(0)[1 - \frac{r^2}{R_o^2}]\,, \qquad (22)$$

u*(0) being the centerline velocity given by

$$u^*(0) = \frac{kR_o^2}{2} \quad , \tag{23}$$

where $k = 4Q/\pi R_o^4$, Q is the volumetric flow rate and R_o the tube radius. Neglecting the effect of the wall, an isolated sphere moves with the corresponding fluid velocity at its center [1] as given by (22), and rotates with an angular velocity

$$\omega'(r) = \frac{kr}{2} \quad , \tag{24}$$

since kr is the velocity gradient at r.

To describe the collisions in the tube, a Cartesian coordinate system is constructed at the sphere center (Fig. 1c). Assuming local Couette flow [2] (i.e. neglecting the curvature in the velocity profile) the collision frequency is still given by (6), and we can equate Δr and Δy so that radial fluctuations are also given by Equations (8) to (18). The mean free path now becomes

$$\bar{\ell}(r) = \frac{\pi(R_o^2 - r^2)}{16cr} = \frac{3(R_o^2 - r^2)}{64rnb^3} \; ; \tag{25}$$

the mean time between collisions, corrected for the average life time of the doublets, is

$$\bar{t}(r) = \frac{\pi^2 R_o^4(1 - 8c)}{32Qcr} \quad . \tag{26}$$

The mean free path for all particles in the tube is obtained by averaging over all values of r

$$\bar{\bar{\ell}} = \frac{\int_0^{R_o} \bar{\ell}(r)\; 2\pi rndr}{\int_0^{R_o} 2\pi rndr} \quad , \tag{27}$$

where n is the number of particles (singlets) per unit volume. Integration of (27) yields

$$\bar{\bar{l}} = \frac{\pi R_o}{12c} = \frac{R_o}{16b^3 n} \quad . \tag{28}$$

Equation (6) and those for τ have been confirmed experimentally [2, 3]; this provides an indirect verification of (20), (21), (25) and (26). In the experiments described later (9) and (17) were tested, by measuring the displacements suffered by tracer spheres in dilute suspensions.

The theory developed above is limited to very low concentrations since the formation of triplets and higher order multiplets has been neglected. As c increases to the region where n-body ($n > 2$) interactions become appreciable, the average radial distance of the reference sphere no longer remains constant because of these inherently unsymmetrical collisions [4]; as a consequence, the reference sphere describes an erratic path in the flowing suspension. Furthermore, it is known [5] that the paths of approach and recession are curvilinear and the doublet rotates as an ellipsoid of $r_e = 2$ and, therefore, the calculated values of $|\overline{\Delta y_t}|$, $|\overline{\Delta r_t}|$ will tend to be lower than those actually observed.

EXPERIMENTAL PART

1. Apparatus

The experiments in Poiseuille flow were performed in precision bore ($\pm$ 5 x 10^{-4} cm) glass tubes of radius R_o = 0.2 to 1.0 cm. vertically mounted on a mechanically driven travelling microscope [1] whose optical axis was normal to the tube axis and which could travel a distance 50 cm. along the tube. Those in Couette flow were conducted between counter-rotating concentric cylinders [4, 6] which permitted observations to be made through a microscope directed along either the Y- or Z- axes; different sets of cylinders made from plexiglass and precision-machined <u>in situ</u> could be attached and the annular gap ΔR varied.

Apparent viscosities were calculated from flow curves obtained both in tubes and in a rotational viscometer. In the tube flow measurements, pressure drops over a length = 30 R_o of tube were measured over a range of accurately known flow rates using a differential pressure transducer (Model CP 51 DS 0.1 psi Pace Engineering Co.). The viscometer was a variable-shear coaxial cylinder Couette-type (Epprecht Rheomat 15).

2. <u>Suspensions</u>

In the experiments with spheres and discs a polyglycol oil (Ucon oil 50-HB-5100, Union Carbide) containing 4% by volume tetrabromoethane was used as suspending phase (viscosity η_o = 24.6 p. and density ρ = 1.139 g.cm.$^{-3}$). The spheres were screen-fractionated samples of polyvinyl acetate (PVA) of radius b ranging from 0.0035 $\pm$ 0.0015 cm. to 0.0280 $\pm$ 0.0040 cm. The discs were prepared from the PVA spheres by compressing them between heated platens of a hydraulic press as described elsewhere [7]; their thickness was 2a' = 0.0125 cm. and their diameter 2b' = 0.0625 $\pm$ 0.0225 cm.

Rods were prepared from continuous nylon filament of diameter 2b' = 0.0156 cm., embedded in wax and cut to a length 2a' = 0.124 $\pm$ 0.01 cm. in a sliding microtome [8]; they were suspended in a mixture of Pale 4 oil (oxidized castor oil, Baker Castor Oil Co.) and tetrabromoethane to yield η_o = 13.6 p. and ρ = 1.138 g.cm.$^{-3}$

Both suspending solutions were found to be Newtonian. The tetrabromoethane was added slowly to the oil until the refractive index of the mixture was the same as that (1.4672) of the PVA spheres and discs or that (1.5135) of the nylon rods, thus rendering the suspensions completely transparent. A small fraction of particles of identical size but of different refractive index and nearly the same density was added to serve as visible tracer particles. In suspensions of spheres these were polystyrene (PS) or polymethylmethacrylate (PMM) at about 0.8% by volume; PS discs and aluminum coated nylon rods were used in the other suspensions.

The sedimentation velocities in the suspensions of spheres, calculated from Stokes' law were negligibly small, never exceeding 3×10^{-4} cm.sec.$^{-1}$; for all practical purposes they were neutrally buoyant.

3. Procedures

Velocity profiles in both Poiseuille and Couette flows were determined by photographing the suspensions as they flowed past the microscope at rest. A Paillard Bolex 16 mm. reflex cine camera was used, and the films analyzed by projecting them onto a drafting table. Particle velocity profiles were obtained by measuring the average velocities of the tracer spheres. In the systems containing PMM tracer spheres, it was also possible to measure the average angular velocities by following optical imperfections in them. Liquid velocity profiles were determined from the measured average translational velocities of tiny aluminum tracer particles ($< 2.5 \times 10^{-3}$cm) in the suspension.

Concentration profiles across the tube were obtained by counting the number of tracer spheres N situated in strips of equal width lying in the median plane. Starting from the wall, all the spheres whose surface (on the wall side) crossed the line separating the first from the second strip were counted as belonging to the first strip, and so on; this was done over a 15.3 cm. length of the tube. The surfaces of the spheres rather than their centers were used as reference points because of the presence of the wall; if the sphere centers had been selected, then a lower concentration of tracer spheres would have been measured in the strips adjacent to the wall, because of the finite dimensions of the particles. Only those spheres sharply in focus were counted; at the magnification used, the depth of the field was approximately one particle diameter.

The path of an individual particle in tube flow was determined by matching the axial speed of the microscope to that of the particle and recording the variation with time of its radial position r. Displacements also occurred in the direction of the microscope axis but these were not measured. Values of $|\overline{\Delta r_t}|$ were obtained by measuring r at the end of equal time intervals of the total time during which the average radial position $\bar{r}$ of the particle remained sensibly constant (within $\pm$ 0.002 cm.). A similar procedure was followed in Couette flow to determine $|\Delta y_t|$; in this case the cylinder speeds were continuously adjusted so that the reference sphere was in the stationary layer. The distribution function $P(\xi)$ was determined from the plots of r against t by counting the number of crossings (which are proportional to $1 - P(\xi)$) in a given time interval at various values of ξ.

RESULTS AND DISCUSSION

1. Poiseuille Flow

(a) Velocity profiles in suspensions of spheres

At sufficiently low values of c and b/R_o the velocities of particles $u'(r)$ and suspending liquid $u(r)$, were identical and parabolic, following (22). As c and/or b/R_o increased $u'(r)$ and $u(r)$ continued to be equal but a pronounced blunting of the velocity profile developed in the center of the tube, with a core of radius r_c in which $u'(r)$ = constant for $r < r_c$. We shall designate this to be "partial plug flow", although it must be emphasized at the outset that this is done as a matter of convenience and does not mean that the profile is mathematically flat when $r < r_c$ with a discontinuous drop in the velocity gradient $G(r)$ to zero at r_c; rather, it is a region where there is no measurable gradient. There is some uncertainty in determining r_c from plots of the type shown in Fig. 2 and for this reason there is an inevitable scatter in the values of r_c given in Table I in which the results are summarized.

Table I contains other measures of the deviation from parabolic flow. The ratio $u'(0)/u^*(0) = 1$ for parabolic flow and < 1 for blunting, where $u^*(0)$ is the axial velocity for parabolic flow for the same Q. When the flow is parabolic the velocity ratio

$$\frac{u'(r)}{u'(0)} = 1 - \frac{r^2}{R_o^2} \qquad (29)$$

and when the profile is blunted the ratio is greater; measured values at r/R_o = 0.2, 0.5 and 0.8 for which the corresponding parabolic flow ratios are 0.96, 0.75 and 0.36 are included in the table.

The influence of the pertinent variables on the blunting of the profile may be summarized as follows:

Concentration. As shown in Fig. 2a and Table I, when c was increased from 0.14 to 0.22 and higher (at constant $b/R_o = 0.028$) there was a transition from parabolic to partial plug flow, with r_c increasing with c.

Particle size. Increasing b/R_o (at $c = 0.33$) also had a pronounced effect on the transition with r_c increasing and becoming equal to R_o at $b/R_o = 0.112$ which corresponds to complete plug flow (Fig. 2b, Table I). Observation of tracer spheres adjacent to the wall revealed, however, that the plug flow did not always extend to the wall since the spheres could often be seen to rotate. This is illustrated in Fig. 3 where the angular rotation Φ of several peripheral spheres is shown. On starting flow the spheres began to rotate erratically; often the rotation stopped after a time (curves 1 and 2) and sometimes started again (curve 3) suggesting stick-slip behaviour. In all cases the translational velocity was constant within the precision of measuring $u'(r)$, independent of $(d\Phi/dt)$.

Flow rate and Viscosity. In contrast (within the experimental error due mainly to small displacements of the observed tracer spheres from the median plane of the tube), the relative velocity profiles were independent of the flow rate over a 10-fold range provided that the particle Reynolds number was kept below the value at which radial migration of particles due to inertial effects becomes appreciable [9]; this is illustrated in Fig. 2c. The velocity profile was also independent of the viscosity as was shown by measurements in a suspension ($c = 0.27$,

$b/R_o = 0.070$, $Q = 3.56 \times 10^{-2}$ cm^3. sec^{-1}., $R_o = 0.4$ cm.) at three temperatures between 22 and 45°C resulting in a 5-fold change in viscosity η of the suspension.

Figure 2d shows that $u(r) = u'(r)$ except for a scatter due to experimental error. Further proof of the absence of any appreciable net slip between particles and suspending fluid is shown by comparing the volume flow rates Q calculated from

$$Q = \int_0^{R_o} 2\pi r u'(r) dr \qquad (30)$$

by graphical integration of measured values $u'(r)$, with those obtained by weighing the amount of suspension expelled from the tube in a given time; the two sets of values (Table I) are in good agreement.

When $r > r_c$ the particles could be clearly seen to rotate, although the rotation of a given particle was not always steady because of frequent interactions evident from the radial displacements which are considered later; it was possible to measure the mean $\omega'(r)$ from the mean period measured while travelling the length of the tube. When $r < r_c$ the particles had neither measurable rotation nor fluctuations in radial distance. Table II gives directly measured values of $\omega'(r)$ for two suspensions which compare favorably with those calculated from (24) using the values of $G'(r)$ determined from the slopes of the velocity profiles, indicating that the field rotation and particle rotation are the same and hence that $G'(r) = G(r)$. As expected, near the tube wall the velocity gradient corresponding to a parabolic distribution $kr < G'(r)$, and away from it $kr > G'(r)$ (Table II).

The fact that the velocity profile varied with c and b/R_o but was independent of Q and η_o suggested that the development of the partial plug flow was a wall effect rather than a manifestation of non-Newtonian behavior by the suspensions. This was further confirmed by measurements in the rotational viscometer which showed the apparent viscosity to be independent of shear rate (Fig. 4a).

At a fixed b/R_o, a linear relationship was also found between ΔP and Q in tube flow (Fig. 4b). As b/R_o increased the slope of the lines for the two most concentrated suspensions decreased, indicating a decrease in the apparent viscosity. This effect has been observed in a variety of suspensions [10-14] and has been explained in terms of wall effects [14, 15] and finite particle size [16]. For spheres Higginbotham et al [10] found that Vand's wall correction factor [14] yielded the true suspension viscosity when $cb/R_o < 1.5$ approximately. According to the present results partial plug flow develops in the tube about this value of cb/R_o. It is likely that this may cause an additional decrease in the apparent viscosity from that predicted by Vand [14], but more extensive viscosity measurements are required before more definite conclusions can be drawn.

(b) Rods and Discs

Concentrated suspensions of rods and discs showed similar behavior, namely, above a certain value of c partial plug flow developed in the tube and yielded profiles similar to those in Fig. 2. As with spheres, no dependence on the flow rate was found. Moreover, the velocity distribution was independent of time, indicating that the particles quickly attained the equilibrium distribution of orientations.

In the region of plug flow the particles did not rotate; the axes of revolution of most discs were nearly normal and those of rods nearly parallel to the direction of flow (Fig. 5a). This might be due to the effect of the convergent entry from the reservoir into the tube or to particle-particle interactions [17]. At $r > r_c$ the particles exhibited erratic rotations and radial displacements.

The results are summarized in Table III. The velocity profile of a suspension of discs with $b'/R_o = 0.078$ and $a'/R_o = 0.0156$ and $c = 0.30$ was nearly identical to that of spheres with $b/R_o = 0.056$ at the same concentration (Fig. 5b), indicating that the characteristic dimension of the cylindrical particles (i.e. the one which produces the same blunting in the velocity profile as a suspension of rigid spheres at the same c) lies between a' and b'. The limited amount of data, however, do not permit any quantitative correlation between a', b' and b.

(c) Concentration profiles

The explanation for plug flow which first comes to mind is that a dilution of the peripheral suspension occurs from inward migration of particles near the wall, although there was no visual evidence of this and the velocity profiles did not change over prolonged times of flow. To check this directly, concentration profiles of tracer spheres in the tube at the beginning of the experiment and after the suspension had flowed back and forth through the tube over a period of 4 hrs were measured. The results are summarized in Table IV and show a uniform concentration profile both at the beginning and at the end of the experiment. The total number of particles N counted after 4 hrs was well within the random statistical error $\sqrt{N}$ of the initial values, and showed reasonable agreement (better than 6%) with that calculated from b, the volume fraction of the tracer spheres in the suspension, the depth of the field and the length of the tube (15.3 cm.) used in the measurements. It is concluded from these experiments that, except for the geometrical requirement that particle centers must be displaced at least b from the wall, the concentration of particle centers is uniform across the tube.

(d) Radial displacements of spheres

In dilute suspensions $\bar{r}$ remained constant over relatively long periods of time as a result of the symmetrical behavior of doublets. This is shown in Fig. 6a where several paths of PS spheres at c = 0.02 are plotted. Each arrow indicates when an n-body ($n > 2$) collision could be seen and which, because such collisions are unsymmetrical, caused a shift in $\bar{r}$; these collisions also caused net displacements from the median plane so that eventually the tracer sphere went out of focus in the microscope and then became lost from view.

The measured values of $|\overline{\Delta r_t}|$ resulting from 2-body collisions only were independent of $\bar{r}$ (Table V) but about twice those calculated from (9). The sign of this discrepancy is as expected since the theory assumes rectilinear approach of two colliding spheres whereas it is known to be curvilinear. Analysis of the doublet geometry of several collisions from previous work [2, 5] shows that $|\overline{\Delta y_\tau}|.\tau$ is of the order of 20% greater than given by (5). In addition, displacements occur by interaction of two spheres which on the basis of the rectilinear-approach theory do not collide.

This effect is revealed by comparing the calculated number of 2-body collisions ft of the reference sphere over the period of observation with the number of discernible displacements Δr made over the same period; the latter is always greater. Thus over the period of 510 sec at $\bar{r} = 0.366$ cm. (Fig. 6a, Table V) the calculated ft = 10 whereas at the scale of resolution used about 23 disturbances in Δr could be detected. This discrepancy points up one of the limitations of the simple geometrical theory of 2-body collisions which cannot be overcome until a theory based on the Stokes-Navier equation is solved in detail. A start on this problem has been made for interacting cylinders in 2-dimensional Couette flow by Raasch [18)] and for spheres at $\theta_o = \pi/2$ by Wakiya et al [19)] but further discussion of this must be deferred.

Surprisingly, values of $1 - P(\xi)$ calculated from the experimental data showed agreement with the theory (Fig. 6c). The scatter is undoubtedly due to the relatively small number of total crossings (< 40 at $\xi = 0$) within the time of observation. This suggests that the collision theory could be improved by substituting a "collision radius" $b_c (> b)$ in the collision equations.

At concentrations at which plug flow developed, the paths of the particles showed radial displacements whose magnitude and frequency decreased with decreasing r (Fig. 6b), until when $r < r_c$ the fluctuations disappeared and, as stated earlier, the spheres moved with identical velocities and without any measurable rotation over the length of the tube.

2. Couette Flow

(a) Velocity profiles

Further evidence of a wall effect at high c was obtained from velocity profile measurements in Couette flow. In the annulus between two counter-rotating cylinders, the clockwise angular velocity $\Omega(R)$ of a homogeneous Newtonian liquid at distance R from the center of rotation is given by [6)]

$$\frac{\Omega(R) + \Omega_1}{\Omega_1 + \Omega_2} = \frac{R_2^2}{R_2^2 - R_1^2}\left\{1 - \frac{R_1^2}{R^2}\right\}, \qquad (31)$$

Ω_1 being the counter-clockwise angular velocity of the inner cylinder, Ω_2 the clockwise angular velocity of the outer cylinder and R_1 and R_2 the respective radii of the cylinder walls. The translational velocity and the velocity gradient at R are given by

$$u(R) = R\Omega(R) \quad , \qquad (32)$$

and

$$G(R) = R\,\frac{d\Omega(R)}{dR} \quad . \qquad (33)$$

Because of the finite curvature of the cylinders the velocity gradient is not strictly constant but decreases with increasing R. However, by increasing both R_1 and R_2, G can be made effectively constant across the annulus.

The measured particle velocity profile plotted in the dimensionless form in Fig. 7a shows good agreement with (31) for spheres at $c = 0.01$. At $c = 0.38$ particle and fluid velocity profiles are identical over a range of values of Ω_1 and Ω_2 , but deviate appreciably from (31); as in tubes, the gradient near the wall is greater than given by the theory for a homogeneous liquid. The theoretical and experimental curves intersect each other near the center of the annulus indicating a similar deviation at each wall. The effect of particle size at the same c (= 0.38) is illustrated in Fig. 7b and 7c; although the ratio $2b/\Delta R$ was increased by a factor of about 3.5 the effect on the velocity profile was not as pronounced as in Poiseuille flow, since at these values of c and b/R_o complete plug flow would have occurred in the tubes. Reasons for this pronounced difference are discussed later.

In contrast, the velocity profiles obtained from measurements of the translational velocities of aluminum tracers in a viscoelastic liquid (4% by weight of polyacrylamide in water) and shown in Fig. 7d were found to deviate markedly from that given by (31), to be unsymmetrical and dependent on the cylinder velocities, the profile asymmetry increasing as the average velocity gradient was increased by keeping Ω_2 constant and increasing Ω_1.

(b) Normal displacements

As expected, the displacements $\Delta y = (\bar{R} - R)$ in dilute suspensions in Couette flow were similar to those in the tube. This is illustrated in Fig. 8a where some of the paths of tracer spheres in a c = 0.035 suspension of PVA spheres are shown. As before $\bar{R}$ remained constant until a multi-body collision (indicated by an arrow) occurred, and the observed $|\overline{\Delta y_t}|$ was twice as large as calculated from (19). Table V also contains values of ft calculated from (6), where the asterisk indicates the number of 2-body collisions prior to the shift of $\bar{r}$ or $\bar{R}$.

In Poiseuille flow the time interval during which an individual particle could be observed was limited by the length of the tube so that it was impossible to establish the extreme limits of the radial fluctuations. In the Couette apparatus, on the other hand, a particle could be observed for very long times as illustrated in Fig. 8(b and c) where it is seen that at sufficiently high concentrations a particle can travel almost from the one wall to the other. It may be concluded from these observations that in very long tubes a particle can in time traverse all radii for which $G > 0$.

3. Reversibility

When appropriate precautions were observed, the rotational and translational displacements of individual particles (and, indeed, domains of the suspending liquid) in Poiseuille flow could be made reversible, i.e. reversing the direction of flow had the effect of reversing time as when a cine-film is run backwards. This was demonstrated by the following simple, but very striking, experiments.

When a drop of dye solution (Victoria blue in the polyglycol oil) was introduced into the same oil in the tube and flow was started the drop was progressively deformed into an extended ribbon; on reversing flow the drop recovered its initial shape as could readily be shown by superposition of photographs. It is important to use a dye which has a low diffusion coefficient; in the system used the cycle could be repeated five times before the irreversible effects of molecular diffusion of the dye became appreciable. The same experiment was performed in dilute and concentrated suspensions ($c \leq 0.4$) of spheres with similar results, except that the deformation of the dyed regime was considerably enhanced by convection due to rotation of the particles when $r > r_c$. Similar results have been obtained in Couette flow [4] and in a fixed particle bed [20].

The interactions of rigid particles are also reversible. Fig. 9 shows the behavior of an isolated triplet of PS discs located near the median plane (MM') of the tube (Fig. 1c). The coordinates r, Φ and Θ of the axis of revolution of each disc were perfectly reproducible when the flow was cycled. The limiting configurations of the triplet are shown pictorially in Fig. 9c.

The reversible behavior of r and Φ of individual spheres in concentrated suspensions is shown in Fig. 10. It is remarkable that the translational and rotational coordinates of a single sphere, and hence all of the complex configurations of the dynamically interacting assembly of spheres, were conserved. Similar behavior was shown by a tracer disc in a concentrated suspension of discs, as illustrated by the variation of r, Θ and Φ in Fig. 11.

The requirements in these experiments were stringent; it was particularly important to have isothermal flow (to avoid irreversible thermal convection currents), to match particle and liquid densities (to avoid irreversible sedimentation) and to have low flow rates (to avoid irreversible inertial effects). It proved to be much more difficult to obtain reversibility with discs than with spheres, possibly because of the additional two degrees of rotational freedom of the discs, but this point is not certain since nothing is known about the rotation of single spheres about the X- and Y- axes (Fig. 1c) in concentrated suspensions.

A formalized theoretical basis for such time-reversed flows has recently been given by Slattery [21] based on the linearized form of the Stokes-Navier equation.

CONCLUDING REMARKS

It is evident from the foregoing considerations that deviations from the parabolic profile in flow through tubes at the low Reynolds numbers employed in the experiments are due to interactions between the outer layers of particles and the rigid walls. Even limiting consideration to single particles presents a formidable problem and has been attempted only for several simple cases [14,18,19,22]. Observations of single isolated spheres touching the wall reveal that there is a definite slip of the particles in both Couette and Poiseuille flows [24]. The spheres rotate, but their translational velocity $u' > \omega' b$ yielding a slip velocity equal to $0.5u'$ approx. The unsymmetrical two-body collisions near the wall reported by Goldsmith and Mason [2] should also be mentioned as a possibly related phenomenon.

The significance of these observations on isolated particles near the wall to the phenomena discussed earlier and which occur at high concentrations is not clear. As the concentration increases the particle-particle interaction effects, which are greatly complicated by the dynamic nature of the particle aggregates, will play an increasingly important role and it is conceivable that theories based on single particles will become irrelevant. However, all arise from the presence of the wall, and knowledge of the behavior of single particles near the wall may contribute to a better understanding of the flow mechanism of concentrated dispersions.

Vand's consideration of the wall effect with rigid spheres led him to conclude that "in the region of high concentrations considerable slip at the wall might develop due to layers of low viscosity along the walls which might completely overshadow the effect of shear inside the suspension". Following Vand's suggestion, the wall effect can be represented by considering the suspension to be a continuum which has an effective viscosity varying from η_o (that of the pure medium) at the wall to η (that of the suspension) at some characteristic distance away which is only a function of b. Assuming several functional relationships for the variation of the effective viscosity with distance from the wall [23] the velocity profiles of concentrated suspensions in both Couette and Poiseuille flows and the decrease in apparent viscosity with increasing b/R_o can be qualitatively explained [23]. Moreover, at a given b/R_o ($= 2b/\Delta R$) and η/η_o Vand's model predicts a smaller effect of the wall in Couette than in tube flow presumably because of the different geometry of the boundary; this is in accordance with the experimental results.

LIST OF SYMBOLS

a'	=	semi-axis of revolution of cylindrical particles
b; b'	=	radius of sphere; equatorial semi-axis of cylinder
c	=	volume fraction of particles in suspension
f	=	2-body collision frequency per particle
G; $G(r)$; $G(R)$	=	velocity gradient; at r in tube flow; at R in Couette flow
k	=	$4Q/\pi R_o^4$
$\bar{\ell}$; $\bar{\ell}(r)$; $\bar{\bar{\ell}}$	=	mean free path; at r; average over the tube
n	=	number of particles per unit volume of suspension
N	=	number of tracer particles (Table IV)
$p(\xi)$; $P(\xi)$	=	differential and integral distribution functions of lateral displacements
Q	=	volumetric flow rate
r; $\bar{r}$; $\lvert\overline{\Delta r_t}\rvert$	=	radial distance from tube axis; time average radial distance; time average absolute radial displacement from mean
r_c	=	radius of core of plug flow
r_e	=	axis ratio of spheroid
R_1, R_2	=	radius of inner and outer cylinder of Couette apparatus
ΔR	=	$R_2 - R_1$
R; $\bar{R}$	=	radial distance of a fluid element from the axis of rotation in Couette flow; time average radial distance
R_o	=	tube radius
u, v, w	=	velocity components in the X-, Y- and Z- directions
$u(r)$, $u^*(0)$	=	fluid translational velocities at r and tube axis
$u(R)$, $u(y)$	=	fluid translational velocities at R and y in Couette flow
$u'(r)$, $u'(0)$	=	particle translational velocities at r and tube axis respectively in Poiseuille flow

t; $\bar{t}$; $\bar{t}(r)$	=	time; average time between collisions in Couette flow; and at r in Poiseuille flow
x, r, ψ	=	cylindrical polar coordinates
X, Y, Z	=	Cartesian coordinates in Couette flow
Δy; Δy_o; $\lvert\overline{\Delta y}_t\rvert$	=	normal displacement; maximum normal displacement during a collision; time average absolute displacement
η_o, η	=	viscosity of suspending fluid and suspension
θ, Φ	=	spherical polar coordinates (Z = polar axis) of axis of revolution of cylinders or line joining centers of a doublet of spheres
θ_o, Φ_o	=	spherical polar coordinates of the doublet at initial collision
ξ	=	$\Delta y_o/b$
ρ	=	density of suspending medium
τ; $\bar{\tau}$	=	life time of doublet; mean value
$\omega'(r)$	=	angular velocity of sphere about Z-axis
Ω_1, Ω_2; $\Omega(R)$	=	angular velocities of inner and outer cylinders of the Couette apparatus; angular velocity of a fluid element at R

REFERENCES

1. Goldsmith, H.L. and Mason, S.G. J. Colloid Sci. 17, 448 (1962)
2. Goldsmith, H.L. and Mason, S.G. Proc. Roy. Soc. 282A, 559 (1964)
3. Manley, R.St.J. and Mason, S.G. J. Colloid Sci. 7, 354 (1952)
4. Darabaner, C.L. and Mason, S.G. Forthcoming publication
5. Bartok, W. and Mason, S.G. J. Colloid Sci. 12, 243 (1957)
6. Trevelyan, B.J. and Mason, S.G. J. Colloid Sci. 6, 354 (1951)
7. Goldsmith, H.L. and Mason, S.G. J. Fluid Mech. 12, 88 (1962)
8. Nawab, M.A. and Mason, S.G. J. Phys. Chem. 62, 1248 (1958)
9. Karnis, A. and Mason, S.G. To be published
10. Higginbotham, G.H., Oliver, D.R. and Ward, S.G. Brit. J. Appl. Phys. 9, 372 (1958)
11. Schofield, R.K. and Scott Blair, G.W. J. Phys. Chem. 34, 248 (1930)
12. Schofield, R.K. and Scott Blair, G.W. J. Phys. Chem. 35, 1212 (1931)
13. Fahraeus, R. and Lindquist, T. J. Amer. Phys. 96, 562 (1931)
14. Vand, V. J. Phys. Colloid Chem. 52, 277, 300 (1948)
15. Whitmore, R.L. Rheology of Disperse Systems Edited by C.C. Mill Pergamon Press (1959)
16. Dix, F.J. and Scott Blair, G.W. J. Appl. Phys. 11, 514 (1940)
17. Anczurowski, E. and Mason, S.G. Forthcoming publication
18. Raasch, J. Z. angew. Math. Mech. 41, T 147 (1961)
19. Wakiya, S., Darabaner, C.L. and Mason, S.G. Forthcoming publication
20. Hiby, J.W. Proceedings of the Symposium of the Interaction of Fluids and Particles. London, 312 (1962)
21. Slattery, J.C. J. Fluid Mech. 19, 625 (1965)
22. Chaffey, C.E., Brenner, H. and Mason, S.G. Rheol. Acta 4, 64 (1965)
23. Karnis, A. Ph.D. Thesis McGill University 1965 p. 196
24. Darabaner, C.L., Karnis, A. and Mason, S.G. To be published

TABLE I

Velocity profiles in concentrated suspensions of rigid spheres in tubes

c	$\frac{b}{R_o}$	$\frac{r_c}{R_o}$	$\frac{u'(0)}{u^*(0)}$ a)	$u'(r)/u^*(0)$ b) $\frac{r}{R_o} = 0.20$	$\frac{r}{R_o} = 0.50$	$\frac{r}{R_o} = 0.80$	$Q \times 10^2\ cm^3.sec^{-1}$. Calc. c)	Meas. d)
0.085	0.028	0	1	0.96	0.75	0.36	-	0.711
0.14	0.028	0	1	0.96	0.75	0.36	-	1.78
0.17	0.039	0	1	0.96	0.75	0.36	-	1.78
0.22	0.028	0.19	0.87	0.99	0.86	0.46	3.55	3.56
0.25	0.024	0	1	0.96	0.75	0.36	-	3.56
0.27	0.070	0.26	0.78	1.0	0.89	0.50	-	3.56
0.32	0.052	0.40	0.74	1.0	0.98	0.63	3.53	3.56
0.33	0.039	0.38	0.75	1.0	0.94	0.57	-	3.56
0.34	0.056	0.43	0.73	1.0	0.97	0.62	0.695	0.711
0.34	0.056	0.43	0.73	1.0	0.97	0.62	3.54	3.56
0.34	0.056	0.43	0.73	1.0	0.97	0.62	6.95	7.11
0.34	0.112	1.0	0.50	1.0	1.0	1.0	0.18	0.18
0.38	0.030	0.31	0.78	1.0	0.93	0.49	3.56	3.56
0.41	0.030	0.32	0.77	1.0	0.93	0.53	3.54	3.56

Mean $\frac{Q_{calc}}{Q_{meas}} = 0.99$

a) u*(0) is centreline velocity for parabolic flow at same Q calculated from (23).

b) u'(r) and u'(0) are the measured particle translational velocities at radial distance r and at the tube axis.

c) From (30) using measured u'(r) .

d) By weighing the suspension expelled from tube.

TABLE II

Average angular velocities of tracer spheres in concentrated suspensions in tubes

r/R	$\omega'(r)$ radians sec.$^{-1}$ Measured	Calculated [a]	$kr/2$ [b] sec.$^{-1}$
$c = 0.34$ $R_o = 0.4$ cm. $Q = 3.56 \times 10^{-2}$ cm^3.sec^{-1}. $b/R_o = 0.056$ $r_c/R_o = 0.43$			
0.954	0.60	0.45	0.34
0.908	0.37	0.35	0.32
0.854	0.32	0.30	0.31
0.795	0.31	0.27	0.28
0.736	0.28	0.25	0.26
0.628	0.19	0.17	0.22
0.325	0	0	0.12
0.275	0	0	0.10
0.075	0	0	0.03
$c = 0.32$ $R_o = 0.2$ cm. $Q = 0.356 \times 10^{-2}$ cm^3.sec^{-1}. $b/R_o = 0.052$ $r_c/R_o = 0.40$			
0.890	0.35	0.33	0.25
0.840	0.25	0.25	0.23
0.790	0.26	0.20	0.22
0.775	0.24	0.19	0.21
0.710	0.16	0.17	0.20
0.650	0.12	0.09	0.18
0.460	0	0	0.13
0.280	0	0	0.08
0.225	0	0	0.06

a) Calculated from (24) using values of $G'(r)$ obtained from the experimentally measured velocity profile.

b) Calculated from (24) using measured Q.

TABLE III

Velocity profiles in concentrated suspensions of rigid rods and discs in tubes

System	c	$\frac{a'}{R_o}$	$\frac{b'}{R_o}$	$\frac{r_c}{R_o}$	$\frac{u'(0)}{u^*(0)}$	$\frac{u'(r)}{u'(0)}$			$Q \times 10^2$ $cm^3.sec^{-1}$.	
						$\frac{r}{R_o} = 0.25$	$\frac{r}{R_o} = 0.50$	$\frac{r}{R_o} = 0.75$	Calc.[a]	Meas.[b]
Discs	0.10	0.0312	0.156	0	1	0.94	0.75	0.43	-	3.56
"	0.10	"	"	0	1	0.94	0.75	0.43	-	3.56
"	0.17	"	"	0.25	0.91	1.0	0.90	0.56	1.86	1.78
"	0.25	"	"	0.37	0.80	1.0	0.95	0.69	1.87	1.78
"	0.25	0.0156	0.078	0.32	0.84	1.0	0.93	0.63	3.66	3.56
"	0.25	"	"	0.32	0.84	1.0	0.93	0.63	0.738	0.711
"	0.30	"	"	0.38	0.77	1.0	0.95	0.72	3.80	3.56
Rods	0.08	0.310	0.039	0.25	0.85	1.0	0.88	0.60	1.71	1.78

$$\text{Mean } \frac{Q\text{calc}}{Q\text{meas}} = 1.03$$

a,b) Evaluated by same methods as in Table I

TABLE IV

Concentration profiles of tracer spheres in tube flow

$\frac{b}{R_o} = 0.039 \quad R_o = 0.4$ cm. $\quad Q = 3.56 \times 10^{-3}$ cm^3.sec^{-1}.

c = 0.17			c = 0.33		
Range of r cm.	No. of tracer particles N t = 0	No. of tracer particles N t = 4 hr.	Range of r cm.	No. of tracer particles N t = 0	No. of tracer particles N t = 4 hr.
0.334 - 0.400	62	57	0.300 - 0.400	71	71
0.267 - 0.333	56	58	0.200 - 0.299	72	69
0.200 - 0.266	56	51	0.100 - 0.199	76	76
0.134 - 0.199	55	65	0.000 - 0.099	80	84
0.067 - 0.133	63	64			
0.000 - 0.066	61	66			
Totals	353	361		299	298

TABLE V

Time average radial displacements in dilute suspensions of rigid spheres

Poiseuille Flow					
$c = 0.02$	$b = 0.016$ cm.	$R_o = 0.4$ cm.	$Q = 0.78 \times 10^{-2}$ cm^3.sec^{-1}.		
$\bar{r}$ cm.	t sec.[a)]	ft [b)]	$G(r)$sec.$^{-1}$	$10^3 \times \lvert\overline{\Delta r_t}\rvert$ Eq.(9)	cm. Meas.
0.366	510	10*	0.326	0.64	1.1
0.357	214	3.5	0.318	0.64	1.3
0.282	420	5.4	0.251	0.64	1.5
0.174	226	-	0.157	0.64	1.2
				Mean $\frac{\text{Meas}}{\text{Calc}}$ = 2.0	
Couette Flow					
$c = 0.035$	$b = 0.0172$ cm.	$\Delta R = 0.638$ cm.			
$(R_2 - \bar{R})$ cm.	t sec.[a)]	ft [b)]	G sec.	$10^3 \times \lvert\overline{\Delta y_t}\rvert$ Eq.(9)	cm. Meas.
0.313	148	3.7*	0.277	1.2	2.4
0.304	188	4.6*	0.277	1.2	2.6
0.265	200	7.2*	0.403	1.2	2.4
0.255	147	5.3	0.403	1.2	2.6
				Mean $\frac{\text{Meas}}{\text{Calc}}$ = 2.1	

a) The total time interval over which $\lvert\overline{\Delta r_t}\rvert$ and $\lvert\overline{\Delta y_t}\rvert$ were evaluated.

b) Calculated from (6); the asterisk indicates the number of two body collisions in time t before the change in $\bar{r}$ or $(R_2 - \bar{R})$ occurred.

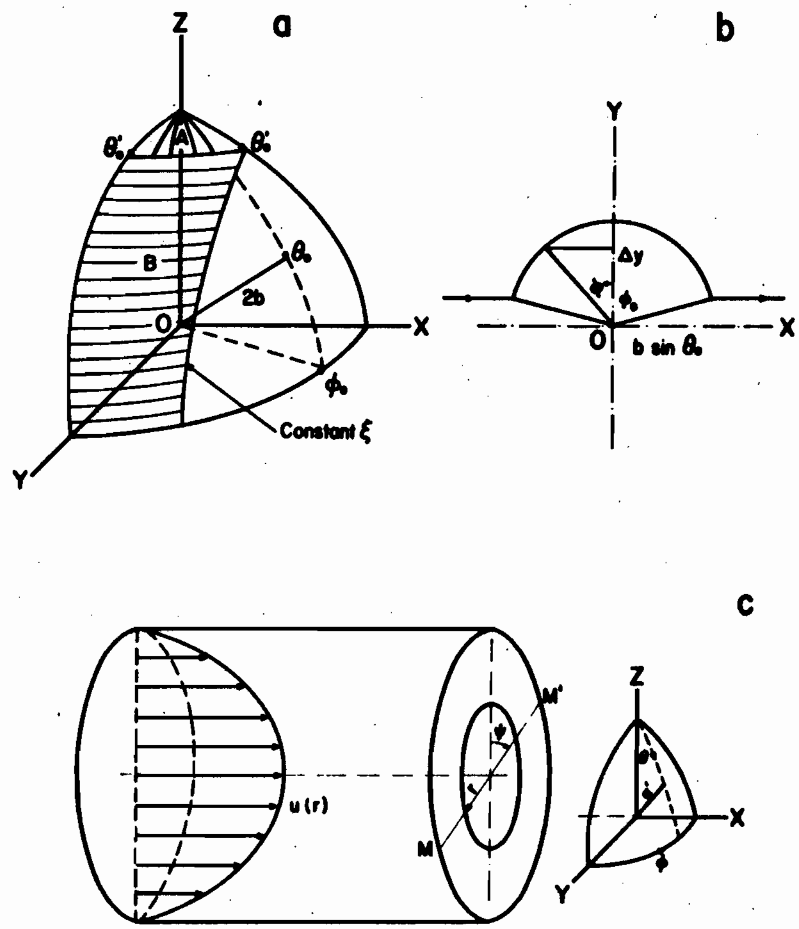

<u>Figure 1</u> (a) Spherical polar co-ordinate system for the collisions of spheres in Couette flow.

(b) Assumed path of a sphere center in the XY plane before, during and after collision with the reference sphere. The origin is at the mid-point of the doublet.

(c) Co-ordinate system to describe the collisions in Poiseuille flow. A Cartesian co-ordinate system is constructed at $x = 0$, r and $\psi = 90°$ at the center of the particle; x, r, ψ are the cylindrical polar co-ordinates.

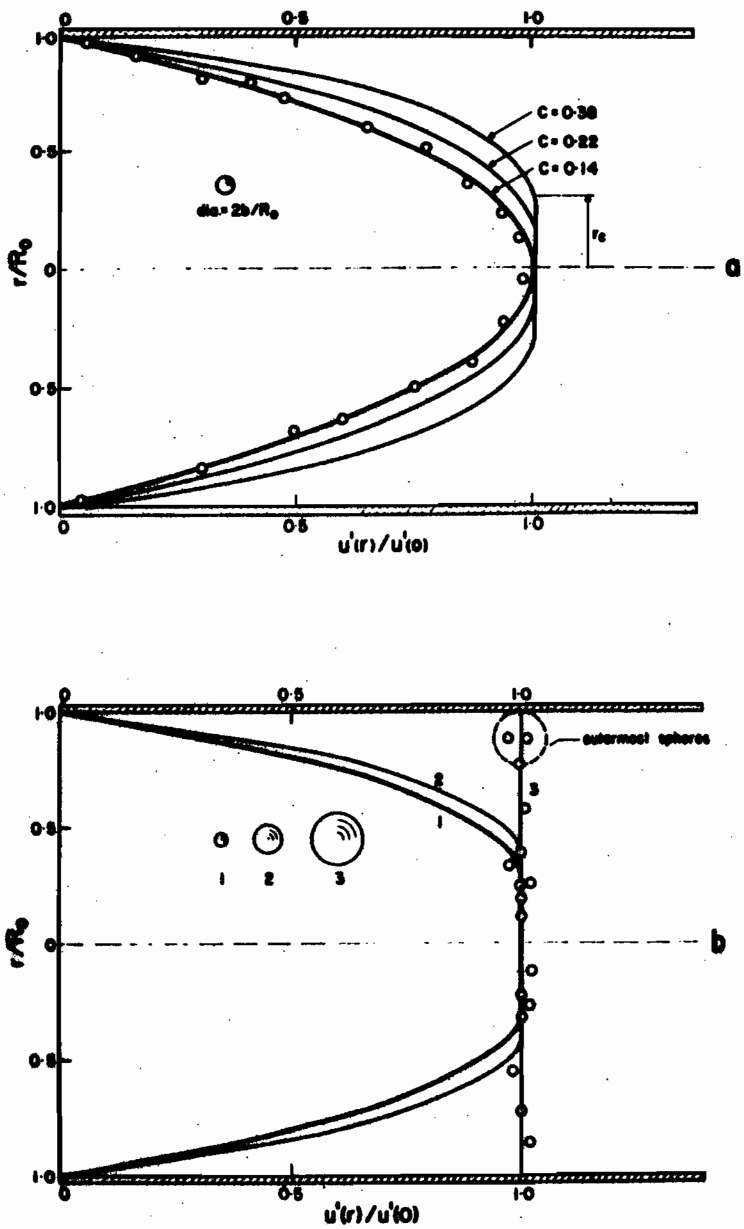

Figure 2 Dimensionless plots of velocity profiles in suspensions of rigid spheres. In each case the sphere diameter ($2b/R_o$) is inset.

(a) Effect of concentration for R_o = 0.4 cm., b/R_o = 0.028 and $Q = 3.56 \times 10^{-2}$ $cm^3.sec^{-1}$. The solid lines are the best fit through the experimental points. The c = 0.14 (open circles) curve is parabolic.

(b) Effect of particle size. Curve 1 (r_c/R_o = 0.31) is the best fit line through the experimental points for a suspension c = 0.32, R_o = 0.4 cm., b/R_o = 0.026, curve 2 (r_c/R_o = 0.43) for a suspension c = 0.34, R_o = 0.4 cm., b/R_o = 0.056; and curve 3 (open circles r_c/R_o = 1) is for a suspension c = 0.34, R_o = 0.2 cm. and b/R_o = 0.112 .

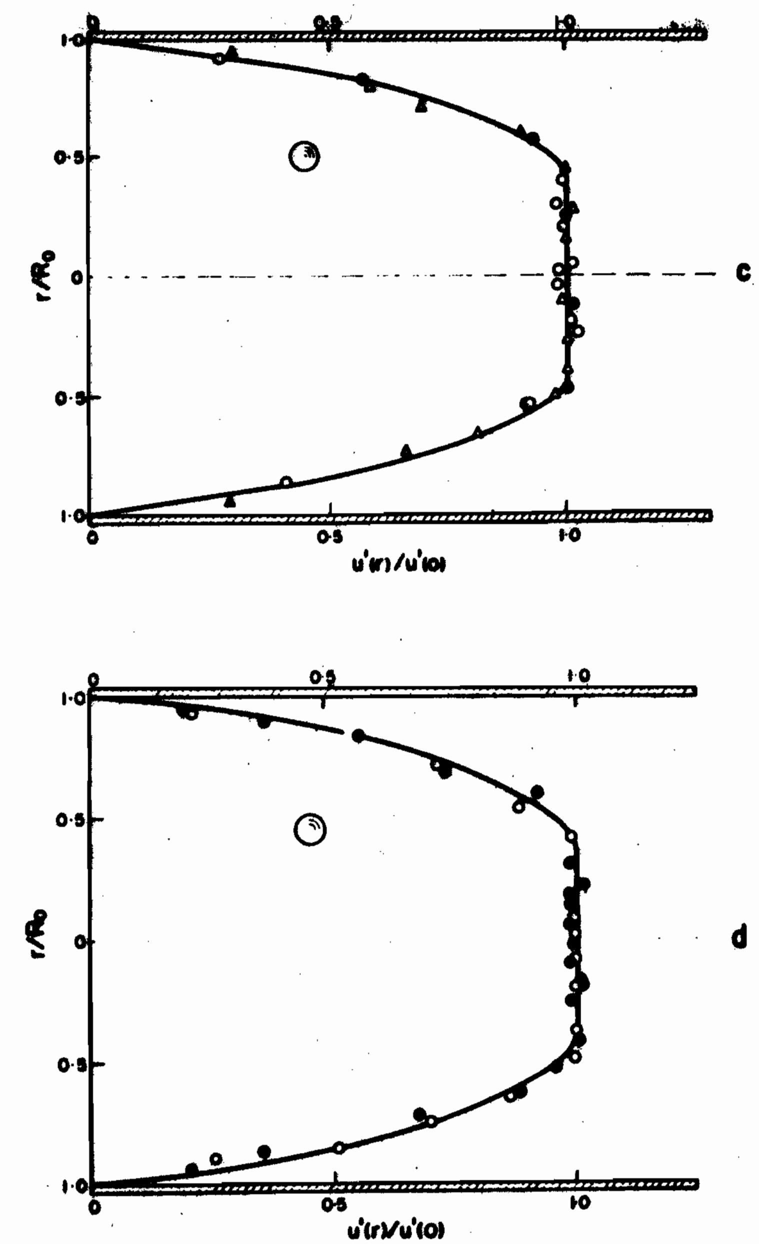

Figure 2 (c) Effect of flow rate for c = 0.34, R_0 = 0.4 cm. and b/R_0 = 0.056. The solid line is the best fit of the experimental points. Closed circles: Q = 0.711 x 10^{-2} $cm^3.sec^{-1}$.; open circles: Q = 3.56 x 10^{-2} $cm^3.sec^{-1}$.; open triangles: Q = 7.11 x 10^{-2} $cm^3.sec^{-1}$.

(d) Comparison of particle and fluid velocity profiles in suspensions of rigid spheres (r_c/R_o = 0.38) for c = 0.30, Q = 3.56 x 10^{-2} $cm^3.sec^{-1}$., b/R_0 = 0.056 and R_0 = 0.4 cm. Experimental points are: open circles (polystyrene spheres); closed circles (aluminum tracer particles).

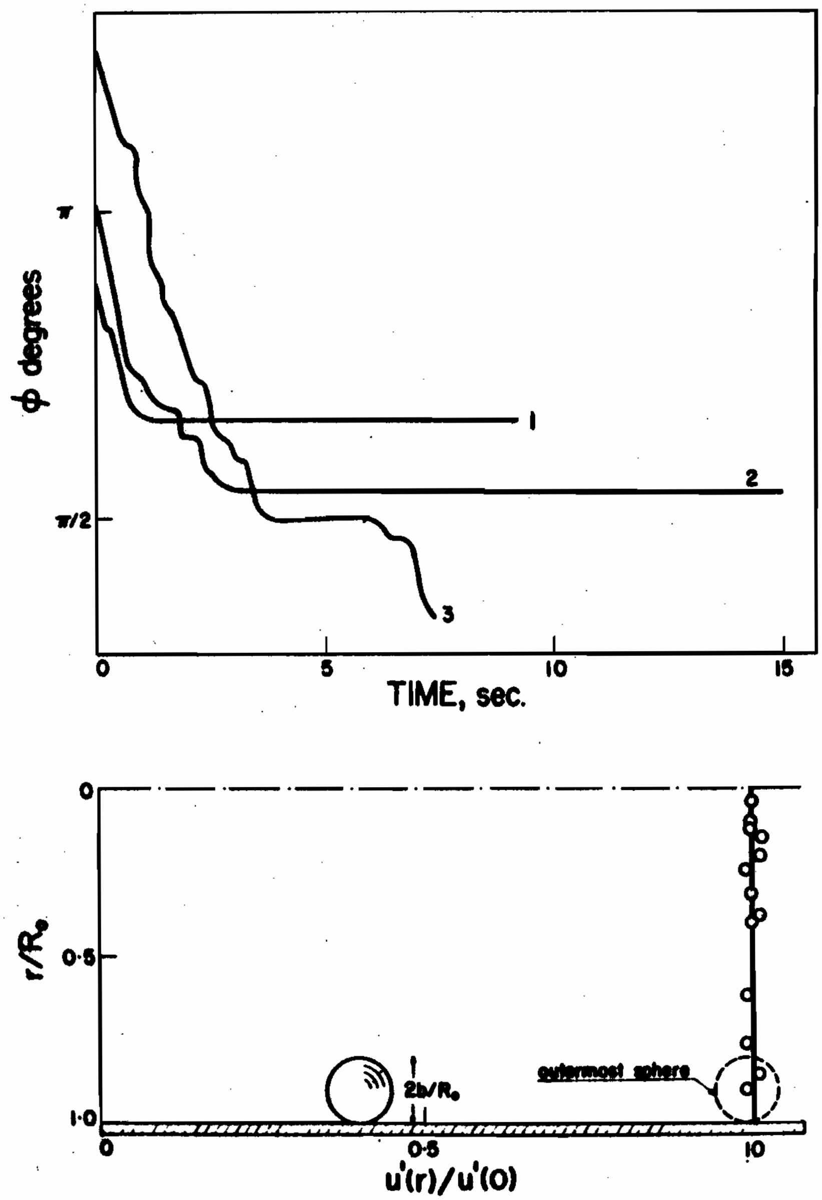

<u>Figure 3</u> Variation of Φ with time of spheres adjacent to the wall in a suspension c = 0.38 exhibiting complete plug flow in the tube; $Q = 1.78 \times 10^{-2}$ $cm^3.sec^{-1}$., $R_o = 0.3$ cm., $b/R_o = 0.1$. The particle velocity profile and the relative size and location of the spheres are also shown in the lower portion.

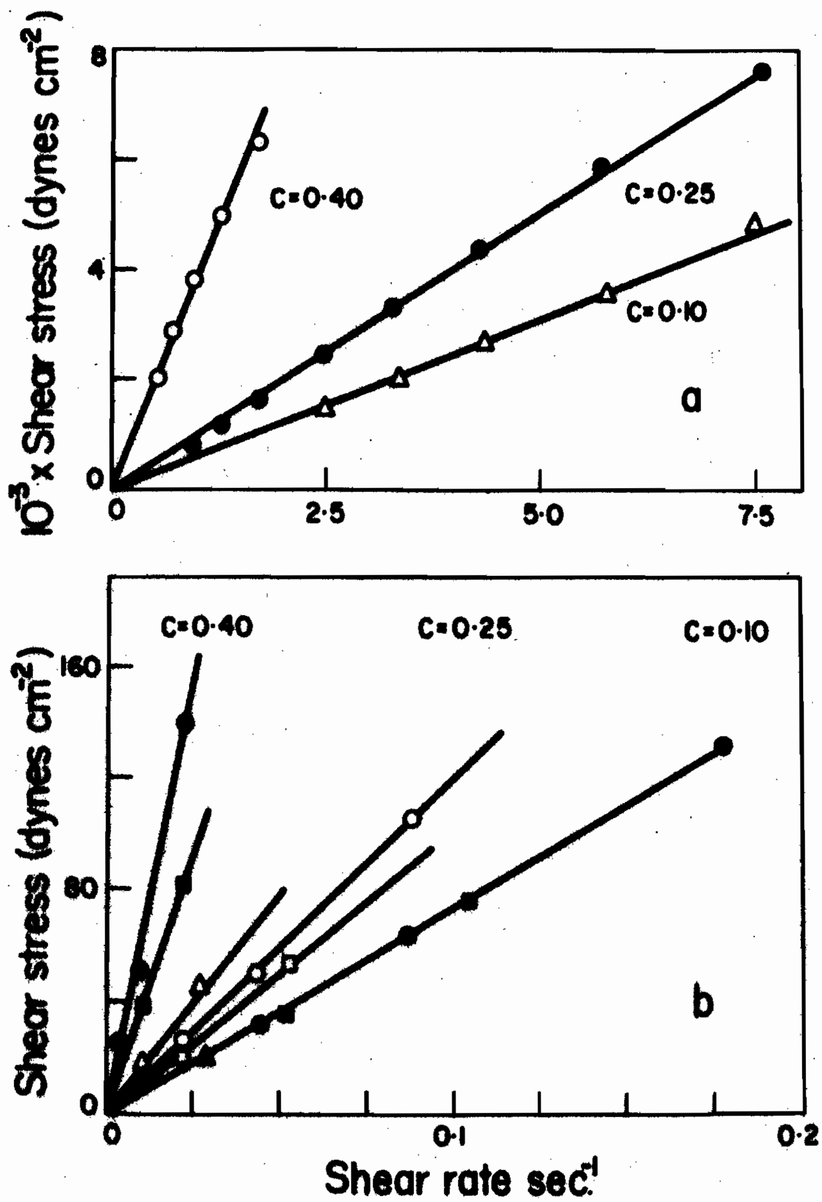

Figure 4 Flow curves in concentrated suspensions of rigid spheres.

(a) Shear stress vs shear rate in a rotational viscometer; radius of the cup R_2= 1.00 cm., radius of the bob R_1= 0.680 cm. and $2b/\Delta R$ = 0.140 .

(b) Plot of shear stress ($R_o \Delta P/2L$) vs nominal shear rate ($4Q/\pi R^3$) at the tube wall. Experimental points are: squares R_o= 0.3 cm., b/R_o= 0.075; circles: R_o= 0.4 cm., b/R_o= 0.056 and triangles R_o= 1.0 cm., b/R_o= 0.022 .

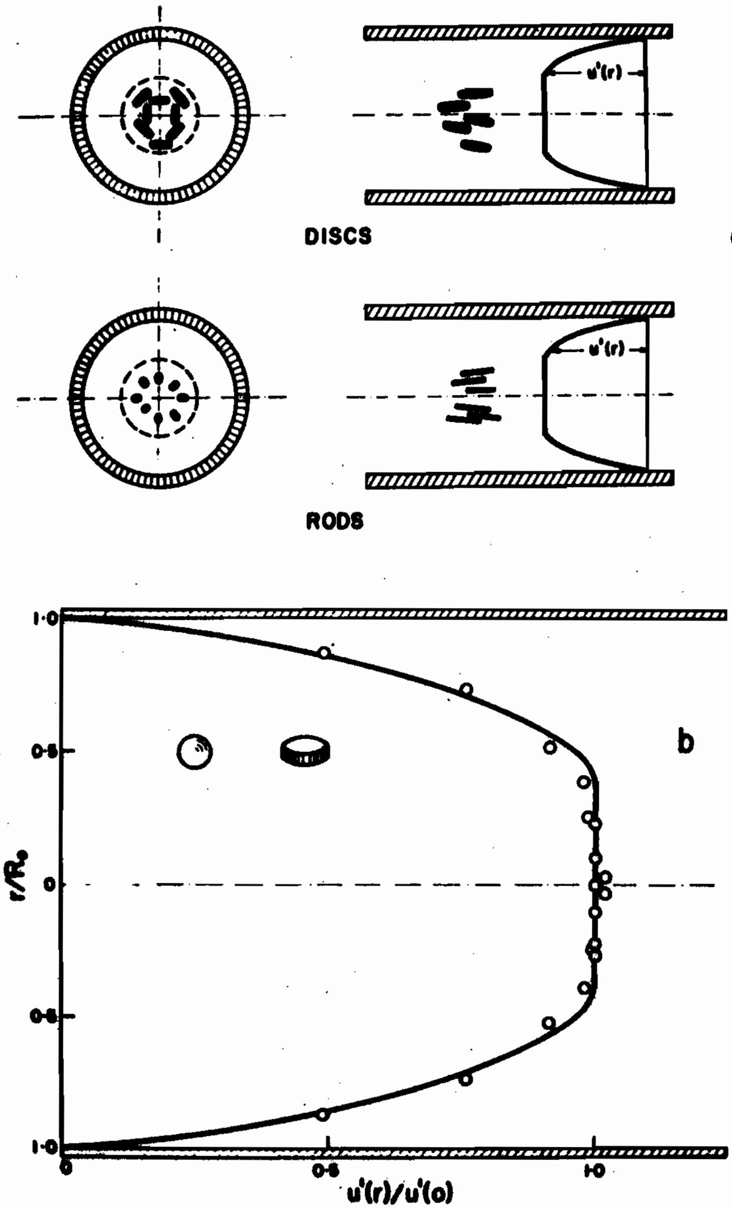

Figure 5 (a) Steady orientation of cylindrical particles viewed along tube axis (left) and in median plane (right) in the region of plug flow in concentrated suspensions of rods and discs (schematic).

(b) Similarity of velocity profile in a suspension of spheres and discs. The solid line is for the spheres shown in Fig. 2d. The experimental points are for a suspension of rigid discs at the same concentration $c = 0.30$; $R_o = 0.4$ cm., $Q = 3.56 \times 10^{-2}$ $cm^3.sec^{-1}$., $b'/R_o = 0.078$ and $a'/R_o = 0.0156$. The relative sizes of spheres and discs in the suspensions are also shown.

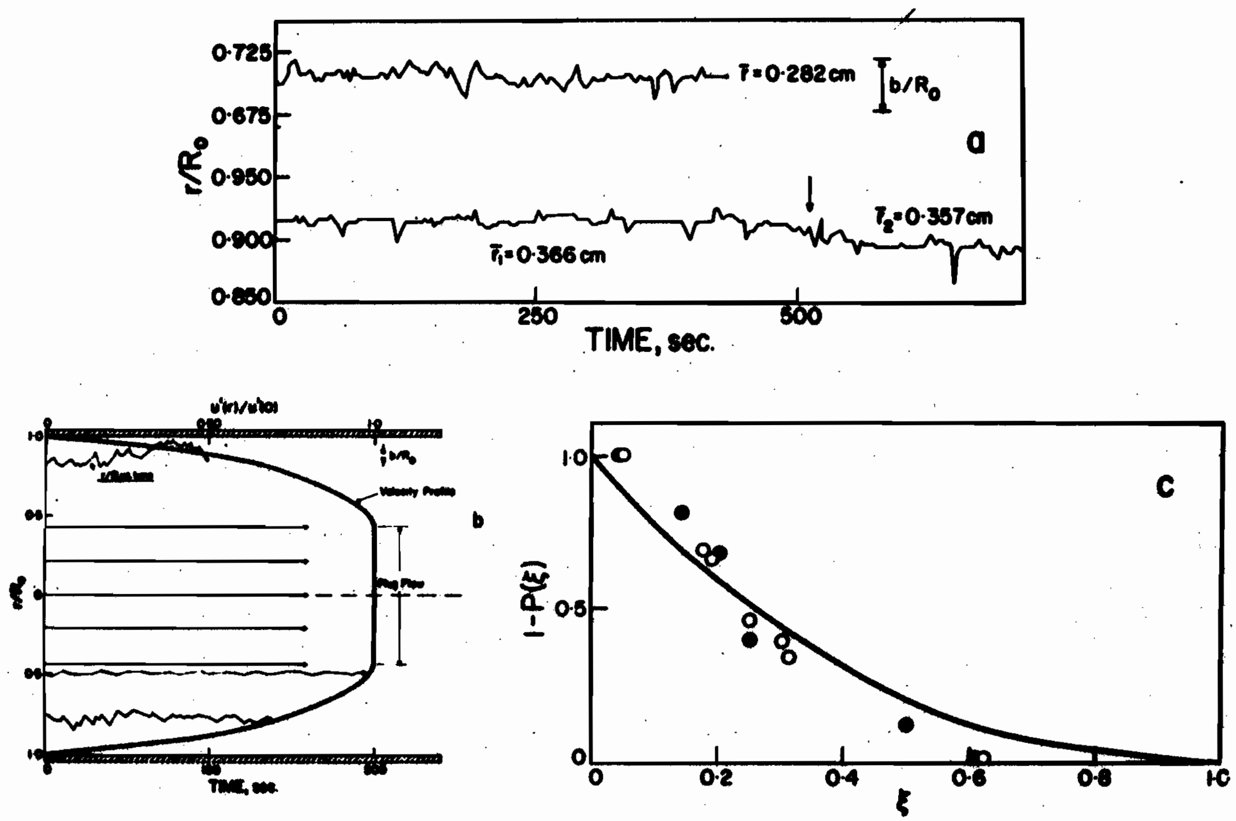

Figure 6 Parts (a) and (b) Variation of the radial distance r with time of tracer spheres in dilute and concentrated suspensions of rigid spheres undergoing Poiseuille flow.

(a) $c = 0.02$, $R_o = 0.4$ cm., $b = 0.0160$ cm., $Q = 1.78 \times 10^{-2}$ cm^3.sec^{-1}. The arrow indicates a 3-body collision which resulted in a shift in $\bar{r}$; measurements taken every 3 secs.

(b) $c = 0.33$, $R_o = 0.4$ cm., $b = 0.0155$ cm., $Q = 3.56 \times 10^{-2}$ cm^3.sec^{-1}., $r_c/R_o = 0.43$; measurements taken every 2 secs.

(c) Plot of $1 - P(\xi)$ vs ξ. The solid line is the theoretically calculated from Eq. (17) the points are experimental data shown in Fig. 6a (open circles) and Fig. 8a (closed circles).

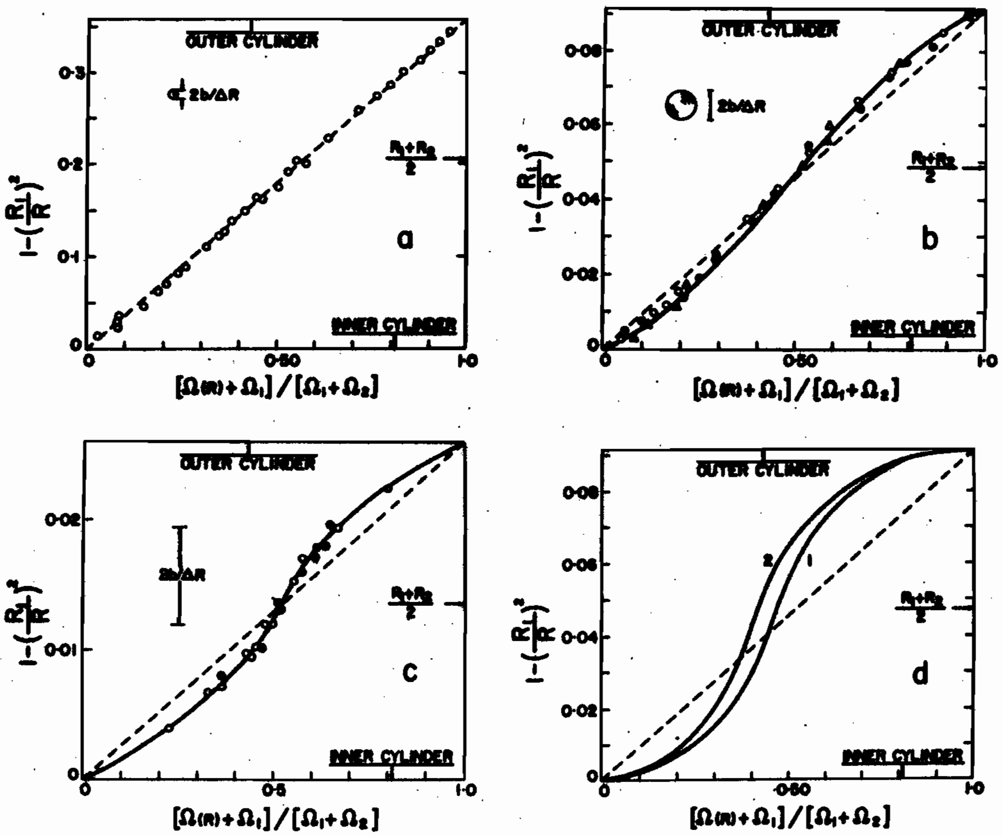

Figure 7 Dimensionless plots of velocity profiles according to Eq.(31). The dashed lines are the theoretically calculated for a Newtonian liquid, the solid lines are the best fit of experimental points. The relative size of the spheres and the mid-point $(R_1+R_2)/2$ are also shown.

(a) $c = 0.01$, $R_1 = 4.644$ cm., $R_2 = 5.795$ cm., $\Omega_1 = 0.00543$ sec^{-1}., $\Omega_2 = 0.00841$ sec^{-1}. and $2b/\Delta R = 0.026$.

(b) $c = 0.38$, $R_1 = 13.942$ cm., $R_2 = 14.625$ cm. and $2b/\Delta R = 0.083$; experimental points are open circles: $\Omega_1 = 0.00259$ sec^{-1}., $\Omega_2 = 0.00614$ sec^{-1}.; closed circles: $\Omega_1 = 0.00259$ sec^{-1}., $\Omega_2 = 0.0205$ sec^{-1}.. and open triangles: $\Omega_1 = 0.0149$ sec^{-1}., $\Omega_2 = 0.00614$ sec^{-1}.

(c) $c = 0.38$, $R_1 = 14.427$ cm., $R_2 = 14.624$ cm. and $2b/\Delta R = 0.287$; open circles: $\Omega_1 = 0.00422$ sec^{-1}., $\Omega_2 = 0.00851$ sec^{-1}. and closed circles: $\Omega_1 = 0.00422$ sec^{-1}., $\Omega_2 = 0.0139$ sec^{-1}.

(d) A viscoelastic liquid (4% by weight of polyacrylamide in water solution), $R_1 = 13.942$ cm., $R_2 = 14.625$ cm.; curve 1: $\Omega_1 = 0.00091$ sec^{-1}., $\Omega_2 = 0.00372$ sec^{-1}.; curve 2: $\Omega_1 = 0.0124$ sec^{-1}., $\Omega_2 = 0.00372$ sec^{-1}.

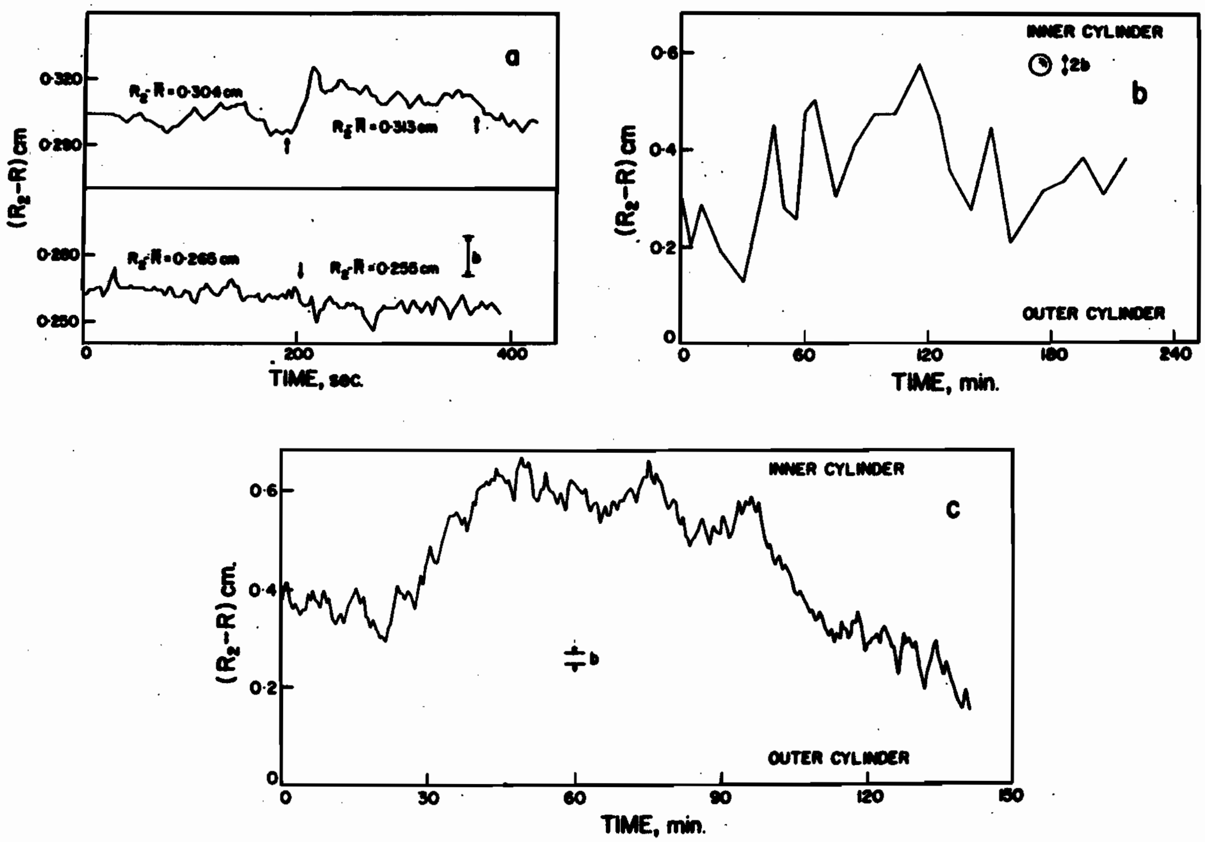

<u>Figure 8</u> Variation of y co-ordinate of tracer spheres from the outer cylinder in dilute and concentrated suspensions of rigid spheres undergoing Couette flow; R_1 = 13.942 cm. and R_2 = 14.625 cm. The variation in z was compensated by focussing the microscope but was not measured.

(a) c = 0.035 , b = 0.0172 cm.; for the lower particle G = 0.403 sec^{-1}. and for the upper G = 0.277 sec^{-1}. The arrows indicate the occurrence of 3-body or higher order collisions causing a change in $\bar{r}$.

(b) c = 0.07 , b = 0.0172 cm., G = 0.05 to 0.42 sec^{-1}; readings at 5 min. intervals.

(c) c = 0.19 , b = 0.0172 cm., G = 0.05 to 0.42 sec^{-1}; readings at 30 sec. intervals.

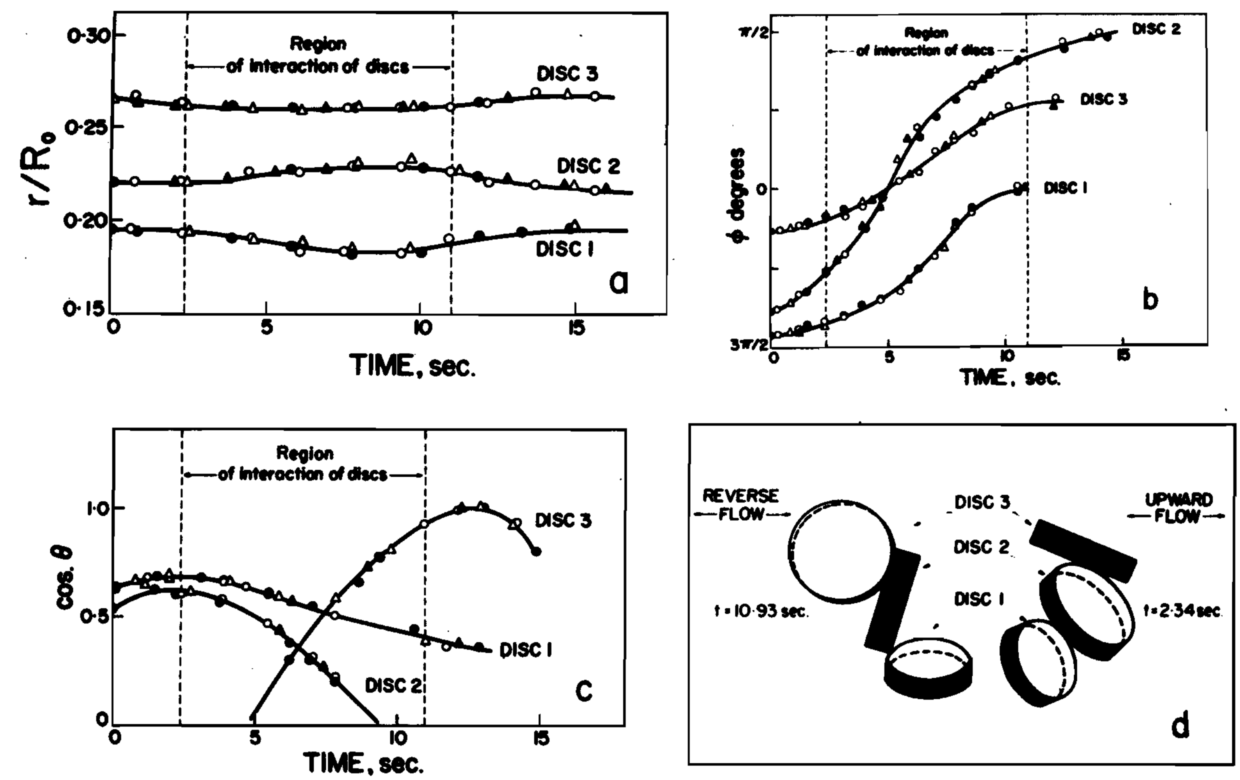

Figure 9 Reversibility of collisions in a system of three interacting PS discs for four consecutive collisions; $R_o = 0.4$ cm., $2a' = 0.0125$ cm. and $Q = 7.11 \times 10^{-2}$ $cm^3.sec^{-1}$. Disc 1: $2b' = 0.0375$ cm.; disc 2: $2b' = 0.0470$ cm. and disc 3: $2b' = 0.0480$ cm. Experimental points are; closed circles: flow upwards, open circles: flow downwards, closed triangles: flow upwards for second time, and open triangles: flow downwards for second time. The vertical dashed lines indicate the region of visible interaction of the discs.

(a) Variation of r with time.

(b) Variation of angle Φ with time.

(c) Variation of angle Θ with time.

(d) Projection of discs in the median plane MM' (XY plane) (see Fig. 1c) traced from microphotographs, illustrating their configuration at the time of collision (t = 2.34 secs.) and separation (t = 10.93 secs.).

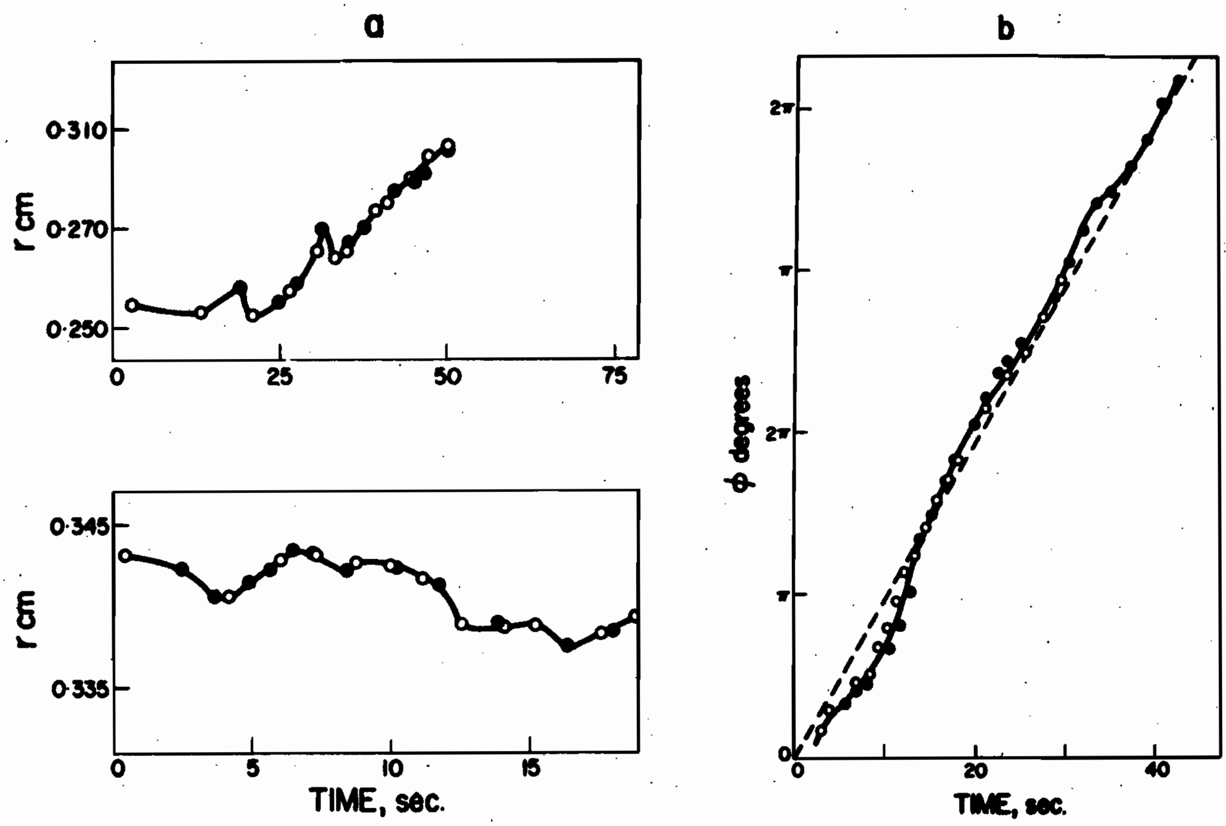

<u>Figure 10</u> Reversibility of collisions in concentrated suspensions of rigid spheres; $R_o = 0.4$ cm., $Q = 3.56 \times 10^{-2}$ $cm^3.sec^{-1}$. The open circles are experimental points obtained during flow in the upward direction, the closed circles when the flow was reversed.

(a) Variation of r with time; for the lower portion $c = 0.17$, $b/R_o = 0.039$ and for the upper $c = 0.34$, $b/R_o = 0.056$.

(b) Variation of Φ with time; $c = 0.17$ and $b/R_o = 0.039$. The dashed line is calculated from Eq.(24) for a single sphere assuming a parabolic velocity distribution (see Table I) and using the average radial distance of the sphere center over the two complete rotations.

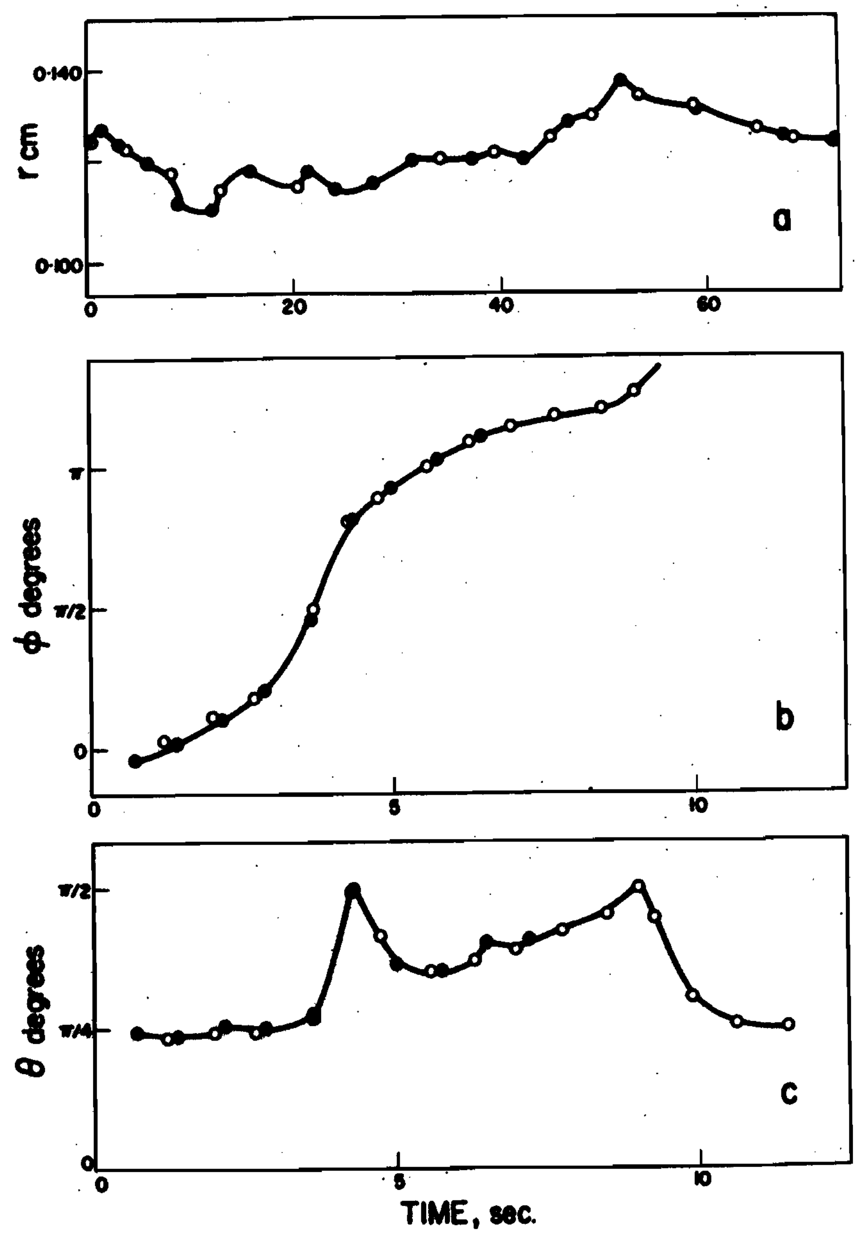

Figure 11 Reversibility of collisions in concentrated suspensions of rigid discs; $R_o = 0.2$ cm., $b'/R_o = 0.156$, $a'/R_o = 0.0062$. Experimental points are; closed circles: flow upwards, and open circles: flow downwards.

(a) Reversibility of path of a tracer disc in a c = 0.10 suspension at $Q = 0.711 \times 10^{-2}$ $cm^3.sec^{-1}$. Parts (b) and (c) are for a suspension c = 0.25 at $Q = 1.78 \times 10^{-2}$ $cm^3.sec^{-1}$.

(b) Variation of angle Φ with time.

(c) Variation of angle Θ with time.

PART III

INERTIAL EFFECTS

ABSTRACT

The behaviour of particles suspended in newtonian liquids undergoing Couette and Poiseuille flows at Reynolds numbers at which inertial effects become significant was investigated.

Rigid spheres rotated with an angular velocity equal to the rotation of the undisturbed field. The rotation and spin of rigid cylinders was similar to that observed in the Stokes flow regime, but they attained limiting rotational orbit constants corresponding to the maximum energy dissipation in Couette flow.

In Poiseuille flow, rigid particles migrated across the planes of shear to an equilibrium radial position which depended on the density difference of two phases, the directions of sedimentation velocity and flow, and the ratio of particle to tube radius. Neutrally buoyant particles which were deformed by flow always migrated to the tube axis.

In concentrated suspensions of spheres a plasmatic layer, free of particles developed near the tube wall as a consequence of radial migration. The formation of this layer modified the velocity profile and caused a reduction in the apparent viscosity coefficient.

Pf p77

INTRODUCTION

The behaviour of rigid and deformable particles in dilute and concentrated suspensions in shear flow in the Stokes (or creeping) flow regime has been described in a number of papers[1-6] from this laboratory.

Goldsmith and Mason[5] found that in Poiseuille flow at effectively zero Reynolds numbers, the radial position of single rigid particles remained constant over prolonged periods of flow. In contrast, fluid drops migrated to tube axis, and a theory to account for this migration was proposed[5] and improved by Chaffey et al[7,8].

The rotation and spin of isolated rigid cylinders in both Couette[1,2,4] and Poiseuille[5] flows were shown to follow Jeffery's equations[9] for a spheroid in an unbounded Couette flow, provided that the "equivalent ellipsoidal" axis ratio[1] was used and wall effects were negligible. Moreover, the cylinders rotated in fixed spherical elliptical orbits which depended only on the initial conditions of release[4,10].

At low Reynolds numbers where inertial effects become important, Segré and Silberberg[11,12] working with dilute neutrally buoyant suspensions of rigid spheres, discovered the "tubular pinch effect" whereby the particles migrated away both from the tube axis and tube wall reaching equilibrium at an eccentric radial position; at this position and at very low concentrations the spheres became regularly spaced in chains extending parallel to the tube axis[13,14].

The observation of Segré and Silberberg have spawned a number of theoretical and experimental studies because of the importance of radial migration phenomena to suspension rheology.

The investigation reported here deals with the behaviour of rigid and deformable particles in dilute and concentrated suspensions at the flow regime where inertial effects start to become significant, and is an extension of a brief preliminary study reported earlier[15] (see Appendix I).

In the Theoretical Part which follows, the relevant theories of the phenomena considered in this Part of the thesis and especially of radial migration are presented in some detail to provide the background necessary to discuss the results.

THEORETICAL PART

1. Poiseuille and Couette flows

In Couette flow the velocity field is defined by

$$u = Gy \;;\quad v,\, w = 0 \;, \tag{1}$$

where u, v, w are the respective fluid velocities along the X-, Y-, Z- axes and G the velocity gradient (Fig. 1a). When the flow is produced between counter-rotating cylinders, G is not strictly constant across the gap but varies with distance from the axis of rotation, being maximum at the inner cylinder (radius R_1) and minimum at the outer cylinder (radius R_2)[1]; however, when $(R_1 - R_2)/R_1$ is small, G may be considered constant across the annular gap.

In Poiseuille flow, G increases linearly with the radial distance r from the tube axis according to the relation[5]

$$G(r) = -\,kr \;, \tag{2}$$

where $k = 4Q/\pi R^4$, Q the volumetric flow rate and R the tube radius. In terms of cylindrical polar coordinates r, Ψ, x (Fig. 1b) integration of (2) yields the component of fluid velocity in the X- direction

$$u(r) = \frac{k}{2}\,(R^2 - r^2) \;. \tag{3}$$

When the particle is small relative to R the local field can be replaced by an equivalent Couette field translating with velocity u(r) (Fig. 1b).

2. Radial migration in Poiseuille flow

Although Segré and Silberberg[11,12] were the first to observe the two-way migration of rigid spheres in Poiseuille flow, Müller[16] working with suspensions of rubber discs, Vejlens[17] using single rigid spheres, and Starkey[18] using carbon black suspensions had previously observed migration away from the wall of the tube at Reynolds numbers at which the tubular pinch effect operates. The principle of least action[18,19] and of minimum energy dissipation in flow[17] were used to explain the migration. However, it has been shown theoretically[20,21] that no lateral force can arise from the creeping equations of motion but that the observed migration is due to inertial effects.

(a) Unbounded flows

The creeping or Stokes flows may be regarded as the leading terms in an asymptotic solution of the Navier-Stokes equation for small Reynolds numbers. To obtain solutions at higher Reynolds numbers various perturbations schemes have been used; a lengthy discussion of the methods used is given by Brenner[22].

Rubinow and Keller[23] have studied the flow around a rigid sphere of radius b spinning with an angular velocity ω' and moving in an unbounded stationary viscous fluid with velocity V; using Stokes and Oseen expansions they showed that the lift force acting on the sphere (to the zero order of Reynolds number) is

$$F_L = \pi b^3 \rho \omega' V \ , \tag{4}$$

where ρ is the density of the fluid. This force, which arises from a "slip-spin", is akin to Magnus force used to explain phenomena such as the curving of a spinning ball, and is due to inertial effects in the neighbourhood of the particle.

Assuming that the sphere is propelled radially with the Stokes velocity the migration velocity is found from (4) to be

$$U = \frac{1}{6} \cdot Vb^2 \cdot \frac{\omega' \rho}{\eta_o} , \tag{5}$$

where η_o is the viscosity of the suspending fluid.

In applying (5) to neutrally buoyant systems in Poiseuille flow, it was assumed[23)] that the relative particle-fluid velocity V is given by[24,25)]

$$V = -\frac{2}{3} u(o)\left(\frac{b}{R}\right)^2 + O\left(\frac{b}{R}\right)^3 , \tag{6}$$

where the negative sign indicates that the particle lags the flow, and u(o) denotes the centerline fluid velocity corresponding to a parabolic distribution; furthermore, it was assumed that $\omega' = G(r)/2$, the value which (as will be seen later) corresponds to Stokes flow, and thus becomes from (2) and (3)

$$\omega' = \frac{u(o)r}{R^2} . \tag{7}$$

Substitution of (6) and (7) into (5) yields

$$U = -\frac{1}{9} u(o) \, \Re \left(\frac{b}{R}\right)^4 \frac{r}{R} , \tag{8}$$

where $\Re = u(o)R \, \rho/\eta_o$ is the tube Reynolds number.

The radial velocity given by (8) is always directed inwards. Rubinow and Keller[23)] multiplied the r.h.s. of (8) by the factor $(r - r^*)/r^*$, where r^* denotes the equilibrium radial position of the sphere, to make (8) agree, at least qualitatively, with the experimental observations[11,12)].

Saffman[20)] also considered the motion of a small sphere in an unbounded parabolic velocity profile in presence of inertial effects and, by iterating the Navier-Stokes equations, calculated the sideways velocity

$$U = -0.86\, u(o)\, \Re \left(\frac{b}{R}\right)^4 \frac{r}{R}\, , \tag{9}$$

which, except for the numerical coefficient, is similar to (8).

In a more rigorous treatment using singular perturbation methods, Saffman[26] analysed the motion of a rigid spherical particle relative to an unbounded, uniform, simple shear flow, the translational velocity of the sphere lying parallel to the streamlines of the undisturbed flow. Three independent particle Reynolds numbers arise from the equations of motion:

Slip:

$$\Re_p = \frac{2bV\rho}{\eta_o}\, , \tag{10}$$

Shear:

$$\Re_G = \frac{4b^2 G\rho}{\eta_o}\, , \tag{11}$$

rotation:

$$\Re_\omega = \frac{4b^2|\omega'|\rho}{\eta_o}\, . \tag{12}$$

Only the case in which

$$\Re_p,\ \Re_G\ \Re_\omega << 1 \text{ and } \Re_G,\ \Re_\omega >> \Re_p^{\ 2}\, , \tag{13}$$

was considered, and the lift force F_L and the torque M around the sphere center were calculated to be

$$F_L = 81.2\ \eta_o b^2 V \left(\frac{G\rho}{\eta_o}\right)^{1/2} + O\left(\frac{\eta_o}{\rho}\right)^{-1/2}\, , \tag{14}$$

and

$$M = -\ 8\ \pi\eta_o b^3 \left(\frac{G}{2} - \omega'\right) + O(\eta_o)\ . \tag{15}$$

The lateral migration velocity, when the Stokes hydrodynamic force $-\ 6\pi\eta_o bU$ is added to (14) and the total lift force is set equal to zero, is

$$U = \frac{81.2}{6\pi}\ Vb\ \left(\frac{G\rho}{\eta_o}\right)^{1/2}\, , \tag{16}$$

which is an order of magnitude greater than (5).

Unlike the Rubinow-Keller theory[23] which depends critically on particle rotation, Saffman's[26] "slip-shear" lift force is independent of the angular velocity of the sphere ie. the particle would migrate even if it was prevented from rotating, in accord with the experimental observations[27,28]. While Saffman's analysis demonstrated the lack of universal applicability of Rubinow-Keller theory it could be argued that when $\mathfrak{R}_p >> \mathfrak{R}_G$ the lift force due to slip-spin might have dominated or been comparable with that due to slip-shear. However, Brenner[22] has pointed out that with neutrally buoyant sphere of small b/R ratio where the axial slip velocity is given by (6) and where it can be shown that

$$\frac{\mathfrak{R}_G}{\mathfrak{R}_p^2} = 0(\frac{1}{Re_p}) \ , \tag{17}$$

ie. as $\mathfrak{R}_p \longrightarrow 0$ the ratio becomes infinite, Saffman's conditions (equation (13)) are always met and the Rubinow-Keller theory is inapplicable.

(b) Bounded flows

While each one of the above theories is able to predict qualitatively certain of the observed features of the radial migration in a tube, especially in non-neutrally buoyant systems, they are unable to account for the two-way migration of neutrally buoyant particles. The experimental results indicate that the presence of the walls are of fundamental importance, and as has been pointed out[8,12,22], no theory which does not explicitly consider inertial and wall effects may be expected to explain the tubular pinch effect.

Repetti and Leonard[29] proposed a semi-empirical model based on (5); V was not evaluated from (6) but from an empirical relation based on velocity data of Goldsmith and Mason[5]. Their final equation contains an adjustable parameter defined as the distance past the sphere surface within which the sphere influences the surrounding fluid. By adjusting the value of the parameter they obtained a reversal in the sign of F_L around r*. However, Brenner[22] has pointed out on theoretical grounds that their equation cannot be correct; it ignores the fact that for small b/R, V is correctly given by (6) and assumes that the Rubinow-Keller theory is applicable to Poiseuille flow.

A full treatment of the problem of a freely rotating and translating parallel to the tube axis rigid sphere in a tube of finite radius, has been attempted by Cox and Brenner[30]. The first order solution of the Navier-Stokes equation was obtained and the lateral force required to maintain the sphere at a fixed r was computed and converted into an equivalent radial migration velocity by application of Stoke's law. The only restriction imposed is that the sphere is not too close to the wall, i.e. $b/(R - r) << 1$. Five cases were considered, ranging from the neutrally buoyant particle to that of the sphere settling in stagnant liquid. For the neutrally buoyant case

$$U = \frac{1}{2}\, u(o)\, \Re \left(\frac{b}{R}\right)^3 f\left(\frac{r}{R}\right) , \tag{18}$$

where f(r/R) is a function of the radial position of particle center. Equation (18) has the same form with the empirical equation used by Segré and Silberberg[12] to correlate their data i.e.

$$\frac{dr}{dt} = U = 0.17\, u(o) \Re \left(\frac{b}{R}\right)^{2.84} \frac{r}{R} \left(1 - \frac{r}{r*}\right) . \tag{19A}$$

Integrating (19A) yields:

$$\log_e \frac{r(r_o - r*)}{r_o(r - r*)} = 0.17\, \frac{\eta_o}{\rho R^2}\, \Re^2 \left(\frac{b}{R}\right)^{2.84} . t , \tag{19B}$$

where r_o is the initial radial position of the sphere.

3. Rotation and spin of rigid particles

Jeffery[9] studied theoretically the rotary motion and axial spin of a single neutrally buoyant rigid spheroid with centre at the origin of an infinite field of Couette flow defined by (1). In terms of spherical polar coordinates θ and ϕ with the Z axis as polar axis (Fig. 1a), the angular velocities of the axis of revolution predicted by the theory, when inertial effects are absent and there is no slip at the particle-liquid interface, are[9]

$$\omega' = \frac{d\phi}{dt} = \frac{G}{(r_e^2 + 1)} (r_e^2 \cos^2\phi + \sin^2\phi) \ , \tag{20}$$

and

$$\frac{d\theta}{dt} = \frac{G(r_e^2 - 1)}{4(r_e^2 + 1)} \sin 2\phi \sin 2\theta \ , \tag{21}$$

where r_e is the equivalent ellipsoidal axis ratio[1]. The spheroid undergoes spin around its axis of revolution given by

$$\omega'_s = \frac{G}{2} \cos \theta \ . \tag{22}$$

Integration of (20) and (21) yields

$$C^2 r_e^2 \cot^2\theta = 1 + (r_e^2 - 1) \cos^2\phi \ , \tag{23}$$

and

$$\tan \phi = r_e \tan \left(\frac{2\pi t}{T}\right) \ , \tag{24}$$

where T is the period of rotation of spheroid given by

$$T = \frac{2\pi}{G} \left(r_e + \frac{1}{r_e}\right) \ , \tag{25}$$

and C is the orbit constant[1].

For the simple case of a sphere ($r_e = 1$), the particle rotates at a constant angular velocity which from (20) is found to be

$$\omega' = \frac{G}{2} \ , \tag{26}$$

and with a period of rotation given by (25) which for $r_e = 1$ reduces to

$$T = \frac{4\pi}{G} \ . \tag{27}$$

It should be noted that (26) is employed to derive (7).

For prolate spheroids (and rods) $r_e > 1$, and (20) indicates that ω' is greatest when the axis of revolution is perpendicular to the direction of fluid flow ($\phi = 0$) and least when it is aligned with the flow ($\phi = \pi/2$); the converse is true when $r_e < 1$, i.e. for oblate spheroids (and discs).

It follows from (23) that, at a given C, the ends of axis of revolution describe a spherical ellipse with major axis θ_1 and minor axis θ_2 (Fig. 1a) where θ_1 and θ_2 are defined by (23) setting $\phi = \pi/2$ and $\phi = 0$ respectively, yielding:

$$\tan \theta_1 = Cr_e \text{ , and } \tan \theta_2 = C \text{ .} \tag{28}$$

4. <u>Variation of orbit constant of rigid spheroids</u>

Saffman[20] studied the effect of inertia of the fluid on the orbit constant of a spheroid in Couette flow, and calculated the rate of change of C to be

$$\frac{1}{C} \cdot \frac{dC}{dt} = A\,\frac{G^2 a(a-b)\rho}{\eta_o} \tag{29}$$

where 2a and 2b are the length of axis of revolution and the equatorial diameter respectively and $A = -0.24$. It follows from (29) that the axis of revolution of an oblate spheroid tends to set itself parallel to the Z-axis ($C = 0$), and that of an oblate spheroid in the XY plane ($C = \infty$). These are the orbits in which the particles make the minimum contribution to the suspension viscosity[9].

In Couette flow, where G is constant, (29) may be integrated to give

$$\log_e \frac{C}{C_o} = A\,\frac{G^2 a(a-b)\rho t}{\eta_o} \tag{30}$$

where C_o is the initial value.

In Poiseuille flow, where G varies with r, substitution of (2) into (29) and integration yields

$$\log_e \frac{C}{C_o} = A\,\frac{k^2 a(a-b)\rho}{\eta_o}\int_0^t r^2 dt \text{ .} \tag{31}$$

EXPERIMENTAL PART

1. Methods

(a) Poiseuille flow

The techniques of observing particles flowing in vertically mounted glass tubes have been described previously[5,6].

The particle translational velocities were determined by matching the speed of the viewing microscope to that of the particle and computing the distance along the tube axis from the readings of a revolution counter. At high flow rates, the speed of a particle was measured by timing it between the cross hairs of two telescopes of a cathetometer mounted 37 cm. apart. The distance of the particle center from the tube wall was measured by means of a calibrated micrometer eyepiece. For suspending liquids of refractive index different from that of glass a correction was applied to give the true radial distance[31].

Liquid velocity profiles were determined by means of a calibrated Hycam 16 mm. high speed camera (Red Lake Laboratories Inc., Sunnyvale, California) operating at about 1,000 frames per sec. The films were subsequently analysed by projecting them onto a drafting table.

The rotations as well as the variations in the orbit constant of cylindrical particles were studied by photographing them with the aid of a Paillard 16 mm. Bolex camera. When the particles are observed along the Z-axis, the projected length $a'(\phi)$ of the semi-axis of revolution in the XY plane at ϕ becomes

$$a'(\phi) = a \sin \theta \ . \tag{32}$$

The projection of the equatorial plane is the ellipse of axis ratio

$$s(\phi) = \frac{b'(\phi)}{b} = \cos \theta \ , \tag{33}$$

where $2b'(\phi)$ is projected length of equatorial diameter at ϕ. The orbit constant was calculated from (28), (32) and (33) by measuring $s(\phi)$ for discs and $a'(\phi)$ for rods at $\phi = 0$.

Liquid drops were formed by using a stainless-steel hypodermic needle connected to a 0.1 ml. capacity microburette. The needle tip was placed under the suspending liquid surface near the upper end of the tube, and the drops released during flow in the downward direction.

(b) Couette flow

Direct observations of particles along the Z-axis in Couette flow were made in the coaxial cylinder device ($R_1 = 13.354$ cm. and $R_2 = 15.234$ cm.) described elsewhere[3]. The photographic techniques for measuring the rotations and orbit constant were similar to those used in tube flow.

2. Materials

The properties of the suspensions used are listed in Table I. In all the experiments the densities of particles and medium were closely matched ($\Delta\rho \leq \pm 0.01$ g.cm.$^{-3}$) except in System 10 ($\Delta\rho = 0.13$ g.cm.$^{-3}$) where sedimentation was deliberately sought, and System 11 where the aluminum tracer particles were so small that sedimentation was negligible.

All experiments were performed in a thermostated room maintained at 22 ± 0.5°C.

RESULTS AND DISCUSSION

1. Rotation and spin of rigid particles

(a) Spheres

The measured angular velocities of spheres in Couette flow (Table II) are in good agreement with (26) although in System 1 there is some scatter in $\omega'_{calc}/\omega'_{meas}$ about the mean value of unity pressumably because of the low η_o and the resulting high values of $\mathfrak{R}_\omega$. The agreement with (26) and (27) over a wide range of $\Re_\omega$ is further illustrated in Figure 2.

Equation (26) was derived for the Stokes flow regime; when small inertial effect are considered, Saffman's analysis[26] indicates that, to the terms of lowest order, ω' is still given by (26), as may be seen from (15) by setting $M = 0$.

(b) Rods and discs

Axial spin: The observed axial spins of discs for the special case of $C = 0$ are given in Table III and indicate good agreement with the values calculated from (22) by setting $\theta = 0$.

Rotation: The variation of ϕ with time for a rigid rod and disc in Poiseuille flow is illustrated in Figure 3a, and follows (24) provided that r_e instead of the actual axis ratio $r_p = a/b$ is used. The values of r_e calculated from (25) using the measured TG[1], agreed to better than 5% with those obtained at low $\Re_p$[4]. Figure 3a also indicates that, as predicted by (20), $d\phi/dt$ is maximum at $\phi = \pi/2$ for the disc ($r_e < 1$) and at $\phi = 0$ for the rod ($r_e > 1$), and is independent of C (and θ).

A more sensitive test of the theory is to plot $\tan \phi$ against $\tan 2\pi t/T$; this was done for rigid cylinders both in Poiseuille (Fig. 3b) and Couette (Fig. 4a) flows and as may be seen the agreement was excellent.

Variation of θ: The variation of θ with ϕ during a complete rotation is shown in Fig. 4b where the results have been plotted in linearized form as suggested by (23) using the experimental values of C and r_e; the agreement with theory is very good. In a number of cases, expecially with discs, the variation of θ with ϕ was not identical in two successive half-orbits. This was also observed at low $\Re_p$ and was attributed to a lack of perfect symmetry (e.g. variation in a) of the particles[5]; the explanation appears to be the same at high $\Re_p$, since the deviations failed to show any correlation with $\Re_p$.

2. Drift in orbits of rods and discs

When a particle was observed over many rotations a steady drift in the orbit constant was observed, until it attained the limiting value $C = \infty$ for rods and $C = 0$ for discs, after which there was no further change confirming the preliminary observations[15]. Contrary to (29), the particles attained the asymptotic orbit values for which the energy dissipation in Couette flow is greatest[9]. At these orientations, a disc possesses a steady spin about its axis of revolution which is oriented along the Z-axis; on the other hand, a rod rotates periodically without spin of axis of revolution lying in the XY plane. This is illustrated schematically in Figure 5a.

(a) Couette flow

As predicted by (30) log (C/C_o) varied linearly with time (Fig. 5b) when $C/C_o < 10$ for rods and $C/C_o > 0.1$ for discs, after which deviations from linearity became apparent. It should be noted, however, that the extreme orbit constants near $C = 0$ for discs and $C = \infty$ for rods are difficult to measure accurately. The rate of change of C increased with G and particle size (Fig. 5b) in accordance with (29); as may be seen from Fig. 6a, however, the rate was not proportional to G^2. At low G, C remained constant (Fig. 5b curve 4) in agreement with earlier results in the creeping flow regime[4,10]. As G increased there was an abrupt increase in the rate of orbit drift (Fig. 6a).

(b) Poiseuille flow

In Poiseuille flow there was also simultaneous radial migration, considered later, to the equilibrium position r* as the long axes of the rods and the faces of the discs became oriented in planes passing through the axis of the tube (Fig. 5a). The rate of change of C increased with increasing r, and was zero for particles near $r = 0$ as shown for a rod in Table IV. As may also be seen from Table IV a particle initially located at r* did not migrate whereas C changed towards its asymptotic value. Thus while the drift in both

C and r are related effects due to fluid inertia, radial migration is not a necessary condition for the variation in C; this is to be expected from the results in Couette flow.

(c) Orbit drift parameter A

Values of A calculated from the experimental data using (30) for Couette flow and (31) in Poiseuille flow are listed in Table V. Because of radial migration in tube flow the integral in the r.h.s. of (31) was evaluated graphically from the experimental data by plotting r^2 against t and measuring the area under the curve. As may be seen from Table V, A was smaller in tube than in Couette flow possibly because of the closer proximity of the wall; it also depended on G and r_p being smaller with rods than discs (Table V). It is clear that A is not constant as predicted by (29) which was, however, derived for spheroids of small r_p. Saffman[20] has pointed out, that, when the aspect ratio is large ($r_p << 1$ or $r_p >> 1$), it is probable that

$$\frac{1}{C} \cdot \frac{dC}{dt} = A_1 b^2 G^2 (\log r_p)^2 \frac{\rho}{\eta_o}, \tag{34}$$

where A_1 is a constant. A comparison between (29) and (34) shows that for rods ($r_p > 1$) $|A_1| > |A|$, while for discs ($r_p < 1$) $|A_1| < |A|$. Values of $|A_1|$ calculated from (34) for Couette flow are plotted in Fig. 6b as a function of G. As may be seen, (34) yielded $|A_1|$ values of the same order of magnitude for both rods and discs, although $|A_1|$ is not constant but increases with G.

3. Radial migration in Poiseuille flow

(a) Neutrally buoyant systems

Rigid spheres. As previously found[11,12,14,15,27], rigid spheres initially placed near the wall migrated inwards, while spheres situated close to the tube axis migrated outwards until, independently of the direction of migration, they reached an equilibrium radial position r* between the tube axis and tube wall (Fig. 7a). At high values of Q and b/R, the particles sometimes overshot r*, after which the migration oscillated until the sphere settled at r* where it remained (Fig. 7b curve 2); there was no tangential movement, i.e. ϕ remained constant as would be expected from the axi-symmetric flow field. Brenner[22)] states that Denson[34)] observed an oscillatory motion of the particles across the equilibrium position at $\Re_p = 15$ to 120.

The rate of migration increased with increasing Q. At a given Q and particle size, and when $b/R \leq 0.4$, the migration velocity did not increase monotonically with increasing the radial displacement from the equilibrium position, but showed a maximum at some intermediate value of r/R; (Fig. 7a Fig. 7b curves 1,2); when $b/R > 0.4$ this was not detectable as may be seen from Fig. 7b. The migration rate also increased with increasing particle size when $b/R < 0.4$, but when $b/R > 0.4$ the rate decreased (Fig. 7b) possibly because of the influence of the other wall of the tube.

As shown in Fig. 8a the translational velocities of the spheres u'(r) were identical for the upward and downward flow but lagged behind the undisturbed fluid velocity u(r) at all radial positions; u(r) at the flow rates used was parabolic and thus followed (3).

The equilibrium radial position r* depended on particle size, decreasing as b/R increased (Figs. 7b and 8b). The values of r*/R found were somewhat lower than those reported in the literature[12,14,27)] perhaps because the present experiments were performed at much lower $\Re$ (≤ 1.1). Scrutiny of the data of Segré and Silberberg[11,12)] with spheres and of Müller[16)] with discs, suggests that r* shifts closer to the wall as the $\Re$ increases. This does not contradict (18) which implies that r*/R is independent of $\Re$ and b/R because (18) applies only when both $\Re$ and b/R are small.

It was not possible to verify (16) because the condition $\Re_G / \Re_p^2 >> 1$ was not fulfilled in these experiments. Saffman's analysis requires high Q and small b/R so that $G^2\eta_o/V^2\rho >> 1$, and under the most favorable conditions of the present investigation (using the measured V) $\mathfrak{R}_G/\mathfrak{R}_p^2$ was of the order of 10^2; hence, the calculated migration rates were about 10^3 greater than those actually observed. Also a direct test of (5) was not possible because ω' was not measured simultaneously with V and U, and use of (7) is not justified for the range of b/R employed.

The data for b/R = 0.25 to 0.305, in which measurement of U were most extensive, were correlated with an equation similar to (19B), i.e.

$$\log \frac{r(r_o - r^*)}{r_o(r - r^*)} = 0.02\, \frac{\eta_o}{\rho R^2}\, \mathfrak{R}^2 \left(\frac{b}{R}\right)^2 \,.\, t \qquad (35)$$

as illustrated in Fig. 8c. It should be noted that (8), after multiplication of the r.h.s. by $(r - r^*)/r^*$ and integration, yields an equation similar to (19B) but with b/R in the fourth power. It seems that the numerical value of the exponent in b/R depends on particle size. With no wall effects[20,23] i.e. as $b/R \rightarrow 0$ its value is 4, whereas with finite but small b/R, both theory[30] and experimental results[11,12] (for b/R = 0.029 to 0.152) yielded values of approximately 3; in the present work, in which b/R was still larger (0.25 - 0.305), the exponent was 2.

<u>Rods and Discs</u>. Rigid cylinders (Fig. 9a and 9b), like spheres, drifted radially either inwards or outwards to the equilibrium position, their orbit constants simultaneously drifting as described earlier.

<u>Deformable particles</u>. In contrast to rigid particles, liquid drops and elastomer filaments, which were deformed by the shear field, migrated to the tube axis (Table VI) as they did at low $\mathfrak{R}_p$[5]. The radial position of the fibres was measured by photographing them. Since they were deformed and bent while flowing in the tube, an arithmetic average radial distance was determined from the photographs; the fibres were divided into

equal segments along the length (about 0.05 cm.) and the distance of each segment from the tube axis was measured. The inward migration to the tube axis of an elastomer fibre is illustrated in Fig. 10 by tracings of photographs taken at various time intervals.

The rate of migration of fluid drops decreased with increasing the viscosity ratio; at p = 50 liquid drops behaved as rigid spheres i.e. there was no migration at low $\Re_p$, and migration to $r^*/R = 0.5$ appr. at high $\Re_p$. For a given system the rate of migration increased with increasing b/R, Q, and radial displacement from the equilibrium position (Table VI) as at low $\Re_p$[5].

(b) Systems with density difference

A few experiments were performed with System 10 in which the spheres were denser than the suspending fluid yielding sedimentation velocities V_b from 0.2 to 0.25 cm. sec.$^{-1}$. The results are tabulated in Table VII. With the flow upwards spheres migrated towards the tube axis at all radial positions, in accordance with previous observations[14,27,29], due to the large value of the slip velocity and the influence of the wall. When the flow was in the downward direction, spheres behaved as in the neutrally buoyant Systems i.e. they possessed a two-way migration depending on their initial r/R, confirming earlier observations[27,29]. Because of the limited length of the tube, r* could not be measured; Oliver's[27] experiments and Brenner's[22] analysis indicate that r* should be closer to the wall than in a corresponding neutrally buoyant system.

It is interesting to note that in the case of downward flow and when the particles were close to the wall they migrated inwards although $u'(r) > u(r)$ (Table VII). It is as if the wall has a repulsive effect on the spheres, an effect which is also present when a sphere sediments near the tube wall in a quiescent liquid of low viscosity. The latter arises from inertial effects which result to a source-like behaviour of the flow at distant points from the sphere not lying within the wake[22]. This was observed by placing a sphere ($b/R \sim 0.4$) at the wall of a vertical tube containing a stagnant liquid of low viscosity (0.13p); the sphere quickly migrated to the tube axis. When the viscosity of the liquid was increased to about 25p without changing the density the sphere rolled down the wall without migrating.

It may be concluded, therefore, that when the sedimentation velocity is in the direction of flow, the particles reach equilibrium at the radial positions at which the inward directed force arising from the proximity of the wall balances the outward directed lift force.

4. <u>Suspensions of rigid spheres in Poiseuille flow</u>

(a) <u>Particle-free layer near the wall</u>

When a suspension of rigid spheres was allowed to flow in the tube a particle-free zone developed near the wall. The formation of this "plasmatic" layer was also observed in suspensions of spheres undergoing oscillatory flow[35] and in pulp fibre suspensions[36] although in the latter case it was probably a deformation rather than an inertial effect.

The thickness δ of the particle-free layer was measured by photographing the flowing suspensions using flash illumination to stop the motion. Since particle-particle interactions, caused δ to vary from point to point along the tube the arithmetic mean $\bar{\delta}$ was calculated from a number of photographs taken simultaneously along the tube.

Fig. 11a shows the gradual increase in $\bar{\delta}$ with time for suspensions of various volume fractions c. At a given Q the time required for $\bar{\delta}$ to reach its equilibrium thickness $\bar{\delta}_\infty$ decreases with increasing c (Fig. 11a).

The asymptotic values of $\bar{\delta}$ are shown plotted in dimensionless form against c in Fig. 11b and as may be seen $\bar{\delta}_\infty/R$ (and $\bar{\delta}_\infty/b$) decreases as c increases. The distribution of particles in the core of the suspension was not measured but, at least in the lower range of c, a peak in the concentration profile around r* should be expected[11,12].

The development of particle-free layer near the wall changed the velocity distribution of the suspension in the tube and caused a drop in the apparent viscosity coefficient η_a. This is illustrated in Fig. 12 and Table VIII.

(b) Velocity profile

To study the modification in the velocity profile, transparent suspensions of polyvinyl acetate spheres (System 5) of various c were used and the velocity distribution measured as described elsewhere[6]. The suspensions were introduced at low Q in the tube and the initial velocity profile determined; Q was then increased and the suspensions were recycled in the tube until $\bar{\delta} = \bar{\delta}_\infty$ after which the initial Q was restored and the velocity profile was again measured. As may be seen from Fig. 12 and Table VIII, the suspensions initially possessing a parabolic velocity distribution developed a central core of effectively zero G whose radius r_c increased with increasing c. At concentrations at which the velocity profile was initially blunted, r_c was further increased by the formation of the plasmatic layer. Partial plug flow in the tube was also observed (Fig. 12) when the suspensions were subjected to an oscillatory flow of high frequency[35] to increase the $\Re_p$.

A similar blunting in the velocity profiles in suspensions of high c undergoing Poiseuille flow was reported at low $\Re_p$ and attributed to a wall effect[6]; at high $\Re_p$ the blunting is due to the radial migration which gives rise to a two-phase flow in the tube with a low viscosity liquid ($= \eta_o$) near the wall and a high viscosity near the axis.

(c) Pressure drop

Because of lubricating action of the plasmatic layer the pressure drop ΔP over a given length L (= 65.1 cm.) of the tube (measured by means of a differential pressure transducer[6]) decreased with time as the layer was developed (Fig. 12, insert) until $\bar{\delta} = \bar{\delta}_{\infty}$ whereafter it remained constant. Similar observations in dilute suspension of spheres were reported by Segré and Silberberg[37].

If $\bar{\delta}_{\infty}/R$ and c for a suspension are known the apparent viscosity η_a may be defined by

$$\eta_a = \frac{\pi R^4 \Delta P}{8QL} , \tag{36}$$

from which η_a may be calculated assuming an annulus of suspending phase thickness $\bar{\delta}_{\infty}$ surrounding an inner core of suspension of uniform concentration c' and viscosity η_c[38-40]. A material balance per unit length of the tube yields

$$c = \gamma^2 c' , \tag{37}$$

where $\gamma = 1 - \bar{\delta}_{\infty}/R$. Mooney's equation[41], recently confirmed by Brodnyan[42] for latexes up to c = 0.4, may be used to evaluate η_c:

$$\eta_c = \eta_o \exp\left(\frac{2.5c'}{1 - 1.57c'}\right) . \tag{38}$$

Neglecting for the time being the effect of the wall the apparent viscosity is given by[40]

$$\eta_a' = \frac{\eta_o}{1 - \gamma^4(1 - \eta_o/\eta_c)} . \tag{39}$$

Combining (36) and (39) yields the pressure drop

$$\frac{\Delta P'}{L} = \frac{8Q\eta_o}{\pi R^4\left[1 - \gamma^4(1 - \eta_o/\eta_c)\right]} . \tag{40}$$

A correction should now be applied to (39) and (40) to account for the hydrodynamic interaction between particles and the wall. If δ_v denotes the thickness of Vand's[38] equivalent plasma layer it can be readily shown[38,40] that η_a (corresponding to (36)) is given by

$$\gamma_v{}^4 = \frac{1 - \eta_o/\eta_a}{1 - \eta_o/\eta_a{}'} \tag{42}$$

where $\gamma_v = 1 - \delta_v/R$, and $\delta_v = 0.7b$ for spheres[38,40,43]. Substitution of (42) into (37) and (40) yields

$$\eta_a = \frac{\eta_o}{1 - (\gamma\gamma_v)^4(1 - \eta_o/\eta_c)}, \tag{43}$$

and

$$\frac{\Delta P}{L} = \frac{8Q\eta_o}{\pi R^4\left[1 - (\gamma\gamma_v)^4(1 - \eta_o/\eta_c)\right]} \, . \tag{44}$$

Comparison between the measured and calculated apparent viscosities and pressure drops for the two suspensions of Fig. 12 (insert) is made in Table IX. As expected $\eta_a{}'$ and $\Delta P'/L$ (i.e. with no correction for the wall) were greater than the measured values. After correcting for the wall, (Eqs. (43) and (44)) the measured and calculated η_a and $\Delta P/L$ were in excellent agreement; this may be fortuitous since the hydrodynamic interaction effect implicit in δ_v may be over-compensated by the existence of the real plasma layer $\bar{\delta}_\infty$.

CONCLUDING REMARKS

The radial migration at high $\Re_p$ is undoubtedly due to inertial effects since no radial (lift) force can arise under comparable conditions in the Stokes flow regime[20,21]. In sedimenting systems the experimental data appear to be in qualitative agreement with several theoretical interpretations[22,23,26] in that the direction of migration depends on the sign of the slip velocity. However, in neutrally buoyant systems the theoretical treatments of Rubinow and Keller[23] and Saffman[20,26] cannot be expected to explain the two-way migration observed in Poiseuille flow because both neglect the variable G and the presence of boundary walls. On the other hand, the theory of Cox and Brenner[30], which takes into account the variation in G and the finite dimensions of the particle, is incomplete, and quantitative comparison with the data cannot be made. Qualitatively, however, the present work shows that for the narrow range of $\Re$ investigated, U varies proportionaly to $\Re$ as predicted by (18); on the other hand, U is proportional to the second rather to the third power in b/R, perhaps because of the large ratio of b/R.

Two interesting consequences of the development of $\bar{\delta}_{\infty}$ are the reduction in ΔP and the change in the velocity profile in suspensions flowing through tubes at high $\Re_p$. These may be of interest in the transport of suspensions through tubes and pipes, since the power expenditure is reduced, and particle rotation is inhibited by the development of plug flow; the latter effect may reduce mechanical attrition and aggregation of the particles as they flow, desirable in some systems[35,36].

The change in the orbit distribution of rods and discs may be important in making viscosity measurements in capillary tubes. The drift towards orbits of maximum energy dissipation will lead to an increase in the apparent viscosity of a suspension of cylindrical particles; this increase may, however, be overshadowed by a decrease resulting from migration from the wall. The two simultaneous effects may produce apparent non-newtonian effect similar to that reported for spheres[37] whose magnitude depends on the relative rates of radial migration and change in orbit constants. This possibility deserves experimental study.

LIST OF SYMBOLS

a; $a'(\phi)$	=	semiaxis of revolution of spheroid; XY projection at ϕ
A, A_1	=	orbit drift parameters
b; $b'(\phi)$	=	radius of the sphere and undistorted drop, and semiaxis of equatorial diameter of spheroid; XY projection at ϕ
c	=	volume fraction of suspended phase
C; C_o	=	orbit constant; initial value
F_L	=	lift force
G; $G(r)$	=	velocity gradient; at r in Poiseuille flow
k	=	$4Q/\pi R^4$
L	=	tube length
M	=	torque about the sphere center
p	=	viscosity ratio of particle to medium
ΔP; $\Delta P'$	=	pressure drop; predicted value uncorrected for Vand's wall effect
Q	=	volumetric flow rate through tube
r; r_o, r^*	=	radial distance from the tube axis; initial and equilibrium radial position of particle
r_c	=	radius of the core of zero velocity gradient (Table VIII)
r_e	=	equivalent ellipsoidal axis ratio of rigid cylinders
r_p	=	a/b
R	=	tube radius
$\mathfrak{R}$, $\mathfrak{R}_G$	=	tube Reynolds number; shear Reynolds number
$\mathfrak{R}_p$, $\mathfrak{R}_\omega$	=	particle Reynolds numbers based on slip and angular velocity respectively
R_1, R_2	=	radius of inner and outer cylinder walls of Couette apparatus
$s(\phi)$	=	$b'(\phi)/b$

t; T	=	time; period of rotation through $\phi = 2\pi$
u, v, w	=	components of fluid velocity along the X, Y, Z axes
u(r), u(o)	=	fluid translational velocities at r and at r = o
u'(r), u'(o)	=	particle translational velocities at r and tube axis
U	=	migration velocity of particles (= dr/dt in Poiseuille flow)
V	=	relative particle-fluid velocity
V_b	=	sedimentation velocity
x, y, z	=	Cartesian coordinates
r, Ψ, x	=	cylindrical poral coordinates
Υ; Υ_v	=	$1 - \bar{\delta}_{\infty}/R$; $1 - \delta_v/R$
δ, δ_{∞}; $\bar{\delta}$, $\bar{\delta}_{\infty}$	=	thickness of particle-free layer near the wall and its equilibrium value; arithmetic averages
δ_v	=	thickness of Vand's pseudo-layer near the wall
η, η_a; η_o, η_c	=	true viscosity and apparent viscosity of the suspension; medium viscosity and viscosity of the core
θ	=	angle of axis of revolution with Z-axis
ρ; $\Delta\rho$	=	density of suspending liquid; density difference of drop and medium
ϕ	=	aximuthal angle of axis of revolution
ω'	=	angular velocity $\dot{\phi}$ of rigid particles
ω'_s	=	axial spin of rigid cylinders

REFERENCES

1. TREVELYAN, B.J. and MASON, S.G. J. Colloid Sci. 6, 354 (1951).
2. MANLEY, R. ST. J. and MASON, S.G. J. Colloid Sci. 7, 354 (1952).
3. BARTOK, W. and MASON, S.G. J. Colloid Sci. 12, 243 (1957).
4. GOLDSMITH, H.L. and MASON, S.G. J. Fluid Mech. 12, 88 (1962).
5. GOLDSMITH, H.L. and MASON, S.G. J. Colloid Science 17, 448 (1962).
6. This Thesis Part II.
7. CHAFFEY, C.E., BRENNER, H. and MASON, S.G. Rheol.Acta 4, 56 (1965).
8. CHAFFEY, C.E., BRENNER, H. and MASON, S.G. Rheol.Acta 4, 64 (1965).
9. JEFFERY, G.B. Proc. Roy. Soc. (London) A 102, 161 (1922).
10. ANCZUROWSKI, E. and MASON, S.G. Forthcoming publication.
11. SEGRE, G. and SILBERBERG, A. Nature 189, 209 (1961).
12. SEGRE, G. and SILBERBERG, A. J. Fluid Mech. 14, 136 (1962).
13. SEGRE, G. 4th Int. Cong. Rheology, Part 4, Ed. by A.L. Copley p.103, Interscience, New York (1965).
14. JEFFREY, R.C. Ph.D. Thesis Cambridge University (1964).
15. KARNIS, A., GOLDSMITH, H.L. and MASON, S.G. Nature 200, 159 (1963).
16. MULLER, A. Abhandlungen zur Mechanic der Flussigkeiten I University of Freiburg Press, Freiburg Switzerland (1936).
17. VEJLENS, G. Acta Path. Microbiol. Scand. Suppl. No. 33 (1938).
18. STARKEY, T.V. Brit. J. Appl. Phys. 7, 52 (1956).
19. STARKEY, T.V., HEWLETT, V.A., ROBERTS, J.H.A. and JAMES, R.E. Brit. J. Appl. Phys. 12, 545 (1961).
20. SAFFMAN, P.G. J. Fluid Mech. 1, 540 (1956)
21. BRETHERTON, F.P. J. Fluid Mech. 14, 284 (1962).
22. BRENNER, H. Advances of Chemical Engineering Volume 6, Academic Press (In Press 1965).
23. RUBINOW, S.I. and KELLER, J.B. J. Fluid Mech. 11, 447 (1961).

24. SIMHA, R. Kolloid Z. 76, 16 (1936)

25. BRENNER, H. and HAPPEL, J. J. Fluid Mech. 4, 195 (1958)

26. SAFFMAN, P.G. J. Fluid Mech. 22, 385 (1965)

27. OLIVER, D.R. Nature 194, 1269 (1962)

28. THEODORE, L. Eng. Sc. D. Dissertation, New York University, New York (1964)

29. REPETTI, R.V. and LEONARD, E.F. Nature 203, 1346 (1964)

30. COX, R.G. and BRENNER, H. Forthcoming Publication

31. GOLDSMITH, H.L. Ph.D. Thesis McGill University, Montreal (1961)

32. BARTOK, W. Ph.D. Thesis McGill University, Montreal (1957)

33. MANLEY, R.ST.J. Ph.D. Thesis McGill University, Montreal (1953)

34. DENSON, C.D. Ph.D. Thesis University of Utah, Salt Lake City (1965)

35. SHIZGAL, B., GOLDSMITH, H.L. and MASON, S.G. Canad. J. Chem. Eng. 43, 97 (1965)

36. FORGACS, O.L, ROBERTSON, A.A. and MASON, S.G. Fundamentals of Papermaking Fibres 447 (1958)

37. SEGRE, G. and SILBERBERG, A. J. Colloid Sci. 18, 312 (1963)

38. VAND, V. J. Phys. Colloid Chem. 52, 277, 300 (1948)

39. THOMAS, H.W. Biorheology 1, 41 (1962)

40. This thesis Appendix III

41. MOONEY, M. J. Colloid Sci. 6, 162 (1951)

42. BRODNYAN, J.G. and KELLEY, E.L. J. Colloid Sci. 20, 7 (1965)

43. HIGGINBOTHAM, G.H., OLIVER, D.R. and WARD, S.G. Brit. J. Appl. Phys. 9, 372 (1958)

TABLE I

Properties of Suspensions. Temp. 22°C

System	medium	ρ g.cm.$^{-3}$	η_o poises	Particles	p a)	range of particle dimensions x 10^3cm.
1	aqueous glycerol	1.05	0.018	polystyrene spheres		b = 62
2	Ucon oil b) 50-HB-260 + tetrabromoethane	1.05	1.2	polystyrene spheres		b = 40 to 71
3		1.05		polystyrene discs		a = 6 to 6.5 b = 22 to 45
4		1.09		aluminum-coated nylon rods		a = 40 to 60 b = 4 to 4.8
5		1.17	1.1	polyvinyl acetate spheres		b = 15 to 29
6		1.06	1.2	elastomer filaments c)		a = 221 to 690 b = 2.8 to 4.6
7	Ucon oil b) 50-HB-55 + tetrabromoethane + benzylalcohol	1.05	0.137	polystyrene spheres		b = 15 to 61
8		1.05		polystyrene discs		a = 6 to 6.5 b = 22 to 45
9		1.08		aluminum-coated nylon rods		a = 40 to 60 b = 4 to 4.8
10		1.05		polyvinyl acetate spheres		b = 36
11		1.05		aluminum particles		< 2
12	Ucon oil 50-HB - 260 + tetra-bromoethane + benzylalcohol	1.049	0.864	polystyrene spheres		b = 11 to 191
13	dibutyl phthalate + Ucon oil LB-1715	1.026	1.26	$Cd(NO_3)_2$ in water	~0	b = 48
14	Ucon oils b) LB-285 + LB-1715	1.259	1.15	glycerol	10	b = 37 to 48
15	Ucon oil b) LB-285 + benzene	0.975	1.0	silicone oil 50_p d)	50	b = 37 to 48

a) Ratio of the suspended to suspending phase viscosity.

b) Polyglycol oils (Union Carbide).

c) E. I. du Pont de Nemours.

d) Dow Corning Silicone oil Series 200.

TABLE II

Angular velocities of rigid spheres in Couette flow

System 1				System 2			
G sec.$^{-1}$.	$\Re_\omega$	ω' rad.sec.$^{-1}$ Eq(26)	Meas.	G sec.$^{-1}$	$\Re_\omega$	ω' rad.sec.$^{-1}$ Eq(26)	Meas.
0.486	0.22	0.243	0.234	3.52	0.033	1.76	1.77
0.680	0.29	0.340	0.322	6.46	0.059	3.23	3.21
1.75	0.82	0.875	0.914	7.70	0.14	3.85	3.83
2.90	1.4	1.45	1.54	8.76	0.16	4.38	4.36
				10.52	0.19	5.26	5.32

Mean $\frac{\text{Calc}}{\text{Meas}} = 1.004$

Mean $\frac{\text{Calc}}{\text{Meas}} = 0.999$

TABLE III

Axial spin of discs at C = 0

Couette flow, System 3			Poiseuille flow, System 8				
G $sec.^{-1}$	ω'_s $rad.sec.^{-1}$ Eq.(22)	Meas.	Q $cm.^3 sec.^{-1}$	R cm.	G $sec.^{-1}$	ω'_s $rad.sec.^{-1}$ Eq.(22)	Meas.
2.58	1.29	1.30	0.356	0.4	5.04	2.52	2.43
3.00	1.50	1.48					

TABLE IV

Drift in orbit constant in Poiseuille flow

$R = 0.2\text{cm.} \quad Q = 0.356 \text{ cm.}^3\text{sec.}^{-1} \quad \Re = 1$

discs, System 3			rods, System 4		
t sec	r/R [a]	C	t sec	r/R [a]	C
0	0.800	∞	0	0.750	0.78
23	0.750	∞	52	0.695	1.2
306	0.560	26	123	0.670	3.6
559	0.550	0.55	356	0.575	∞
709	0.540*	0	-	0.490*	∞
0	0.735	5.0	0	0.485*	0.54
65	0.640	3.3	51	0.495	0.60
133	0.535	0.91	136	0.490	1.3
308	0.530	0	241	0.485	∞
505	0.525	0			
805	0.525*	0	0	0.005	1.8
			67	0	1.9
			182	0.125	1.8
			382	0.230	2.7
			-	0.490*	∞

a) The asterisks indicate the value of r^*/R.

TABLE V

Orbit Drift Rate

Couette flow					Poiseuille flow						
Discs, System 3					Discs						
G sec.$^{-1}$	r_p	$10^3 x \frac{a(a-b)\rho}{\eta_o}$ sec.	$10^3 \frac{\log_e C/C_o}{t}$ sec.$^{-1}$ (a)	A Eq.(30)	System	k cm.$^{-1}$ sec.$^{-1}$	Range of G sec.$^{-1}$ (b)	$10^3 \frac{a(a-b)\rho}{\eta_o}$ sec.	$\int_0^t r^2 dt$ cm.^{2} sec.^{2} (c)	$\log_e C/C_o$	A Eq.(31)
4.35	0.159	− 0.19	− 1.4	0.90							
3.79	0.192	− 0.15	− 0.81	0.86	3	282.9	30.7 − 41.9	− 0.19	0.68	− 0.74	0.16
3.70	0.264	− 0.10	− 0.37	0.62							
4.58	0.264	− 0.10	− 0.66	0.72	8	17.68	4.9 − 5.9	− 0.62	6.23	− 0.88	0.16
4.64	0.264	− 0.10	− 0.66	0.71							
7.0	0.264	− 0.10	− 0.95	0.47							
Rods, System 4					Rods						
5.34	10.03	2.4	0	0							
8.66	10.03	2.4	0.17	0.0022	4	282.9	27.8 (d)	2.1		0.38	0.0039
9.49	10.03	2.4	6.4	0.068	4	282.9	38.2 − 42.7	2.1	1.66	0.66	0.0055
11.6	10.03	2.4	14.6	0.104							

(a) Evaluated from the slopes of $\log_e C/C_o$ vs. t plots (Fig. 5b).

(b) At the initial and final radial positions.

(c) Evaluated by graphical integration.

(d) Initially located at r*.

TABLE VI

Radial migration of deformable particles in Poiseuille flow.

Fluid drops, R = 0.4 cm.							Elastomer filaments (System 6) $Q = 0.356$ cm.^{3}sec.$^{-1}$ R = 0.2 cm.				
System	$10^2 \times Q$ cm.^{3}sec.$^{-1}$	$10^2 \times b$ cm.	$10^3 \times \Re_p$ a)	r/R initial	r/R final	$10^4 \times \frac{dr}{dt}$ cm.sec.$^{-1}$ initial	$10^3 \times b$ cm.	a cm.	r_p	$\bar{r}/R$ b) initial	$\bar{r}/R$ b) final
13	7.1	4.8	0.5	0.250	0	135	2.9	0.54	185	0.460	0.050
13	7.1	4.8	0.5	0.083	0	13	4.6	0.69	150	0.554	0.110
14	7.1	4.8	0.72	0.250	0	22	2.8	0.221	78	0.745	0.050
14	7.1	3.7	0.29	0.290	0	16	2.8	0.221	78	0.568	0.060
15	14.2	4.8	1.3		0.50						
15	14.2	3.7	0.54		0.53						

a) From (6) and (10) using the radius b of the undeformed drop.

b) Average radial position.

TABLE VII

Radial migration of sedimenting rigid spheres

(System 10) in Poiseuille flow

b/R = 0.18 Q = 1.78 X 10^{-2} $cm.^3 sec.^{-1}$ R = 0.2 cm. V_b = 0.20 - 0.25 $cm.sec.^{-1}$

r/R initial	r/R final	t sec	u'(r) $cm.sec.^{-1}$	u(r) $cm.sec.^{-1}$ initial r/R	u(r) $cm.sec.^{-1}$ final r/R	Direction of flow	$10^4 \times \Delta r/t$ [a] $cm.sec.^{-1}$
0.140	0.175	45.2	0.395	0.277	0.275	Downwards	1.6
0.465	0.140	37.7	0.380	0.222	0.278	"	- 17
0.250	0.340	49	-	0.265	0.250	"	3.7
0.080	0.080	120.5	0.102	0.281	0.281	Upwards	0
0.175	0.130	125.6	0.0886	0.275	0.278	"	- 0.72
0.160	0.010	123.4	0.0952	0.276	0.283	"	- 2.4
0.060	0.025	101.7	0.0877	0.282	0.283	"	- 1.1

a) Migration towards the tube axis is negative.

TABLE VIII

<u>Effect of radial migration on the velocity profile in suspensions of spheres undergoing Poiseuille flow.</u>

System 5 $R = 0.2$ cm. $Q = 0.356$ cm.^{3}sec.$^{-1}$ $b = 0.015$ cm. $\Re_p = 0.7 \times 10^{-3}$

c	Initial velocity profile					Final velocity profile				
	r_c/R [a]	$u'(o)/u(o)$ [b]	$u'(r)/u'(o)$ [b]			r_c/R [a]	$u'(o)/u(o)$ [b]	$u'(r)/u'(o)$ [b]		
			r/R = 0.25	r/R = 0.50	r/R = 0.75			r/R = 0.25	r/R = 0.50	r/R = 0.75
0.05	0	1.0	0.94	0.75	0.43	0.12	0.97	0.95	0.79	0.46
0.10	0	1.0	0.94	0.75	0.43	0.24	0.93	1.0	0.83	0.50
0.15	0.20	0.94	0.98	0.82	0.53	0.35	0.84	1.0	0.93	0.61
0.20	0.38	0.84	1.0	0.90	0.64	0.40	0.78	1.0	0.95	0.69

a) r_c is the radius of the core i.e. the region of plug flow in the tube within which the particles move with identical translational velocities and without rotating.

b) $u'(o)$ = particle translational velocity at $r = 0$.

TABLE IX

Comparison of measured and calculated values of apparent viscosity and pressure drop in suspensions of spheres; System 5, $b/R = 0.096$.

c	Q a) $cm^3 sec^{-1}$	$\bar{\delta}_\infty/R$ b)	c' Eq. (37)	η c) poises	η_c poises Eq. (38)	η'_a poises Eq. (39)	$\Delta P'/L$ dyn. cm^{-3} Eq. (40)	η_a poises Calc d)	Meas.	$\Delta P/L$ dyn. cm^{-3} Calc d)	Meas.
0.15	0.142	0.050	0.167	1.80	1.93	1.69	73	1.49	1.45	65	63
0.30	0.071	0.012	0.308	4.24	4.94	4.20	96	3.24	3.5	74	79

a) Volumetric flow rate at which ΔP was measured.

b) From Fig. (11b); for the $c = 0.3$ suspension an extrapolated value was used.

c) The true viscosity of the suspension claculated from (38) using c.

d) From (42), (43) and (44) with $\delta_v = 0.7\ b$.

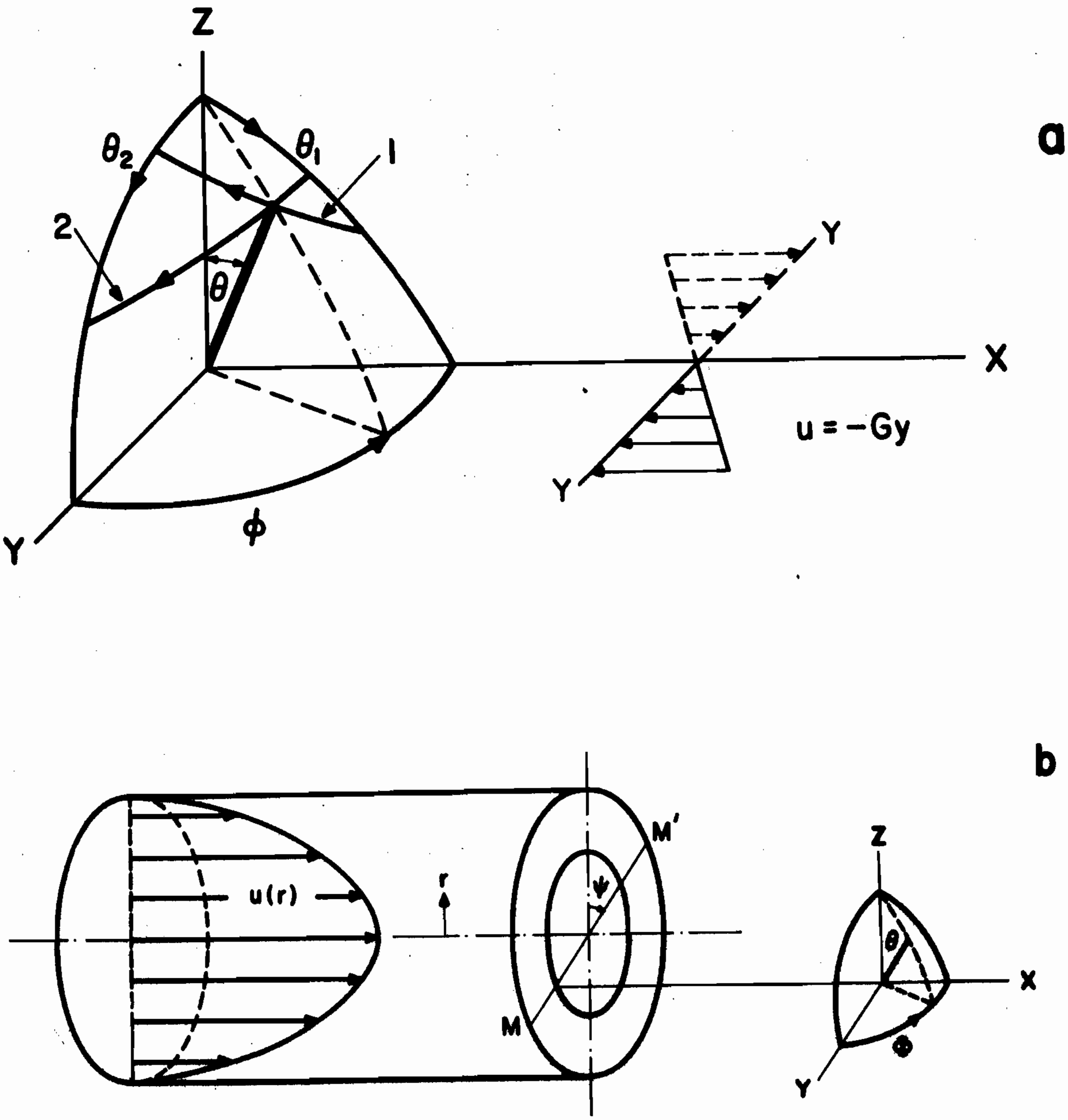

<u>Figure 1</u> (a) Spherical polar coordinate system describing the orbits of cylindrical particles in Couette flow. A spherical elliptical orbit of the axis of revolution of a rod ($r_e > 1$) and a disc ($r_e < 1$) are shown by curves 1 and 2 respectively.

(b) Cylindrical polar coordinates r, ψ, x in Poiseuille flow; (right) Cartesian coordinate system constructed at x = 0 and $\psi = -90°$.

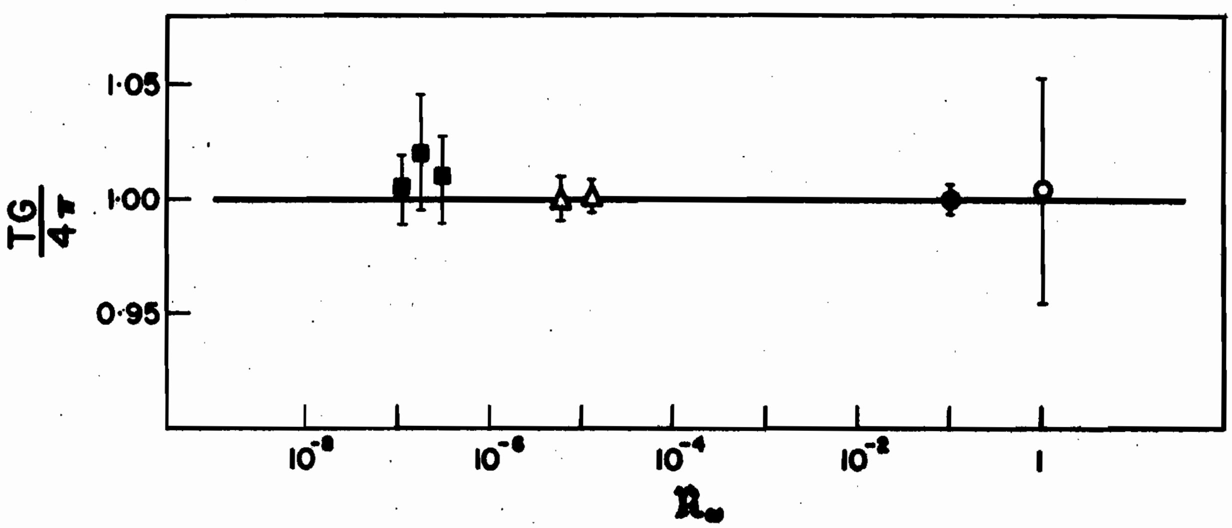

<u>Figure 2</u> Angular velocity of rigid spheres as a function of $\mathfrak{R}_\omega$. The horizontal line is from (27) and the points are experimental data.

Circles: present work for System 1 (open circles) and System 2 (closed circles) in Couette flow;
triangles: previous data for Couette flow[2,3,32,33]; and
squares: previous data for Poiseuille flow[6,31].

The vertical lines indicate the standard deviation for each set of data.

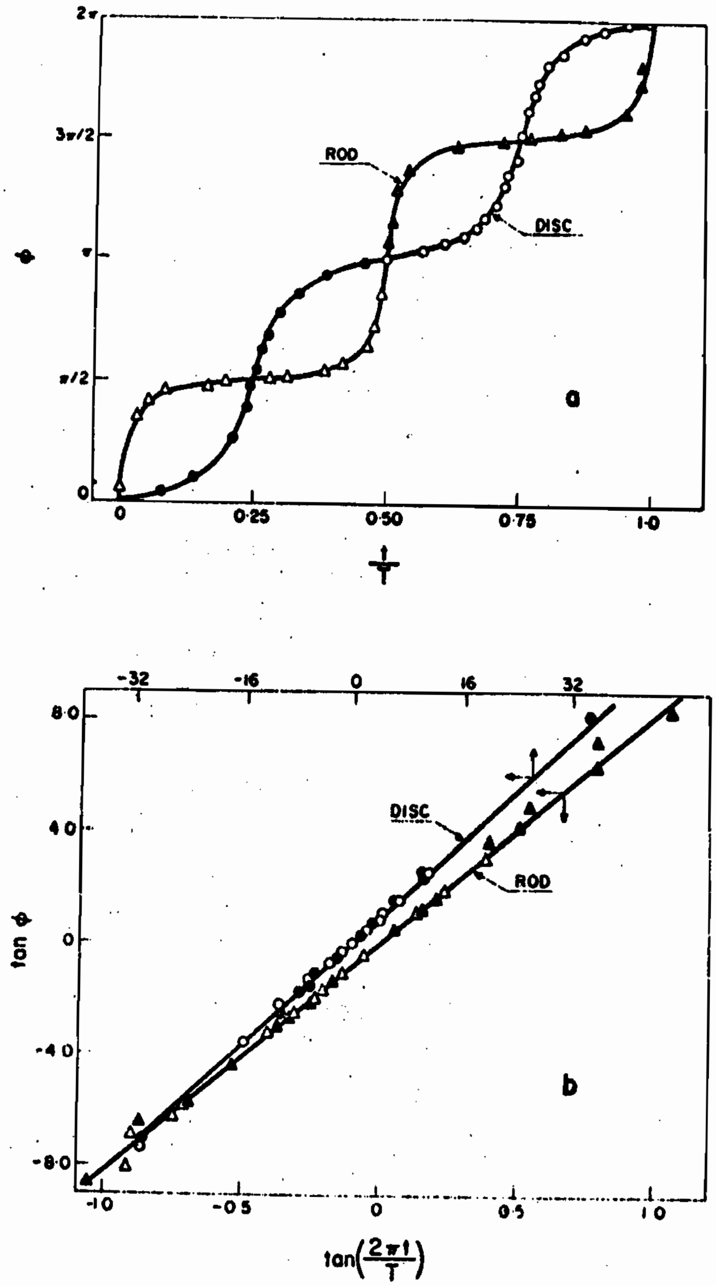

<u>Figure 3</u> Variation of ϕ with time in Poiseuille flow for a rigid disc $r_e = 0.245$ (System 8, circles) and for a rigid rod $r_e = 8.2$ (System 9, triangles). The lines are calculated from (24). The experimental points are: -
closed circles: $r/R = 0.740$, $G = 5.24\ \mathrm{sec}^{-1}$, $C = 11$;
open circles: $r/R = 0.790$, $G = 5.58\ \mathrm{sec}^{-1}$, $C = 2.1$;
closed triangles: $r/R = 0.702$, $G = 4.97\ \mathrm{sec}^{-1}$, $C = \infty$;
open triangles: $r/R = 0.675$, $G = 4.76\ \mathrm{sec}^{-1}$, $C = 3.5$.

(a) Plot of ϕ against t/T. Note that the angular velocity is maximum at $\phi = 0$ for the rod and at $\phi = \pi/2$ for the disc and that, as predicted by (20), the variations of ϕ with time are independent of G (or C).

(b) Variation of tan ϕ with tan $(2\pi t/T)$.

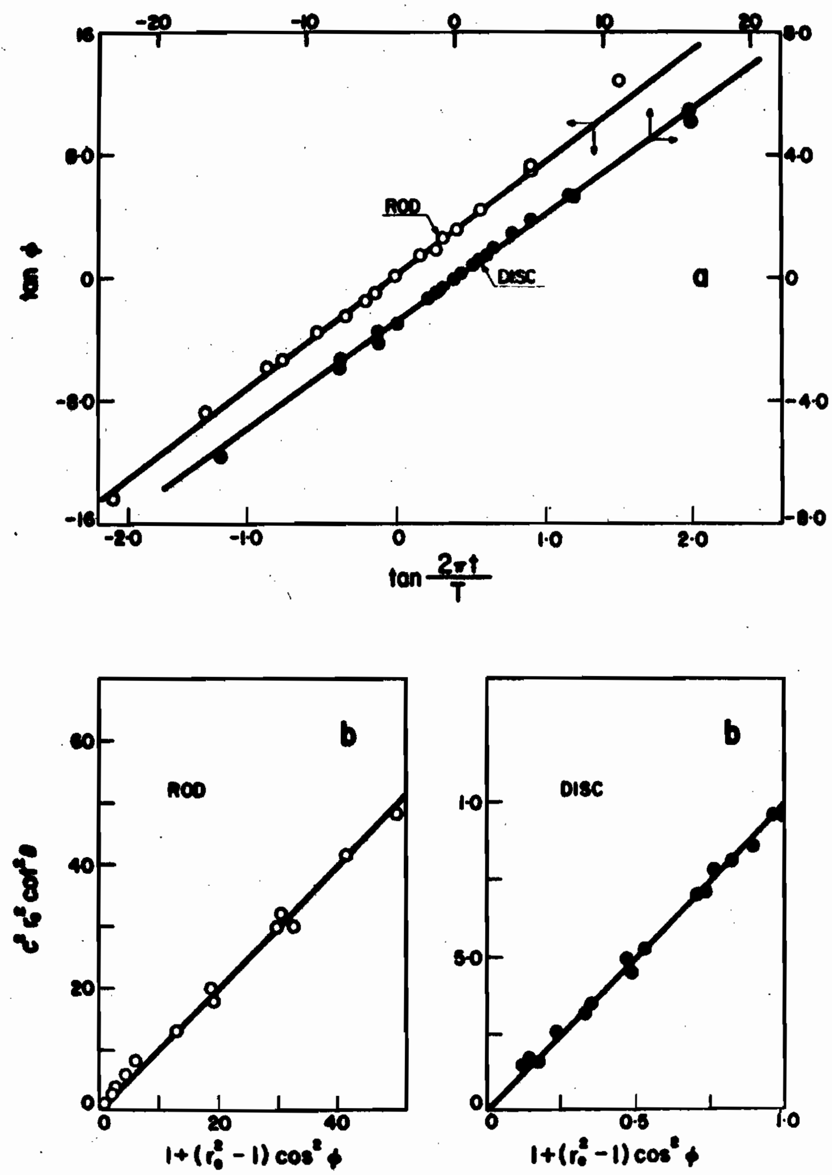

Figure 4 (a) Variation of angle ϕ with time in Couette flow for a rigid disc (System 3) and rod (System 4). The lines are calculated from (24), and the points are experimental data. Open circles: G = 6.01 sec^{-1}, r_e = 7.24 and C = 0.26; closed circles: disc G = 4.41 sec^{-1}, r_e = 0.35 and C = 2.8.

(b) Variation of θ with ϕ for the same rod and disc shown in Figure 3. The lines are calculated from (23) using the measured C and r_e the points are experimental data.

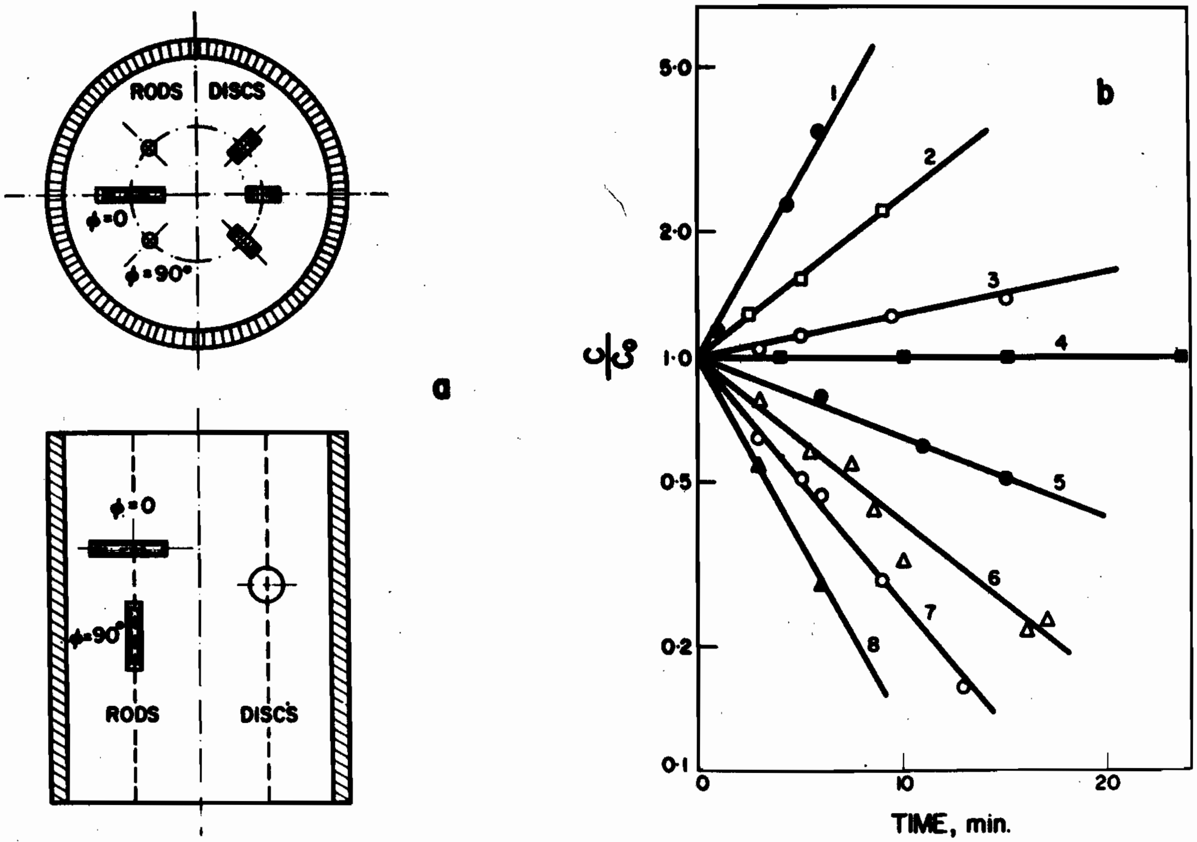

Figure 5 (a) Projection of rods and discs in tube flow viewed along the tube axis (upper) and in the median plane (lower) after they have attained the respective limiting value $C = \infty$ and $C = 0$.

(b) Variation of log C with time showing the effect of G and particle size on the rate of change of C in Couette flow. Lines 1 to 4 inclusive are for rods (System 4, $2a = 0.098$ cm, $2b = 0.0095$ cm) and lines 5 to 8 for discs (System 3, $2a = 0.012$ cm). Rods: line 1: $G = 11.6\ \text{sec}^{-1}$, $C_o = 0.69$; line 2: $G = 9.49\ \text{sec}^{-1}$, $C_o = 0.44$; line 3: $G = 8.66\ \text{sec}^{-1}$, $C_o = 0.32$; line 4: $G = 5.34\ \text{sec}^{-1}$, $C_o = 0.23$.
Discs: line 5: $2b = 0.0455$ cm, $G = 3.70\ \text{sec}^{-1}$, $C_o = 2.9$; line 6: $2b = 0.0455$ cm, $G = 4.6\ \text{sec}^{-1}$, $C_o = 1.8$; line 7: $2b = 0.0455$ cm, $G = 7.0\ \text{sec}^{-1}$, $C_o = 3.4$; line 8: $2b = 0.0755$ cm, $G = 4.35\ \text{sec}^{-1}$, $C_o = 2.3$.

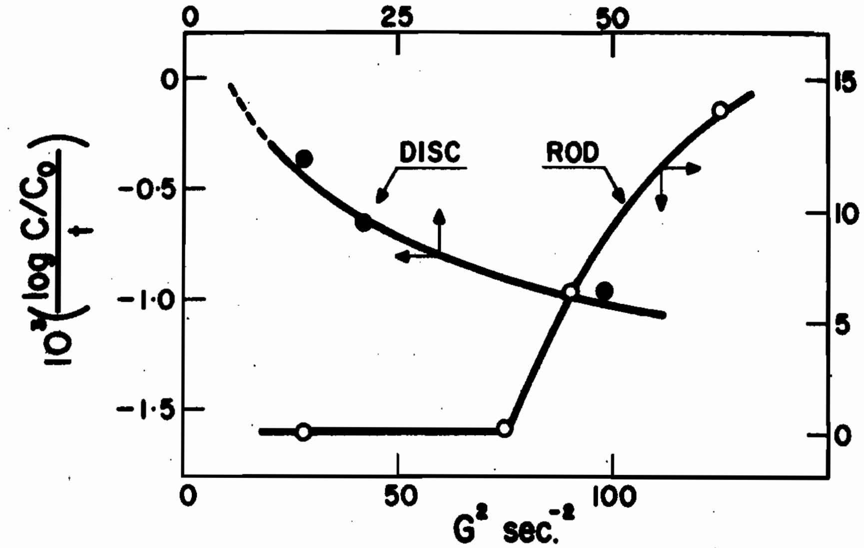

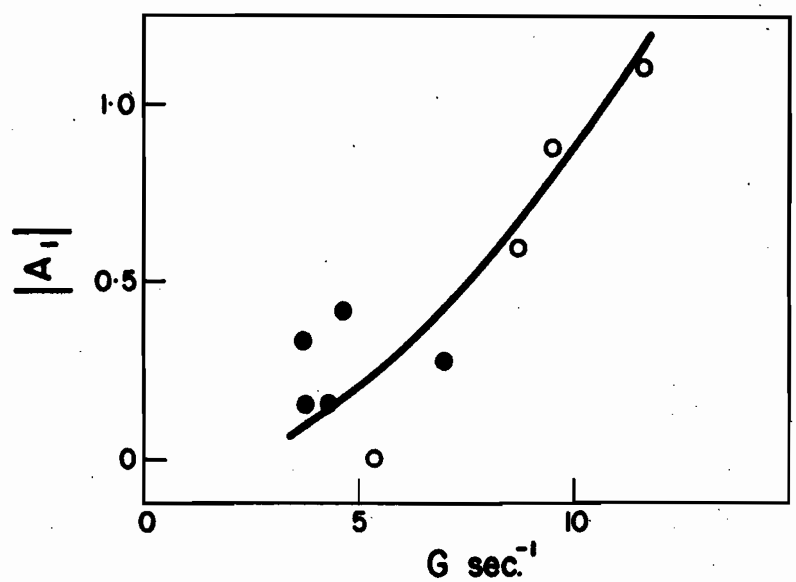

<u>Figure 6</u> (a) Plot of log $[C/C_0]$ /t against G^2 for rods (open circles) and discs (closed circles) in Couette flow which according to (30) should be linear.

(b) Plot of $|A_1|$ calculated from (34) against G in Couette flow for the rod (open circles) and discs (closed circles) in Table V.

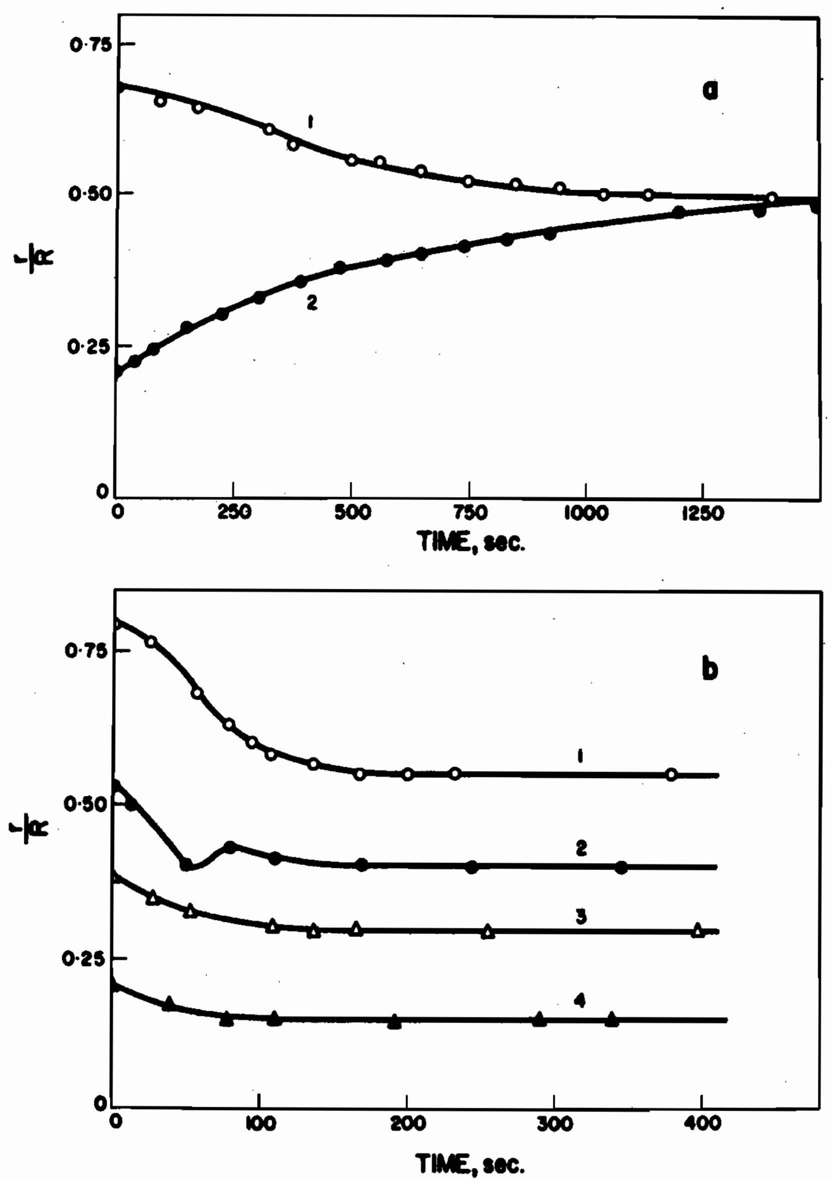

<u>Figure 7</u> Radial migration of rigid spheres in Poiseuille flow.

(a) System 2, $Q = 7.11 \times 10^{-2}$ cm.^{3} sec^{-1}, $b/R = 0.305$, $R = 0.2$ cm, and $\Re_p = 7.4 \times 10^{-3}$. Curve 1: inward migration. Curve 2: outward migration.

(b) System 12, $Q = 7.11 \times 10^{-2}$ cm.^{3} sec^{-1}, $R = 0.1$ cm. Curve 1: $b/R = 0.155$, $\Re_p = 2.7 \times 10^{-3}$. Curve 2: $b/R = 0.40$, $\Re_p = 4.7 \times 10^{-2}$. Curve 3: $b/R = 0.525$, $\Re_p = 1.1 \times 10^{-1}$. Curve 4: $b/R = 0.778$, $\Re_p = 0.36$.

Particle Reynolds numbers are based on (6) and (10). The arrows are points of inflection where dr/dt passes through a maximum.

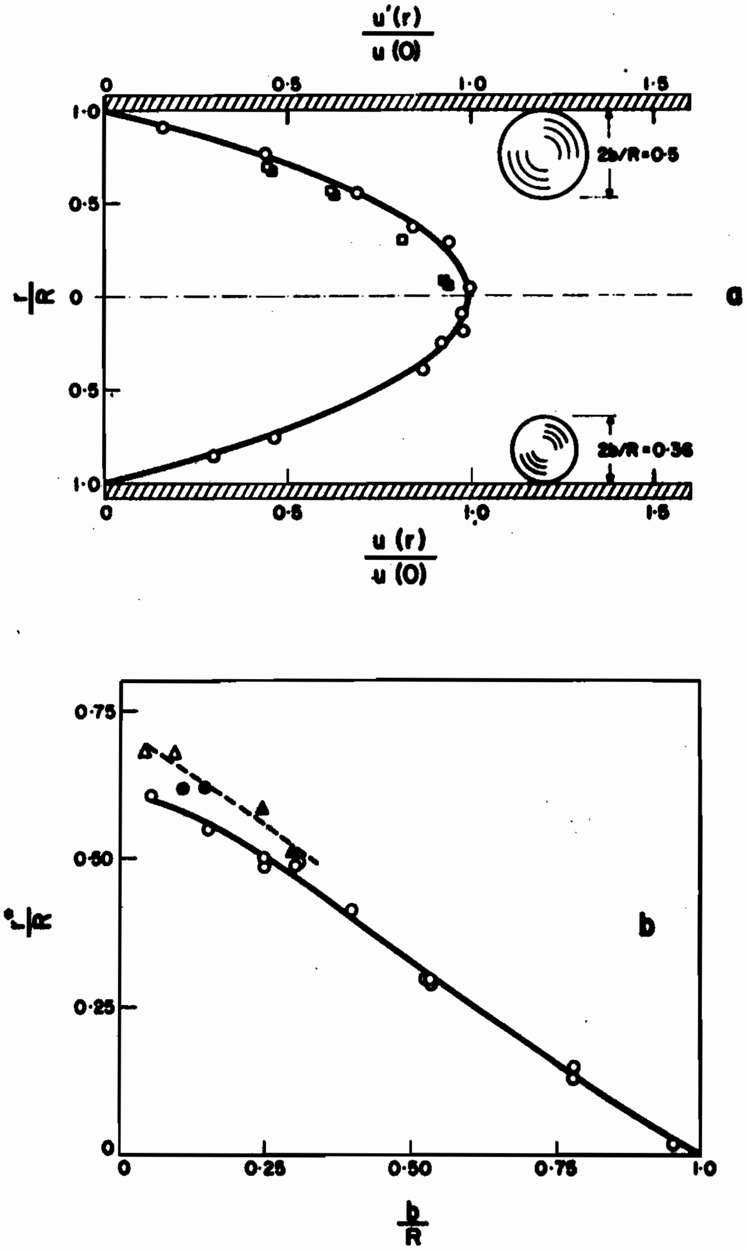

Figure 8 (a) Particle and fluid translational velocities in Poiseuille flow in a tube R = 0.2 cm. at Q = 0.071 to 0.356 $cm^3\ sec^{-1}$. The line is calculated from (3). The points are experimental data for System 11 (circles, $\Re$ = 8.8) and Systems 2 and 7, (squares, 2b/R = 0.36 to 0.50) during flow in the upward (open squares) and downward (closed squares) direction at $\Re_p$ (based on (6) and (10)) from 1.4 x 10^{-2} to 2.1 x 10^{-2}.

(b) Dimensionless plot showing the effect of b on r*.
Open circles: present work $\Re \leq 1.1$;
closed circles: data[12] at $\Re < 30$;
open triangles: data[14] at $10 < \Re < 80$;
closed triangles: data[27] $145 < \Re < 510$.

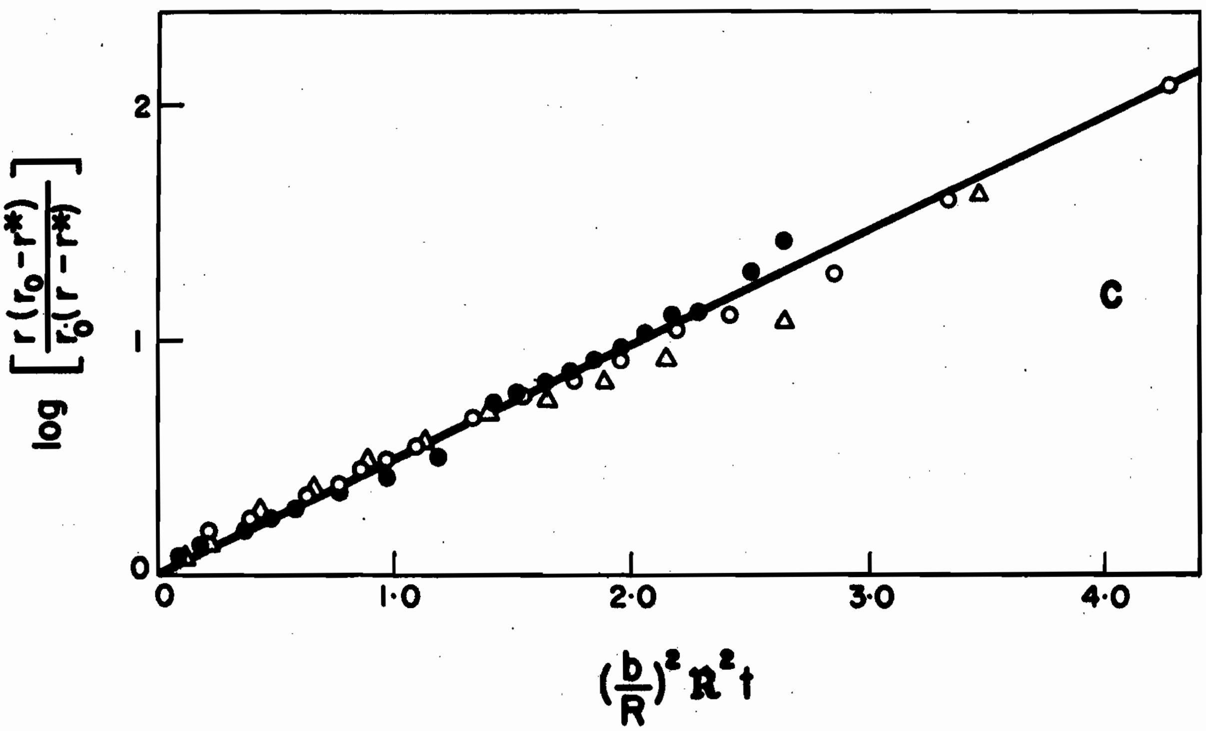

Figure 8 (c) Plot according to (19B) System 2, R = 0.2 cm. Circles: b/R = 0.305 and $\mathfrak{R}$ = 0.195 for outward (closed circles) and inward (open circles) migration. Triangles: for outward migration of a sphere b/R = 0.25 and $\mathfrak{R}$ = 0.390.

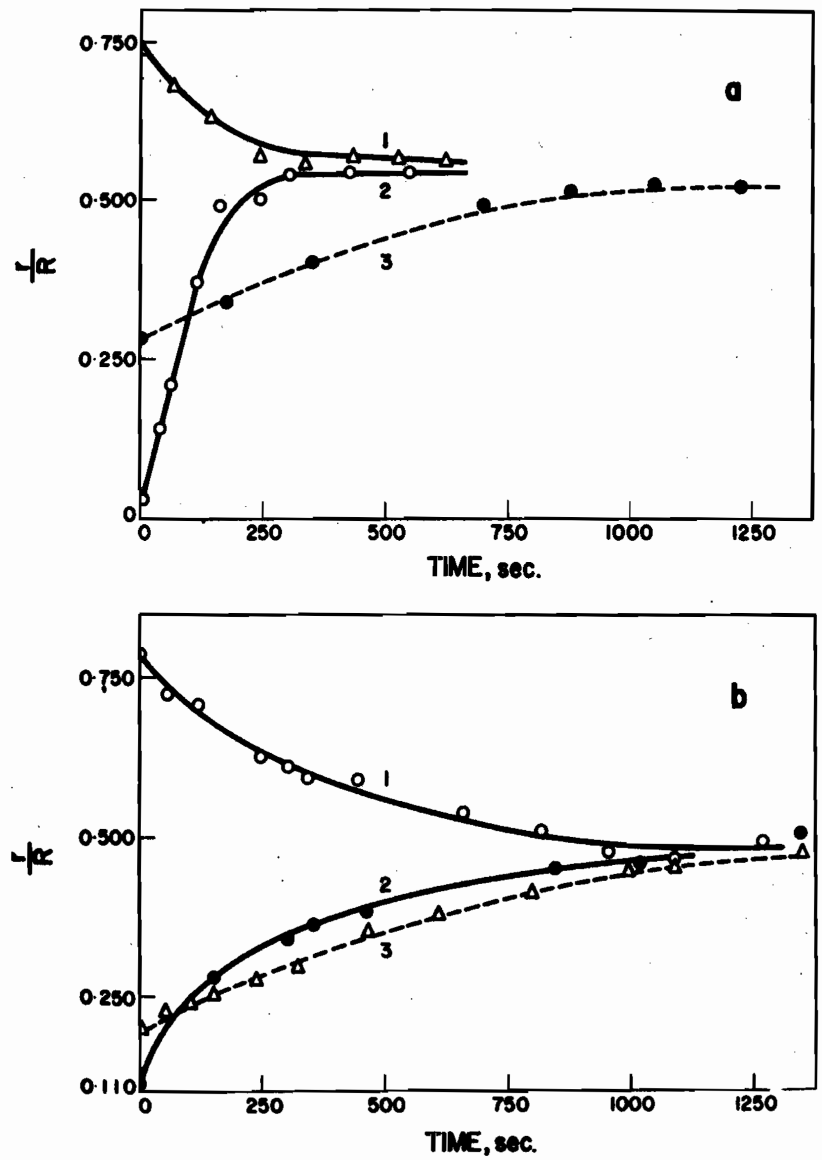

Figure 9 Radial migration of rigid cylinders in Poiseuille flow at $\Re$ from 0.4 to 1.

(a) Discs; System 3, R = 0.2 cm. and 2a = 0.012 cm. Curve 1: Q = 0.356 $cm.^3$ sec^{-1}, 2b = 0.0684 cm; curve 2: Q = 0.356 $cm.^3$ sec^{-1}, 2b = 0.0934 cm. and curve 3: Q = 0.142 $cm.^3$ sec^{-1}, 2b = 0.0897 cm.

(b) Rods; System 4, R = 0.2 cm, Q = 0.356 $cm.^3$ sec^{-1}. Curve 1: 2a = 0.0892 cm, 2b = 0.0083 cm, curve 2: 2a = 0.114 cm, 2b = 0.0085 cm. and curve 3: 2a = 0.108 cm, 2b = 0.0084 cm.

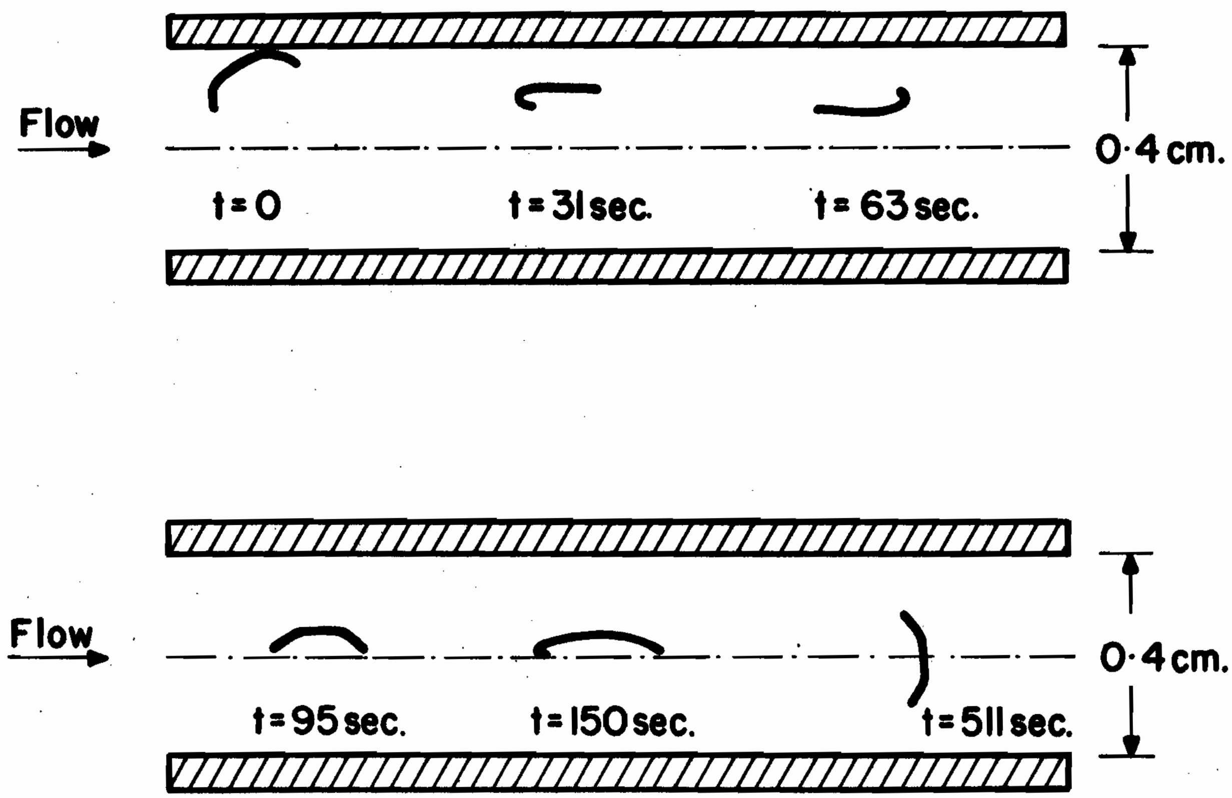

Figure 10 Tracings from photographs of an elastomer fibre (No. 4 in Table VI) showing its radial migration to the tube axis and its configuration at various time intervals. System 6, $Q = 0.356$ cm.^{3} sec^{-1}, $R = 0.2$ cm. and $r_p = 78$.

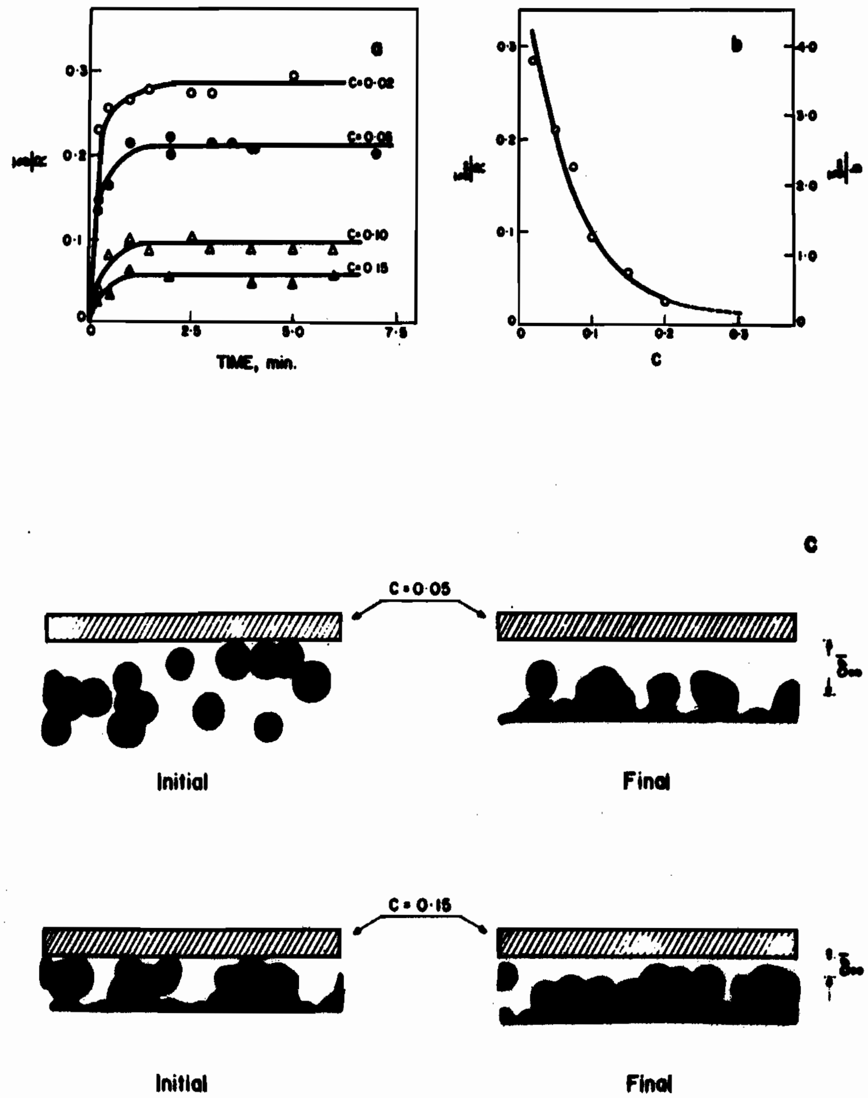

<u>Figure 11</u> The development of particle-free layer in suspensions of rigid spheres. System 7, R = 0.2 cm, b/R = 0.075, Q = 0.356 cm.^{3} sec^{-1}, $\mathfrak{R}_p = 5 \times 10^{-3}$.

(a) Variation of $\bar{\delta}/R$ with time. The points are; open circles: c = 0.02, closed circles: c = 0.05, open triangles: c = 0.10 and closed triangles c = 0.15.

(b) Effect of concentration on $\bar{\delta}_\infty/R$ and $\bar{\delta}_\infty/b$.

(c) Tracings from photographs of the particle-free zone for two suspensions.

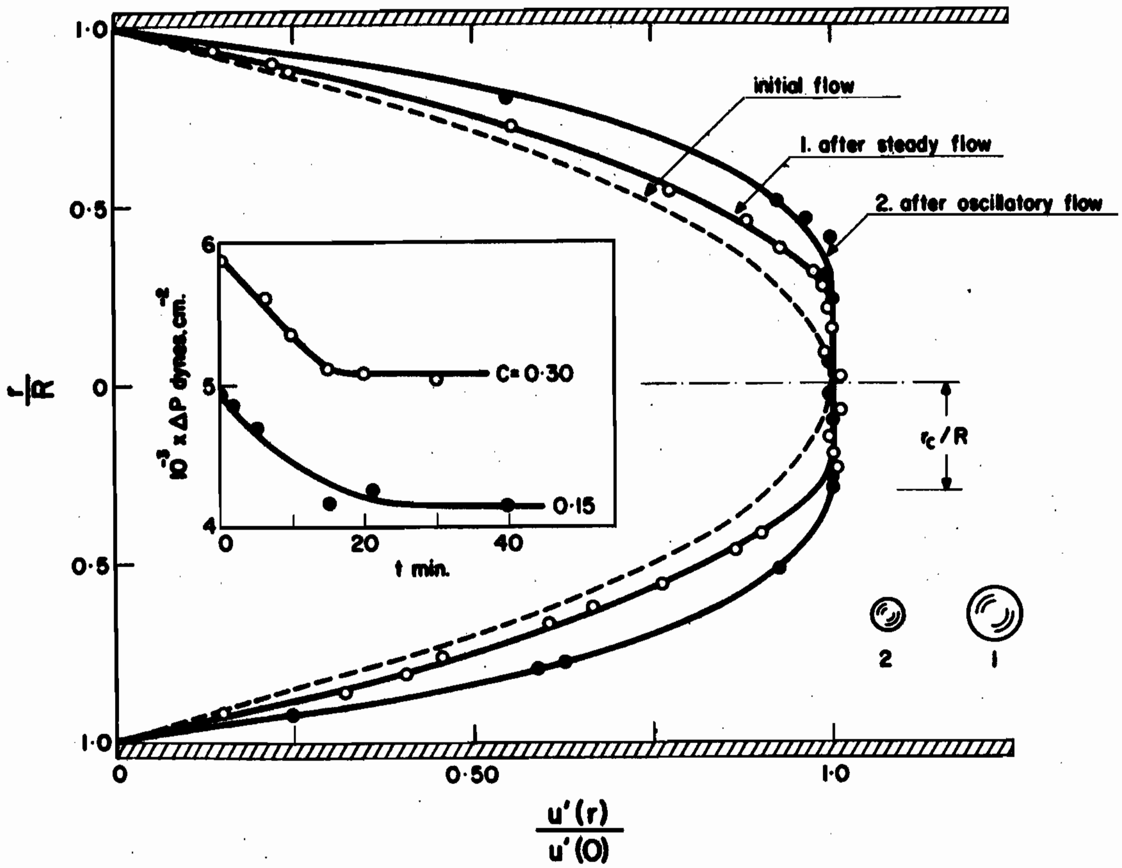

Figure 12 Effect of particle-free zone on the apparent viscosity and velocity profile of concentrated suspensions of spheres (System 5) in Poiseuille flow. Plot of $u'(r)/u'(o)$ against r/R for two suspension ($u'(o)$ is the centerline particle translational velocity). The dashed line is the initial parabolic velocity profile. The solid lines are the final velocity distributions when $\delta = \delta_\infty$. Curve 1 (open circles): steady flow c = 0.10 Q = 0.356 cm.^{3} sec^{-1}, R = 0.2 cm, b/R = 0.075 and $\Re_p = 0.7 \times 10^{-3}$. Curve 2 (closed circles): oscillatory flow, frequency 17.1 sec^{-1}, amplitude 1.1 cm^3, c = 0.22, R = 0.5 cm, b/R = 0.040 and $\Re_p = 2.2 \times 10^{-3}$.

The insert shows the decrease in ΔP with time for two suspensions c = 0.15 (closed circles) and c = 0.30 (open circles) in a tube R = 0.3 cm; b/R = 0.096 and $Re_p = 2 \times 10^{-3}$.

Particle Reynolds numbers are based in (6) and (10); the relative sizes of the spheres are also shown.

PART IV

MENISCUS EFFECTS

ABSTRACT

This investigation deals with the accumulation of particles which occurs behind an advancing air-liquid meniscus in a tube. It is shown that near the meniscus the radial component of velocity of the liquid containing the particles plays an important part.

The measured axial and radial velocities of a liquid without particles are in qualitative agreement with a theory due to Bhattacharji and Savic for homogeneous fluids.

Isolated spheres suspended in the liquid which reached the meniscus, suffer an inward displacement as they are transported by the radial flow near the tube wall which increases with increasing particle size. An inward displacement of spheres also occurs at a tube convergence in positions remote from the meniscus. In both cases, the inward displacement presumably is due to the interaction of spheres with the wall.

Two-body collisions near the advancing meniscus result in an inward displacement of the individual spheres of the doublet greater than that of isolated spheres.

The phenomena account for the observed accumulation and also for a predicted size-fractionation in suspensions of rigid spheres and emulsions.

INTRODUCTION

In studying the velocity profiles in concentrated suspensions of rigid spheres undergoing Poiseuille flow[1)] an increase in concentration behind the advancing meniscus was observed (but not reported) as the suspensions were pumped into the tube.

Concentration changes in suspensions flowing through tubes have been observed by many workers in a number of systems[2-8)]. In aqueous pulp-fiber suspensions Forgacs et al[2)] have shown, using a vertically mounted rotating circular loop of glass tubing device half-filled with the suspension, that a depletion of pulp fibres at the receding and an accumulation at the advancing meniscus occurred; the phenomenon was attributed to the formation of a particle-free layer as a result of migration from the tube wall of deformable pulp fibres. In blood flowing through capillary tubes, a dilution of the red cells in the tube was observed, the drop in concentration becoming more pronounced as the tube radius decreased[3-4)]; moreover, it was observed that the region behind an advancing meniscus showed a much stronger red colour than the bulk of the suspension in the tube[5)]. Vejlens[5)] has also shown that the first drop of blood from a finger tip puncture contained a relatively greater number of white corpscules than the subsequent drops.

The reduction in concentration of a suspension in a tube and the accumulation of particles near an advancing meniscus have been explained[6-8)] in terms of inward displacement of particles from the wall at the tube inlet and the near the meniscus, which causes them to travel faster than the original streamline in which they entered the tube.

Recently Bhattacharji and Savic[9)] made a theoretical study of the flow of a viscous liquid ahead an inviscid liquid piston in an attempt to explain the concentration gradients observed in natural formations of minerals. This theory is relevant to the present work which was undertaken to study the nature and causes of concentration changes in flowing dispersions. Starting with the flow of pure liquid, velocity profiles and streamline patterns behind the advancing meniscus were measured. The paths of single rigid spheres and two-body interactions behind advancing liquid menisci were studied. Concentration measurements along the tube in dilute and concentrated suspensions were made. Entrance effects were investigated, and, finally, some experiments on particle fractionation in dilute emulsions and suspensions were performed.

THEORETICAL PART

Consider the axi-symmetric flow of an incompressible viscous fluid in a tube radius R with cylindrical polar coordinates x, r having an origin at the center of the air-liquid meniscus (Fig. 1a). Far behind the meniscus (which for simplicity is considered to be flat) the velocity profile $u^*(\alpha)$ is parabolic[10)]

$$u^*(\alpha) = 2\,\bar{u}\,(1 - \alpha^2)\ , \tag{1}$$

where $\alpha = r/R$ and $\bar{u}$ the average fluid velocity given by

$$\bar{u} = \frac{Q}{\pi R^2}\ , \tag{2}$$

Q being the volumetric flow rate through the tube. The flux at α is

$$q^*(\alpha) = R^2 \int_0^\alpha 2\pi\alpha u^*(\alpha) d\alpha \ . \tag{3}$$

The meniscus advances in the direction of positive x with velocity $\bar{u}$. To render the flows stationary we consider the tube to move with a velocity $-\bar{u}$ yielding a velocity distribution relative to the mensicus $u(\alpha) = u^*(\alpha) - \bar{u}$ which from (1) and (2) becomes

$$u(\alpha) = \bar{u}\,(1 - 2\alpha^2) \ . \tag{4}$$

Now consider a long fluid cylinder of radius r (Fig.1a) whose base (BB') is on the meniscus and whose top AA' is remote from the meniscus. The flux through AA' is given by

$$q(\alpha) = Q\alpha^2(1 - \alpha^2) \ , \tag{5}$$

whereas that through BB' is zero. Since no accumulation of fluid within the cylinder is possible the liquid flows radially outwards from its side as illustrated by the arrows in Fig. 1a. Thus the transition from a parabolic to a uniform velocity distribution must result in a radial flow behind the advancing meniscus; as may be seen from (5) the maximum $q(\alpha)$ ($= Q/4$) occurs at $\alpha = 1/\sqrt{2}$.

Bhattacharji and Savic[9)] have solved the Navier-Stokes equation in the Stokes (creeping flow) regime assuming no slip at the tube wall and that the viscous shear vanishes at the liquid surface x = 0. An approximate analytic solution, which is sufficient for our purposes, is given by the Stokes stream function

$$\Psi = \frac{Q}{2\pi}\,\alpha^2(1 - \alpha^2)\left[1 - \exp(-\sqrt{6}\beta^2)\right] \ , \tag{6}$$

where $\beta = -x/R$. As $\beta^2 \rightarrow \infty$, (6) reduces to the stream function for parabolic flow:

$$\Psi = \frac{Q}{2\pi}\,\alpha^2(1 - \alpha^2)\ . \tag{7}$$

Equation (6), which is exact at high β, predicts that the streamlines turn backwards near the advancing meniscus. The radial position α_m at which a streamline goes through a maximum β_m is found by differentiating (6) partially with respect to α and equating to zero; it can then be shown that the loop occurs at constant $\alpha_m (= 1/\sqrt{2})$.

The axial and radial velocities follow from the stream function:

$$u(\alpha) = \frac{1}{r}\,\frac{\partial\Psi}{\partial r} = \bar{u}(1 - 2\alpha^2)\left[1 - \exp(-\sqrt{6}\beta^2)\right]\ , \tag{8}$$

and

$$v(\alpha) = \frac{1}{r}\,\frac{\partial\Psi}{\partial r} = \pm\,\frac{\sqrt{6}}{2}\,\bar{u}\alpha(1 - \alpha^2)\exp(-\sqrt{6}\beta^2)\ , \tag{9}$$

When the meniscus is advancing ($\beta < 0$) the sign in (9) is +, the radial flow is from the axis to the wall, and the reverse for a receding meniscus ($\beta > 0$). In both cases as $\beta \to \infty, v(\alpha) \to 0$ and (8) reduces to (4). Moreover, (8) predicts that $u(1/\sqrt{2}) = 0$ for all values of β; also by differentiating (9) partially with respect to α and equating to zero, it can be readily shown that at constant β, $v(\alpha)$ goes through a maximum at $\alpha = 1/\sqrt{3}$ for all values of β.

In the experiments described later $v(\alpha)$ was measured, as a matter of convenience, at Ψ = constant rather than at β = constant; $v(\alpha)$ along a streamline may be calculated by combining (6) and (9) to yield

$$v(\alpha) = \pm\,\frac{\sqrt{6}}{R^2}\left[\frac{\alpha(1 - \alpha^2)Q}{2\pi} - \frac{\Psi}{\alpha}\right]. \tag{10}$$

The radial position of maximum $v(\alpha)$ is found by differentiating (10) with respect to α and equating to zero which gives

$$\alpha(v_m) = \left[\frac{1 + (1 + 24\pi/Q)^{1/2}}{6}\right]^{1/2} . \qquad (11)$$

Equation (11) shows that, at a given Q, $\alpha(v_m)$ is least when $\Psi = 0$ (streamline passing through the tube axis) and equal to $\pm 1/\sqrt{3}$ and increases with increasing Ψ.

EXPERIMENTAL PART

Direct observations of particle movements flowing through vertical tubes were made using the travelling microscope system previously described[1,10]. Neutrally buoyant suspensions of screen-fractionated samples of polystyrene (PS) or polyvinyl acetate (PVA) spheres of radius $b = (35 \pm 15)$ to $(650 \pm 50)\mu$. in a polyglycol oil (Ucon oil 50-HB-5100) containing tetrabromoethane of density $\rho = 1.05$ to 1.14 g.cm.$^{-3}$ and viscosity $\eta_o = 24.6$ poises were employed.

Liquid velocity profiles and streamline patterns behind the meniscus were measured by cine-photography (using a Paillard Bolex 16 mm. reflex camera) of tiny 25μ aluminum tracer particles suspended in the liquid. Near the meniscus the axial and radial velocities changed continuously and the average values were measured. The average axial velocity was determined by counting the number of frames between two positions of a tracer particle at a distance $x \pm \Delta x$ from the meniscus ($\Delta x < 0.03$ cm.) and $r \pm \Delta r$ from the axis ($\Delta r < 0.008$ cm.); similarly the average radial velocity was evaluated at $r \pm \Delta r (\Delta r < 0.09$ cm.).

Two-body collisions were studied by locating two spheres close together near the meniscus and in the median plane of the tube normal to the viewing axis and photographing their interaction. The variation of the azimuthal angle ϕ of the line joining the sphere centers with the Y-axis (Fig. 1a) as well as the radial positions of each particle were measured on a projection table.

Convergent entrance effects at positions remote from the meniscus were investigated in a very dilute suspension of PS spheres (volume fraction $c < 0.001$) which flowed in a tube of radius $R_1 = 0.4$ cm. which converged smoothly over a length of 0.8 cm. to a tube $R_2 = 0.1$ cm., thus simulating the conditions existing at the entrance of the tube from the reservoir. The distance of the particle centers from the wall was measured by means of a calibrated filar eyepiece.

In dilute suspensions, the increase in concentration near the meniscus due to radial flow was determined by photographing the suspension near the advancing meniscus.

Concentration gradients along the tube in concentrated suspensions of PVA spheres, due both to entrance effects and radial flow, were determined by flowing the suspensions through an initially empty tube $R = 0.2$ cm. and length $L = 85$ cm. Successive samples of known volume between 0.2 to 2 cm.^{3} expelled from the other end of the tube were collected and c for each was determined by weighing both wet and dry.

All the experiments were performed in a thermostated room maintained at 22 ± 0.5°C.

RESULTS

1. General observations

At the values of Q used in most of the experiments an advancing (rising) meniscus was almost flat, slightly concave to the air near the tube wall (Fig. 1b); when it receded at the same $\bar{u}$ the shape was quite different (Fig. 1b).

As expected spheres approaching the advancing meniscus moved radially from the axis towards the wall. Upon reversing flow the radial movement became directed inwards; however, spheres situated close to the wall were entrapped by the liquid left behind the receding meniscus and remained at the tube wall. For this reason it was easier to make quantitative measurements behind advancing menisci.

A marked increase in concentration behind an advancing meniscus occurred, with particles accumulating progressively as the meniscus travelled along the tube. At higher c, the suspensions exhibited complete plug flow[1)] over a distance $|\beta|$ which gradually increased with time.

2. Flow near an advancing meniscus

(a) Axial velocity

Figure 2 shows the measured axial velocity profiles of the liquid with no particles present as a function of β; when $|\beta| \geqq 0.75$ the velocity distribution was parabolic. As the meniscus was approached the profile deviated from (4), and as predicted by (8) $u(\alpha)$ was greater than given by (4) when $1/\sqrt{2} < \alpha < 1$ and less when $0 < \alpha < 1/\sqrt{2}$. At $|\beta| = 0.5$ a central core of effectively zero velocity gradient developed around the tube axis (Fig. 2) its width increasing towards the meniscus. At $\beta = 0$ the velocity of the meniscus was constant across the tube up to the wall. However, since there is no slip at the wall, there should be a transition layer near the wall in which the velocity goes from 0 to $-\bar{u}$. In two carefully executed experiments the meniscus velocity was about 2% higher than $\bar{u}$ calculated from (2), corresponding to a calculated layer thickness of 2×10^{-3}cm. With the optical equipment used the resolution was better than 10μ and the accuracy of Q was within 2%. It was concluded, therefore, that the thickness of the layer was small ($<10\mu$) and that for all practical purposes the entire meniscus front travels at $u^* = \bar{u}$ as illustrated in Fig. 2. The curves (Fig. 2) intersect each other at $\alpha = 1/\sqrt{2}$ where $u(\alpha) = 0$ in accord with (8).

The volume flow rates calculated from (3) by graphical integration using the measured $u^*(\alpha)$ and the limits of integration from 0 to 1 were in good agreement with those obtained by weighing the amount of liquid expelled from the tube in a measured time (Table I).

(b) Streamlines

The streamline pattern behind the advancing liquid surface is illustrated in the upper part of Fig. 3. As expected from the velocity profiles, circulation at high $|\beta|$ occurred around $\alpha = 1/\sqrt{2}$. Although the axial flow is effectively parabolic at $\beta = -0.75$, Fig. 3 shows that there is still some circulation at $|\beta| > 0.75$.

The radial position α_m of the loop (indicated by the solid circles in Fig. 3) increased from the value of $1/\sqrt{2}$ predicted by (6) as the meniscus was approached; a more exact solution for Ψ which is valid for smaller $|\beta|$[9] indicates that α_m increases with decreasing $|\beta|$ in accord with the present observations. The results were extrapolated to $\alpha = 1$, $\beta = 0$ (dashed line, Fig. 3) since the streamline $\Psi = 0$ should turn on the meniscus at the tube wall.

(c) Radial velocity

Measured values of $v(\alpha)$ for various initial radial positions $\alpha_1 (< 1/\sqrt{2})$ are shown plotted as a function of α in Fig. 4 and compared with those calculated from (10). Although the measured and calculated $v(\alpha)$ are of the same order of magnitude, however, in all cases $v(\alpha)$ meas. > $v(\alpha)$ calc. The observed $\alpha(v_m)$ as well as the values of α at which, for a given Ψ, $v(\alpha)$ vanishes are in good agreement with the theory.

3. Single spheres

(a) Meniscus effects

When a sphere, initially located at $\alpha_1 (< 1/\sqrt{2})$, approached the advancing meniscus it was transported by the radial flow towards the tube wall. The final $\alpha_2 (> 1/\sqrt{2})$ of the sphere center was smaller than for the corresponding streamline by an amount which depended on particle size (Fig. 5a). The displacement $\Delta\alpha = \alpha_2(0) - \alpha_2(\Upsilon)$, the difference in α_2 from the corresponding value when $\Upsilon = b/R = 0$, is shown plotted against α_1 in Fig. 5b. It increases with increasing Υ and decreasing α_1, and is greatest ($= \Upsilon$) when $\alpha_1 = 0$, and is zero at $\alpha = 1/\sqrt{2}$.

When $\alpha_1 < \Upsilon$, $\Delta\alpha = \Upsilon$ because the particles cannot penetrate the wall. A $\Delta\alpha > 0$ occurs at all $\alpha_1 < 1/\sqrt{2}$, although the magnitude diminishes with decreasing α_1, which suggest that a hydrodynamic rather than a mechanical wall effect of the type proposed by Whitmore[6] operates; the spheres presumably interact with the free liquid surface and tube wall, and this interaction results in a deflection of sphere centers from their original streamline.

(b) Entrance effects

A re-arrangement of the sphere centers was also observed in the converging tube at positions remote from the meniscus (Table II). As the particles entered the smaller tube they were displaced inwards. The magnitude $\Delta\alpha' = \alpha_1' - \alpha_2'$ of this displacement between the large and small tube increased with increasing α_1 and b. In the case of a streamline (i.e. $\Upsilon = 0$) $\alpha_1' = \alpha_2'$ as may be seen by applying (5) to the smaller and larger tube respectively, and comparing values α so that the continuity condition is satisfied. Thus, $\Delta\alpha'$ represents the displacement of a particle center from its entering streamline. As may be seen from Table II particles initially located close to the axis of the large tube passed into the smaller tube almost unhindered; moreover, their paths were reversible when the direction of flow was reversed. On the other hand, the paths of spheres which were initially located near the wall ($\alpha_1 > 0.75$) were irreversible; the outward displacement occurring at the exit of the small tube was smaller than the corresponding inward movement when the particles entered the tube.

4. Two-body collisions

When two spheres collided in the median plane of the tube near the advancing meniscus, α_2 for each individual sphere after separation was often (but not always) smaller than the corresponding for non-interacting particles at the same Υ and α_1. In the first and second columns of Table IIIthe radial positions of the two spheres before and after their interactions are listed; in the third, α_2 for pairs of single non-interacting spheres (from Fig. 5a) of the same γ and α_1 are tabulated. The fourth column shows the additional displacement $\Delta\alpha_2$ i.e. the difference between α_2 of each sphere of the doublet after separation and the value for a non-interacting spheres. In most cases $\Delta\alpha_2$ was positive indicating an additional inward displacement. The magnitude of $\Delta\alpha_2$ depended on the way that the spheres interacted; when the doublet did not rotate as it was transported by the radial flow of the liquid (i.e. when ϕ = constant), then $\Delta\alpha_2 < 0.02$, but when it rotated the resulting values of $\Delta\alpha_2$ (for one or both spheres) were appreciably greater.

A collision involving a rotation of the doublet near the advancing meniscus is shown in Fig. 6; in Part (a) the angle ϕ is plotted against time, the arrows indicating the angles ϕ_o and $-\phi_o$ at which the spheres appeared to collide and separate unsymmetrically with the angle of approach ϕ_o being numerically less than the angle of separation $-\phi_o$ in contrast to collisions at high $|\beta|$[11]. The variation in α for each sphere of the doublet is plotted as a function of β in Fig. 6b with $\Delta\alpha_2$ and the corresponding $\Delta\alpha$ also shown.

There are two possible reasons for $\Delta\alpha_2 > 0$: i) the doublet has a higher effective γ than a singlet and hence experiences a higher $\Delta\alpha$ as would be expected from Fig. 5; and ii) because the angle of approach is numerically smaller than that of separation, the sphere centers at the time of separation, are located closer to the tube axis. The data (Table III) suggest that the second effect may be the more important since $\Delta\alpha_2$ was greatly reduced when the doublet did not rotate (i.e. ϕ = constant).

5. Suspensions of rigid spheres

The paths of sphere centers behind the advancing meniscus in a dilute ($c = 0.025$) suspension of rigid spheres produced an irregular pattern often crossing one another because of the change in $\Delta\alpha$ caused by particle interaction. This is illustrated in the lower part of Fig. 3.

The accumulation behind the meniscus may be defined as

$$A = \int_0^\infty \left[c(\beta) - c \right] \pi R^3 d\beta , \qquad (12)$$

where $c(\beta)$ is the concentration at β and c the concentration in the bulk of the suspension; (12) represents the net total increase in volume of particles behind the advancing meniscus. In the experiments A was determined approximately because of the change in the velocity profile as the suspension comes out of the tube makes exact measurement difficult. Assuming plug flow, when $c(\beta)$ is plotted against β, the area under the curve lying above c is a measure of the particle accumulation behind the meniscus.

The results are shown in Fig. 7 and Table IV. As may be seen the accumulation, after traversing a given length of the tube, increased with increasing c and Υ but remained unaffected by a tenfold increase in Q. The amount of suspension expelled from the tube before $c(\beta)$ reached the steady value c appeared to be independent of Υ but increased with increasing c. At high c and Q the leading edge of the suspension became pointed and did not wet the tube wall and exhibited plug flow.

The dependence on Υ and c suggests that the accumulation at the meniscus is due to particle-wall and particle-particle interactions. Because of the complex behaviour of particle aggregates it is difficult to establish a model to explain the accumulation quantitatively. However, the results for singlets and doublets can provide a qualitative explanation. It was shown that $\Delta\alpha$ increases with increasing Υ so that accumulation is more pronounced with increasing particle size. At high c, the effect is enhanced because of particle-particle interactions which result in greater inward displacement.

The accumulation can be caused by both converging-entrance and meniscus effects, and in the experiments with concentrated suspensions described above both effects were undoubtedly present. The following experiments were performed to separate and study each effect independently.

(i) The reservoir was filled with a pure liquid (Silicone oil 50p. + Freon 112) immiscible with the suspension but of the same viscosity (44.5 p.). When the surface of the pure liquid was about 1 cm. above the bottom of the tube (R = 0.2 cm.) a 10 cm. column of a suspension c = 0.18 was placed on its surface. The suspension, from which the entrance effect had now been eliminated, was displaced by the pure liquid and flowed for the same tube length (85 cm.) as in the experiments of Fig. 7. The first 0.26 $cm.^3$ of the suspension expelled from the tube ($0<|\beta|<10.4$) were collected and c determined and the result compared with that obtained for the c = 0.18 suspension of Fig. 7a at the same range of $|\beta|$. As may be seen from Table V, which summarizes the results, entrance effects account only for a 15% of the total accumulation.

(ii) The increase in c near the meniscus, in positions remote from the entrance to the tube, was measured directly for two dilute suspensions by counting the number of particles accumulated near the meniscus. Both dynamic and static methods of particle counting were used. In the dynamic method the microscope moved at $\bar{u}$ to follow the meniscus at a fixed distance $\beta = -1.5$ where the velocity profile was parabolic. The total number of particles N_+ which, during the time of observation, crossed the plane at $\beta = -1.5$ towards the meniscus ($u'(\alpha) > 0$) and N_- in the other direction were counted. In the static method the number of particles N_1 contained in the volume $\pi R^2|x|$ ($x = -1.5R$) at the beginning and at the end (N_2) of the experiment were counted. Both methods yielded similar results (Table VI) for the accumulation near the meniscus.

Both sets of experiment suggest that the observed accumulation near the advancing suspension-air interface is largely a meniscus effect and to a minor extent only an entrance effect.

6. Particle fractionation

Since the displacement $\Delta\alpha$ increases with increasing Υ (Fig. 5b) a size separation should occur behind a meniscus, with larger particles accumulating faster at the meniscus. This was confirmed by experiments with both rigid spheres and emulsions.

(a) Dilute suspensions of rigid spheres

The results obtained with three binary suspensions of different b_1/b_2, where the subscripts 1 and 2 refer to larger and smaller particles respectively, are tabulated in Table VII. After the suspensions had flowed in the tube for approximately 40 cm. the ratio n'_1/n'_2 of the number of larger to smaller particles per cm.^{3} at the meniscus was always greater than that in the bulk (n_1/n_2) of the suspension. The ratio $(n'_1/n'_2)/(n_1/n_2)$ increased with increasing b_1/b_2, and at a given b_1/b_2 it decreased with decreasing b_1 and b_2.

(b) Dilute emulsions

A similar phenomenon was observed in a coarse polydisperse emulsion (Fig. 8). The variation in the size distribution behind the meniscus was determined by photographing the region near the meniscus at various time intervals. The proportion of larger drops behind the advancing meniscus increased as the emulsion travelled in the tube; this is illustrated in Fig. 8a where the relative frequence n_i/n, n_i being the number of particles of radius $b_i \pm \Delta b$ and n the total number of particles counted, is plotted against b_i. After the emulsion had travelled about 60 cm. in the tube and before the meniscus reached the end of the tube, the flow was stopped and the size distribution at various β was determined by photographing a small volume ($= 1.5 \times 10^{-4}$ cm.^{3}) of the emulsion. The maximum in the distribution curves shifted to larger drops as the meniscus was approached. The volume average particle radius $\bar{b}$

$$\bar{b} = \left[\frac{\sum n_i b_i^{\,3}}{n}\right]^{1/3} \qquad (13)$$

decreased as $|\beta|$ increased (Fig. 8b) reaching a constant value at about $\beta = -0.67 \times 10^2$. No coalescence of drops was observed during the experiments.

DISCUSSION

1. Rigid spheres

Although radial flow of the liquid near the meniscus has been mentioned by Whitmore[6)] as a possible factor to the particle accumulation behind it, it was implied that its contribution is small compared to convergent entry effects. The experimental evidence presented above suggest that it is caused by the combined effects of radial flow and interactions of particles with one another and with the walls, and that entrance effects, on the other hand, are negligible. The possible reasons for this are discussed below.

(a) Entrance effects

The spheres are displaced inwards at the convergent entry of the tube because of their interaction with the wall[6] and the radial flow existing near the entrance as the parabolic velocity profile is developed in the smaller tube[12]. This inward radial displacement, it has been argued, may be expected to result, on the average, in a greater axial velocity of the particles relative to their entering streamlines[6-8]. This mechanism, however, neglects completely the relative particle-fluid velocity resulting from the wall. The slip velocity and the inward displacement $\Delta\alpha$ work in opposite directions, the former causing a depletion and the latter an accumulation of particles behind the advancing meniscus.

To estimate the effect of $u'(\alpha)$ on particle accumulation at the meniscus, $u'(\alpha)$ must be known as a function of α. Figure 9 was constructed from the theoretical calculations of Brenner[13] for the axial velocity of a sphere in a uniform flow near a single plane wall and is accurate up to $\alpha = 0.997$. Using this plot and (1), $u^*(\alpha)$ and $u'(\alpha)$ for the spheres of Table II were calculated. By comparing the 6th and 9th columns of Table VIII it may be seen that only in one case (marked with asterisk) the axial velocity of the sphere in the tube $R_2 = 0.1$ cm. exceeded the velocity of the streamline in which it entered the tube. This lag velocity of the particles may be the reason why entrance effects were found small in our experiments.

(b) Mean concentration

If entrance effects are small then the average concentration of a suspension in a tube, under steady state conditions, would be approximately the same as in an infinitely large feeding reservoir. Experiments to confirm this have not yet been performed; to resolve this question further experimental study is required especially near $\Upsilon = 1$ when the behaviour would probably be very different.

A marked reduction in the tube concentration has been reported in experiments with blood[3-4] and suspensions of rigid spheres[6-7]. However, red cells are deformed by the shear[14] and may migrate inwards[10,15,16]. On the other hand, the experiments[7] cited by Whitmore[6] were performed at particle Reynolds numbers ($4u^*(o)b^3\rho/3\eta_oR^2$) of the order of 10^{-2} where the tubular pinch effect operates, and rigid particles migrate towards an eccentric equilibrium radial position[17]. It was perhaps the radial migration of particles and not the radial displacement at the convergent entry that produced the observed reduction in the concentration of the suspensions in the tube.

(c) Meniscus effects

The concentration of the suspension at $\alpha < 1/\sqrt{2}$ reaching the advancing meniscus may, (at any rate for small Υ's) be assumed to be equal to the reservoir concentration c. The accumulation at the meniscus in a dilute suspension (i.e. neglecting particle-particle interactions) due to radial flow of the liquid at the meniscus may now be calculated and compared with the results of Table VI.

For simplicity we assume that the concentration at $\alpha > 1/\sqrt{2}$ is uniform and equal to $c_w (>c)$ up to $\alpha = 1 - \Upsilon$ when it drops to zero (solid line, Fig. 9 insert). This is an approximation since it may be seen by examining Fig. 5a that, because $\Delta\alpha$ decreases with increasing α_1, the concentration is maximum at $\alpha = 1 - \Upsilon$ and decreases to c at $\alpha = 1/\sqrt{2}$ (dashed line, Fig. 9 insert).

A material balance with respect to suspended phase per unit length of the tube yields

$$c_w\pi\left[(R - b)^2 - \frac{R^2}{2}\right] = \frac{c\pi R^2}{2} , \qquad (14)$$

from which it follows that

$$n'_w = \frac{n}{1 - 4\Upsilon} , \qquad (15)$$

where n and n_w are the number of particles per cm.^{3} at $\alpha < 1/\sqrt{2}$ and $\alpha > 1/\sqrt{2}$ respectively.

At $|\beta| > 1.5$ the positive flux of the particles is

$$\frac{1}{t} N_+ = R^2\int_0^{1/\sqrt{2}} n2\pi\alpha u'(\alpha)d\alpha , \qquad (16)$$

and the negative flux

$$\frac{1}{t} N_- = R^2\int_{1/\sqrt{2}}^{1-\Upsilon} n_w 2\pi\alpha u'(\alpha)d\alpha . \qquad (17)$$

Assuming moreover that $u'(\alpha) = u(\alpha)$, (16), and (17) after substitution from (15) become

$$N_+ = \frac{nQt}{4} \qquad (18)$$

and

$$N_- = -\frac{nQt}{1 - 4\Upsilon}\left[\frac{1}{2} - (1 - \Upsilon)^2\right]^2 ; \qquad (19)$$

$N_- = 0$ when $1 - \Upsilon = 1/\sqrt{2}$. The net accumulation is

$$\Delta N = N_+ + N_- = nQt\left(\frac{\Upsilon}{1 - 4\Upsilon}\right)\left[(2 - \Upsilon)(1 - \Upsilon)^2 - 1\right] . \qquad (20)$$

Values of N_+ and N_- calculated from (18) and (19) are listed in Table VI. The measured and calculated N_+ are in good agreement.

At $\alpha > 1/\sqrt{2}$, and when c_w is not constant but decreases between $\alpha = (1 - \Upsilon)$ and $1/\sqrt{2}$, N_- tends to increase numerically; the slip velocity of the particles tend also to increase N_-. For these reasons N_- calc./N_- meas. < 1 and the resulting values of ΔN are about twice those measured experimentally.

(d) Binary systems

Applying (20) to a dilute binary suspension of rigid spheres yields

$$n_i' = n_i \left[1 + Qt\left(\frac{\Upsilon_i}{1 - 4\Upsilon_i}\right)\right]\left[(2 - \Upsilon_i)(1 - \Upsilon_i)^2 - 1\right], \; i = 1, 2 \qquad (21)$$

from which it follows

$$\frac{n_1'}{n_2'} = \frac{n_1\left[1 - 4\Upsilon_1 + Qt\Upsilon_1\left[(2 - \Upsilon_1)(1 - \Upsilon_1)^2 - 1\right]\right]\left[1 - 4\Upsilon_2\right]}{n_2\left[1 - 4\Upsilon_2 + Qt\Upsilon_2\left[(2 - \Upsilon_2)(1 - \Upsilon_2)^2 - 1\right]\right]\left[1 - 4\Upsilon_1\right]} \qquad (22)$$

Calculated values of $(n'_1/n'_2)/(n_1/n_2)$ from (22) are listed in Table VII, and as may be seen are greater than those observed. It was shown earlier that for a monodisperse suspension $\Delta N_{calc.} > \Delta N_{meas.}$ Because $\Upsilon_1 > \Upsilon_2$ the particles of species 1 lag the flow more than those of 2 and consequently $(\Delta N_1/\Delta N_2)_{meas.} < (\Delta N_1/\Delta N_2)_{calc.}$

2. Emulsions

It has been shown[10,15,16] that, at positions remote from the meniscus where the velocity is given by (1), deformed fluid drops migrate towards the tube axis due to the influence of the wall. The rate of migration increases with increasing b; in the emulsion used the theory[16] predicts that a drop $b_1 = 10^{-2}$cm. near the tube wall has a radial velocity $- dr/dt = 0.03$ cm.sec.$^{-1}$, while for $b_2 = 0.5 \times 10^{-2}$cm. the migration velocity is only 0.002 cm.sec.$^{-1}$. Thus, n_1/n_2 should vary along the tube and be higher near the meniscus.

An exact calculation of the variation of n_1/n_2 along the tube in a flowing emulsion is complicated but an estimate of the relative effects of radial migration of fluid drops at high $|\beta|$ and of radial flow at low $|\beta|$ on particle accumulation behind an advancing meniscus may be obtained as follows.

Consider a binary emulsion of $b_1 = 10^{-2}$cm. and $b_2 = 0.5 \times 10^{-2}$cm. under the conditions defined in Fig. 8; n_1/n_2 may be obtained from the initial distribution curve of Fig. 8a. Since the emulsion is dilute and particle-particle interactions are neglected, n'_1/n'_2 for the binary system considered here, would be the same as for the polydisperse emulsion of Fig. 8a, and thus may be obtained from the final distribution curve. The values so obtained are listed in Table IX.

Consider next a binary suspension of rigid spheres of the same radius (i.e. $b_1 = 10^{-2}$cm. and $b_2 = 0.5 \times 10^{-2}$cm.); $(n'_1/n'_2)/(n_1/n_2)$ was evaluated from (22) and is given in Table IX. Comparison between $(n'_1/n'_2)/(n_1/n_2)$ for drops and rigid spheres indicates that the effect is mainly due to the radial migration of drops. This is in line with the explanation of Forgacs et al[2] for the accumulation at the meniscus observed with deformable pulp fibre suspensions.

Corresponding effects (particle depletion and size separation) may logically be expected in front of receding menisci, and warrant study.

It is conceivable that these interesting meniscus effects may lead to useful techniques of phase separation and of particle fractionation.

LIST OF SYMBOLS

A	=	net total increase in volume of suspended phase behind the meniscus Eq.(12)
b; $\bar{b}$	=	radius of rigid sphere and undeformed drop; mean value
c; c_w, $c(\beta)$	=	volume fraction of the suspended phase; at $(1 - \Upsilon) > \alpha > 1/\sqrt{2}$ and at β
L	=	tube length
n, n'; n_w	=	number of particles per $cm.^3$ in the bulk of the suspension and at the meniscus; at $(1 - \Upsilon) > \alpha > 1/\sqrt{2}$
N_1, N_2	=	number of particles contained in the volume $\pi R^2 \lvert x \rvert$ initially and at the end of the experiment
N_+, N_-	=	number of particles entering and leaving a cross-section of the tube remote from the meniscus in time t
ΔN	=	$N_+ + N_-$
$q^*(a)$; $q(a)$	=	flux at α with the tube fixed; with the tube moving at velocity $- \bar{u}$
Q	=	volumetric flow rate through the tube
r; Δr	=	radial distance from the tube axis; difference in r
r, x	=	cylindrical polar coordinates
R	=	radius of tube
t	=	time
$u^*(\alpha)$; $u(\alpha)$	=	streamline velocity at α with the tube fixed; with the tube moving at velocity $- \bar{u}$
$\bar{u}$	=	average fluid velocity in the tube
$u'(\alpha)$	=	translational velocity of a sphere whose center is at α
$v(\alpha)$	=	radial velocity of fluid
x; Δx	=	axial distance from the meniscus; difference in x
α; α_m	=	r/R; maximum α of a streamline
α_1, α_2; α_1', α_2'	=	initial and final positions of a streamline and particle center near the meniscus; at the tube inlet

$\alpha(v_m)$	=	radial position at which the radial velocity is greatest
$\Delta\alpha$, $\Delta\alpha'$	=	difference in radial positions of sphere center and the reference streamline at the meniscus and tube inlet respectively
$\Delta\alpha_2$	=	difference in radial positions of the centers of interacting and non-interacting spheres
β; β_m	=	$-x/R$; maximum value for a streamline
γ	=	b/R
η_o; ρ	=	viscosity medium; density
ϕ	=	azimuthal angle of the axis of the doublet
ϕ_o, $-\phi_o$	=	angles of collision and separation of the doublet
Ψ	=	Stokes stream function

REFERENCES

1. This Thesis, Part II.
2. FORGACS, O.L., ROBERTSON, A.A. and MASON, S.G. Fundamentals of Papermaking Fibres 447, British Paper and Board Maker's Association, Kenley, Surrey, England (1958)
3. FAHRAEUS, R. Physiol. Reviews 9, 241 (1929)
4. FAHRAEUS, R. and LINDQUIST, T. Amer. J. Physiol. 96, 562 (1931)
5. VEJLENS, G. The distribution of leucocytes in the vascular system. Acta path microbiol. scand. Suppl. XXXIII (1938)
6. WHITMORE, R.L. Rheology of Disperse Systems. Ed. by C.C. Mill. Pergamon Press 49 (1959)
7. MAUDE, A.D. and WHITMORE, R.L. Brit. J. Appl. Phys. 7, 98 (1956)
8. MAUDE, A.D. Brit. J. Appl. Phys. 10, 371 (1959)
9. BATTACHARJI, S. and SAVIC, P. Proc. of the 1965 Heat Transfer and Fluid Mechanics Inst. Ed. by A.F. Charwat et al. Stanford University Press 1965.
10. GOLDSMITH, H.L. and MASON, S.G. J. Colloid Sci. 17, 448 (1962)
11. GOLDSMITH, H.L. and MASON, S.G. Proc. Roy. Soc. A282, 569 (1964)
12. LANGHAAR, H.L. J. Appl. Mech. 9; Trans. Am. Soc. Mech. Engrs. 64, 55A (1942)
13. BRENNER, H. Private communication
14. GOLDSMITH, H.L. and MASON, S.G. Chapter prepared for inclusion in "Rheology" Ed. by F.R. Eirich (1965)
15. This Thesis, Appendix II
16. CHAFFEY, C.E., BRENNER, H. and MASON, S.G. Rheol. Acta 4, 64 (1965)
17. SEGRE, G. and SILBERBERG, A. Nature 189, 209 (1961)

TABLE I

Comparison of measured and calculated volume flow rates behind the advancing meniscus

$R = 0.2$ cm. $\quad Q_{meas.} = 0.178 \times 10^{-2} \text{cm.}^3 \text{sec.}^{-1}$

β	$10^2 \times Q_{calc.}$ a)
0	0.182
- 0.25	0.174
- 0.50	0.175
$\leq$ - 0.75	0.178

$$\text{Mean } \frac{Q_{calc.}}{Q_{meas.}} = 0.996$$

a) Calculated from measured $u^* = u + \bar{u}$ by graphical integration of Equation (3).

TABLE II

Radial displacement of spheres in a convergence

$$Q = 0.711 \times 10^{-2}\,\text{cm.}^{3}\,\text{sec.}^{-1}$$

b cm.	Entrance effects ($R_1 \rightarrow R_2$)					Exit effects ($R_2 \rightarrow R_1$)				
	R_1 = 0.4 cm.		R_2 = 0.1 cm.		a) $\Delta\alpha'$	R_2 = 0.1 cm.		R_1 = 0.4 cm.		a) $\Delta\alpha'$
	$(R_1 - r)$cm.	α_1'	$(R_2 - r)$cm.	α_2		$(R_2 - r)$cm.	α_2'	$(R_1 - r)$cm.	α_1'	
0.016	0.032	0.920	0.016	0.840	0.080	0.016	0.840	0.040	0.900	- 0.060
0.016	0.047	0.883	0.016	0.840	0.043	-	-	-	-	-
0.011	0.030	0.925	0.011	0.889	0.036	0.011	0.889	0.037	0.910	- 0.021
0.011	0.035	0.913	0.011	0.889	0.024	-	-	-	-	-
0.013	0.100	0.750	0.025	0.748	0.002	0.025	0.748	0.100	0.750	- 0.002
0.017	0.142	0.645	0.036	0.640	0.005	0.036	0.640	0.142	0.645	- 0.005
0.014	0.284	0.290	0.072	0.282	0.008	-	-	-	-	-

a) The positive and negative signs indicate an inward and outward displacement respectively.

TABLE III

Two-body interactions near the advancing meniscus

R = 0.4 cm. $\quad \gamma = 0.128 \pm 0.003 \quad Q = 3.56 \times 10^{-2}$ cm.^{3} sec.$^{-1}$

Doublet				Singlet		$\Delta\alpha_2$	
α_1		α_2		α_2			
Sphere 1	Sphere 2	Sphere 1	Sphere 2	Sphere 1	Sphere 2	Sphere 1	Sphere 2
0.335	0.284	0.845	0.837	0.833	0.845	– 0.012	0.008
0.267	0.196	0.837	0.852	0.748	0.860	0.011	0.008
0.514	0.474	0.749	0.807	0.780	0.794	0.031	– 0.013
0.028*	0.017*	0.849	0.849	0.870	0.870	0.021	0.021
0.485*	0.443*	0.715	0.812	0.790	0.803	0.075	– 0.007
0.466	0.398	0.772	0.823	0.797	0.820	0.025	– 0.003
0.517*	0.409*	0.706	0.755	0.730	0.814	0.024	0.059
0.440*	0.358*	0.687	0.817	0.805	0.827	0.118	0.010
0.582*	0.494*	0.720	0.744	0.757	0.786	0.037	0.042
0.421	0.372	0.809	0.812	0.810	0.824	0.001	0.012
0.404	0.414	0.832	0.795	0.815	0.812	0.017	0.017
0.233*	0.188*	0.809	0.789	0.853	0.860	0.044	0.061

The asterisks indicate rotating doublets.

TABLE IV

Particle accumulation behind an advancing meniscus

PVA spheres   R = 0.2 cm.   L = 85 cm.

c	$10^2 \times Q$ $cm.^3 sec.^{-1}$	γ	$10^3 \times A$ $cm.^3$ a)
0.035	1.78	0.078	0.48
0.10	1.78	0.078	1.0
0.18	1.78	0.078	3.2
0.32	1.78	0.078	7.7
0.32	0.356	0.078	7.7
0.32	3.56	0.078	7.7
0.32	0.356	0.018	2.1

a) By graphical integration of Equation (12).

TABLE V

Effect of convergence on particle accumulation near the meniscus

$c = 0.18$ $\tau = 0.078$ $Q = 1.78 \times 10^{-2}$ cm.^{3} sec.$^{-1}$

$c(\beta)$	$c(\beta) - c$	Remarks
0.52 [a)]	0.34	With convergent entrance effects
0.47	0.29	Without convergent entrance effects

a) From Fig. 7a for $|\beta| < 10.4$.

TABLE VI

Particle accumulation near the meniscus

$Q = 0.178 \times 10^{-2} \text{cm.}^3 \text{sec.}^{-1}$ $R = 0.2$ cm. $\gamma = 0.075$ $c = 0.025$

t secs.	Measured						Calculated				$\frac{N_+ \text{calc.}}{N_+ \text{meas.}}$	$\frac{N_- \text{calc.}}{N_- \text{meas.}}$
	N_+	N_-	$\Delta N = N_+ + N_-$ a)	N_1	N_2	$N_2 - N_1$ b)	N_1 c)	N_+ Eq.(18)	N_- Eq.(19)	ΔN Eq.(20)		
131	110	- 94	16	65	80	15	66	102	72	30	0.93	0.77
160	121	- 99	22	74	93	19	66	124	87	37	1.02	0.88

a) Dynamic measurement.

b) Static measurement.

c) From $N_1 = \frac{3c|\beta|}{4\gamma^3}$ using $c = 0.025$, and $|\beta| = 1.5$.

TABLE VII

Particle fractionation behind the meniscus in binary systems of rigid spheres

R = 0.4 cm.   Q = 0.142 $cm.^3 sec.^{-1}$ L = 40 cm.   Qt = 20 $cm.^3$

$10^2 \times c_1$	$10^2 \times b_1$ cm.	$10^2 \times c_2$	$10^2 \times b_2$ cm.	b_1/b_2	n_1/n_2	n_1'/n_2'	$(n_1'/n_2')/(n_1/n_2)$ Meas.	Eq.(22)
0.18	2.2	0.030	0.7	3.1	0.19	0.21	1.1	1.5
2.7	6.5	0.032	0.7	9.3	0.11	0.24	2.2	2.7
16.7	6.5	1.52	2.2	3.0	0.43	0.65	1.5	1.8

TABLE VIII

Effect of slip velocity on particle accumulation behind an advancing meniscus

$$Q = 0.711 \times 10^{-2} \text{cm.}^3 \text{sec.}^{-1} \qquad u_{R_2}/u_{R_1} = 16$$

$R_1 = 0.4$ cm.				$R_2 = 0.1$ cm.				
α_1	$10^2 \times u^*(\alpha_1)$ a) cm.sec.$^{-1}$	$\frac{u'(\alpha_1)}{u^*(\alpha_2)}$ b)	$10^2 \times u'(\alpha_1)$ cm.sec.$^{-1}$	α_2	$10^2 \times u^*(\alpha_1)$ a) cm.sec.$^{-1}$	$10^2 \times u^*(\alpha_2)$ a) cm.sec.$^{-1}$	$\frac{u'(\alpha_2)}{u^*(\alpha_2)}$ b)	$10^2 \times u'(\alpha_2)$ cm.sec.$^{-1}$
0.920	0.423	0.715	0.303	0.840	6.78	13.2	0.815	6.50
0.883	0.622	0.772	0.481	0.840	9.96	13.2	0.815	6.50
0.925	0.396	0.712	0.282	0.889	6.34	9.52	0.760	7.24*
0.913	0.466	0.665	0.310	0.889	7.47	9.52	0.760	7.24
0.750	1.24	0.877	1.19	0.748	19.8	19.9	0.877	17.5
0.645	1.65	0.922	1.52	0.640	26.4	26.7	0.925	24.7
0.290	2.59	0.99	2.56	0.282	41.4	41.6	0.99	41.2

a) From (1).

b) From Fig. 9.

TABLE IX

Effect of radial migration of fluid drops on fractionation of a dilute emulsion at the meniscus

$R = 0.075$ cm. $Qt = 0.53$ cm.^{3}

Fluid Drops					Rigid Spheres		
$10^2 \times b_1$ cm.	$10^2 \times b_2$ cm.	n_1/n_2 a)	n'_1/n'_2 b)	$\frac{n'_1/n'_2}{n_1/n_2}$	$10^2 \times b_1$ cm.	$10^2 \times b_2$ cm.	$\frac{n'_1/n'_2}{n_1/n_2}$ c)
1	0.5	1	2.7	2.7	1	0.5	1.12

a) From the initial distribution curve of Fig. 8a.

b) From the final distribution curve of Fig. 8a.

c) From (22).

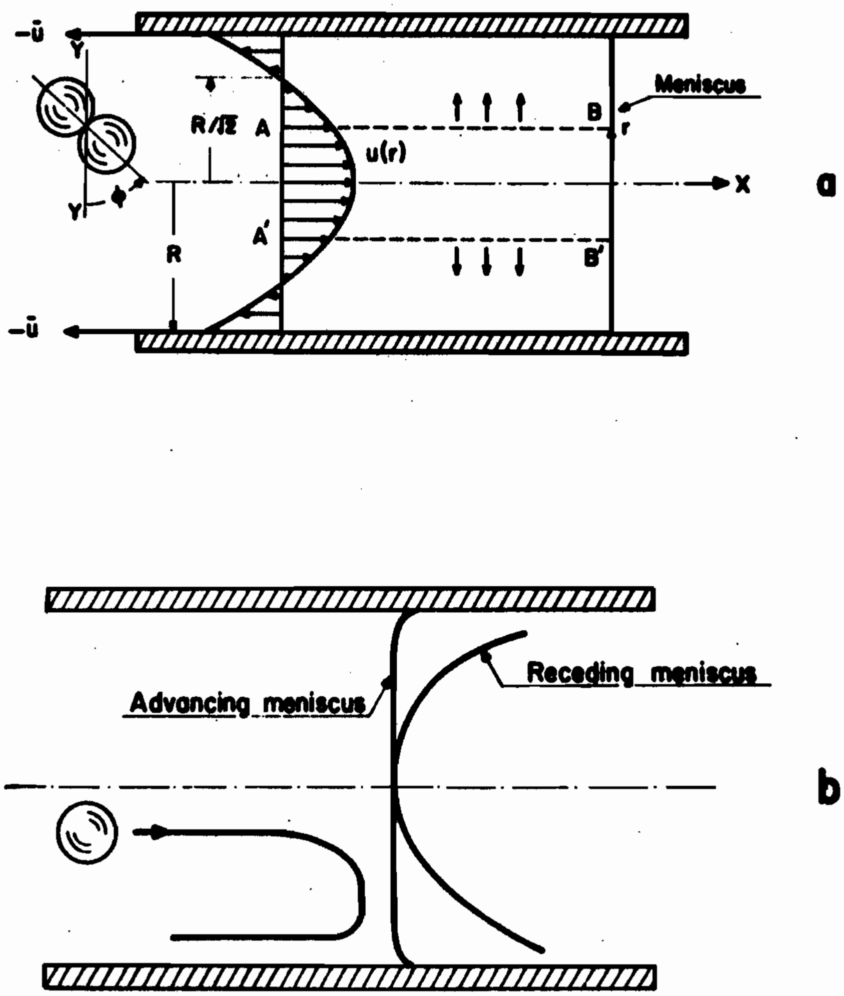

<u>Figure 1</u> (a) Flow behind an advancing meniscus which is rendered stationary by moving the tube with a velocity $-\bar{u}$. The azimuthal angle ϕ of a doublet of spheres is also shown on the left.

(b) Tracings from photographs of an advancing and a receding meniscus in a tube R = 0.2 cm. at $Q = 1.78 \times 10^{-3}$ cm.^{3} sec^{-1}. The path of a sphere center behind the advancing meniscus is also shown.

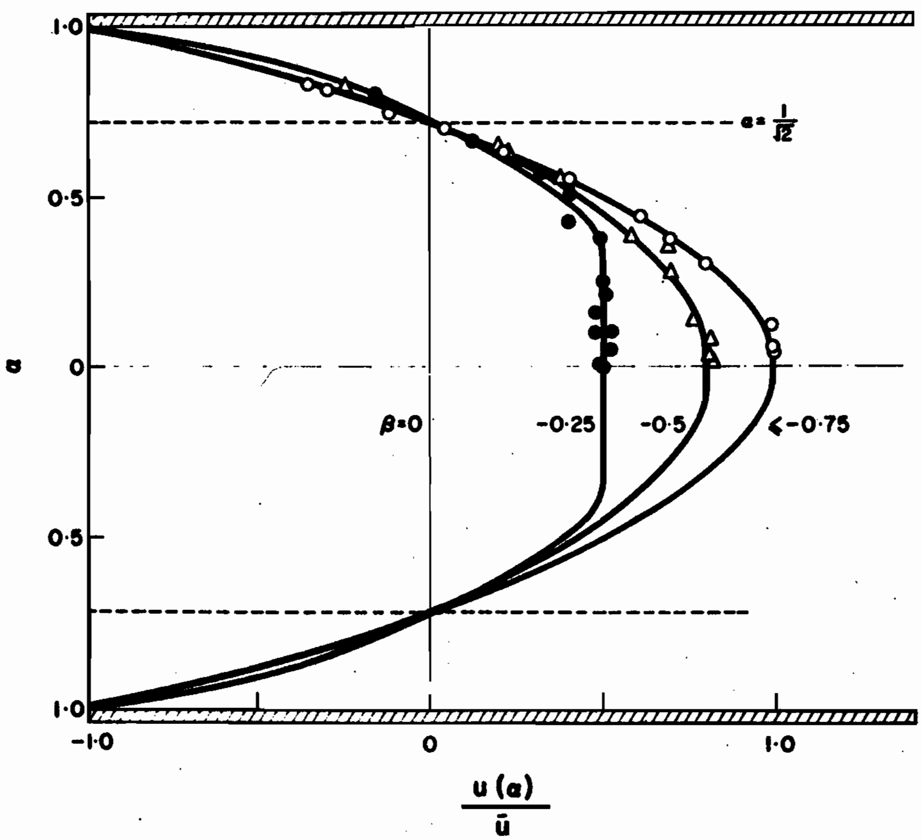

Figure 2 Dimensionless plots of axial velocity profiles of the pure liquid behind the advancing meniscus; R = 0.2 cm. and Q = 1.78 x 10^{-3} cm.^{3} sec.$^{-1}$ and various values of β. The profile becomes parabolic at β = - 0.75.

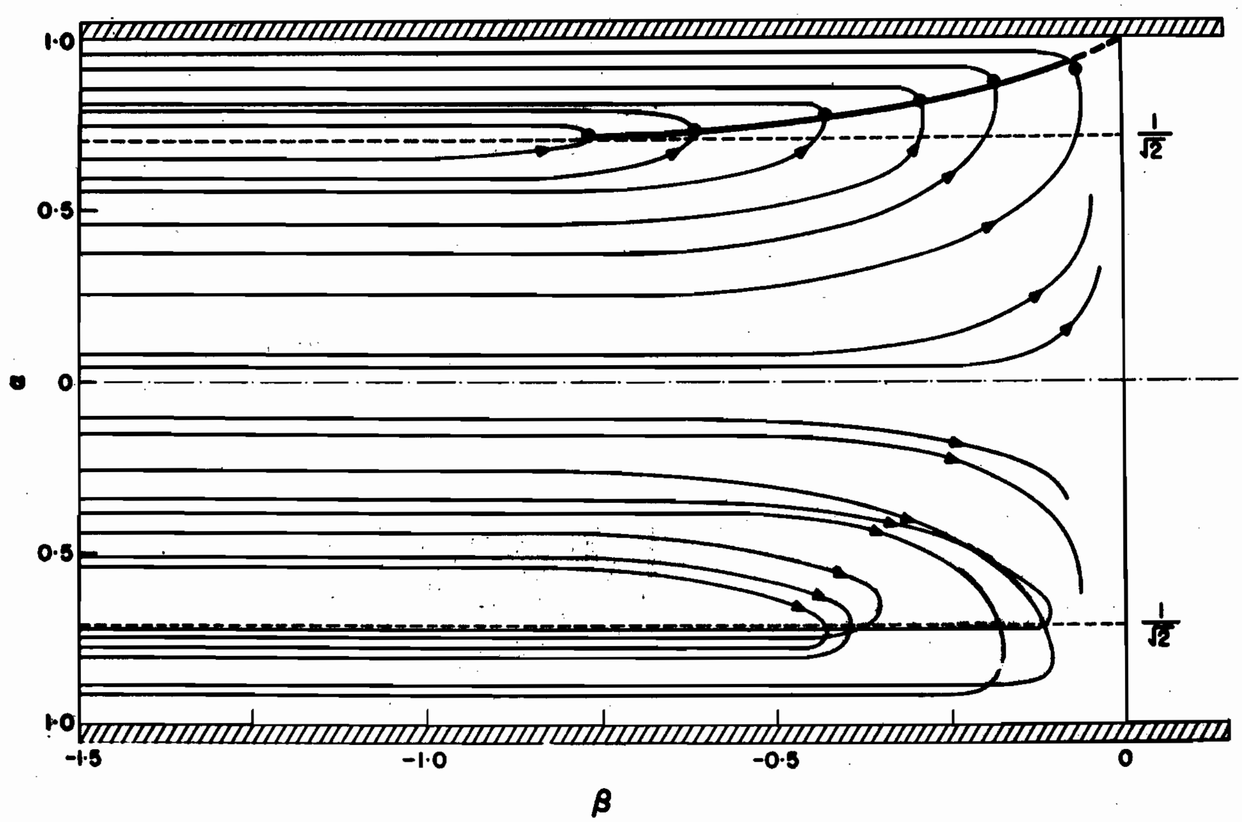

Figure 3 Flow behind the advancing meniscus in a tube R = 0.2 cm. at $Q = 1.78 \times 10^{-3}$ cm.^{3} sec^{-1}.

The upper part shows the streamline pattern behind the advancing meniscus measured with aluminum tracer particles ($\gamma < 0.003$); the closed circles indicate the point at which the streamlines loop backwards.

The lower part shows the loci of sphere centers for c = 0.025 and $\gamma = 0.075$. Because of the difference in $\Delta\alpha$ between interacting and non-interacting particles the paths cross one another.

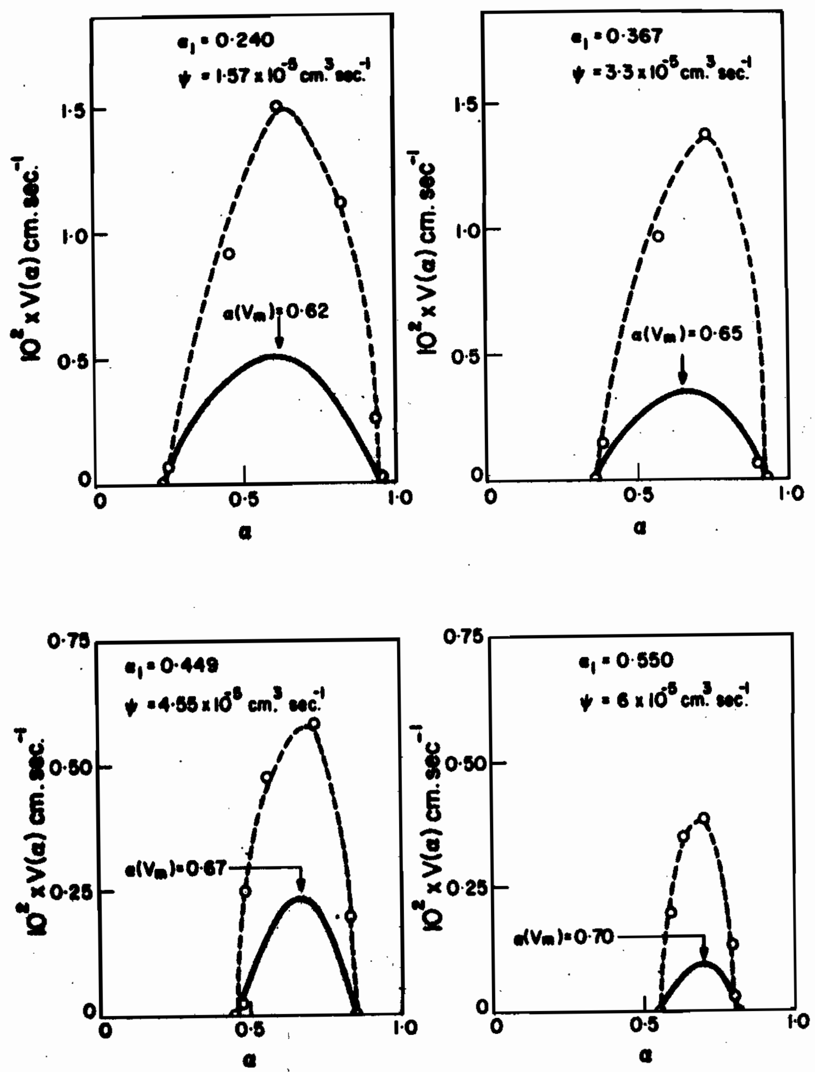

Figure 4 Comparison of measured (broken lines) and calculated (solid lines) from (10) radial velocities of the liquid behind the advancing meniscus in a tube R = 0.2 cm. and Q = 1.78 x 10^{-3} cm.^{3} sec.$^{-1}$ at different α_1. The values of Ψ and $\alpha(v_m)$ calculated from (7) and (11) are also shown.

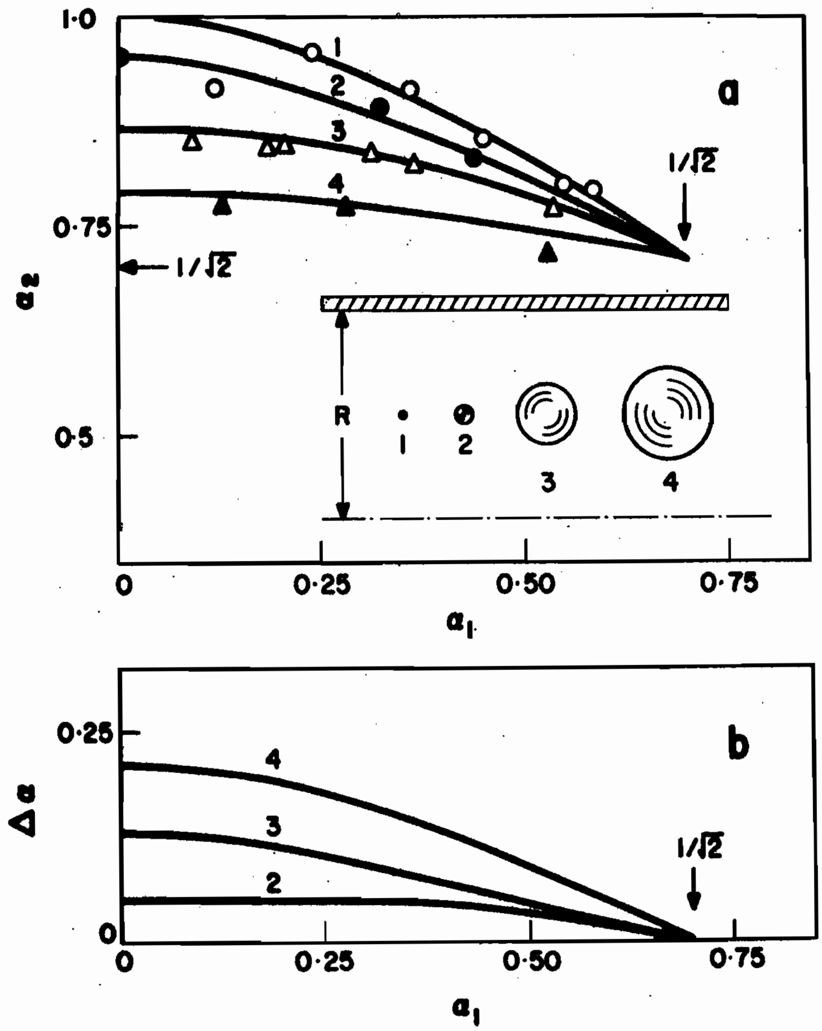

<u>Figure 5</u> Radial displacement of isolated rigid spheres due to radial flow near the advancing meniscus in a tube R = 0.4 cm. at $Q = 3.56 \times 10^{-2}$ cm.^{3} sec^{-1}.

(a) Dimensionless plot showing the effect on α_2 of γ and α_1. Curve 1: $\gamma < 0.003$; curve 2: $\gamma = 0.038$; curve 3: $\gamma = 0.130$ and curve 4: $\gamma = 0.213$. The relative sizes of the spheres are shown in the insert.

(b) Dimensionless plot showing the displacement of spheres from their entering streamlines near the meniscus as a function of α_1. The curves were drawn from Part (a) employing the relation $\Delta\alpha = \alpha_2(o) - \alpha_2(\gamma)$.

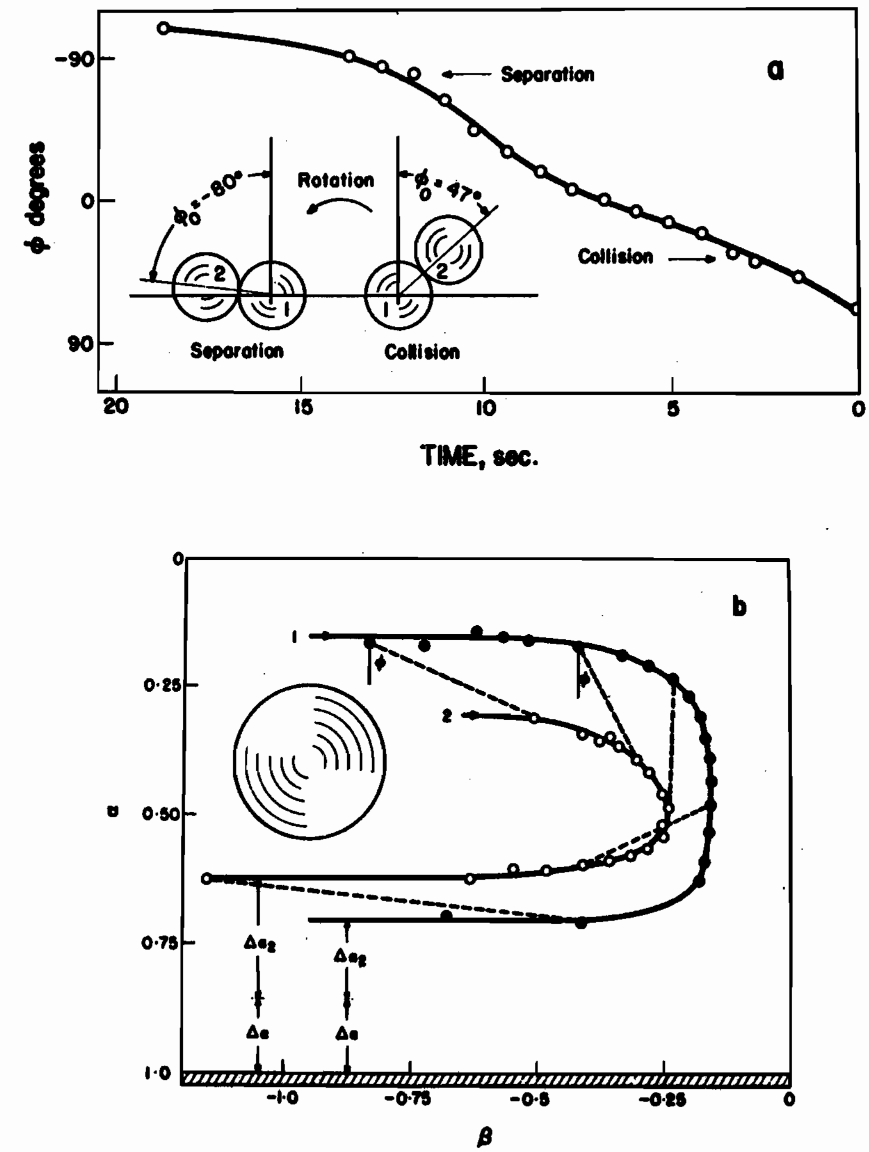

<u>Figure 6</u> Two-body collisions of rigid spheres near the advancing meniscus. $R = 0.3$ cm, $Q = 1.78 \times 10^{-2}$ cm.^{3} sec^{-1}, $b_1 = 0.0455$ cm. and $b_2 = 0.0470$.

(a) Variation of angle ϕ with time. The arrows indicate the angles of collision ϕ_o and separation $-\phi_o$; the configurations of the doublet at collision and separation are also shown.

(b) Dimensionless plot of the paths of particle centers. The numbers in the curves correspond to spheres 1 and 2 of Part (a); the broken lines join the particle centers at a given time and because α and β are drawn to the same scale their angle with the Y-axis is the angle ϕ. The relative size of the spheres, and the values of $\Delta\alpha_2$ for each sphere of the doublet after separation as well as $\Delta\alpha$ are shown. In this doublet the two centers were not both in the plane of the drawing.

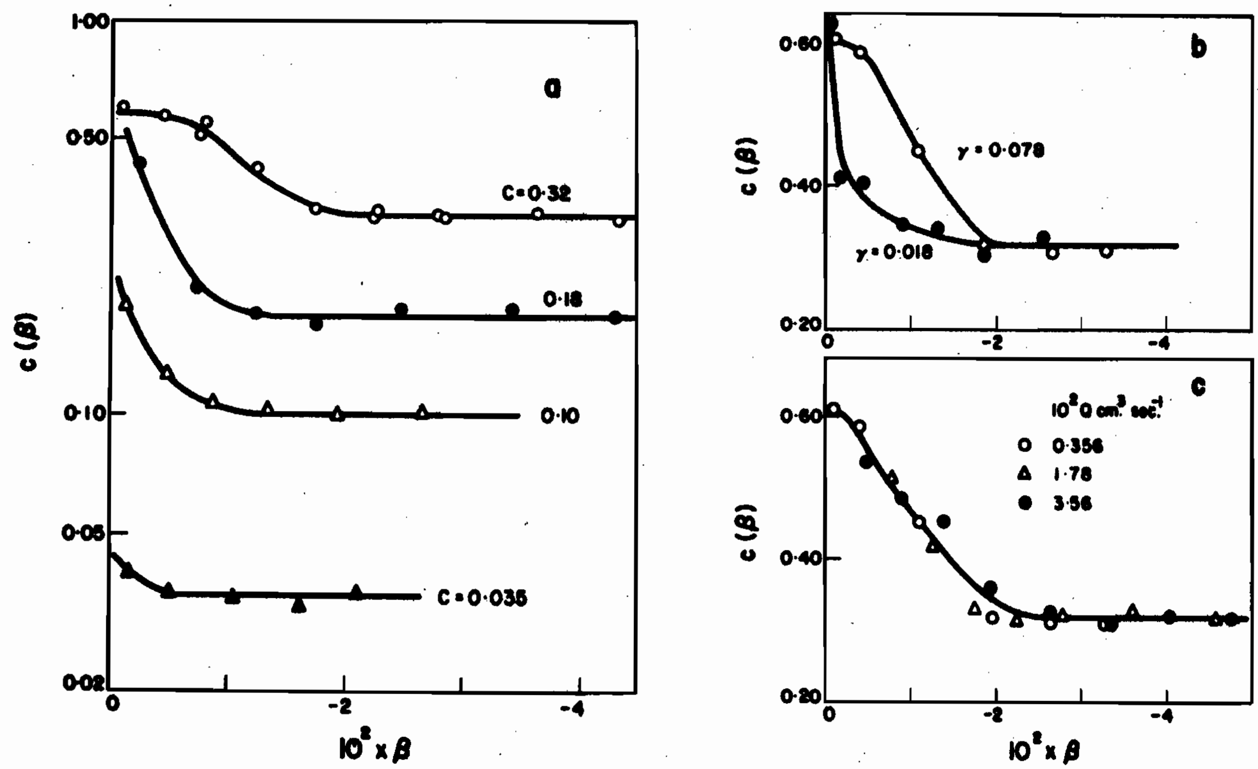

<u>Figure 7</u> Particle accumulation behind the advancing meniscus in suspensions of PVA spheres. R = 0.2 cm. L = 85 cm.

(a) Semi-logarithmic plot showing the effect of concentration; γ = 0.078 and Q = 1.78 x 10^{-2} cm.^{3} sec^{-1}.

(b) Effect of particle size; Q = 0.356 x 10^{-2} cm.^{3} sec^{-1}.

(c) Effect of flow rate; γ = 0.078.

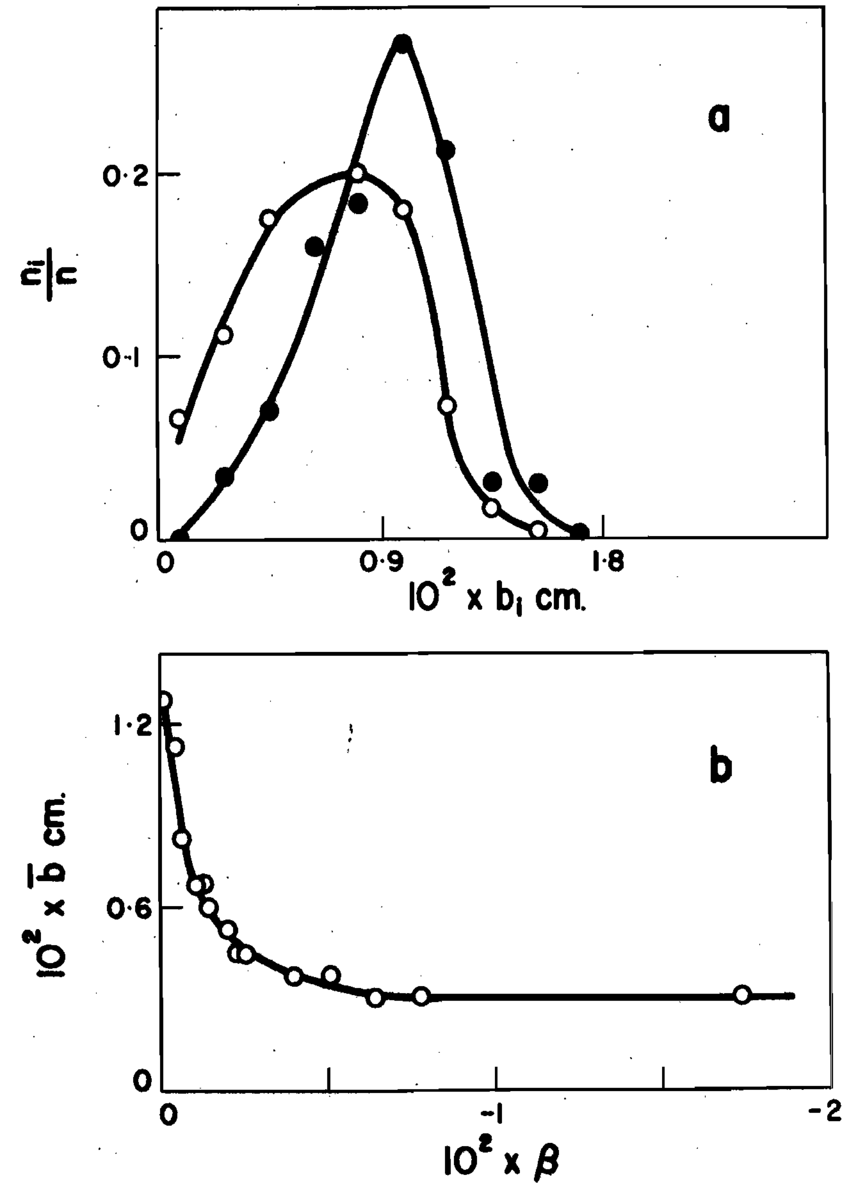

Figure 8 Particle fractionation in a c = 0.01 emulsion of 60% Ucon oil 1715 + 40% Carbon tetrachloride (by volume) in 98% glycerol in water solution flowing in a tube R = 0.075 cm. at $Q = 4 \times 10^{-3}$ cm.^{3} sec^{-1}.

(a) Plot of relative frequency against drop radius near the meniscus initially (open circles) and after the emulsion travelled 30 cm. in the tube (closed circles).

(b) Volume average particle diameter vs. distance from the meniscus after the emulsion travelled approx. 60 cm. in the tube.

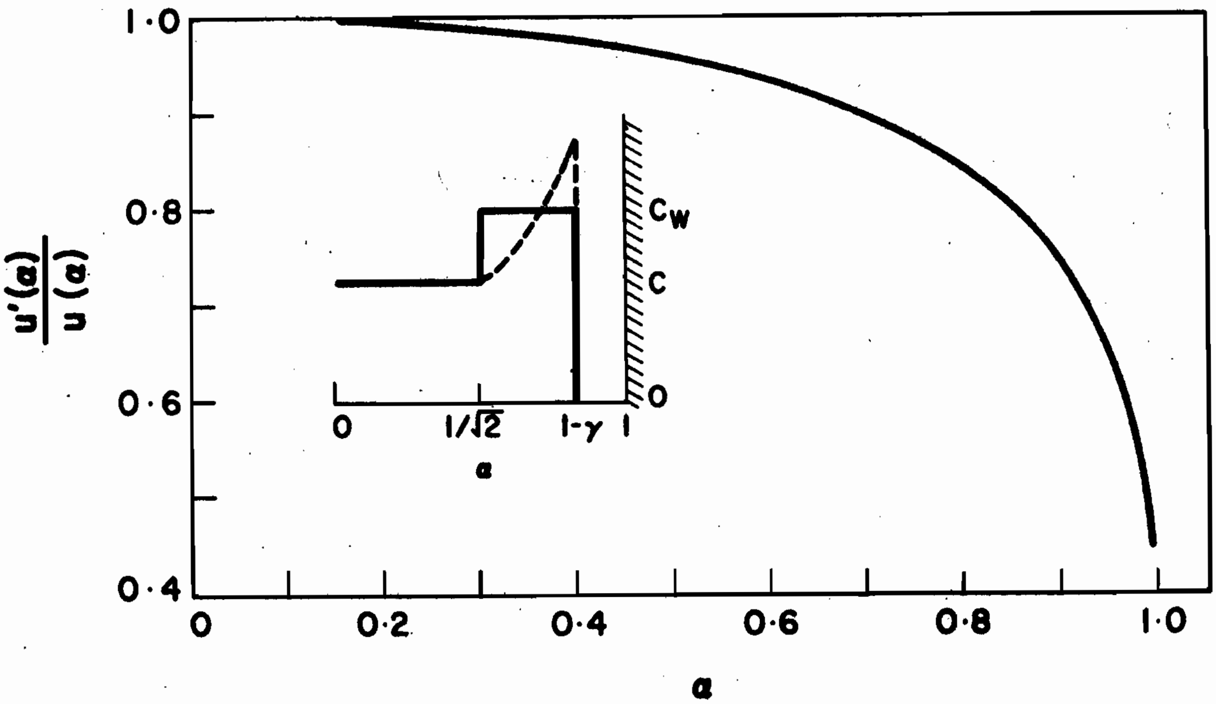

Figure 9 Dimensionless plot showing the effect of the wall proximity on the axial velocity of a sphere[13]. In the insert the assumed distribution of particle centers (solid line) used to calculate the accumulation behind the meniscus is shown; the dashed line is probably a better approximation.

PART V

PARTICLE BEHAVIOUR IN VISCOELASTIC FLUIDS

ABSTRACT

The behaviour of rigid and deformable particles suspended in viscoelastic fluids undergoing slow Couette and Poiseuille flows was studied experimentally.

In tube flow the particles migrated from the wall to a limiting radial position at which the velocity gradient was effectively zero; in Couette flow between concentric rotating cylinders migration occurred towards the outer cylinder wall.

The rotations of rigid rods and discs were similar to those in newtonian liquids, except for a steady drift in orbit constant to asymptotic values which in newtonian liquids correspond to minimum energy dissipation.

Two-body collisions of rigid uniform spheres were unsymmetrical and irreversible.

The deformation and burst of newtonian liquid drops were as in newtonian suspending liquids of comparable suspending phase viscosity, except for the alignment angle of the drop at zero deformation.

INTRODUCTION

Previous publications from this laboratory[1-7] have dealt with the translation, rotation and interactions of small rigid and deformable particles suspended in newtonian liquids undergoing laminar viscous flow in Couette and Poiseuille flows.

This part of the thesis represents an extension of the earlier studies to viscoelastic suspending fluids in which normal stress effects may be expected to influence the behaviour of the suspended particles. A preliminary experimental investigation is described of the radial migration of rigid particles across the planes of shear, the rotation of rigid cylinders, two-body interactions of rigid spheres and the deformation of newtonian liquid drops. Comparisons are made with the corresponding phenomena in newtonian liquids.

EXPERIMENTAL PART

The experimental methods of producing Couette flow between counter rotating cylinders and Poiseuille flow in tubes have been described previously[8]. The experiments were performed in a thermostated room maintained at 22 $\pm$ 0.5°C. Polyisobutylene (PIB) in decahydronaphthalene (Decalin) solutions of weight fractions c_p from 0.01 to 0.063 were used in the tube experiments. Such solutions are viscoelastic and have been well characterized rheologically[9-13]; the density ρ varied from 0.8875 to 0.8908 g.cm.$^{-3}$ and the refractive index from 1.4775 to 1.4793.

The experiments in Couette flow were carried out using a c_p = 0.04 polyacrylamide (PAA) in water solution (ρ = 1.002 g.cm.$^{-3}$) as a viscoelastic suspending phase. To avoid end effects[1] a low viscosity 50:50 mixture of carbon tetrachloride and 10p. silicone oil was used as bottom layer.

Both the PIB and PAA solutions were non-newtonian, the apparent viscosity η_a when measured in a rotational viscometer (Epprecht Rheomat 15) decreasing with increasing the rate of shear G (Fig. 1).

In most of the Couette experiments (except those on radial migration) the particles were rendered stationary[1] by adjusting the angular speeds Ω_1 and Ω_2 of the counter-rotating cylinder walls, and observed through a microscope directed along the Z-axis of the field (Fig. 2a). In the tube, observations were made in the median plane MM' normal to the viewing axis, i.e. along the Z-axis of the field of motion defined in Fig. 2b.

The systems studied and their relevant properties are listed in Table I. System 1 was used to measure the velocity profiles, and 2 to 4 radial migration in tube flow. The velocity profiles were determined by timing the particles between two positions of the observation microscope. The distance along the tube was computed from the readings of a revolution counter, while the distance from the tube wall was measured by means of a calibrated micrometer eyepiece. System 7 was used to study radial migration in Couette flow. The distance of the sphere center from the inner cylinder wall was measured with the aid of a calibrated dial gauge coupled to the microscope.

The rotations and drift in the orbit of rigid cylindrical particles were studied in Systems 4, 5, 6, 8 and 9. The particles were photographed through the microscope by means of a cine camera (Paillard Bolex 16 mm. reflex camera) aligned with the wall of the apparatus, and the films analysed by projecting them onto a drafting table. The azimuthal angle ϕ of the axis of revolution (Fig. 2) was measured directly from the films. The colatitudinal angle θ was computed with the aid of the following relations:

$$\text{rods} \qquad a'(\phi) = a \sin \theta \; ; \tag{1}$$

$$\text{discs} \qquad b'(\phi) = b \cos \theta \; , \tag{2}$$

where 2a, 2b are the length of the axis of revolution and equatorial diameter respectively and $2a'(\phi)$, $2b'(\phi)$ their projected lengths on the XY plane at ϕ.

Two body collisions between rigid spheres were studied in System 7. The paths of approach and recession were determined by measuring the distances Δx and Δy of a sphere center from the mid-point of the line joining the centers of the two interacting spheres. The angles of collision were measured by the method of Allan and Mason[3)] i.e. assuming rectilinear approach and recession.

Liquid drops (Systems 10 to 14) were formed from a stainless steel hypodermic needle tip connected to a 2 $cm.^3$ syringe. The tip was immersed under the suspending liquid surface and the drops released by initiating the flow at the desired moment, so that their size could be varied; the radius b of the undeformed drop was determined from photographs taken under no flow conditions. The orientation and deformation of liquid drops were investigated by photographing the deformed drop. The deformation D defined as[14)]

$$D = \frac{L - B}{L + B} \; , \tag{3}$$

and the alignment angle ϕ_m were measured; L and B are the length and breadth of the elliptical equator of the drop (Fig. 2c).

1. Poiseuille Flow

(a) General Observations

When $c_p < 0.04$ the polymer solutions showed newtonian behaviour at the shear rates existing in the tube and no radial migration of rigid particles was observed over prolonged periods of flow (2 to 3 hrs.); when $c_p > 0.04$, they migrated away from the wall.

The rotation about the Z-axis of rods and discs in solutions of $c_p > 0.04$ were found to be in partial agreement with Jeffery's[15] equations for the rotation of a spheroid suspended in a newtonian liquid undergoing plane Couette flow of gradient G:

$$\frac{d\phi}{dt} = \frac{G}{(r_e^2 + 1)} (r_e^2 \cos^2\phi + \sin^2\phi) , \qquad (4)$$

$$\frac{d\theta}{dt} = \frac{G(r_e^2 - 1)}{4(r_e^2 + 1)} \sin 2\phi \sin 2\theta , \qquad (5)$$

where θ, ϕ are the spherical polar coordinates of the axis of revolution (Fig. 2a) and r_e the equivalent ellipsoidal axis ratio[7]. It was observed that rods and discs followed (4), but not (5); instead, as discussed below, they showed a continuous drift in orbit constant to limiting values.

(b) Velocity profiles

The velocity distribution of a newtonian liquid flowing in a straight circular tube is parabolic[4,8], the streamline velicity u(r) at radial distance r from the tube axis being

$$u(r) = \frac{kR_o^2}{2} (1 - \frac{r^2}{R_o^2}) , \qquad (6)$$

where R_o is the tube radius, $k = 4Q/\pi R_o^4$ and Q the volumetric flow rate; the rotation of the field at r is

$$\omega(r) = -\frac{kr}{2} . \qquad (7)$$

When $c_p < 0.04$ it was found that the relative velocity profile determined by measuring the translational velocity $u'(r)$ and the angular velocity $\omega'(r)$ of small Eccospheres at several values of Q followed (6) and (7) (Fig. 3). This is to be expected since the polymer solutions behave as newtonian liquids, their apparent viscosity being constant over the range of G employed (Fig. 1). When $c_p > 0.05$, deviations from the parabolic distributions became apparent and the profile was blunted near the central region of the tube (Fig. 4).

(c) Spheres : radial migration

At c_p about 0.05, rigid spheres migrated inwards to a radial position at which the velocity profile was flat (Fig. 4a). The rate of migration increased with increasing particle radius b and radial distance from the tube axis; spheres initially located in the flat portion of the velocity profile neither rotated nor migrated radially (Fig. 4a).

The observed radial migration may arise from the combined action of normal stresses and velocity gradient. In PIB solutions the normal stresses increase with r[11,17] and consequently the pressure exerted on the sphere surface from the wall side may be greater than from the axis side, which can conceivably yield a net force pushing the sphere towards the tube center. The normal stresses depend only on the rate of shear[11], and when G = 0 the force would be expected to vanish. This is probably why the sphere stopped migrating inwards where the velocity profile became effectively flat. Brodnyan *et al*[12] on the other hand have shown that at low shear rates, where the viscosity is independent of G, the normal stresses are not observable. This may be the reason that no measurable radial migration was found in solutions of low c_p; it is conceivable that it would have been observed by greatly increasing Q.

When the concentration of spheres was increases, a marked dilution occurred at the wall because of radial migration. In contrast to the particle-free zone formed near the wall in suspensions of spheres in newtonian fluids at high Reynolds numbers[18)], the peripheral layer in viscoelastic liquids did not become particle-free but merely diluted. This is illustrated by photographs (Fig. 5a) of a suspension of polyvinyl acetate spheres of weight fraction c = 0.125; as may be seen after a period of flow the particles formed a central core consisting of aggregates, while the region near the tube wall contained only isolated particles. The layer thickness δ was defined as the distance from the wall in which only isolated spheres were present; since it was not constant along the tube the mean $\bar{\delta}$ was evaluated from the photographs (insert in Fig. 5b); $\bar{\delta}$ increased slowly with time and approximately 2 hrs. of flow were required before $\bar{\delta}/R_o$ (Fig. 5b) reached an equilibrium value $\bar{\delta}_\infty/R_o$ and which decreased with increasing c (Fig. 5c).

(d) Rods and discs : radial migration

Like spheres rigid cylinders rotated and migrated towards the tube axis until they reached the flat portion of the velocity profile after which rotation and radial migration ceased (Fig. 4b). At the same time, they drifted to limiting rotational orbits which in newtonian fluids in Couette flow correspond to the minimum energy dissipation[15)].

Period of rotation

Integration of (4) yields

$$\tan \phi = r_e \tan\left(\frac{2\pi t}{T}\right) , \qquad (8)$$

where T is the period of rotation given by

$$T = \frac{2\pi}{G}\left(r_e + \frac{1}{r_e}\right) . \tag{9}$$

G was evaluated from the experimentally determined velocity profile with an accuracy of better than $\pm$ 0.01. As found in newtonian liquids[4,5] the periods of rotation were less than those predicted by (9) when the actual axis ratio $r_p = a/b$ of the cylinders was used. Following earlier practice[7], the equivalent axis ratio r_e was evaluated from (9) using the experimental value of TG. For the rod and disc shown in Fig. 6 the values of r_e calculated from (9) were in reasonably good agreement (within 8%) with those obtained for similar particles in newtonian liquids[5,19].

Variation of ϕ

Fig. 6a shows the variation in ϕ for a rigid rod and disc plotted according to (8); the solid lines were calculated from (8) using the measured r_e, and as may be seen the agreement is good. Radial migration over a single rotation was effectively zero.

Drift in the orbit

The integrated form of (2) after rearranging the terms is

$$C^2 r_e^{\,2} \cot^2\theta = 1 + (r_e^{\,2} - 1) \cos^2\phi \tag{10}$$

where C is the orbit constant which can vary between 0 and ∞ depending on the initial orientation. It has been found experimentally that in newtonian liquids rigid cylinders maintain a constant C over more than a hundred particle rotations[5,19]; moreover, it has been shown[18] that the variation of $\cot^2\theta$ with $\cos^2\phi$ follows (10).

In non-Newtonian liquids Saffman[16] has shown theoretically that spheroidal particles should assume preferred orbits which are independent of the initial C. Assuming that the liquid deviates slightly from newtonian behaviour, and neglecting the fluid inertia, the rate of change of C with time is[16)]

$$\frac{1}{Cg(C/r_e)} \cdot \frac{dC}{dt} = \frac{G^2 \alpha_2}{\eta_o} \tag{11}$$

where α_2 is a phenomenological coefficient which measures the non-newtonian nature of the fluid, and $g(C/r_e)$ a function which depends on the particle shape and the suspending fluid; (11) does not predict in which direction C changes. Subsequent experiments by Saffman in Couette flow indicated that prolate spheroids (and rods) drift towards $C = 0$ their axes of revolution being parallel to the Z-axis, and oblate spheroids (and discs) towards $C = \infty$ the axis rotating in the XY plane (Fig. 7a); in these orbits rods exhibit a steady spin, whilst discs rotate with an angular velocity which (from (4)) is greatest at $\phi = \pi/2$ and least at $\phi = 0$.

Analogous behaviour was found in the present experiments, i.e. C evaluated from (10) using the measured θ and r_e, increased with time for discs and decreased for rods. This is illustrated in Fig. 7b and 7c by plotting $C/(1 + C)$ as a function of time; since this fraction varies from 0 to 1 as C changes from 0 to ∞, this is a convenient way of including $C = \infty$ in the plot.

The cylindrical particles did not reach their corresponding limiting orbit values until they were near the tube axis (Fig. 7c). Initially C changed rapidly over an interval of negligible radial migration to a value which depended on r/R_o and which was smaller for rods and larger for discs the farther the particle was initially located from the wall (Fig. 7b). This phenomenon was not observed in Couette flow and was probably due to the influence of the tube wall.

As a result of the drift in C the variation of θ with ϕ did not follow (10) as may be seen from Fig. 6b where $\cot^2\theta$ has been plotted against $\cos^2\phi$ for 1/4 of particle rotation. The solid lines were calculated from (10) using the experimental r_e and C, the latter evaluated at $\phi = 0$, and assuming newtonian behaviour (i.e. C = constant). As expected, the measured $\cot^2\theta$ deviated from those calculated from (10) towards higher values for rods (limiting $C = 0$, $\cot\theta = \infty$) and smaller for discs (limiting $C = \infty$, $\cot\theta = 0$).

2. Couette Flow

(a) Radial migration

In the Couette apparatus rigid spheres migrated towards the outer cylinder. This is shown in Fig. 8 where the radial distance of the sphere center from the inner cylinder is plotted in dimensionless form against time, R_1 and R_2 denoting the radii of the inner and outer cylinders and R the distance of the particle center from the axis of rotation of the concentric cylinders.

The direction of migration was independent of the sense of rotation (Fig. 8) and whether the inner or outer cylinder was rotating, although the rate of migration (for the same angular velocity of the cylinder wall) was greater when the inner cylinder was moving (Fig. 8 curves 2 and 3). The rate of migration increased with increasing particle radius b (Fig. 8 curves 1 and 4) and increasing the apparent velocity gradient (Fig. 8 curves 1 and 2); it also decreased with increasing R.

As in tube flow, the observed migration may arise from the combined action of normal stress and G which are both greatest at the inner and least at the outer cylinder wall. For the set of cylinders used $G(R_1)/G(R_2) = 1.65$[7] (assuming newtonian behaviour) and consequently

G is higher on the one side of the sphere (that facing the inner wall) than on the other; the elastic suspending medium is under tension (strangulation) as a result of straining and this may yield a net force pushing the particle towards the outer cylinder.

(b) <u>Two-body collisions of rigid spheres</u>

Interactions between two rigid uniform spheres in viscoelastic fluids were found to be unsymmetrical and irreversible (Fig. 9, Table III). The paths of approach and recession were curvilinear (Fig. 9), and upon coming into apparent contact the spheres rotated together as was previously found for spheres in newtonian fluids[1,6]. The rectilinear angle[3] of approach $|\phi_a|$ was greater than the angle of recession $|\phi_r|$; upon reversing the direction of rotation of the field the path was retraced until re-collision and $|\phi_a'| = |\phi_r|$ but $|\phi_a'| < |\phi_r'|$ (Fig. 9 and Table II). Each time the spheres were brought into contact by reversing the flow the y distance between their centers gradually increased ($|\phi_r'| < |\phi_a|$) until finally they did not collide.

This doublet behaviour is different from that in newtonian liquids. With rigid spheres[1,6] the collisions were symmetrical the paths of recession being mirror images of the paths of approach. With fluid drops[3,6], although the collisions were unsymmetrical, resulting also in a separation of colliding drops after repeated collisions, $|\phi_a|$ was always greater than $|\phi_r|$.

The observed behaviour of colliding rigid spheres in viscoelastic fluids is probably due to the anisotropic nature of the suspending phase. It is likely that the force generated by the suspending fluid along the doublet axis[3], which is compression in the quadrant of approach and tension in that of recession, is not symmetric around $\phi = 0$. Moreover, it would appear that by reversing the field rotation, not only the sign of this force is reversed but its magnitude is altered as well; the latter might have been due to an elastic recovery effect, during the brief period when the apparatus was stopped before reversing flow.

(c) Drift in orbit of rods and discs

The behaviour of rigid cylindrical particles was similar to that in Poiseuille flow. The variation of θ with ϕ did not follow (10), and C drifted towards its asymptotic values of $C = 0$ for rods and $C = \infty$ for discs as may be seen from Fig. 10.

(d) Deformation of liquid drops

In the systems studied the modes of drop deformation were similar to those observed in newtonian liquids of comparable suspending phase viscosity. Drops possessing class A deformation[2)] assumed a spheroidal shape, D and ϕ_m increasing with increasing the speed of rotation (Fig. 11a). At sufficiently high speeds the ends of the drop became pointed and fragments of liquid were released (Fig. 11a, Part 5). With Pale 4 as suspending phase (class B-2 deformation[2)]), even at very low G, the drop extended into a long cylindrical thread oriented along the X-axis which upon stopping the apparatus disintegrated in a large number of tiny drops (Fig. 11a, Part 3) by growth of Rayleigh capillary waves[20)].

The deformation D increased with increasing the speed of rotation of the cylinders and drop radius (Fig. 11b). The angle ϕ_m also increased with increasing the speed of rotation towards $\phi_m = \pi/2$. Cerf[21)] has shown theoretically that in newtonian liquids the alignment ϕ_m is given by

$$\phi_m = \frac{\pi}{4} + (1 + \frac{2p}{5})\ D\ , \tag{12}$$

where p is the ratio of suspended to suspending phase viscosity; when $D = 0$, $\phi_m = \pi/4$. The validity of (12) has been verified experimentally[2)]. In viscoelastic fluids the major axis of the ellipsoid is oriented closer to the lines of flow[22] and consequently when $D = 0$, $\phi_m > \pi/4$. This is shown in Fig. 11c where the results for the Systems having class A deformation are plotted according to (12). The data are well correlated on a single line because of the high viscosity of the suspending solution at the low G used in the experiments (< 0.5 sec.$^{-1}$ assuming newtonian behaviour), which resulted in values of p very close to zero for all the Systems studied. The straight line calculated by the least square method has an intercept 61°.

SUMMARY

The motions of single rigid spheres, rods and discs, and newtonian liquid drops suspended in viscoelastic fluids undergoing slow Couette and Poiseuille flows have been studied experimentally. The results were compared with similar observations in newtonian suspending media, and the difference in the behaviour explained on the basis of normal stress effects.

It was shown that rigid particles migrated across the planes of shear and in the direction of diminishing G in both Couette and Poiseuille flows. The variations of angle ϕ with time of rigid rods and discs were in good agreement with the theory of Jeffery, provided that the experimental G and the equivalent ellipsoidal axis ratio r_e were used, but the particles attained limiting rotational orbit constants as predicted by Saffman. Two-body interactions of rigid uniform spheres were unsymmetrical and irreversible in contrast to the symmetry found in newtonian suspending media. The deformation and burst of liquid newtonian drops were similar to those observed previously in newtonian suspending fluids of comparable suspending phase viscosity, except for the alignment angle of the drops at zero deformation.

LIST OF SYMBOLS

a; $a'(\phi)$	= semi-axis of revolution of rigid cylinder; projection on the XY plane at ϕ.
b; $b'(\phi)$	= radius of rigid sphere, undeformed drop and semi-axis of the equatorial diameter of rigid cylinder; projection on the XY plane at ϕ
B	= minor axis of a deformed liquid drop
c; c_p	= weight fraction of suspension; weight fraction of polymer in suspending solution
C	= orbit constant
D	= Taylor's deformation parameter = $(L - B)/(L + B)$
G; $G(r)$	= velocity gradient; at r in Poiseuille flow
k	= $4Q/\pi R_o^4$
L	= major axis of a deformed liquid drop
p	= viscosity ratio of the suspended to suspending phase
Q	= volumetric flow rate through tube
r; Δr	= radial distance from the tube axis; difference in r
r_p	= a/b
r_e	= equivalent ellipsoidal axis ratio
R; R_1, R_2	= radial distance of the particle center from the axis of rotation in Couette flow; radius of inner, and outer cylinder of Couette apparatus
R_o	= tube radius
t; T	= time; period of rotation of particle
$u(r)$, $u'(r)$	= streamline velocity, particle translational velocity at r
x, r, ψ	= cylindrical coordinates
x, y, z	= Cartesian polar coordinates
Δx, Δy	= distances along the X and Y axes of a sphere center from the mid-point of the doublet axis
α_2	= phenomenological coefficient Eq. (11)

δ, δ_∞; $\bar{\delta}, \bar{\delta}_\infty$	=	thickness of the reduced particle concentration layer, and its equilibrium value; mean values
η_a, η'	=	apparent viscosity of suspending phase, viscosity of suspended phase
θ	=	angle of axis of revolution with the Z-axis
ρ	=	density
ϕ; ϕ_m	=	azimuthal angle of axis of revolution; orientation of the major axis of the deformed drop
ϕ_a, ϕ_r	=	rectilinear angles of approach and recession of collision doublet of rigid spheres
$\omega(r)$, $\omega'(r)$	=	rotation of field and angular velocity of sphere at r
Ω_1, Ω_2	=	angular velocities of inner and outer cylinder of Couette apparatus

REFERENCES

1. BARTOK, W. and MASON, S.G. J. Colloid Sci. 12, 243 (1957)
2. RUMSCHEIDT, F.D. and MASON, S.G. J. Colloid Sci. 16, 238 (1961)
3. ALLAN, R.S. and MASON, S.G. J. Colloid Sci. 17, 383 (1962)
4. GOLDSMITH, H.L. and MASON, S.G. J. Colloid Sci. 17, 448 (1962)
5. GOLDSMITH, H.L. and MASON, S.G. J. Fluid Mech. 12, 88 (1962)
6. GOLDSMITH, H.L. and MASON, S.G. Proc. Roy. Soc.(London) A 282, 559 (1962)
7. TREVELYAN, B.J. and MASON, S.G. J. Colloid Sci. 6, 354 (1951)
8. This Thesis, Part II
9. GREENSMITH, H.W. and RIVLIN, R.S. Nature 186, 664 (1951)
10. PHILIPPOFF, W. Trans. Soc. Rheol. 1, 95 (1957)
11. GREENSMITH, H.W. and RIVLIN, R.S. Trans. Roy. Soc.(London) A 245, 399 (1953)
12. BRODNYAN, J.G., GASKINS, F.H. and PHILIPPOFF, W. Trans. Soc. Rheol. 1, 109 (1957)
13. MARKOVITZ, H. Trans. Soc. Rheol. 1, 37 (1957)
14. TAYLOR, G.I. Proc. Roy. Soc. (London) A 138, 41 (1932)
15. JEFFERY, G.B. Proc. Roy. Soc. (London) A 102, 161 (1922)
16. SAFFMAN, P.G. J. Fluid Mech. 1, 540 (1956)
17. ERINGEN, C.A. "Non linear Theory of Continuous Media" pp. 221 - 249, McGraw Hill (1962)
18. This Thesis, Part III
19. ANCZUROWSKI, E. and MASON, S.G. Forthcoming publication
20. RUMSCHEIDT, F.D. and MASON, S.G. J. Colloid Sci. 17, 260 (1962)
21. CERF, R. J. Chim. Phys. 48, 59 (1951)
22. LODGE, A.S. "Flow properties of Blood" Ed. by A.L. Copley and G. Stainby. Pergamon Press (1960)

TABLE I

Description of Systems

Temperature 22°C

System	Suspending phase	Suspended phase	b cm.	Axis ratio (a/b)	η' poises [a]	Deformation class
1	PIB [b]	Eccospheres [c]	< 0.006			
2		Polymethylmethacrylate spheres	0.008 - 0.011			
3		Polyvinyl acetate spheres	0.042			
4		Polyvinyl acetate discs		0.097 - 0.165		
5		metal coated Polystyrene discs		0.2 - 0.32		
6		metal coated nylon rods		12.2 - 12.4		
7	PAA [d]	Polystyrene spheres	0.014 - 0.065			
8		Polystyrene discs		0.17		
9		metal coated nylon rods		10		
10		Silicone oil [e]	0.085 - 0.0965		10	A
11		Silicone oil [e]	0.062 - 0.177		0.5	A
12		dibutylphthalate	0.0707		0.21	A
13		Ucon oil LB-1715 [f]	0.0315 - 0.074		10	A
14		Pale 4 [g]	-		60	B - 2

a) Viscosity of the suspended phase

b) Vistanex L-100 (Enjay Chemical Co.)

c) Hollow glass spheres (Emerson and Cuming, Canton, Mass.)

d) Cyanamer P-250 (American Cyanamid Co., Wayne, N.J.)

e) Dow Corning Silicone fluid (Series No. 510)

f) Union Carbide polyglycol oil

g) Oxidized castor oil (Baker Castor Oil Co., N.Y.)

TABLE II

Two-body collisions in Couette flow

$\theta = \pi/2$

Collision doublet	Clockwise		Counter Clockwise	
	$\lvert \phi_a \rvert$ degrees	$\lvert \phi_r \rvert$ degrees	$\lvert \phi'_a \rvert$ degrees	$\lvert \phi'_r \rvert$ degrees
1	59	32	32	39
2	50	33	33	35

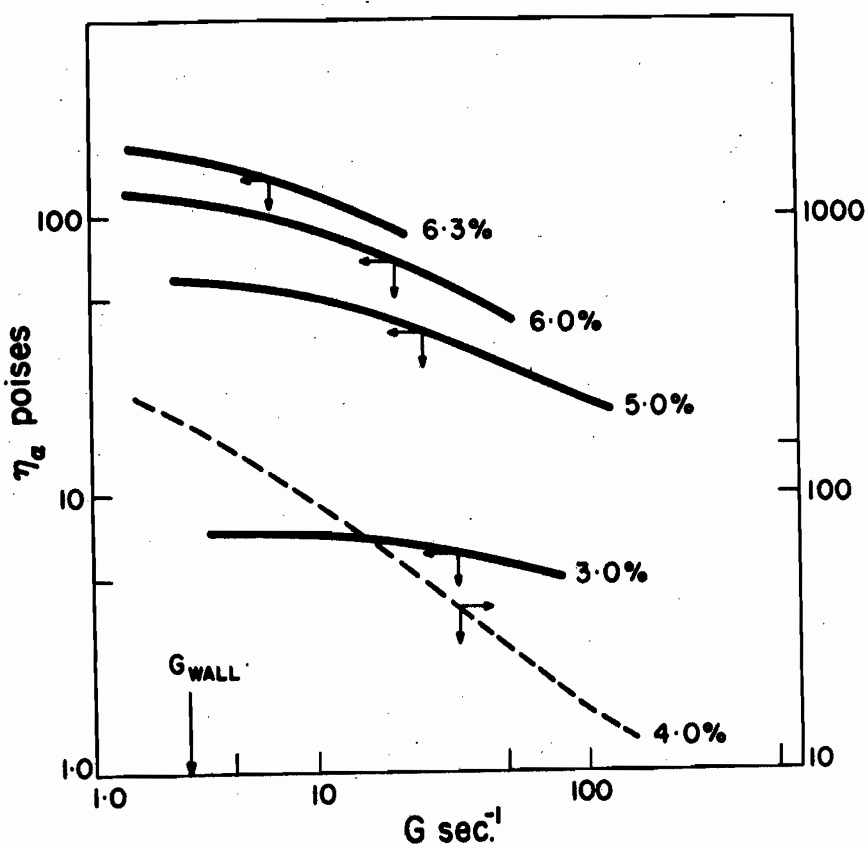

<u>Figure 1</u> Semi-logarithmic plot of the apparent viscosity of solutions of PIB in Decalin (solid lines) and PAA in water (dashed line) plotted as a function of the shear rate at various concentrations of polymer. The arrow indicates the maximum G at the tube wall at the flow rates used in most experiments assuming newtonian behaviour.

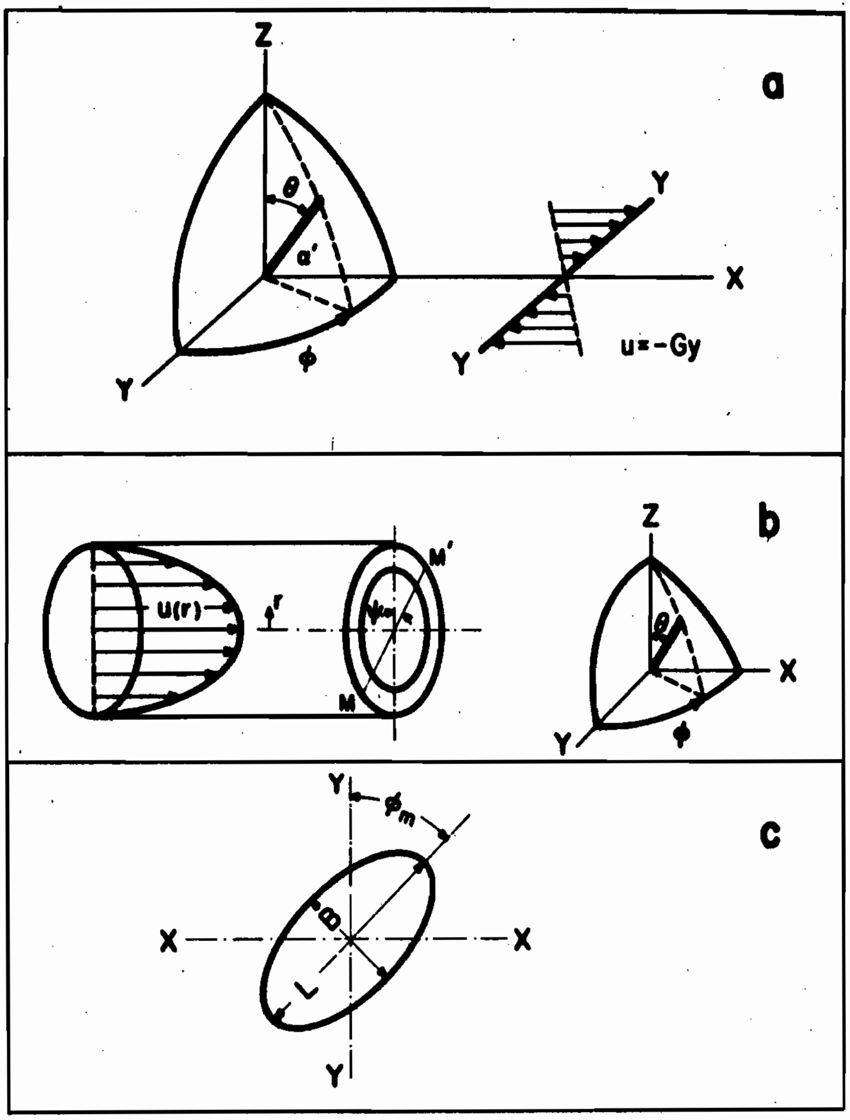

Figure 2 (a) Spherical polar coordinate system for Couette flow.

(b) Cylindrical polar coordinate system r, ψ, x for Poiseuille flow. A Cartesian coordinate system is constructed at the particle center located at x = o, r, ψ = - 90°.

(c) Deformation parameters of a deformed liquid drop.

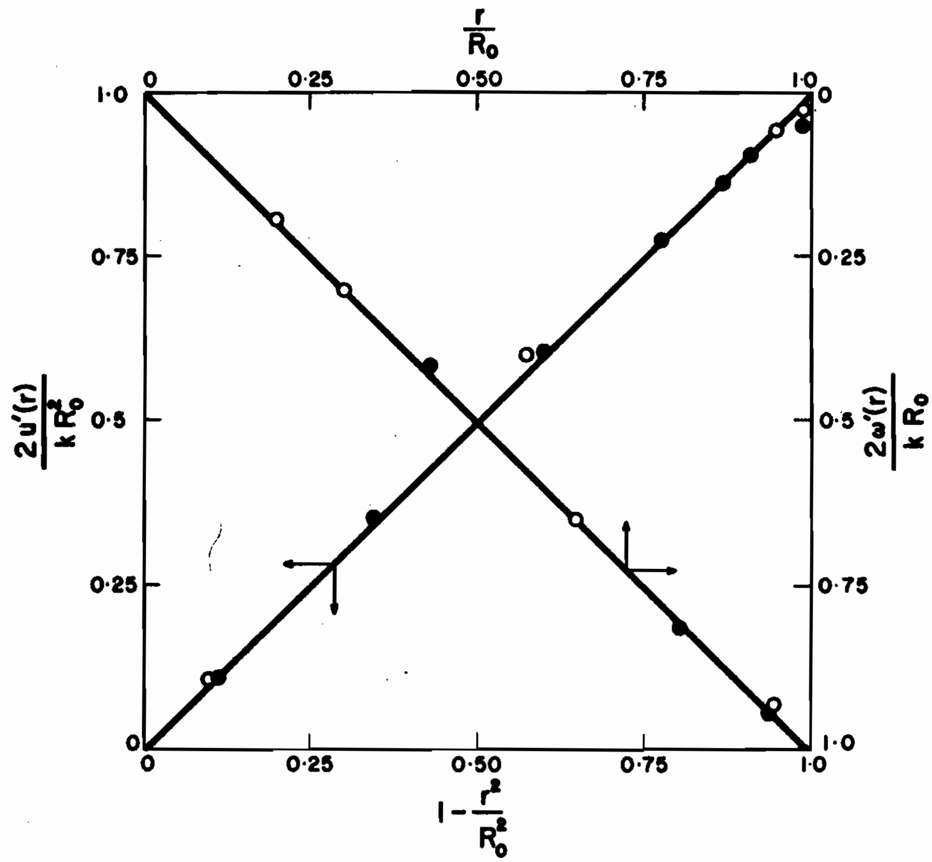

Figure 3 Translational and angular velocities of small spheres in System 1; $c_p = 0.02$ and $R_o = 0.3$ cm. The solid lines are calculated from (6) and (7) and the points are experimental. Open circles: $Q = 1.78 \times 10^{-2}$ cm.^{3} sec.$^{-1}$ and closed circles: $Q = 7.11 \times 10^{-2}$ cm.^{3} sec.$^{-1}$

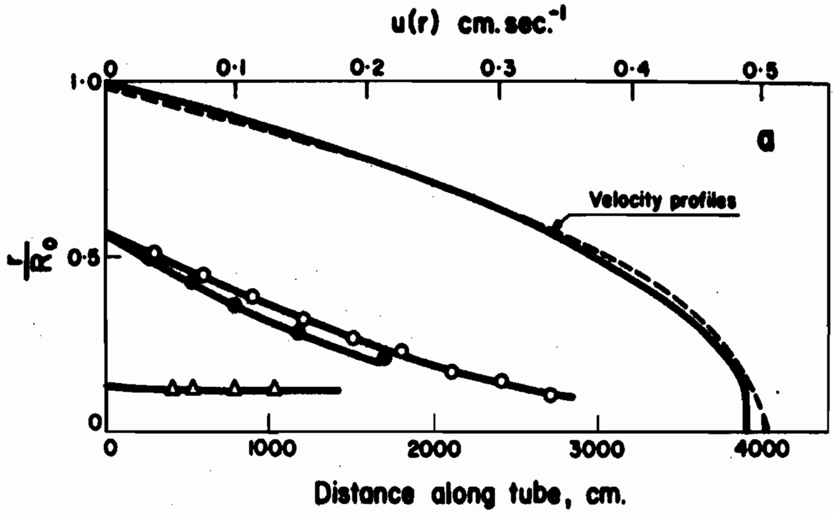

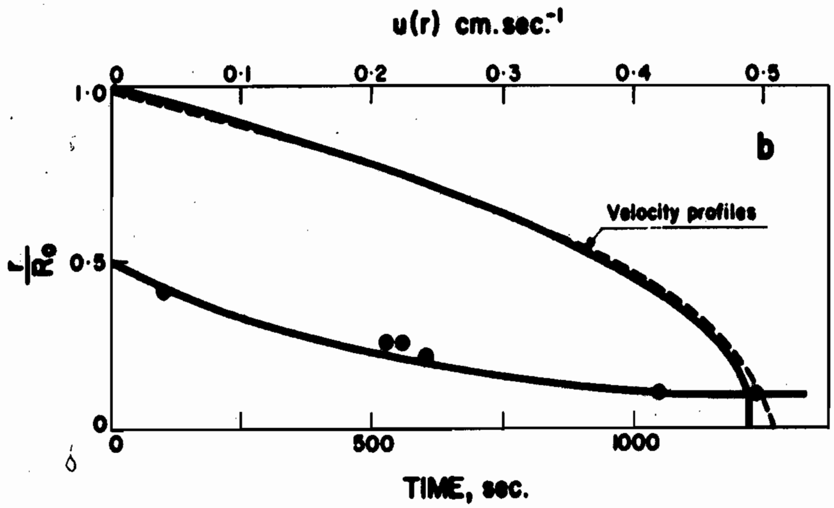

Figure 4 Inward migration of rigid particles from the tube wall in PIB solutions, $R_o = 0.3$ cm, $Q = 7.11 \times 10^{-2}$ cm.^{3} sec^{-1}. The velocity profiles at the same Q for the PIB (solid lines) and the parabolic profile for a newtonian liquid (broken line) are also plotted. Note that there is no migration where the profile is flat.

(a) Spheres: System 2, $c_p = 0.06$; open circles: $b/R_o = 0.027$; closed circles: $b/R_o = 0.037$ and triangles: $b/R_o = 0.035$.

(b) Discs: System 4, $c_p = 0.05$, $2a = 0.0146$ cm. and $2b = 0.151$ cm.

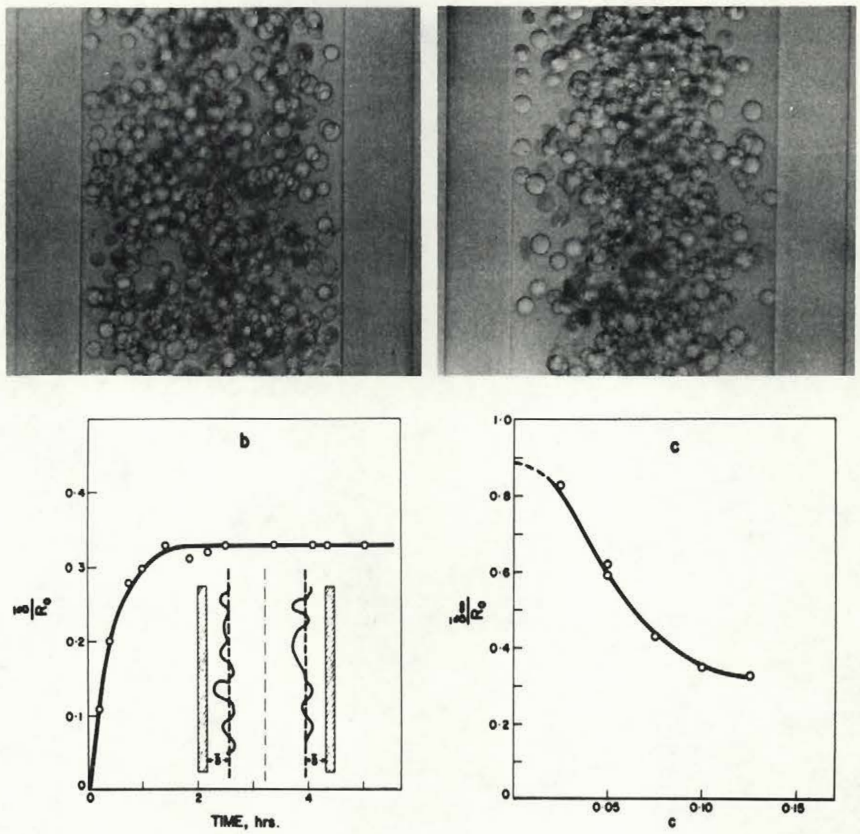

<u>Figure 5</u> The development of the reduced particle-concentration layer near the tube wall in System 3; $c_p = 0.05$, $R_o = 0.3$ cm. and $Q = 7.11 \times 10^{-2}$ cm.^{3} sec^{-1}.

(a) Photographs of a c = 0.125 suspension initially (left) and after 5 hrs. of flow (right).

(b) Increase of $\bar{\delta}/R_o$ with time for the suspension shown in Fig. 5a. The insert is the tracing from the right photograph of Fig. 5a and shows the variation of δ with the tube length (solid lines) and the mean value $\bar{\delta}$ (dashed lines).

(c) Dependence of $\bar{\delta}_\infty/R_o$ on particle concentration; the data were extrapolated to $\bar{\delta}_\infty/R_o = 0.88$ (dashed line) at which the velocity profile becomes flat.

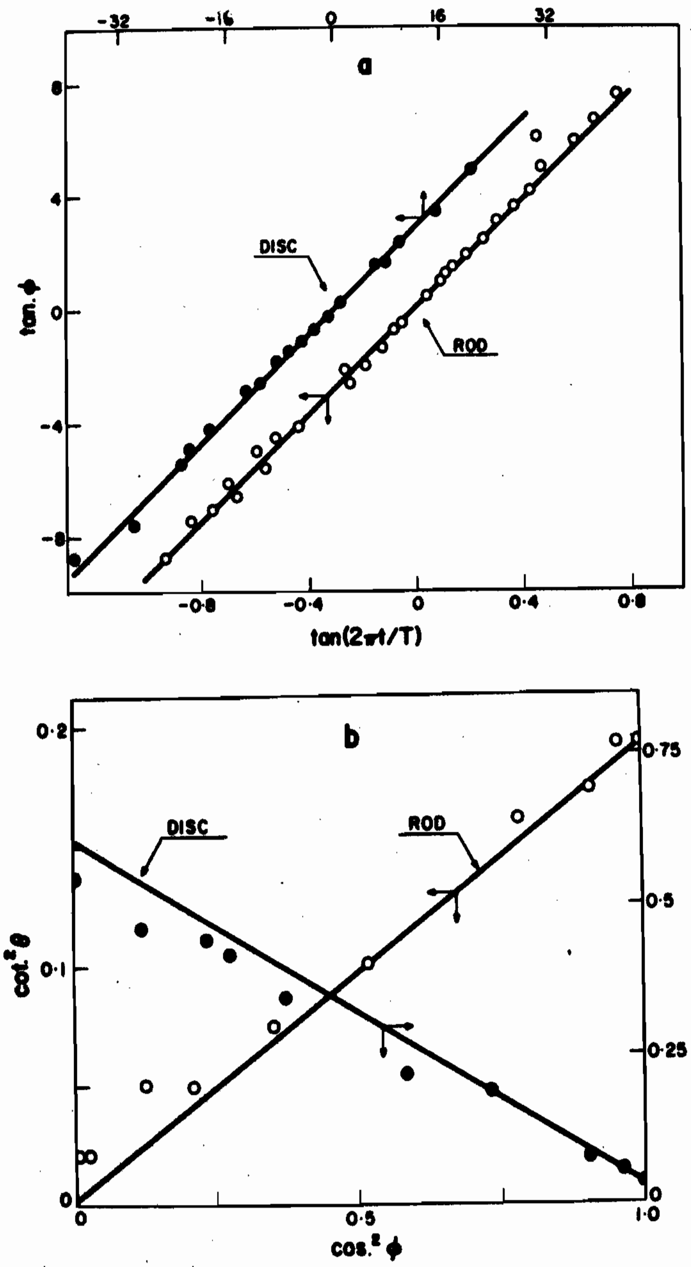

__Figure 6__ Rotation of a rigid rod (System 6) and disc (System 4) in Poiseuille flow; $R_o = 0.5$ cm, $Q = 0.142$ cm.^{3} sec^{-1}, $c_p = 0.05$. The experimental points are;
open circles: for rod $2a = 0.106$ cm, $2b = 0.086$ cm. $r_e = 9.6$, $r/R_o = 0.476$ and $G(r) = 0.65$ sec^{-1};
closed circles: for disc $2a = 0.018$ cm, $2b = 0.109$ cm, $r_e = 0.24$, $r/R_o = 0.330$ and $G(r) = 0.52$ sec^{-1}.

(a) Variation of tan ϕ with time; the solid lines are calculated from (8) using the measured r_e.

(b) Variation of θ with ϕ plotted according to (10). The solid lines are calculated from (10) assuming newtonian behaviour (i.e. C = constant) and using the experimental r_e and the value of C at $\phi = 0$.

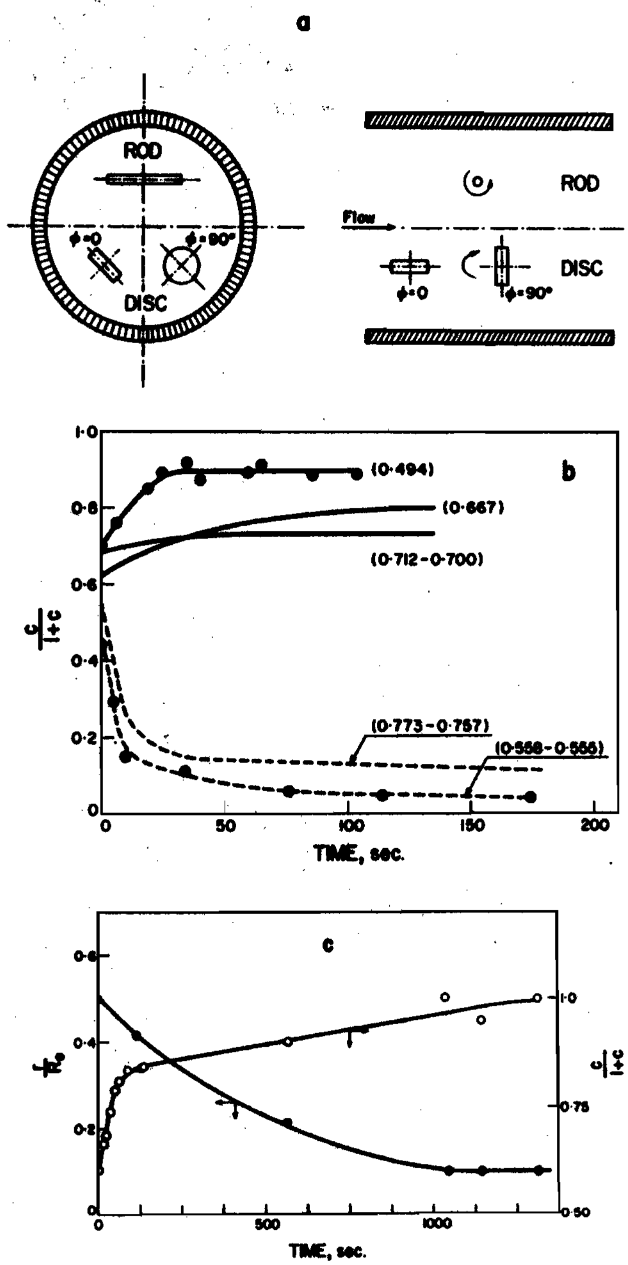

Figure 7 Drift in orbit constant of rigid cylinders in Poiseuille flow in a tube $R_o = 0.3$ cm. at $Q = 7.11 \times 10^{-2}$ cm.^{3} sec^{-1}.

(a) Limiting orbit values of rods and discs viewed along the axis (left) and in the median plane (right); schematic.

(b) Plot of $C/(1 + C)$ against time for rigid discs (System 5, solid lines) and rods (System 6, broken lines); $c_p = 0.063$, rods: $2a = 0.1$ cm., $2b = 0.0082$ cm., and discs: $2a = 0.015$ cm. and $2b = 0.047$ cm. to 0.075 cm. The numbers in parentheses indicate the variation in r/R_o of the particle center over the time interval during which C was measured.

(c) Variation of C and r with time for a rigid disc (System 4), $c_p = 0.05$, $2a = 0.015$ cm. and $2b = 0.151$ cm.

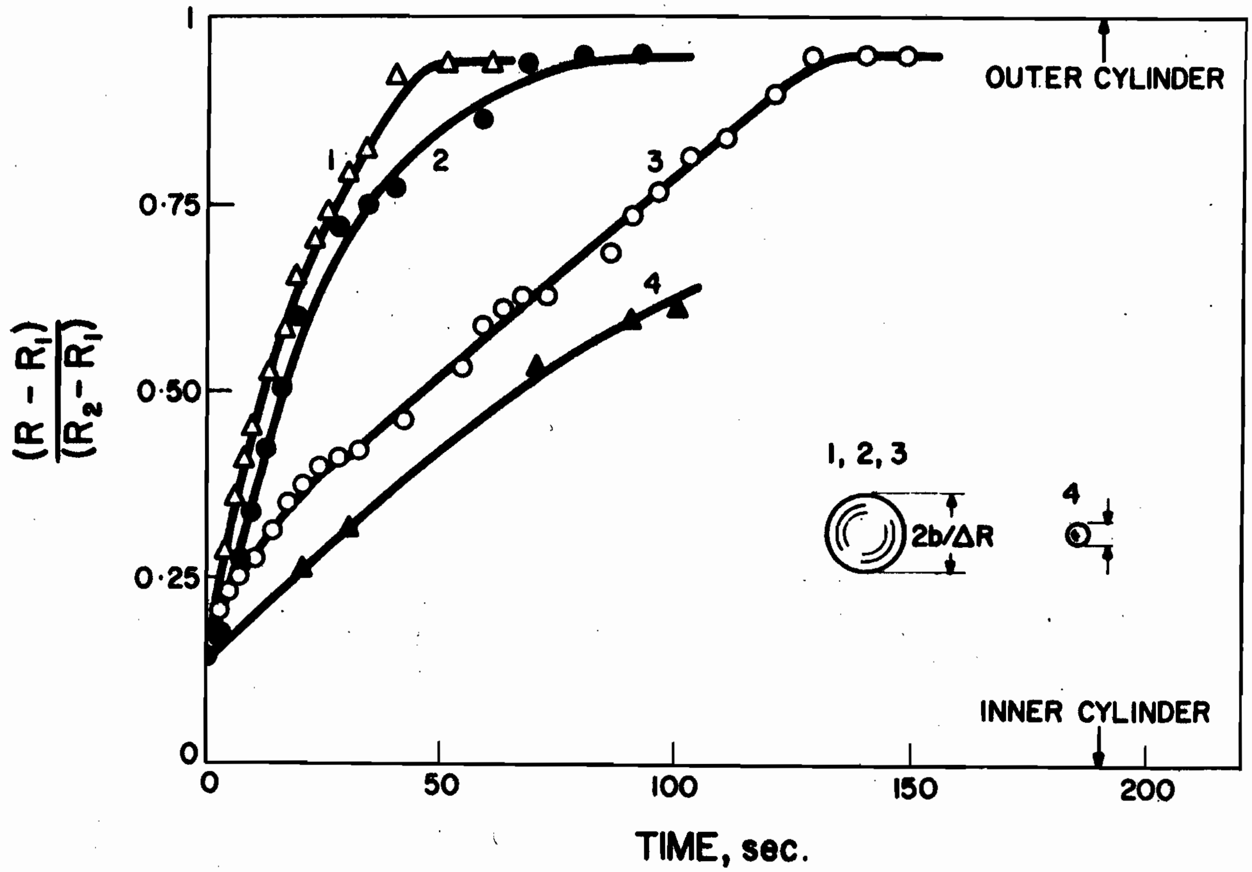

<u>Figure 8</u> Radial migration in Couette flow in System 7; R_2 = 5.795 cm. and R_1= 4.644 cm. Curve 1: b = 0.065 cm, Ω_1= - 0.092 rad.sec.$^{-1}$ and Ω_2= 0; curve 2: b = 0.065 cm, Ω_1= 0.0563 rad.sec^{-1}, and Ω_2= 0; curve 3: b = 0.065 cm, Ω_1= 0 and Ω_2= 0.0563 rad.sec.$^{-1}$ and curve 4: b = 0.014 cm, Ω_1= - 0.092 rad.sec.$^{-1}$ and Ω_2= 0. The positive and negative signs of Ω indicate counterclockwise and clockwise rotation of the cylinders; the size of the spheres relative to the gap width $\Delta R = R_2 - R_1$ of the Couette apparatus is also shown.

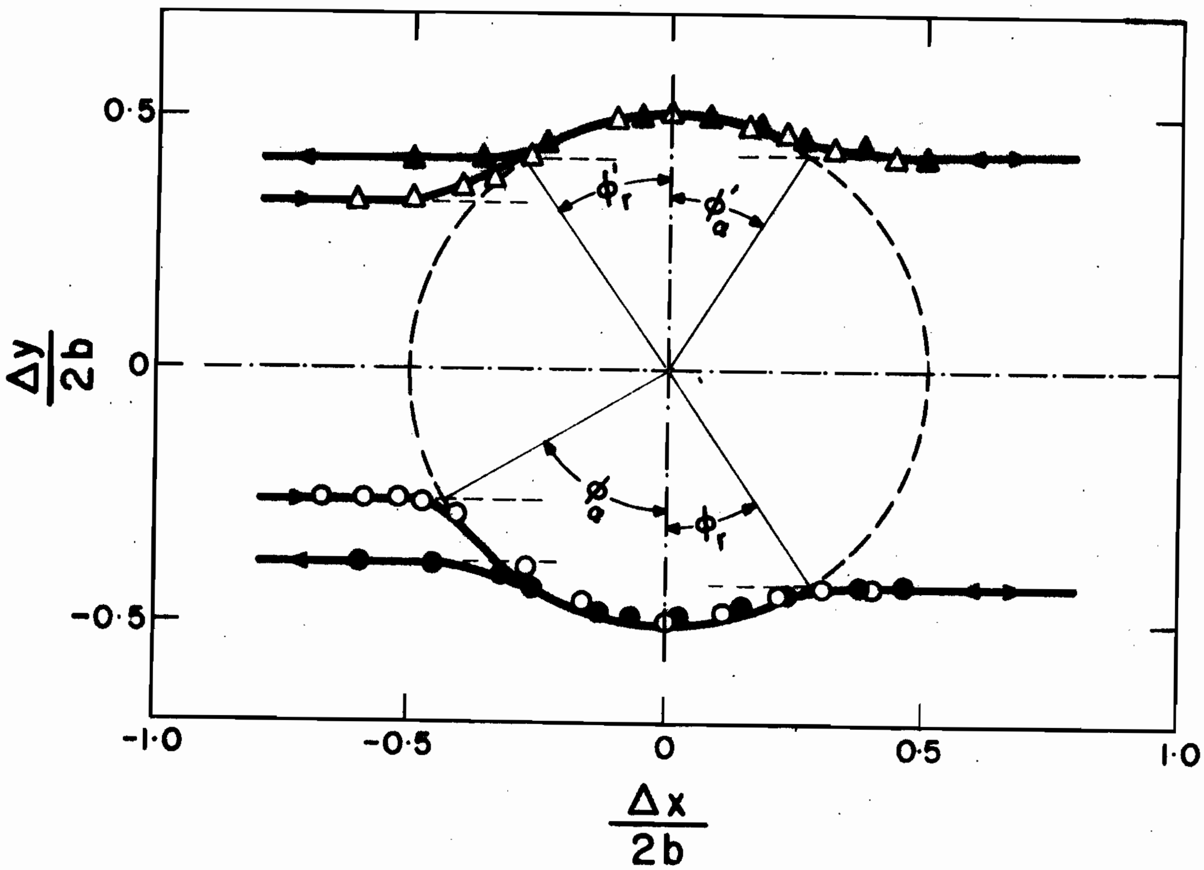

Figure 9 Dimensionless plot of paths of particle centers about the mid-point of the doublets for two equatorial collisions ($\theta = \pi/2$) in Couette flow. The open circles (No. 1, Table III) and open triangles (No. 2, Table III) are experimental points obtained during the first collision, while the closed circles and triangles are those obtained when the spheres recollided on reversing rotation of the Couette cylinders. System 7, $b = 0.0166$ cm, $\Omega_1 = 0.0167$ rad.sec.$^{-1}$ and $\Omega_2 = 0.0112$ rad.sec^{-1}.

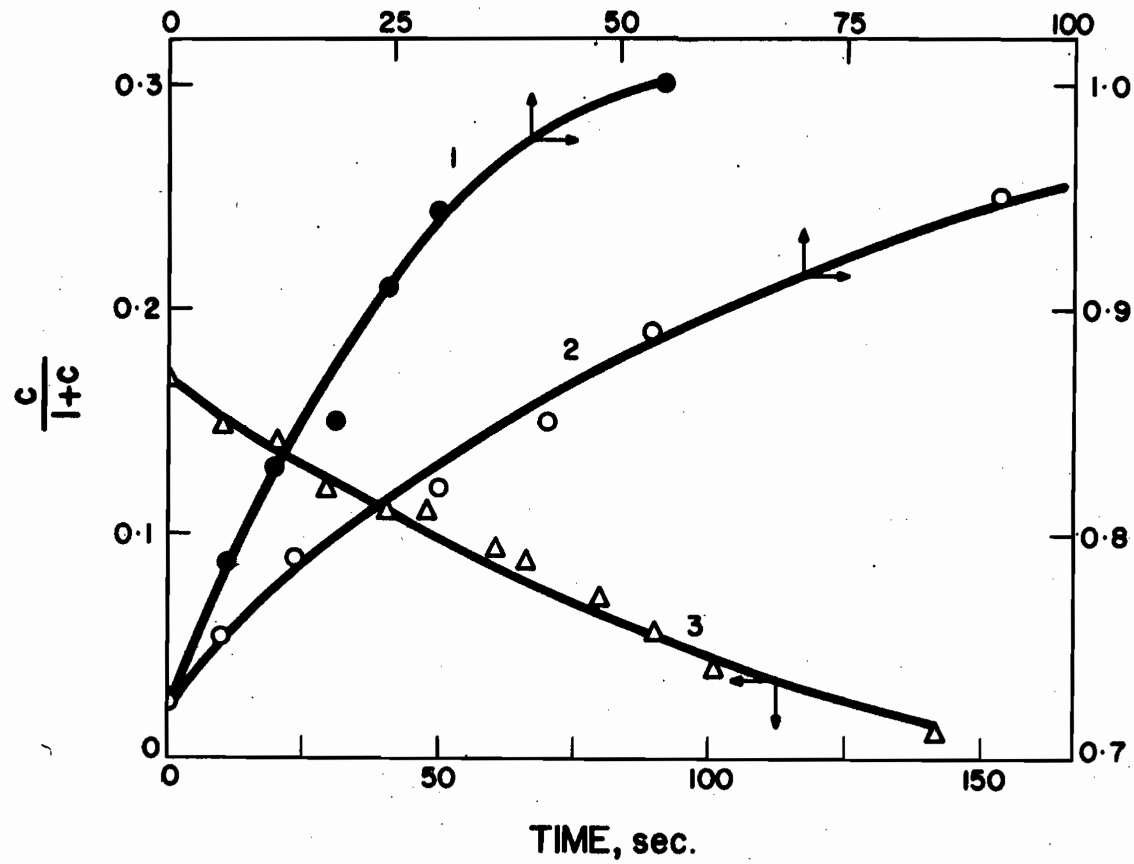

Figure 10 Variation of orbit with time for a disc (circles) $2a = 0.0145$ cm, $2b = 0.0854$ cm, and rod (triangles) $2a = 0.081$ cm, $2b = 0.0081$ cm. in Couette flow (Systems 8 and 9). Curve 1: $\Omega_1 = 0.0237$ rad.sec^{-1}, $\Omega_2 = 0.0216$ rad.sec.$^{-1}$ and curve 2: $\Omega_1 = 0.0089$ rad.sec^{-1}, $\Omega_2 = 0.0079$ rad.sec.$^{-1}$ and curve 3: $\Omega_1 = 0.0114$ rad.sec^{-1}, and $\Omega_2 = 0.0248$ rad.sec^{-1}.

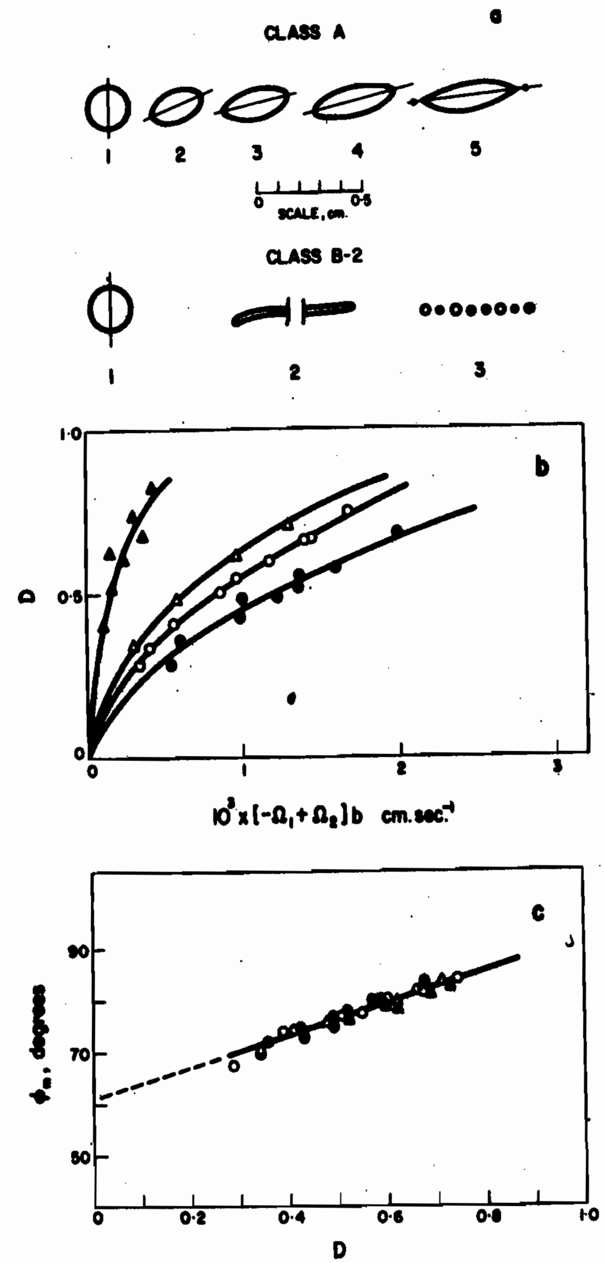

Figure 11 Deformation of newtonian liquid drops in Couette flow.

(a) Tracings from photographs showing the class A deformation (Systems 10 to 13) and class B-2 deformation (System 14).

(b) Effect of b and speed of rotation on the deformation parameter D.

(c) Variation of ϕ_m with D.

In parts (b) and (c) b varied from 0.032 cm. to 0.177 cm. and $\Omega_1 + \Omega_2 \leq 0.0223$ rad.sec^{-1}. The experimental points are: open circles: System 10; closed circles: System 11; open triangles: System 12 and closed triangles: System 13.

PART VI

CONCLUSION

1. General Summary

The main findings and conclusions described in Parts II to V of the thesis may be summarized as follows:

1. In neutrally buoyant concentrated suspensions of rigid particles suspended in newtonian liquids undergoing creeping flow, the velocity distribution deviated from that calculated for a homogeneous newtonian liquid, because of particle-particle and particle-wall interactions. The velocity profile in Poiseuille flow was blunted in the central portion of the tube with individual particles moving at fixed radial positions with identical velocities and without rotating. Outside the region of plug flow, the particles exhibited erratic radial fluctuations and irregular rotations which, however, were reversible with respect to the direction of flow. In dilute suspensions, the distribution of lateral displacements agreed well, whereas the time average lateral displacement was twice than those calculated from a simplified theory based on two-body collisions (Part II).

2. In the flow regime where inertial effects become important, isolated neutrally buoyant rigid cylinders exhibited the tubular pinch effect previously observed for rigid spheres suspended in newtonian liquids undergoing Poiseuille flow. At the same time, they assumed limiting rotational orbit constants which were independent of the initial conditions of release, and which corresponded to the maximum energy dissipation in Couette flow. Deformable particles migrated to the tube

axis, provided that the ratio of particle to suspending fluid viscosity did not exceed 50. In concentrated suspensions of spheres, because of radial migration, a particle-free zone was formed near the wall which modified the initial velocity profile and resulted in a drop in the apparent viscosity coefficient of the suspension which could be accounted for theoretically (Part III).

3. Behind an advancing meniscus the axial and radial velocities of a homogeneous liquid undergoing Poiseuille flow were in qualitative agreement with an approximate theory due to Bhattacharji and Savic[1]. It was shown experimentally that, when a suspension of rigid particles was employed, the radial flow near the advancing meniscus and the interactions of particles with the wall and with one another resulted in inward displacements of the particles, which in turn caused an increase in concentration of the suspension behind the advancing meniscus (Part IV).

4. In viscoelastic suspending media in which there are normal stress effects, isolated rigid particles migrated across the planes of shear, in both Couette and Poiseuille flows, towards the region of lower velocity gradient. In tube flow, this inward migration resulted in a dilution of particles near the wall. Rigid cylinders drifted to rotational orbits which in newtonian liquids correspond to the minimum energy dissipation in Couette flow, independently of the initial conditions of release. Two-body interactions between small uniform spheres were unsymmetrical and irreversible, and the alignment angle of liquid newtonian drops at zero deformation greater than that corresponding to a newtonian suspending phase (Part V).

2. Concluding Remarks and Suggestions for Further Work

The results have already been discussed in detail in Parts II to V and it remains only to comment briefly on some of their implications.

The work with concentrated suspensions of rigid particles shows that the deviations in the velocity profile are probably due to a wall effect proposed by Vand[2] to explain the decrease in the apparent viscosity with decreasing tube radius. This so-called sigma effect is not necessarily a manifestation of a deviation in the velocity distribution since it exists at concentrations where the velocity profile is still parabolic. The development of the partial plug flow in the tube would, however, be expected to produce a further reduction in apparent viscosity not taken into account in Vand's or any other theory. The viscous energy dissipated when a particle is introduced in the flow depends both on its translational and angular velocity. In the region of plug flow, the particles move with identical translational velocities without rotating; for this simple reason the power required to maintain flow is less than that corresponding to a parabolic velocity profile. Near the wall, however, it is greater due to higher translational and rotational velocities of the particles, but the total effect is a net reduction.

The work also demonstrates the importance of considering the tube radius in capillary viscometry and gap width in Couette viscometry. The concentration theory[3-5] proposed to explain the sigma-phenomenon predicts no viscosity change in a Couette viscometer. However, the viscosity measurements in a Couette viscometer on which the theory was based were made with small particles[6] so that any wall effect was probably too small to be detected. It has been shown (Part II) that Vand's wall effect[2], ignored in the concentration theory[3, 4], does in fact operate in both Couette and Poiseuille flows.

The existence of concentration gradients along the tube and the fractionation of particles behind an advancing and ahead a receding menisci demonstrate the importance of properly sampling a suspension when measuring concentration and size distribution[3, 7]. The phenomena suggest some interesting new possibilities for separating and fractionating particles which warrant further examination. Conceivably the principles could apply not only to particles but macromolecules in solution[8].

In view of the considerations listed above and the detailed discussion given in Parts II to V and Appendices II to IV the following recommendations are made for future studies.

(1) <u>Newtonian suspending fluids</u>

(a) <u>Single particles</u>

i) Experiments with improved methods on the behaviour of spheres in close proximity and up to physical contact with a rigid wall to establish conclusively whether or not there is a true slip at the wall.

ii) Migration of neutrally buoyant rigid spheres in Couette flow at high Reynolds numbers and at various distances from the wall.

iii) The direction of radial migration in Poiseuille flow at high Reynolds numbers for non-neutrally buoyant fluid drops of various viscosities, with the sedimentation velocity in the same and/or opposite direction to flow.

iv) Radial migration of liquid drops in Poiseuille flow for a more extensive quantitative test of the theory of Chaffey <u>et al</u>[9]. To include experiments of the effect of surface active agents which will inhibit internal circulation on the wall migration.

v) Examine quantitatively the effects near an advancing meniscus with liquid drops.

(b) Multiplet systems

i) Two-body collisions of uniform spheres in Couette flow at high Reynolds numbers using high-speed cine photography.

ii) Distribution of orbit constants of suspensions of rigid cylinders in dilute suspensions at high Reynolds numbers where the observed drift in orbits depart from the distribution found at low Reynolds numbers[9].

iii) Measurements of the pressure drop at various times in dilute suspensions of rigid cylinders undergoing Poiseuille flow at high Reynolds numbers to study the effect of radial migration and drift in orbit on the apparent viscosity.

iv) Concentration profiles across the tube (using transparent suspensions and tracer particles) in concentrated suspensions of rigid particles at high Reynolds numbers.

v) Simultaneous measurements of velocity profiles and apparent viscosities at low Reynolds numbers in suspensions of rigid particles to correlate viscosity and velocity profile data in a semi-empirical model based on a pseudo-two-phase flow.

vi) Measurements of the mean concentration of a suspension flowing in a tube at low Reynolds numbers and under steady state conditions i.e. when meniscus effects are not present. To compare the results with the concentration of the suspension in the feeding reservoir and thus evaluate quantitatively the effects arising from the convergent entry of the tube.

vii) Concentration changes in front of a receding meniscus in dilute (i.e. without particle-particle interaction) and concentrated suspensions;

to include also experiments with emulsions. In dilute suspensions, because the radial flow is directed inwards, wall effects are expected to be negligible and thus no change in the concentration is anticipated. At high concentrations, however, particle-particle interactions may result in a depletion of particles ahead of a receding meniscus. In the case of an emulsion, on the other hand, it is expected that there would always be a reduction in the concentration near the receding meniscus because of the radial migration of the deformable particles[10,11].

viii) Velocity profiles in concentrated emulsions of various viscosity ratios. The technique described in Part II may be used for transparent emulsions to obtain a velocity distribution across the tube; for non-transparent emulsions an idea of the deviations from the parabolic distribution may be obtained by measuring the translational velocities of the outermost drops of the core.

(2) Non-newtonian suspending media

(a) Single particles

i) Fluid velocity profiles in viscoelastic fluids in Couette flow over a wide range of annular gaps, by measuring the angular velocity of small spheres.

ii) Defprmation of non-newtonian liquid drops in newtonian and non-newtonian media. The non-newtonian systems should include some non-elastic (e.g. Binghan plastic) fluids.

iii) Migration of rigid particles undergoing flow between counter-rotating discs. Migration towards the center of rotation is anticipated due to the variable velocity gradient.

(b) Suspensions

i) Pressure drop measurements in concentrated suspensions in viscoelastic fluids where the radial migration is expected to cause a reduction in the apparent viscosity.

ii) Concentration changes occurring in Couette flow.

PART VII

CLAIMS TO ORIGINAL RESEARCH

1. The velocity distribution in concentrated suspensions of rigid particles was shown to deviate from that calculated for a homogeneous newtonian liquid due to particle-particle and particle-wall interactions; qualitative agreement with Vand's[2)] pseudo-two-phase flow was obtained.

2. The tubular pinch effect for rigid particles other than spheres, but not for particles deformed by the shear was demonstrated.

3. The rotation of small rigid cylinders suspended in newtonian liquids undergoing Couette and Poiseuille flows with inertial effects present was shown to follow Jeffery's[12)] equations provided that the experimentally determined equivalent axis ratio was used. Moreover, rods and discs attained limiting rotational orbit constants which, contrary to Saffman's[13)] prediction, corresponded to maximum energy dissipation in Couette flow [12)].

4. The change in the velocity profile and drop in the apparent viscosity coefficient in suspensions flowing through tubes at high Reynolds numbers was demonstrated.

5. The flow of a homogeneous liquid near a moving meniscus was shown to be in qualitative agreement with the theory[1)]. In a suspension, concentration changes near an advancing meniscus were shown to arise from the radial flow occurring behind the meniscus and by particle-particle and particle-wall interactions.

6. Lateral migration of rigid particles suspended in viscoelastic liquids undergoing slow Couette and Poiseuille flows was demonstrated

and explained qualitatively on the basis of normal stress effects which propelled the particles in the direction of diminishing velocity gradient.

7. The nature of two-body collisions of uniform spheres and of deformation of newtonian liquid drops in viscoelastic liquids in Couette flow were described.

REFERENCES

1. BHATTACHARJI, S. and SAVIC, P. Proc. of the 1965 Heat Transfer and Fluid Mechanics Inst. Ed. by A. F. Charwat et al, Stanford University Press (1965)
2. VAND, V. J. Phys. and Colloid Chem. 52, 277, 300 (1948)
3. WHITMORE, R.L. Rheology of Disperse Systems Ed. C.C. Mill Pergamon Press 49 (1959)
4. MAUDE, A.D. and WHITMORE, R.L. Brit. J. Appl. Phys. 7, 98 (1956)
5. MAUDE, A.D. Brit. J. Appl. Phys. 10, 371 (1959)
6. SWEENY, K.H. and GECKLER, R.D. J. Appl. Phys. 25, 1135 (1954)
7. VEJLENS, G. Acta. Path. Microbiol. Scand. Suppl. No. 33 (1938)
8. BAGLEY, E.B. Trans. Soc. Rheology (In Press 1966)
9. ANCZUROWSKI, E. and MASON, S.G. Forthcoming Publication.
10. GOLDSMITH, H.L. and MASON, S.G. J. Colloid Sci. 17, 448 (1962)
11. CHAFFEY, C.E., BRENNER, H. and MASON, S.G. Rheor. Acta 4, 56 and 64 (1965)
12. JEFFERY, G.B. Proc. Roy. Soc. (London) A102, 196 (1922)
13. SAFFMAN, P.G. J. Fluid Mech. 1, 540 (1956)

(*Reprinted from Nature, Vol.* 200, *No.* 4902, *pp.* 159–160, *October* 12, 1963)

Axial Migration of Particles in Poiseuille Flow

WE have extended recent observations of the radial movements of single rigid[1,2] and deformable[3] spheres suspended in Newtonian liquids flowing through straight circular tubes to include other particle shapes and visco-elastic fluids.

The experiments in Newtonian liquids were conducted as before[3,4] using single rigid spheres, rods and disks of the same density as the liquids but flowing at particle Reynolds numbers (Re_p) between 3×10^{-4} and 7×10^{-3} instead of less than 10^{-6}. The tubular pinch effect previously observed with rigid spheres[1,2] at these Re_p was also exhibited by the rods and disks. Particles placed initially near the tube wall migrated inwards, while particles near the tube axis moved outwards until an equilibrium radial position (r) close to one-half the tube radius (R) was reached (Fig. 1). For a given particle shape, the rate of radial migration increased with increasing flow rate, particle size and radial displacement from

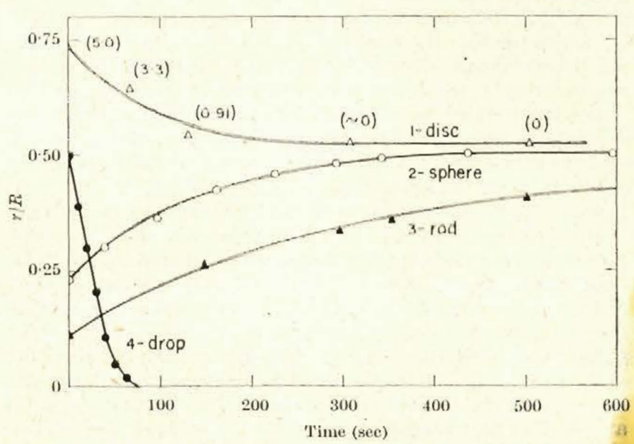

Fig. 1. Radial migration inwards (curve 1) and outwards (curves 2 and 3) to the equilibrium position $r/R = 1/2$ approximately, exhibited by spheres, rods and disks at high Re_p ($> 10^{-3}$) when suspended in polyglycol oils flowing through a tube $R = 0{\cdot}2$ cm. The curves are: (1) polystyrene disk of radius 0·034 cm having an initial orbit constant $C = 5{\cdot}0$, the numbers in parentheses indicating the decrease in C with radial distance and time; (2) polystyrene sphere of radius 0·050 cm; (3) nylon rod of length 0·11 cm. The steady inward migration to the tube centre of a glycerol drop in a polyglycol oil mixture, viscosity ratio suspended phase/suspending phase = 10, is shown by curve 4

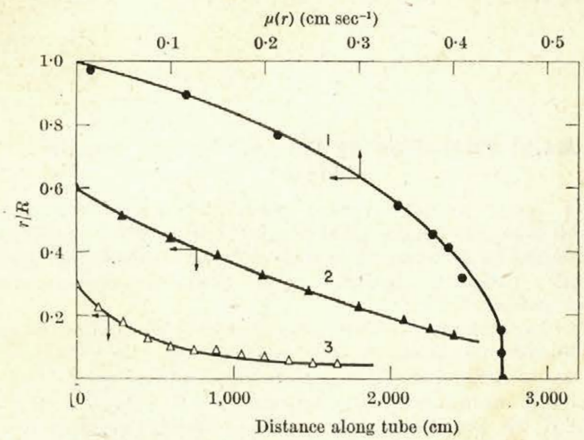

Fig. 2. Inward radial migration of 'Plexiglass' spheres in viscoelastic fluids flowing through a tube $R = 0{\cdot}3$ cm at low Re_p ($< 10^{-6}$). Curve 1 shows the velocity profile, blunted near the tube centre, of a 6 per cent by weight solution of polyisobutylene in 'Decalin'. The inward migration to the central region of no shear of spheres of radii 0·016 and 0·021 cm suspended in the same solution is shown by curves 2 and 3 respectively

the equilibrium position. Furthermore, rods and disks assumed limiting rotational orbits which were independent of the conditions of initial release. The long axis of the rods and the faces of the disks became oriented in planes passing through the axis of the tube, corresponding to spherical elliptical orbit constants $C = \infty$ and 0 respectively[4]; these are the orbits in which the particles make the maximum contribution to suspension viscosity[5] in Couette flow. At low Re_p ($< 10^{-6}$) the radial positions and orbit constants of single rigid rods and disks remained fixed at their initial values[4]. The drift in C and r at higher Re_p presumably are related effects due to inertia[6].

In striking contrast to rigid particles, liquid drops and elastomer filaments, which were deformed by the shear field in the tube, migrated inwards to $r = 0$ just as they did at low Re_p (refs. 3, 4). This behaviour was shown by liquid drops having a viscosity as high as 10 times that of the suspending medium (Fig. 1). When the ratio reached 50, and the drop deformation appeared negligible, the behaviour was as for rigid spheres, that is, no migration at low Re_p and migration to $r/R = 1/2$ at high Re_p. Thus the migration due to deformation[3,4] can dominate that due to inertia, and vice versa.

Inward migration of rigid particles occurred in the viscoelastic fluids at low Re_p ($< 10^{-6}$). Solutions of 3–6·3 weight per cent polyisobutylene ('Vistanex L-100', Enjay Chemical Co.) in decahydronaphthalene ('Decalin'), which have been well characterized rheologically[7], were used as the medium. As expected from the decrease in apparent viscosity with increasing rate of shear, the velocity profile $u(r)$ across the tube, instead of being parabolic as with the Newtonian liquids, was blunted in the central regions (Fig. 2). Rigid spheres, rods and disks placed near the wall rotated and migrated inwards to radial positions at which the velocity profile was nearly flat (Fig. 2). The rate of migration increased with r and particle size. During migration, rods and disks drifted into rotational orbits corresponding to $C = 0$ and ∞ respectively; these orbits correspond to *minimum* energy dissipation in Couette flow and are in agreement with Saffman's theoretical prediction and observations for rigid spheroids in a non-Newtonian fluid of the type used[8]. Particles in the flat portion of the profile, where the velocity gradient was zero, neither rotated nor moved radially. The particle migration observed in these experiments may arise from the combined action of normal stresses in the fluid and the variation in velocity gradient across the particle.

These experiments reveal three distinct mechanisms for radial migration during the flow of suspensions through tubes of which only one, that due to deformation at low Re_p, has been explained with any degree of completeness[4]. It is possible that there are additional mechanisms, especially at concentrations at which appreciable particle interaction can occur. These phenomena are of interest in connexion with the development of particle-free peripheral zones in the flow of various suspensions such as pulp fibre suspensions and blood through tubes.

This investigation was supported (in part) by U.S. Public Health Service research grant H-5911 from the National Heart Institute of the United States Public Health Service.

A. KARNIS
H. L. GOLDSMITH
S. G. MASON

Pulp and Paper Research Institute
of Canada,
and
McGill University, Montreal.

[1] Segré, G., and Silberberg, A., *Nature*, **189**, 209 (1961).
[2] Oliver, D. R., *Nature*, **194**, 1269 (1962).
[3] Goldsmith, H. L., and Mason, S. G., *Nature*, **190**, 1095 (1961).
[4] Goldsmith, H. L., and Mason, S. G., *J. Colloid Sci.*, **17**, 448 (1962).
[5] Jeffery, G. B., *Proc. Roy. Soc.*, A, **102**, 161 (1922).
[6] Segré, G., and Silberberg, A., *J. Fluid Mech.*, **14**, 136 (1962).
[7] Philippoff, W., *Trans. Soc. Rheol.*, **1**, 95 (1957).
[8] Saffman, P. G., *J. Fluid Mech.*, **1**, 540 (1956).

Printed in Great Britain by Fisher, Knight & Co., Ltd., St. Albans

APPENDIX II

WALL MIGRATION OF FLUID DROPS IN COUETTE FLOW

INTRODUCTION

In the creeping flow regime Goldsmith and Mason[1] found that liquid drops suspended in newtonian liquids undergoing Poiseuille flow migrated to the tube axis whereas the center of rotation of single rigid particles remained at fixed radial positions over prolonged periods of flow. An approximate theory based on drop deformation and the variation in velocity gradient across the drop was proposed[1] to explain the inward migration of fluid drops.

A more rigorous theoretical treatment of the problem of drop migration was advanced recently by Chaffey et al[2, 3] for Couette flow. Two cases were considered: (i) migration of a liquid drop in a variable shear field in absence of wall effects, and (ii) migration in a uniform shear field resulting from interaction of the drop with the rigid wall bounding flow. The present brief investigation was undertaken to test the equation derived for the latter case.

THEORETICAL PART

The behaviour of an isolated, neutrally buoyant, and slightly deformed drop near the rigid wall bounding the suspending fluid which undergoes plane Couette flow defined by

$$u = Gy, \quad v = w = o \,, \tag{1}$$

where u, v, w are the respective fluid velocities along the X, Y, Z axes and G the velocity gradient was considered[3]. Using the method of reflections it was shown that interaction with the wall should cause the drop to move away from it. Assuming fully developed circulation inside the drop the predicted migration velocity is[3]

$$\frac{d\ell}{dt} = GD \cdot \frac{b^3}{\ell^2} \cdot \frac{33(79p^2 + 77p + 54)}{280(p+1)^2}, \tag{2}$$

where ℓ is the distance of the drop center from the wall, b the radius of the undeformed drop, p the viscosity ratio of the suspended to suspending phase, and D is the Taylor's[4] deformation parameter given by

$$D = \frac{L - B}{L + B} = \frac{G\eta_o b}{\gamma} \frac{(19\,p + 16)}{(16\,p + 16)}, \tag{3}$$

where L and B are the length and breadth of the deformed drop, η_o the viscosity of suspending fluid, and γ the interfacial tension. Substitution of D from (3) into (2) and integration yields

$$\ell^3 = \ell_o^3 + \frac{3\eta_o}{\gamma} \cdot G^2 b^4 f(p) t, \tag{4}$$

where

$$f(p) = \frac{33(79p^2 + 77p + 54)(19p + 16)}{4480(p+1)^3}, \tag{5}$$

and ℓ_o is the initial distance of the drop center from the wall.

EXPERIMENTAL PART

The theory was tested experimentally in a coaxial cylinder device in which the two cylinders rotated in opposite directions[5]. The velocity gradient G(R) at a distance R from the center of rotation is[6]

$$G(R) = 2\,\frac{\Omega_1 + \Omega_2}{R_2^2 - R_1^2} \cdot \frac{R_1^2 R_2^2}{R^2} \tag{6}$$

where R_1 and R_2 are the respective radii of the inner and outer cylinder walls, and Ω_1, Ω_2 their angular velocities; G(R) is greatest at R_1 and least at R_2; when R_1, R_2 are large G(R) may be considered constant across the annular gap. With the larger set of cylinders (Table I), G(R) was evaluated at the stationary layer at which (6) becomes[6)]

$$G = \frac{2(R_1^{\,2}\Omega_1 + R_2^{\,2}\Omega_2)}{R_2^{\,2} - R_1^{\,2}}\,; \tag{7}$$

the variation in G across the gap was approximately 12%. With the smaller set (Table I), the curvature of the walls could no longer be neglected; since with this arrangement the drops were always released near the outer wall, G was calculated at R_2:

$$G(R_2) = \frac{2R_1^{\,2}}{R_2^{\,2} - R_1^{\,2}}\,(\Omega_1 + \Omega_2)\,. \tag{8}$$

The systems used (Table I) showed negligible drop sedimentation. The distance of a drop from the wall was measured either photographically, or visually using a calibrated dial gauge coupled to the viewing microscope. The interfacial tension, under the conditions of the experiment, was determined by photographing the drop in the stationary layer; the measured values of L, B and b were then used to calculate γ by means of (3).

RESULTS AND DISCUSSION

Liquid drops migrated away from the walls of the Couette apparatus reaching equilibrium about half-way between the two cylinders, where the effects of two walls balanced one another (Fig. 1). The direction of migration was independent of speed and sense of rotation of the cylinder walls. The rate of migration (Fig. 1) increased with decreasing the distance from the wall and increasing the drop radius; it also increased with increasing G (Fig. 2a) and the ratio $f(p)/\gamma$ (Fig. 2b).

In Fig. 3a some of the experimental results have been plotted in accordance with (4); as may be seen the plot of ℓ^3 against G^2b^4t yielded a family of straight lines as predicted by the theory. With the set of narrower-gap cylinders deviations from the linear relationship became apparent as the drops approached their equilibrium positions; these deviations, as expected, were towards lower values of ℓ^3 and were undoubtedly due to the interaction of drops with the other wall so as to reduce the rate of migration.

Values of the observed ℓ^3 are shown in Fig. 3b and compared with those calculated from (4). For the systems investigated the rates were 1/2 to 1/3 those predicted by the theory. The effect of the other wall during the initial stage of migration (calculated from (4)) is too small to account for the discrepancy; this may also be seen from Fig. 3b where no difference in the rates was found in the two apparatus with different gaps. The dependence of the slope of the lines (Fig. 3b) on the physical properties of the systems suggests that the boundary assumptions of the theory might not have been satisfied in the experiments. A key assumption is that there is fully developed internal circulation inside the drops. It has been shown that minute traces of impurities at the drop interface can inhibit the circulation[7] and presumably decrease the migration velocity[8]. It is interesting to observe that deviation from the theory increased at increasing p (Fig. 3b).

The data of Goldsmith and Mason[1] on the migration of liquid drops in Poiseuille flow have also been tested using a relation similar to (4) for flow in tubes[3]. The results were similar to those in Couette flow, the measured migration rates being lower than the theoretically calculated. In the system Silicone oil - Pale 4 for which the agreement was satisfactory[3], there is a numerical error in evaluating f(p), the reported migration rates being about 10 times greater than those actually observed.

CONCLUDING REMARKS

The experimental study of the wall migration of liquid drops in Couette flow is in general agreement with the theory of Chaffey *et al*[3], the observed migration rates being of the same order of magnitude as those predicted by (4). The fact that they were smaller may be due to the inhibition of the internal circulation, although this does not explain completely the magnitude of the observed deviations.

LIST OF SYMBOLS

b	=	radius of the undeformed drop
B	=	minor axis of the deformed drop
D	=	$(L - B)/(L + B)$
$f(p)$	=	function of p Eq. (5)
G; $G(R)$	=	velocity gradient; G at R
ℓ	=	distance of drop center from the wall
L	=	major axis of the deformed drop
p	=	viscosity ratio of suspended to suspending phase
R, R_1, R_2	=	radial distance from the axis of rotation; radius of inner and outer walls of the Couette apparatus
t	=	time
u, v, w	=	components of fluid velocity along the X, Y, Z axes
x, y, z	=	Cartesian coordinates
γ	=	interfacial tension
η_o	=	suspending phase viscosity
$\Delta \rho$	=	density difference
Ω_1, Ω_2	=	angular velocities of inner and outer cylinder walls

REFERENCES

1. GOLDSMITH, H.L. and MASON, S.G. J. Colloid Sci. 17, 448 (1962)
2. CHAFFEY, C.E., BRENNER, H. and MASON, S.G. Rheol. Acta 4, 56 (1965)
3. CHAFFEY, C.E., BRENNER, H. and MASON, S.G. Rheol. Acta 4, 64 (1965)
4. TAYLOR, G.I. Proc. Roy. Soc. (London) A 146, 501 (1934)
5. BARTOK, W. and MASON, S.G. J. Colloid Sci. 12, 243 (1957)
6. TREVELYAN, B.J. and MASON, S.G. J. Colloid Sci. 6, 354 (1951)
7. RUMSCHEIDT, F.D. and MASON, S.G. J. Colloid Sci. 16, 210 (1961)
8. HADAMARD, J. Compt. rend. 152, 1735 (1911)

TABLE I

<u>Properties of Systems</u>

Temperature 22°C

System	R_2 cm.	R_1 cm.	Suspending phase	Suspended phase	p	γ [a)] dyne $cm.^{-1}$	$\Delta\rho$ [b)] $g.cm.^{-3}$
1	15.223	13.354	Silicone oil 50 ps.	Ucon oil LB-1715	0.16	0.23	0.029
2a	15.223	13.354	Silicone oil 50 ps.	Water	2×10^{-4}	10	0.025
2b	9.557	4.754	Silicone oil 50 ps.	Water	2×10^{-4}	26	0.025
3	9.557	4.754	Silicone oil 50 ps.	Pale 4	1.4	4	0.026

a) Calculated from the measured drop deformation using (3).

b) Density difference between the two phases.

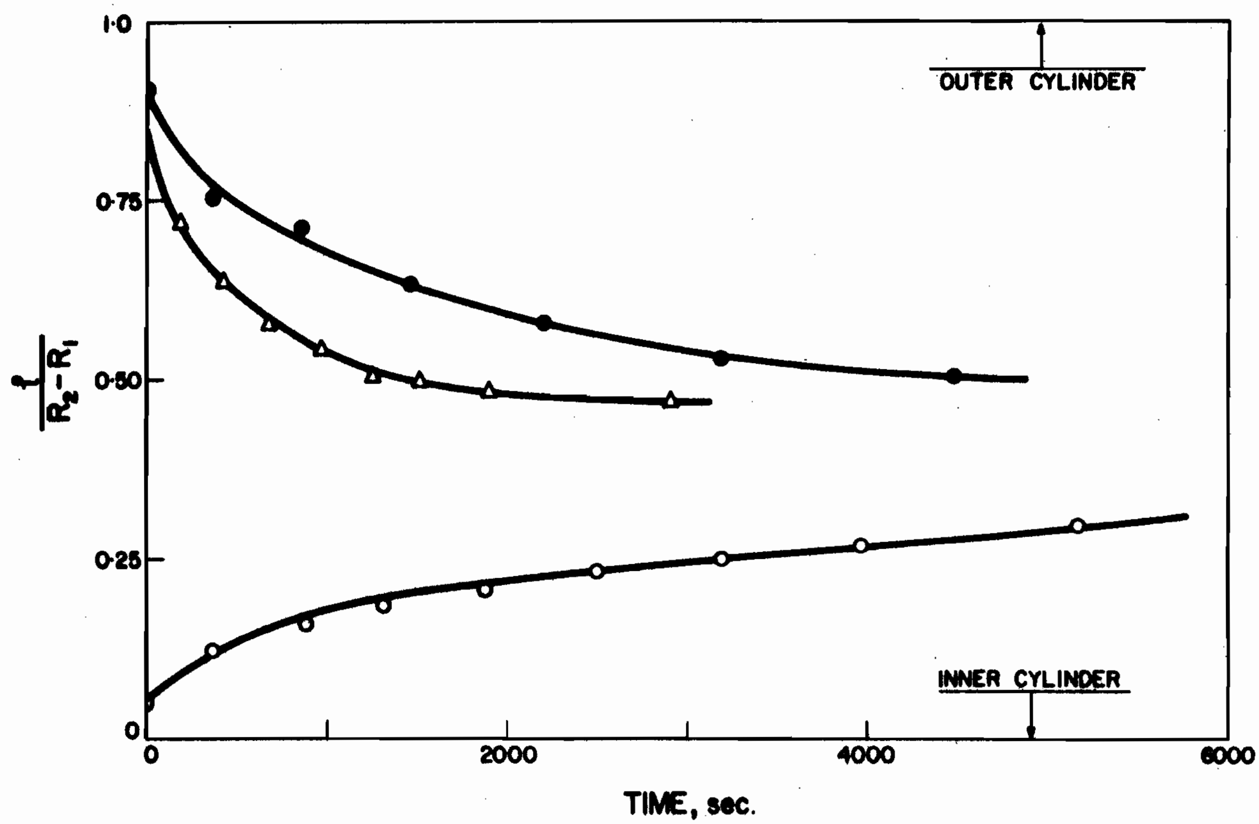

Figure 1 Migration of liquid drops from walls bounding Couette flow. System 2a; open circles: b = 0.063 cm, Ω_1 = 0.0223 rad.sec.$^{-1}$ and Ω_2 = 0.0239 rad.sec^{-1};
closed circles: b = 0.104 cm, Ω_1 = 0.0223 rad.sec^{-1}, Ω_2 = 0.0239 rad.sec.$^{-1}$ and
open triangles: b = 0.135, Ω_1 = 0.089 rad.sec.$^{-1}$ and Ω_2 = 0.0425 rad.sec^{-1}.

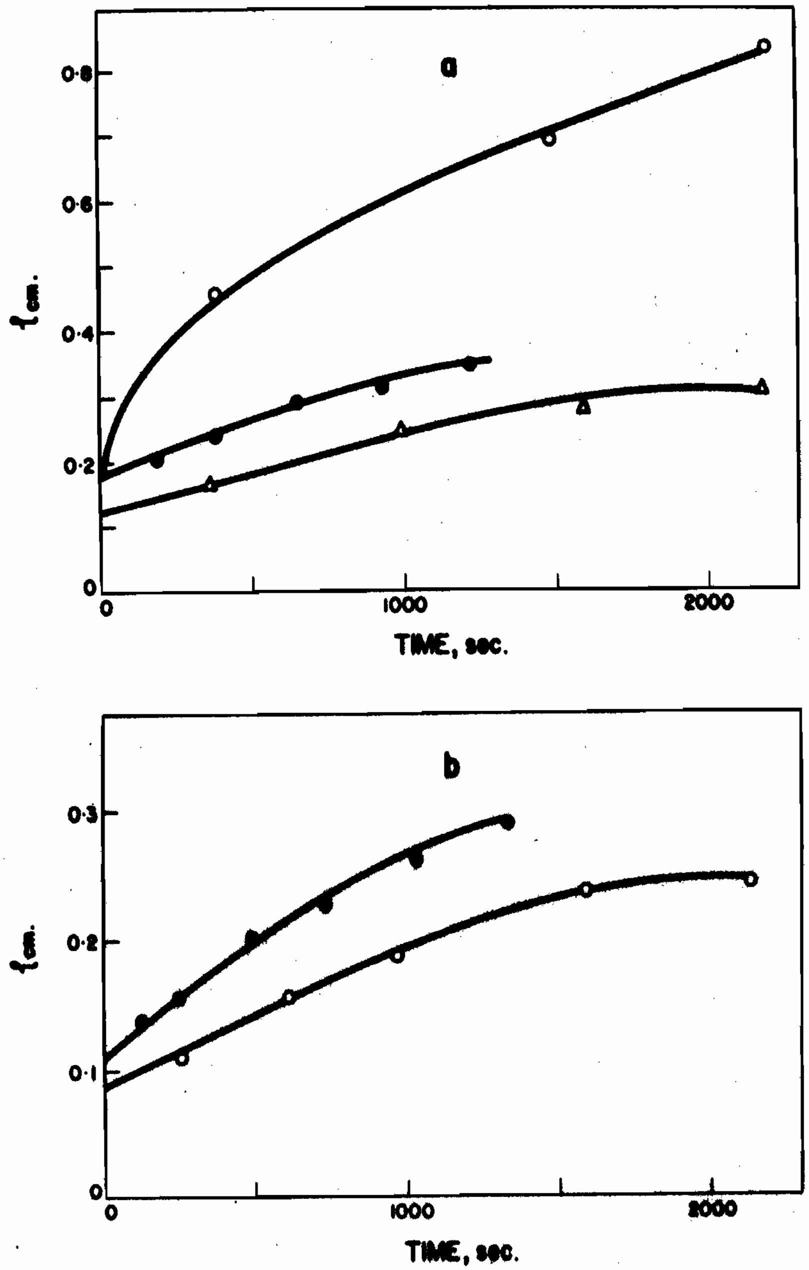

Figure 2 Radial migration of liquid drops undergoing Couette flow.

(a) Effect of velocity gradient on the rate of migration; $b = 0.100 - 0.104$ cm.
Open circles: System 2a, $G = 0.355\ \text{sec}^{-1}$;
closed circles: System 2b, $G = 0.220\ \text{sec.}^{-1}$ and
open triangles: System 2a, $G = 0.186\ \text{sec}^{-1}$.

(b) Effect of physical properties on the rate of migration.
Open circles: System 2b, $G^2b^4 = 2.45 \times 10^{-6}\ \text{cm.}^4\ \text{sec.}^{-2}$ and
$f(p)/\gamma = 0.22\ \text{cm.dyn}^{-1}$;
closed circles: System 3, $G^2b^4 = 2.49 \times 10^{-6}\ \text{cm.}^4\ \text{sec.}^{-2}$ and
$f(p)/\gamma = 1.85\ \text{cm.dyn}^{-1}$.

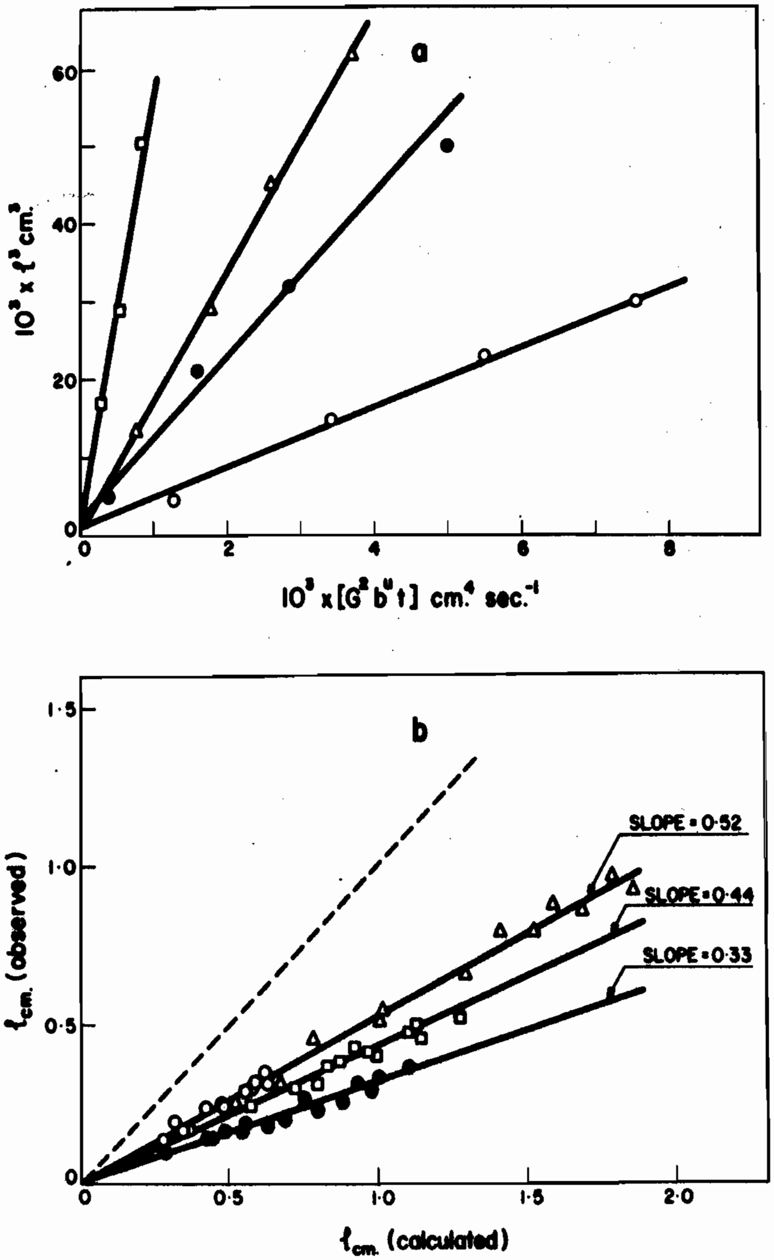

Figure 3 Radial migration of liquid drops in Couette flow.

(a) Plot of ℓ^3 vs. G^2b^4t according to (4).
Open circles: System 2b, b = 0.100 cm, G = 0.186 sec^{-1};
closed circles: System 3, b = 0.098 cm, G = 0.220 sec^{-1};
open squares: System 1, b = 0.0707 cm, G = 0.140 $sec.^{-1}$ and
open triangles: System 2a, b = 0.063 cm. and G = 0.355 sec^{-1}.

(b) Comparison of the observed and calculated (Eq.(4)) values of ℓ. The dotted line is the 45° line of perfect correlation, the solid lines are the ones drawn through the experimental points.
Open circles: System 2b, range of b = 0.083 - 0.103 cm. and range of G = 0.186 - 0.400 sec^{-1};
open triangles: System 2a, range of b = 0.063 - 0.135 cm. and range of G = 0.355 - 0.421 sec^{-1};
open squares: System 1, range of b = 0.0707 - 0.0822 cm, range of G = 0.123 - 0.220 $sec.^{-1}$ and
closed circles: System 3, range of b = 0.057 - 0.098 cm. and range of G = 0.181 - 0.335 sec^{-1}.

APPENDIX III

THE APPARENT VISCOSITY AND VELOCITY DISTRIBUTION IN CONCENTRATED SUSPENSIONS: A SEMI-EMPIRICAL MODEL OF FLOW.

INTRODUCTION

It was shown in Part II that the velocity profiles of concentrated suspensions of spheres deviate from those predicted by the theory with no particles present as a result of the interaction of the outer layers of the suspension with the rigid wall. Following Vand's[1)] suggestion we may represent the wall effect by considering the suspension to be a continuum with a variable viscosity η^* varying from η_o (the viscosity of the medium) at the wall to η (that of the suspension) at some characteristic distance δ from the wall which is only a function of particle size. Using this semi-empirical approach we shall show that the observed velocity profiles both in Couette and Poiseuille flows as well as the variation of the apparent viscosity η_a with particle size may be explained qualitatively.

THEORETICAL PART

1. General

Consider a uniformly dispersed suspension of rigid spheres of volume fraction c flowing in a tube radius R_o, or undergoing shear flow in the annular gap of width ΔR of a Couette device. In Poiseuille flow the origin of the coordinate system is taken at the axis of the tube (Fig. 1a); in Couette flow the origin of y is at one of the walls which, for simplicity, is considered to be at rest. We assume (i) newtonian behaviour of the suspension and suspending medium (ii) continuity of velocities and shear stresses and (iii) steady state conditions. With these assumptions the differential equations of motion are, in Poiseuille flow,

$$\frac{du'(r)}{dr} = \frac{Cr}{\eta^*}, \tag{1}$$

where $u'(r)$ is the translational velocity of the suspension at r, $C = -\Delta P/2L$ and $\Delta P/L$ is the pressure drop per unit length of the tube. In Couette flow

$$\frac{du'(y)}{dy} = \frac{f_s}{\eta^*}, \tag{2}$$

where f_s is the shear stress at the boundary.

To integrate (1) and (2) the explicit form of η^* must be known. By making various assumptions concerning the thickness of the layer and the functional variation of η^* with the distance from the wall, various velocity distributions can be computed. Three simple flow models are treated below.

2. Poiseuille flow

Model A: It is assumed that

$$\eta^* = \eta_o \quad \text{at} \quad r_o \leq r \leq R_o ; \tag{3a}$$

$$\eta^* = \eta \quad \text{at} \quad o \leq r \leq r_o ; \tag{3b}$$

and

$$\frac{\delta}{R_o} <<< 1 ; \tag{3c}$$

there is therefore an abrupt increase of the viscosity from η_o to η at $r = r_o$ (Fig. 1b). Since it has been assumed that $\delta <<< R_o$ its thickness may be neglected; the slip velocity u'_o i.e. the velocity of the inner surface of the δ layer is given by

$$u'_o = -\frac{C\delta R_o}{\eta_o} . \tag{4}$$

Setting $\eta^* = \eta$ in (1) and integrating with the boundary condition that at $r = R_o$ $u'(R_o) = u'_o$ the velocity distribution in the suspension is found to be

$$u'(r) = -\frac{CR_o^2}{2\eta_o}\left[\frac{1-\beta^2}{\eta_r} + \frac{2\delta}{R_o}\right], \tag{5}$$

where $\beta = r/R_o$ and $\eta_r = \eta/\eta_o$ is the relative viscosity. The volumetric flow rate, neglecting the flow in the layer is

$$Q = \int_0^{R_o} 2\pi r u'(r)dr , \tag{6}$$

which upon substitution of $u'(r)$ from (5) and integration yields

$$Q = -\frac{C\pi R_o^4}{2\eta_o}\left[\frac{1 + 4\eta_r \frac{\delta}{R_o}}{2\eta_r}\right]. \tag{7}$$

Inserting (7) into (5) the resulting velocity profile is

$$u'(r) = \frac{2Q}{\pi R_o^2}\left[\frac{1 - \beta^2 + 2\eta_r \frac{\delta}{R_o}}{1 + 4\eta_r \frac{\delta}{R_o}}\right] \tag{8a}$$

$$= u^*(o)\left[\frac{1 - \beta^2 + 2\eta_r \frac{\delta}{R_o}}{1 + 4\eta_r \frac{\delta}{R_o}}\right] , \tag{8b}$$

where $u^*(o)$ is the centerline velocity corresponding to the parabolic distribution at the same Q. At the tube axis (8) becomes

$$\frac{u'(o)}{u^*(o)} = \frac{1 + 2\eta_r \frac{\delta}{R_o}}{1 + 4\eta_r \frac{\delta}{R_o}} . \tag{9}$$

Defining the apparent viscosity of the suspension as

$$\eta_a = -\frac{C\pi R_o^4}{4Q} , \tag{10}$$

then from (7) and (10) is found that

$$\frac{\eta_a}{\eta} = \frac{1}{1 + 4\eta_r \frac{\delta}{R}} \quad . \tag{11}$$

Model B: The same variation of η^* with r as in Model A is assumed (i.e. Equations 3a and 3b) but δ now has a finite thickness (Fig. 1b). Setting $\eta^* = \eta_o$ in (1) and assuming that the liquid adheres to the tube wall integration of (1) leads to the velocity distribution in the δ layer.

$$u'(r) = -\frac{CR_o^{\ 2}}{2\eta_o}(1 - \beta^2) \ . \tag{12}$$

At $r = r_o$ (12) gives the velocity of the inner surface of the δ layer

$$u'(\Upsilon) = -\frac{CR_o^{\ 2}}{2\eta_o}(1 - \Upsilon^2) \ , \tag{13}$$

where $\Upsilon = r_o/R_o$.

In the core of the suspension integration of (1) yields

$$u'(r) = \frac{CR_o^{\ 2}}{2\eta}\beta^2 + A \ , \tag{14}$$

where A is an integration constant. The condition of continuity of the velocity at $r = r_o$ permits the evaluation of A from (13) and (14). The resulting velocity distribution in the core is

$$u'(r) = -\frac{CR_o^{\ 2}}{2\eta_o}\left[\frac{\Upsilon^2 - \beta^2}{\eta_r} + (1 - \Upsilon^2)\right] \ . \tag{15}$$

The total volume flow rate Q is equal to the sum of the volume flows in the layer, Q_1, and in the core, Q_2, i.e.

$$Q = Q_1 + Q_2 \ , \tag{16}$$

where $$Q_1 = \int_{r_o}^{R_o} 2\pi r\, u'(r)dr \,, \tag{17}$$

and $$Q_2 = \int_{0}^{r_o} 2\pi r\, u'(r)dr \,. \tag{18}$$

Using (14) to (18) the total efflux is found to be

$$Q = -\frac{\pi C R_o^4}{4\eta_o}\left[\frac{\gamma^4}{\eta_r} + 1 - \gamma^4\right] \,. \tag{19}$$

Substitution of (19) into (14) and (15) yields

$$\frac{u'(r)}{u^*(o)} = \frac{1-\beta^2}{\left[\frac{\gamma^4}{\eta_r} + 1 - \gamma^4\right]} \qquad \text{for } \gamma < \beta < 1 \,, \tag{20}$$

and $$\frac{u'(r)}{u^*(o)} = \frac{\left[\frac{\gamma^2-\beta^2}{\eta_r} + 1 - \gamma^2\right]}{\left[\frac{\gamma^4}{\eta_r} + 1 - \gamma^4\right]} \qquad \text{for } 0 < \beta < \gamma. \tag{21}$$

At $\beta = 0$ (21) reduces to

$$\frac{u'(o)}{u^*(o)} = \frac{\gamma^2 + \eta_r(1-\gamma^2)}{\gamma^4 + \eta_r(1-\gamma^4)} \,. \tag{22}$$

The apparent viscosity is found from (10) and (19)

$$\frac{\eta_a}{\eta} = \frac{1}{\gamma^4 + \eta_r(1-\gamma^4)} \,, \tag{23}$$

which is the same as Vand's[1)] equation but written in a different form.

<u>Model C</u>: Here it is assumed that η^* varies linearly with the distance from the wall (Fig. 1b) reaching the value of η at $\delta = R_o - r_o$, after which it remains constant, i.e.

$$\eta^* = \eta \qquad \text{at} \qquad 0 \leq r \leq R_o \tag{24a}$$

and $$\eta^* = \eta_o + (\eta - \eta_o)\left(\frac{R_o - r}{\delta}\right) \text{ at } r_o < r \leq R_o . \tag{24b}$$

Then following the same procedure as in Model B it can be shown (see Addendum) that in the layer the velocity distribution is given by

$$\frac{u'(r)}{u^*(o)} = \frac{\dfrac{(1-\gamma)^2}{2(\eta_r - 1)^2}\left[-\left\{\dfrac{\eta_r - 1}{1-\gamma}\right\}(1-\beta) + \left\{\dfrac{\eta_r - \gamma}{1-\gamma}\right\}\log_e\left|-1 - \dfrac{\eta_r - 1}{1-\gamma}(1-\beta)\right|\right]}{\dfrac{\gamma^4}{4\eta_r} + H\gamma^2 + \Lambda - F}, \tag{25}$$

and in the core

$$\frac{u'(r)}{u^*(o)} = \frac{\left[\dfrac{\gamma^2 - \beta^2}{4\eta_r} + \dfrac{H}{2}\right]}{\left[\dfrac{\gamma^4}{4\eta_r} + H\gamma^2 + \Lambda - F\right]} \tag{26}$$

where $$H = \frac{(1-\gamma)^2}{(\eta_r - 1)^2}\left[-(\eta_r - 1) + \frac{\eta_r - \gamma}{1-\gamma}\log_e|\eta_r|\right], \tag{27}$$

$$\Lambda = \left[\frac{1-\gamma}{\eta_r - 1}\right]\left[\frac{3\gamma^2 - 2\gamma^3 - 1}{3}\right], \tag{28}$$

and $$F = \frac{(1-\gamma)^2(\eta_r - \gamma)}{(\eta_r - 1)^3}\left[\left\{\frac{\eta_r - \gamma^2}{\eta_r - 1}\right\}\log_e(\eta_r - 1) - \right.$$

$$\left.\left\{\frac{\eta_r - \gamma}{\eta_r - 1}\right\}(1-\gamma) - \frac{(1-\gamma^2)}{2} - \gamma^2\log_e(\eta_r - 1)\right]. \tag{29}$$

At $\beta = 0$ (26) reduces to

$$\frac{u'(o)}{u^*(o)} = \frac{\gamma^2 + 2\eta_r H}{\gamma^4 + 4\eta_r(H\gamma^2 + \Lambda - F)} \tag{30}$$

The apparent viscosity is found to be

$$\frac{\eta_a}{\eta} = \frac{1}{\gamma^4 + 4\eta_r(H\gamma^2 + \Lambda - F)} \tag{31}$$

3. Couette Flow

Model A: As in the tube it is assumed (Fig. 1b) that

$$\eta^* = \eta_o \qquad \text{at} \qquad 0 \leq y \leq \delta \,, \tag{32a}$$

$$\eta^* = \eta \qquad \text{at} \qquad y \geq \delta \,, \tag{32b}$$

and $\delta <<< \frac{\Delta R}{2}$.

Equations (2) and (32) lead to the following velocity distribution

$$u'(y) = \frac{f_s}{\eta_o}\left[\frac{y}{\eta_r} + \delta\right] \tag{33}$$

At $y = \Delta R/2$ the translational velocity u^* is

$$u^* = \frac{f_s \, \Delta R}{2\eta} \,, \tag{34}$$

and (33) becomes

$$\frac{u'(y)}{u^*} = \frac{2y}{\Delta R} + \eta_r \cdot \frac{2\delta}{\Delta R} \,. \tag{35}$$

By defining an "apparent velocity gradient" G_a as the difference in the velocities of the cylinders divided by the gap, the apparent viscosity is

$$\eta_a = \frac{G\eta}{G_a} \,, \tag{36}$$

where $\qquad G = f_s/\eta \,.$

Combining (35) and (36) yields

$$\frac{\eta_a}{\eta} = \frac{1}{1 + \frac{2\delta}{\Delta R}\eta_r} \,. \tag{37}$$

Model B: The variation of η^* with y is given by (32) but δ is no longer negligible compared with ΔR. In the layer integration of (2), assuming that the liquid sticks at the wall, yields

$$u'(y) = \frac{f_s}{\eta_o} y \,, \tag{38}$$

which at $y = \delta$ becomes

$$u'(\delta) = \frac{f_s}{\eta_o}\,\delta\ . \tag{39}$$

In the core the integrated form of (2) is found to be with the aid of (39)

$$u'(y) = \frac{f_s}{\eta}\left[y + \delta(\eta_r - 1)\right]\ . \tag{40}$$

Combining (34), (38) and (40) the velocity distribution in the layer and the core are

$$\frac{u'(y)}{u^*} = \eta_r\,\frac{2y}{\Delta R} \qquad \text{for} \qquad 0 \leq y \leq \delta\ , \tag{41}$$

and

$$\frac{u'(y)}{u^*} = \frac{2y}{\Delta R} + \frac{2\delta}{\Delta R}\,(\eta_r - 1) \quad \text{for} \quad y \geq \delta\ ; \tag{42}$$

the apparent viscosity is found by combining (36) and (42)

$$\frac{\eta_a}{\eta} = \frac{1}{1 + \frac{2\delta}{\Delta R}\,(\eta_r - 1)}\ . \tag{43}$$

<u>Model C</u>: Equation (24) for Couette flow becomes

$$\eta^* = \eta_o + (\eta - \eta_o)\,\frac{y}{\delta} \quad \text{at} \quad 0 \leq y \leq \delta\ , \tag{44a}$$

and

$$\eta^* = \eta \qquad \text{at} \qquad y \geq \delta\ . \tag{44b}$$

Following the same procedure as in Model B it can readily be shown (see Addendum) that

$$\frac{u'(y)}{u^*} = \left[\frac{\eta_r}{\eta_r - 1}\right]\frac{2\delta}{\Delta R}\log_e\left[1 + (\eta_r - 1)\,\frac{y}{\delta}\right] \quad \text{for} \quad 0 \leq y \leq \delta, \tag{45}$$

$$\frac{u'(y)}{u^*} = \frac{2(y - \delta)}{\Delta R} + \frac{\eta_r}{\eta_r - 1}\,\frac{2\delta}{\Delta R}\log_e \eta_r \qquad \text{for} \qquad y \geq \delta\ , \tag{46}$$

and

$$\frac{\eta_a}{\eta} = \frac{1}{\frac{2\delta}{\Delta R} \cdot \frac{\eta_r \log_e \eta_r}{\eta_r - 1} + 1 - \frac{2\delta}{\Delta R}}\ . \tag{47}$$

4. Comparison with experiment

The true viscosity of the suspension η was calculated from Mooney's[2)] equation

$$\log_e \eta_r = \frac{2.5c}{1 - 1.57c},$$

which has been confirmed recently by Brodnyan and Kelley[3)] for latexes up to $c = 0.4$.

To evaluate δ from the measured velocity profiles a trial and error procedure was used. A value for δ was assumed, and the velocity profiles constructed; then δ was adjusted to provide the best fit of the experimental results for each run, keeping in mind, however, that for each Model δ/b must be constant. The average values of δ found were 0.7b, b and 2.5b for Models A, B and C respectively. It should be noted that for Models A and B the average value of δ obtained from the velocity profile measurements is in good agreement with those reported in the literature by Higginbotham <u>et al</u>[4)] (= 0.7b) and Vand[1)] (= 1.1b) from viscosity measurements using the Model B.

A comparison between the observed $u'(o)/u^*(o)$ and those calculated using the average δ is made in Table I, and in Fig. 2 the predicted and observed velocity distributions of a suspension in Poiseuille (Fig. 2a) and Couette (Fig. 2b) flows are compared. The δ value in Couette was lower than in tube flow because, at the same c and b/R_o or $2b/\Delta R$, deviations in Couette flow were less pronounced. Also Model A predicts a slip at the wall which was not observed experimentally except possibly in the case of complete plug flow. Models B and C appear to provide a more satisfactory agreement with the experimental results.

Each model also predicts a different value for the apparent viscosity. As may be seen from Fig. 3a, η_a increases from Model A to C and at the same η_r and δ the predicted η_a is smaller in Couette than in Poiseuille flow, because of the different geometry of the container and flow conditions.

A unique model should satisfy both viscosity and velocity profile data. In the work described in Part II measurements of η_a were not extensive and were performed with the sole purpose of demonstrating the newtonian behaviour of the suspensions. Simultaneous measurement of velocity distribution and apparent viscosity in both Couette and Poiseuille flows, coupled with various assumptions concerning the variation of η^* with distance from the wall (for instance an exponential relationship) may provide a unique semi-empirical Model based on Vand's theory which would fit both viscosity and velocity data.

ADDENDUM

Derivation of flow equations in Model C

1. Poiseuille flow; velocity distribution in the δ layer

Substitution of η^* from (24b) into (1) and integration yields

$$u'(r) = \frac{CR_o^2}{\eta_o}\int\frac{\beta d\beta}{\left[1 + \frac{\eta_r - 1}{1 - \gamma} - \frac{\eta_r - 1}{1 - \gamma}\beta\right]} + A \qquad (48a)$$

or

$$u'(r) = -\frac{CR_o^2(1-\gamma)^2}{\eta_o(\eta_r - 1)^2}\left[-1 - \left\{\frac{\eta_r - 1}{1 - \gamma}\right\}(1 - \beta) + \left\{1 + \frac{\eta_r - 1}{1 - \gamma}\right\}\log_e\left|-1 - \frac{\eta_r - 1}{1 - \gamma}(1 - \beta)\right|\right] + A \qquad (48b)$$

where the integration constant A is to be evaluated from the boundary condition of no slip at the wall i.e. at $\beta = 1$ $u(r) = 0$;

$$A = -\frac{CR_o^{\,2}(1-\gamma)^2}{\eta_o(\eta_r - 1)^2} \ , \tag{49}$$

and therefore

$$u'(r) = -\frac{CR_o^{\,2}(1-\gamma)^2}{\eta_o(\eta_r-1)^2}\left[-\left\{\frac{\eta_r - 1}{1-\gamma}\right\}(1-\beta)\right.$$

$$\left. + \left\{1 + \frac{\eta_r - 1}{1-\gamma}\right\}\log_e\left|-1 - \frac{\eta_r - 1}{1-\gamma}(1-\beta)\right|\right] \ . \tag{50}$$

At $\beta = \gamma$ (50) yields

$$u'(\gamma) = -\frac{CR_o^{\,2}}{\eta_o} H \ , \tag{51}$$

where H is defined by (27).

<u>Velocity distribution in the core</u>

Substitution of (24a) into (1) and integration yields

$$u'(r) = \frac{CR_o^{\,2}}{2\eta}\beta^2 + A \ , \tag{52}$$

where the integration constant A is evaluated by assuming continuity of the velocities at $\beta = \gamma$. Then using (51) and (52)

$$A = -\frac{CR_o^{\,2}}{\eta_o}\left[\frac{\gamma^2}{2\eta_r} + H\right] , \tag{53}$$

and consequently (52) becomes

$$u'(r) = -\frac{CR_o^{\,2}}{\eta_o}\left[\frac{\gamma^2 - \beta^2}{2\eta_r} + H\right] . \tag{54}$$

<u>Volumetric flow rate</u>

Equation (17) after substitution of $u'(r)$ from (50) yields the efflux in the δ layer

$$Q_2 = -\frac{2\pi CR_o^{\,4}(1-\gamma)^2}{\eta_o(\eta_r-1)^2}\left[I_2 + \ 1 + \frac{\eta_r - 1}{1-\gamma} \ I_2\right] , \tag{55}$$

where $$I_1 = \int_{\gamma}^{1} \left[- \frac{\eta_r - 1}{1 - \gamma} (1 - \beta)\right] \beta d\beta \tag{56a}$$

$$= -\left[\frac{\eta_r - 1}{1 - \gamma}\right]\left[\frac{3\gamma^2 - 2\gamma^3 - 1}{6}\right] , \tag{56b}$$

and $$I_2 = \int_{\gamma}^{1} \left[\log_e \left| - 1 - \frac{\eta_r - 1}{1 - \gamma} (1 - \beta)\right|\right] \beta d\beta \tag{57a}$$

$$= - \frac{(\eta_r - \gamma)}{2(\eta_r - 1)} (1 - \beta) - \frac{1}{4}(1 - \gamma^2)$$

$$- \gamma^2 \log_e|1 - \eta_r| + \frac{1}{2}\left[\frac{\eta_r - \gamma}{\eta_r - 1}\right]^2 \log_e|1 - \eta_r| . \tag{57b}$$

Substitution from (56b) and (57b) into (55) yields

$$Q_2 = - \frac{\pi C R_o^{\ 4}}{\eta_o} (\Lambda - F) , \tag{58}$$

where the functions Λ and F are defined by (28) and (29).

The volumetric flow rate in the core is found by combining (18) and (54)

$$Q_1 = - \frac{C\pi R_o^{\ 4}}{\eta_o}\left[\frac{\gamma^4}{4\eta_r} + H\gamma^2\right]. \tag{59}$$

The total volume flow rate Q is given by

$$Q = \frac{u^*(o)}{2} \pi R_o^{\ 2} , \tag{60}$$

and by combining (16), (58), (59) and (60) is found that

$$- \frac{C R_o^{\ 2}}{\eta_o} = \frac{u^*(o)/2}{\gamma^4/4\eta_r + H\gamma^2 + \Lambda - F} . \tag{61}$$

Substitution of CR_o^2/η_o from (61) into (50) and (54) yields the velocity distribution in the δ layer (Eq. 25) and in the core (Eq. 26).

The expression for the apparent viscosity (Eq. 31) is easily found by combining (10), (60) and (61).

2. Couette flow; velocity distribution in the δ layer

Equation (2) after substitution of η^* from (44a) and integration becomes

$$u'(y) = \frac{f_s}{\eta_o} \cdot \frac{\delta}{\eta_r - 1} \log_e\left(1 + \frac{\eta_r - 1}{\delta} y\right) + A . \qquad (62)$$

The integration constant A is evaluated by assuming that $u'(y) = 0$ at $y = 0$ which yields $A = 0$. Therefore

$$u'(y) = \frac{f_s\delta}{\eta_o(\eta_r - 1)} \log_e\left[1 + (\eta_r - 1)\frac{y}{\delta}\right], \qquad (63)$$

which at $y = \delta$ becomes

$$u'(\delta) = \frac{f_s\delta}{\eta_o(\eta_r - 1)} \log_e\eta_r . \qquad (64)$$

Substitution of f_s from (34) into (63) yields (45).

Velocity distribution in the core

Combining (2) and (44b) one obtains

$$u'(y) = \frac{f_s}{\eta} y + A , \qquad (65)$$

where the constant A is evaluated with the aid of (64) i.e. assuming continuity of the velocity at the interface

$$A = \frac{f_s\delta}{\eta_o(\eta_r - 1)} - \frac{f_s\delta}{\eta} ; \qquad (66)$$

from (65) and (66) the velocity profile in the core is found to be

$$u'(y) = \frac{f_s \delta}{\eta_o(\eta_r - 1)} \log_e \eta_r + \frac{f_s}{\eta}(y - \delta) , \tag{67}$$

and combination of (34) and (67) leads to the velocity distribution given by (46).

Apparent viscosity

At $y = \Delta R/2$ (67) becomes

$$u^* = \frac{f_s}{\eta}\left[\frac{\eta_r \delta \log_e \eta_r}{\eta_r - 1} + \frac{\Delta R}{2} - \delta\right] ; \tag{68}$$

by definition $G_a = 2u^*/\Delta R$ and consequently (68) may be written

$$G_a = G\left[\frac{2\delta}{\Delta R} \cdot \frac{\eta_r \log_e \eta_r}{\eta_r - 1} + 1 - \frac{2\delta}{\Delta R}\right] , \tag{69}$$

which, with the aid of (36) and after rearrangement, reduces to (47).

LIST OF SYMBOLS

A	=	integration constant
b	=	sphere radius
c	=	volume fraction of the suspension
C	=	$-\Delta P/2L$
f_s	=	shear stress
F	=	function of η_r and γ Eq. (29)
G, G_a	=	velocity gradient, apparent velocity gradient
H	=	function of η_r and γ Eq. (27)
L	=	tube length
ΔP	=	pressure drop
Q	=	volumetric flow rate
r	=	radial distance from the tube axis
r_o	=	$R_o - \delta$
R_o	=	tube radius
ΔR	=	width of annulus in Couette apparatus
$u'(r)$, $u'(o)$	=	translational velocity of the suspension of r and tube axis respectively
$u'(y)$, u^*	=	translational velocity of the suspension at y and at the mid-point of the gap in Couette flow
$u^*(o)$	=	centerline velocity in tube flow for parabolic velocity distribution
u'_o	=	velocity of inner surface of plasma layer
y	=	distance from the wall in Couette flow
β	=	r/R_o
γ	=	r_o/R_o
δ	=	thickness of the pseudo-layer
η, η_o	=	viscosity of the suspension and suspending phase
η_a, η_r, η^*	=	apparent viscosity, relative viscosity and effective viscosity
Λ	=	function of η_r and γ Eq. (28)

REFERENCES

1. VAND, V. J. Phys. and Colloid Chem. 52, 277 (1948)

2. MOONEY, U. J. Colloid Sci. 6, 162 (1951)

3. BRODNYAN, J.G. and KELLEY, E.L. J. Colloid Sci. 20, 7 (1965)

4. HIGGINBOTHAM, G.H., OLIVER, D.R. and WARD, S.G. Brit. J. Appl. Phys. 9, 372 (1958)

TABLE I

Comparison of the calculated and measured dimensionless centerline velocity in concentrated suspensions in Poiseuille flow

C	b/R_o	$u'(o)/u^*(o)$ Model A Eq.(9)[a]	Model B Eq.(22)[b]	Model C Eq.(30)[c]	Measured[d]
0.22	0.028	0.92	0.93	0.95	0.87
0.27	0.070	0.81	0.78	0.85	0.78
0.30	0.056	0.81	0.81	0.89	0.79
0.32	0.052	0.79	0.79	0.78	0.74
0.33	0.039	0.81	0.80	0.86	0.75
0.34	0.056	0.71	0.74	0.84	0.73
0.34	0.112	0.66	0.69	0.81	0.50
0.38	0.030	0.77	0.74	0.80	0.78

a) = 0.7b, b) = b, c) = 2.5b, d) See Part II of thesis.

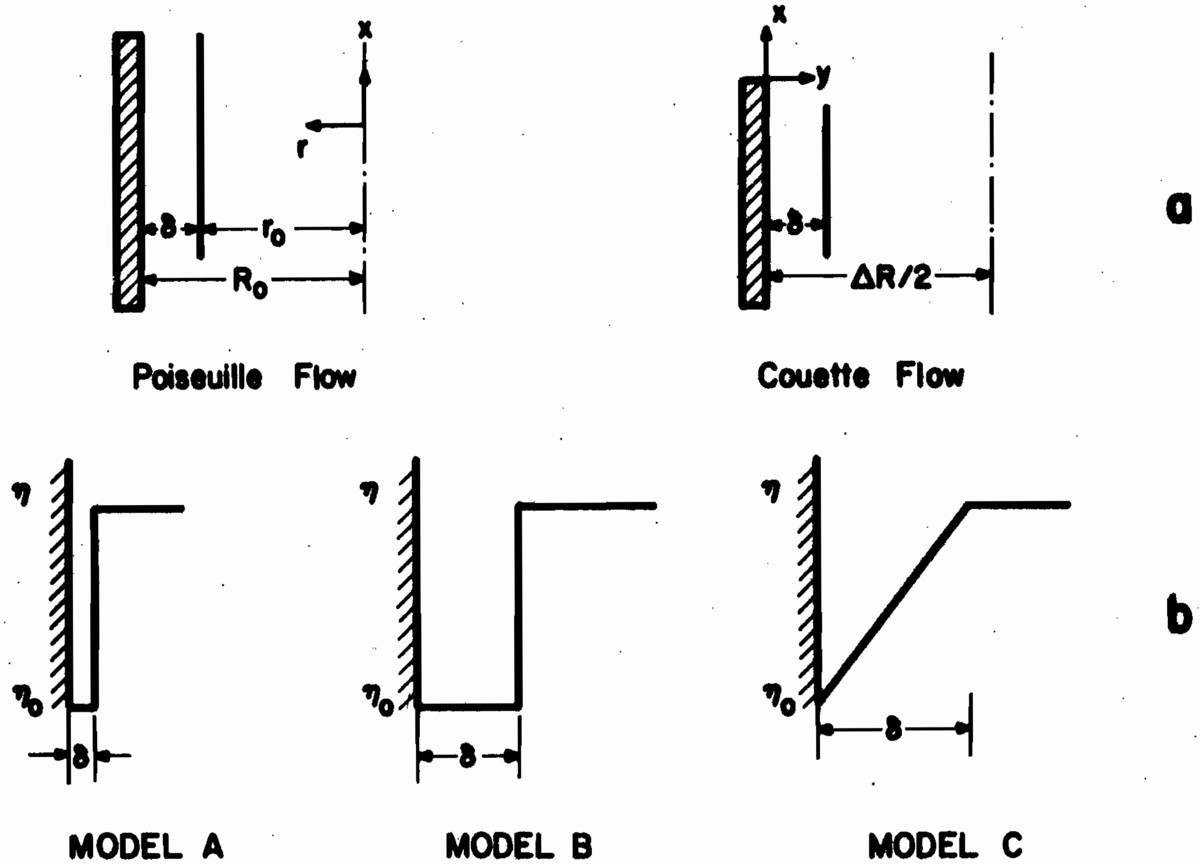

Figure 1 (a) Coordinate system to describe the pseudo two-phase flow in Couette and Poiseuille flows in relation to the wall.

(b) Schematic representation showing the assumed variations of the effective viscosity η^* with distance from the wall.

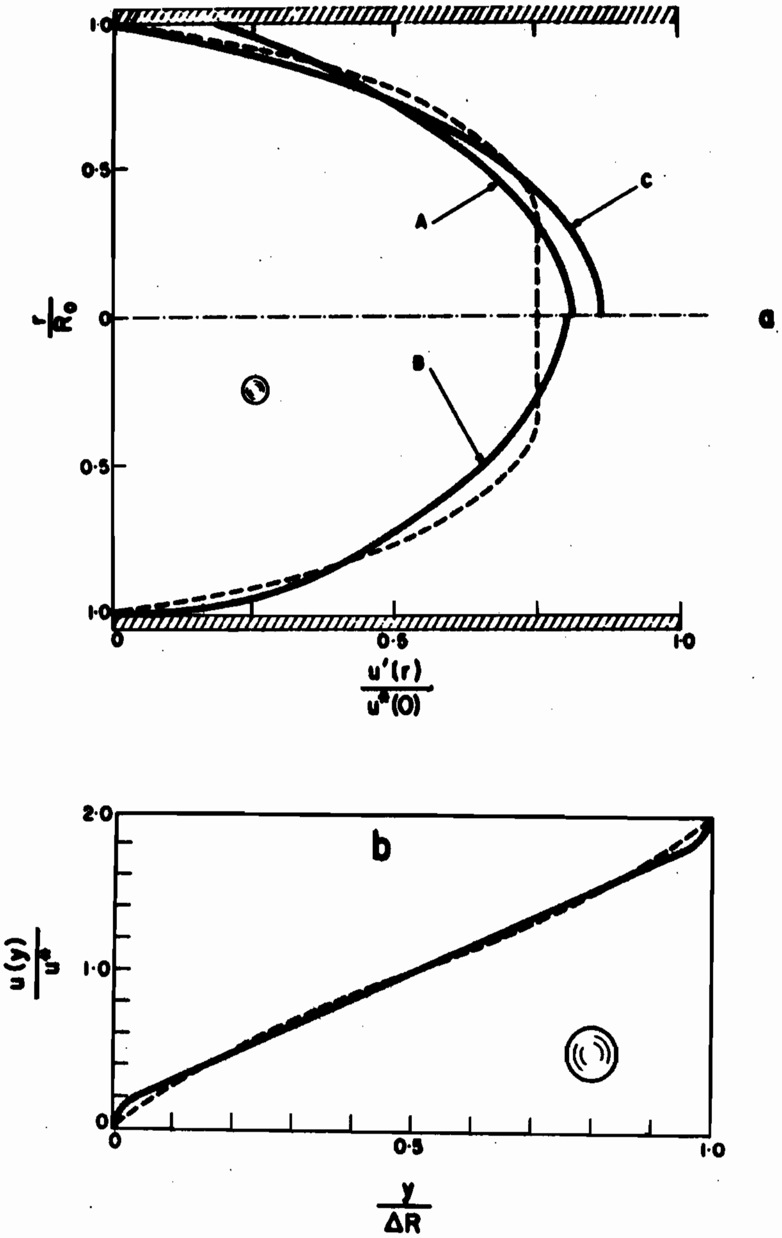

<u>Figure 2</u> Comparison of the calculated (solid lines) and measured (dotted lines) velocity profiles.

(a) Poiseuille flow; $c = 0.33$ and $b/R = 0.039$. For Model A $\delta = 0.7b$, for Model B $\delta = b$ and for Model C $\delta = 2.5b$.

(b) Couette flow; $c = 0.38$ and $2b/\Delta R = 0.083$. Model C with $\delta = b$.

The relative size of the spheres is also shown.

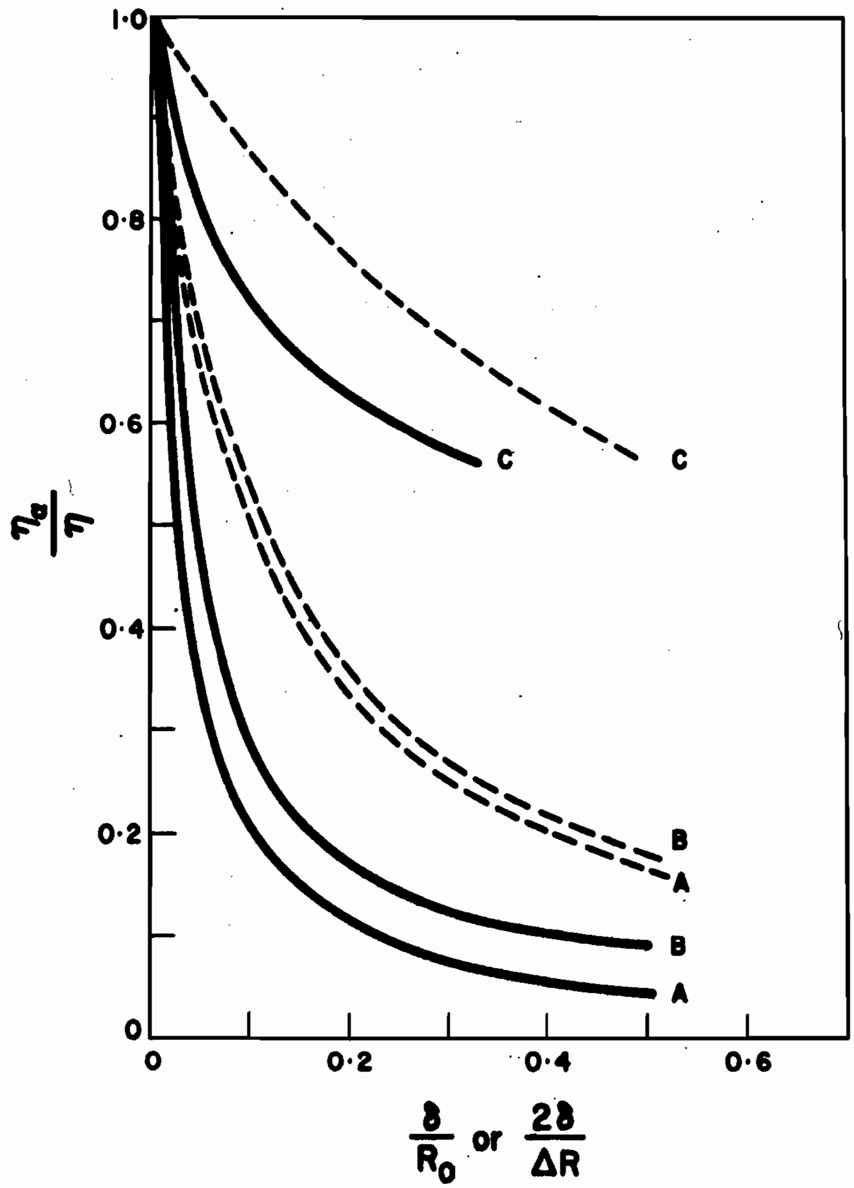

Figure 3 Variation of the apparent viscosity with layer thickness δ in a suspension of η_r = 10 in Couette (dotted lines) and Poiseuille (solid lines) flows for the three assumed Models.

APPENDIX IV

THE BEHAVIOUR OF ISOLATED SPHERES IN CONTACT WITH A RIGID WALL

INTRODUCTION

In Part II experimental evidence was presented suggesting that in concentrated suspensions of spheres the deviations from the parabolic velocity profile and the decrease in the apparent viscosity with decreasing the tube radius are due to particle-particle and particle-wall interactions. In Appendix III an explanation of the two effects was attempted using Vand's pseudo-two-phase flow model.

It was considered to be of interest to measure the translational and rotational velocities of isolated neutrally buoyant rigid spheres in contact with a rigid wall, and to this end a few experiments were performed both in Couette and Poiseuille flows.

EXPERIMENTAL

The methods of producing Couette and Poiseuille flows have already been described[1)]. The Couette Mark II Apparatus (see Appendix V) was used with the stainless steel cylinders of R_1 = 13.354 cm. and R_2 = 15.236 cm. where R_1 and R_2 are the respective radius of inner and outer cylinder wall.

The systems studied are listed in Table I. Systems 1 and 2 were used for the tube experiments, 3 and 4 in Couette flow. Except with System 1 either a magnetic or electric field (5 KV) was applied in order to bring the sphere on the wall. In System 2 the sphere contained a thin iron wire through its center, and with the aid of a magnet, was placed in the median plane of the tube normal to the viewing axis of the microscope and in contact with the wall. The electric field in Systems 3 and 4 was normal to the direction of flow and was applied at the outer (insulated) Couette cylinder by a stabilized 60 c.p.s. AC power supply; the inner cylinder was grounded.

The spheres were photographed through the microscope directed along the Z-axis (Fig. 1a, Part II) by means of a Bolex Paillard 16 mm. reflex cine camera and the films analysed by projecting them onto a drafting table. The angular velocity ω' of the sphere was measured by following small imperfections on its surface, while its translational velocity u' relative to the wall by measuring the distance travelled by the sphere in a given time.

RESULTS AND DISCUSSION

In all cases (as summarized in Table II) the sphere did not execute a pure rolling motion along the wall but instead exhibited a slip velocity V expressed by

$$V = u' - \omega' b \qquad (1)$$

b being the sphere radius. The first experiments were carried out using System 1; although the spheres appeared through the microscope to touch the wall, because of the limited resolution (approx. 5×10^{-4} cm.) obtained with the optical equipment used, it was thought that they might not have been in real contact. Subsequent experiments, however, by applying a magnetic or electric field to break any intervening liquid film between the sphere and the wall yielded similar results.

Recently Goldwan, Cox and Brenner[2)] have obtained an exact solution for the motion of an isolated, neutrally buoyant rigid sphere near a single plane wall in a fluid undergoing a simple shearing motion. The results of their calculations are tabulated in Table III. The numerical solution used, however, did not converge well when the sphere was extremely close to the wall. The application of a type of lubrication theory approximation when the sphere nearly touches the wall indicated that both its angular and translational velocities were proportional to $\left[- \log_e(\ell - b)/b\right]^{-1}$. Thus in the limit of zero gap distance the sphere should not move. Although both ω' and u' tend to zero as gap distance tends to zero, the theory also indicates that $\omega' b/u'$ should tend to a limiting value. However, this limiting value cannot be obtained from the lubrication theory approximation since its calculation requires knowing the fluid velocity field outside the gap region.

The experimental results appear to agree well with Brenner's theory in the sense that when the sphere was very close to the wall $\omega' b'/u' = 0.6$ approx. However, this work leaves unanswered the important question of whether or not the sphere slips on the wall. As mentioned above the limited resolution of the optical equipment makes it uncertain if the spheres were actually touching the wall. For instance a sphere radius $b = 0.05$ cm. located at $b/\ell = 0.997$ yields $(\ell - b) = 1.5 \times 10^{-4}$ cm. which could not be observed experimentally. It can thus be argued that a thin film of liquid always existed between the sphere and the wall, even though a magnetic or electric field was applied, which would produce pseudo-slip. Improved experiments are required to resolve this question.

LIST OF SYMBOLS

b	=	radius of rigid sphere
G	=	velocity gradient of the undisturbed flow
ℓ	=	distance of sphere center from the wall
Q	=	volumetric flow rate through a tube
R_o	=	tube radius
R_1, R_2	=	radius of inner and outer cylinder respectively
u, u'	=	streamline velocity, translational velocity of the sphere
V	=	slip velocity
η_o	=	viscosity of the suspending phase
ω; ω'	=	rotation of the field at the sphere center; angular velocity of the sphere

REFERENCES

1. This Thesis, Part II

2. BRENNER, H. New York University, Personal communication (1965)

TABLE I

Description of Systems

Temperature 22°C

System	Suspended Phase	b cm.[a]	Suspending Phase	η_o (poises)[b]	Remarks
1	Polymethylmethacrylate sphere	0.014	polyglycol oil[c]	25	
2	Nylon sphere	0.163	corn syrup	90	Magnetic field applied before starting experiment.
3	aluminum coated polystyrene sphere	0.0432 to 0.0479	silicone oil[d] containing Freon 113[e]	50	Electric field applied before and during experiment.
4					Electric field applied before experiment.

a) Radius of the sphere.

b) Viscosity of the suspending medium.

c) Ucon oil 50-HB-5100 (Union Carbide).

d) Dow Corning fluid series 200.

e) E.I. du Pont de Nemours.

TABLE II

Slip velocities of isolated rigid spheres on the wall

Poiseuille Flow

System	$10^2 \times Q$ [a) $cm.^3 sec.^{-1}$	R_o [b) cm.	$u' \times 10^2$ $cm.sec.^{-1}$	ω' $sec.^{-1}$	$V \times 10^2 cm.sec.^{-1}$ Eq.(1)	$\omega' b/u'$
1	0.711	0.2	0.860	0.339	0.385	0.552
1	1.78	0.2	1.82	0.848	0.630	0.654
2	1.78	0.4	2.18	0.0730	1.01	0.546

Mean = 0.58

Couette Flow

System	G [c) $sec.^{-1}$	b cm.	$u' \times 10^2$ $cm.sec.^{-1}$	ω' $sec.^{-1}$	$V \times 10^2 cm.sec.^{-1}$ Eq.(1)	$\omega' b/u'$
3	0.289	0.0479	0.574	0.0714	0.231	0.595
3	0.0952	0.0432	0.185	0.0233	0.089	0.544
4	0.291	0.0435	0.593	0.0705	0.186	0.514

Mean 0.55

a) Volumetric flow rate through the tube.

b) Radius of the tube.

c) Velocity gradient of the undisturbed flow at the sphere center.

TABLE III

Calculated translational and rotational velocities of rigid spheres as a function of distance from the wall

(After reference 2)

b/ℓ [a]	ω'/ω [b]	u'/u [b]	$\omega' b/u'$	$\frac{\omega'/u'}{\omega/u}$
0	1.0	1.0	0	1.000
0.0995	0.99952	0.99962	0.049659	0.9999
0.266	0.99430	0.99436	0.13289	0.9999
0.426	0.97780	0.97768	0.21257	1.0002
0.648	0.92368	0.92181	0.32468	1.0020
0.888	0.77916	0.76692	0.45050	1.0160
0.956	0.67462	0.65375	0.49360	1.0320
0.995	0.50818	0.47861	0.52825	1.0618
0.997	0.48300	0.45291	0.53152	1.0664
1.000 [c]	-	-	1.0000	2.000

a) ℓ = distance of the sphere center from the wall.

b) ω, u = undisturbed angular and translational velocities in absence of wall effects.

c) Values obtained from a lubrication theory approximation.

APPENDIX V

THE TUBE AND COUETTE APPARATUS

1. The Tube Apparatus

A view of the apparatus with the tube vertical as in all the present experiments is shown in Figure 1. The apparatus rests on two concrete vibration-free mounts and by rotation about one end the whole assembly can be inclined to any angle to the horizontal. It is equipped with a reversible and continuously variable 1/4 HP direct-current motor drive with magnetic amplifier control. Through a series of pulleys and belts the motion is transmitted to the screw shaft driving the microscope; four gear ratios 16:1 to 1:4 are available to give linear speeds from 10^{-3} to 2 cm.sec.$^{-1}$, the ranges at each gear ratio overlapping to obtain better speed control. Limit switches reverse the direction of the microscope movement at the upper and lower ends of its travel. The microscope support can be rotated by 90° thus enabling observations to be made in two mutually perpendicular directions i.e. along the Y- and Z-axes (Fig. 1c, Part II). A still or cine camera can be attached to the microscope to photograph the particles when required.

Precision glass tubes pass through rubber stoppers into the square glass cell with flat viewing surfaces which contains a solution of the same refractive index as the glass (= 1.474). This provides distortion-free viewing over a length of about 60 cm. of the tube. The ends of the cell rest on circular slots in the steel frame of the apparatus, and the cell can be aligned with the axes of travel by means of levelling screws.

Reproducible flow rates are obtained by the use of an infusion-withdrawal pump (Harvard Apparatus Co. Inc., Dover, Mass.) placed on the shelf as shown in the lower left position of Fig. 1. It is equipped with a synchronous motor which moves the plunger of a syringe connected to the lower end of the tube. The pump can provide continuous operation by means of adjustable limit stops which automatically reverse the motor. Twelve speeds are available covering a 5,000 to 1 range.

2. The Couette Apparatus

The Couette apparatus consists essentially of two vertical coaxial cylinders rotating at independently variable speeds in opposite directions, with the suspension contained in the annulus between them. In the experiments described in Parts III and IV the Couette designated as Mark II was used, while those in Part II were performed in Couette Mark IV. In the experiments on radial migration of liquid drops both were used. A brief discussion of the essential features of each one is given below.

Couette Mark II. A photograph of the apparatus is shown in Fig. 2. The cylinders are made of stainless steel; the outer one has a sealed bottom made from plate glass so that observations along the Z-axis throughout the annulus are possible. The optical equipment (camera, microscope, and illuminator) is mounted on a frame which can be pivoted about the center of rotation of the cylinders and can be also traversed radially across the apparatus. The motors are 1/4 HP with magnetic amplifier control. The gear boxes are equipped with three sets of reduction gears (1:100, 1:50, 1:25) thus providing a wide range of velocity gradients. Shown at the right of Fig. 2 is the speed control panel with the coarse and fine control knobs for each cylinder and the tachometers, whereas on the left is the panel with variable AC and DC outlets to supply the microscope light, camera motor, and electronic timer.

Couette Mark IV. The apparatus is shown in Figure 3. The principle is the same as in Mark II, i.e. two accurately machined spindles rotate in opposite directions, but the device is more versatile. Cylinders and discs of various dimensions made of transparent material (Lucite or epoxy resin) can be mounted on the spindles by means of a chuck assembly, and the surfaces can be machined *in situ* to a tolerance of 8×10^{-4}cm. with a built-in lathe. Lubrication of the spindles is maintained by means of an oil circulation system, which is operated by an oil pump motor that runs whenever the spindles are rotated. Contamination of the suspension by the circulating oil is prevented by the use of two teflon rings. The motion is provided to each spindle independently by a set of motors and gear boxes similar to those of the Mark II.

The frame on which the optical equipment is mounted is designed to permit observations along the Y- and Z-axes. The radial position can be accurately determined to 5×10^{-4}cm. with a dial gauge. The control panel shown on the right is similar to that of Mark II i.e. contains the speed control knobs, tachometers, and variable DC and AC outlets for the illuminator, camera motor, and electronic timer.

FIGURE 1

The tube apparatus in vertical position. The infusion-withdrawal pump is in the lower left-hand side of the picture. The microscope and camera are arranged for viewing along Z-axis.

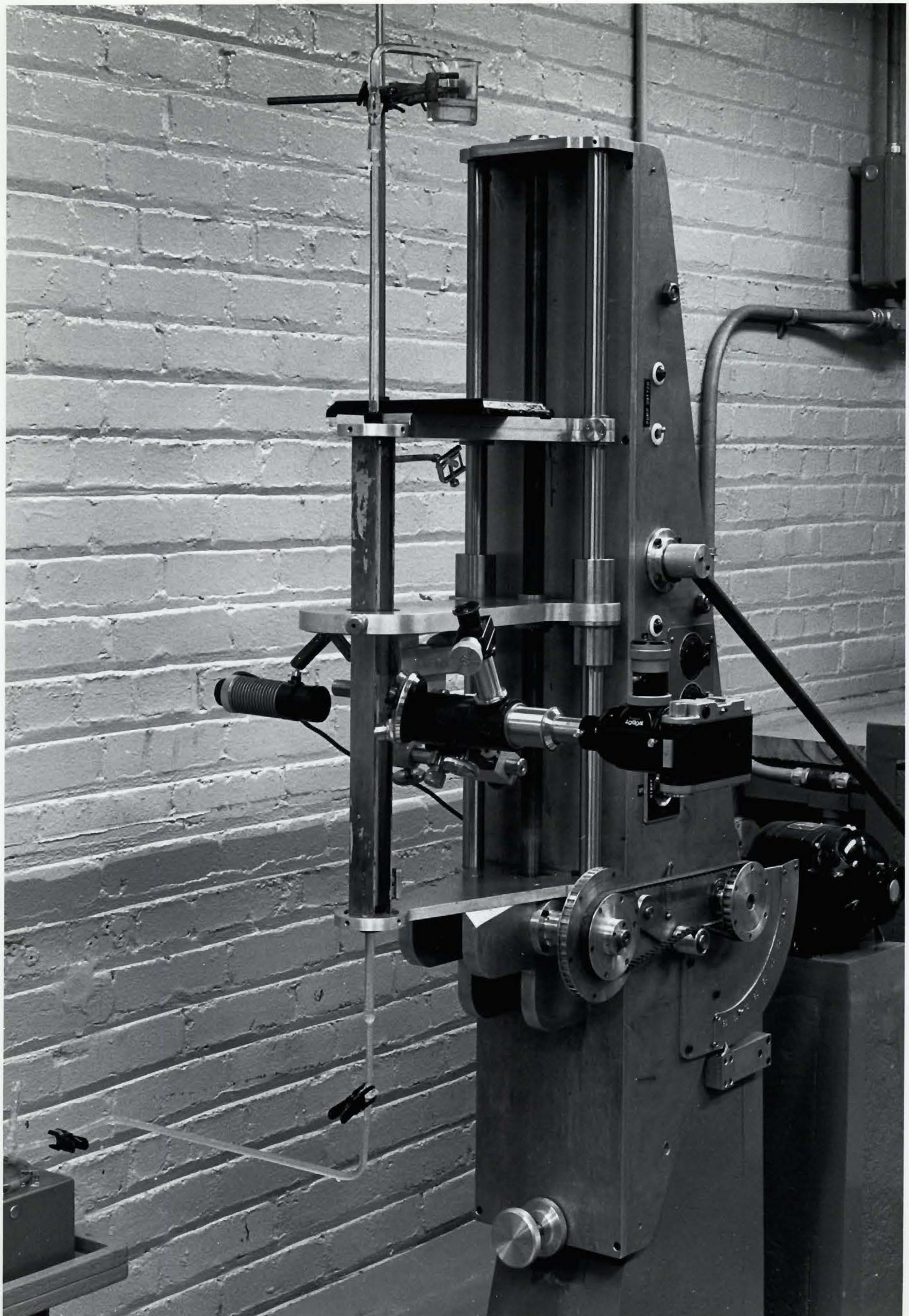

FIGURE 2

The Couette Mark II apparatus. The cylinders are shown in the center of the photograph, the individual motor drives on either side. The microscope and cine camera are arranged for viewing along the Z-axis of the field of the Couette flow.

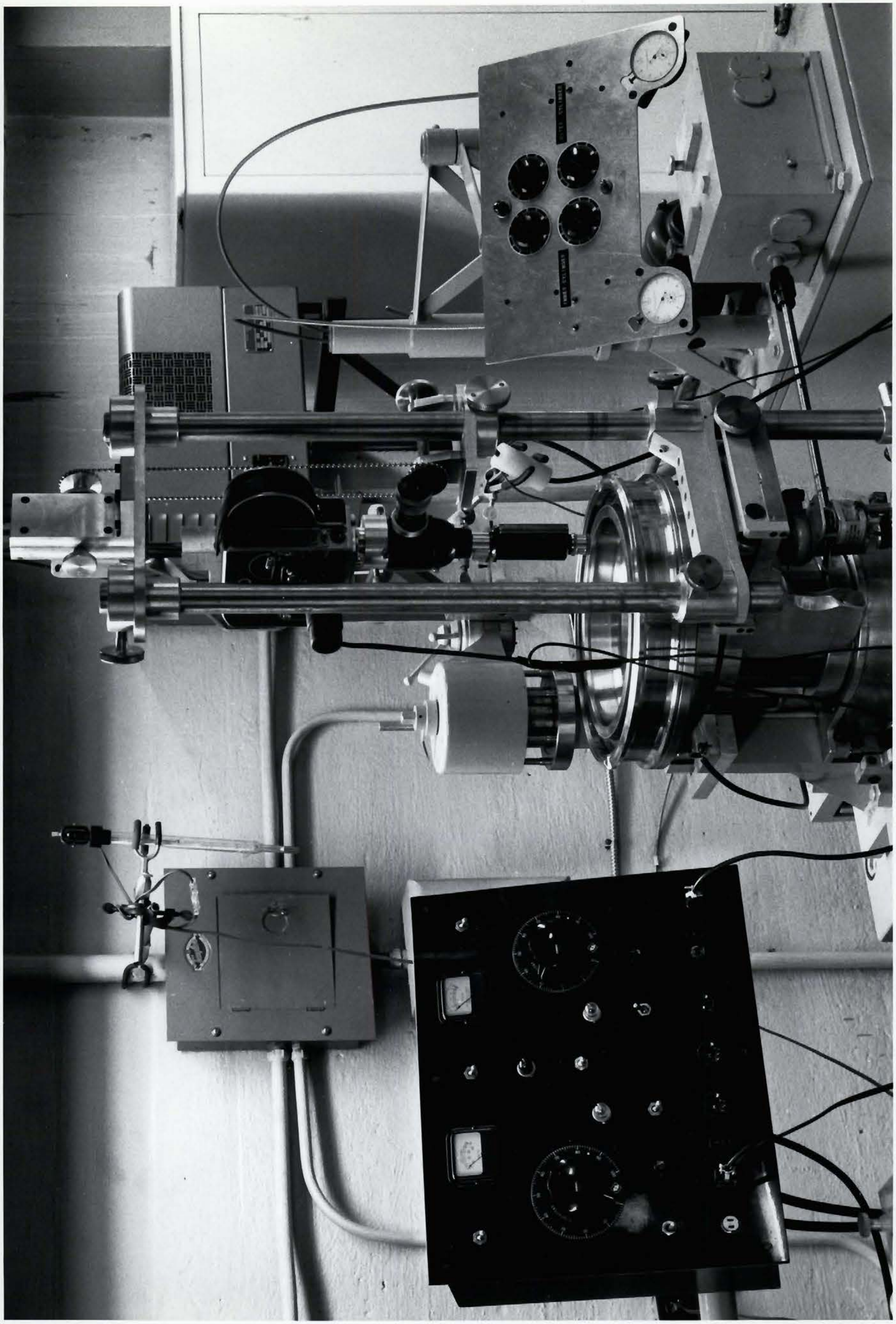

FIGURE 3

The Couette Mark IV apparatus. The Lucite cylinders are shown on the left and the control panel on the right. The microscope and cine camera are arranged for viewing along the Y-axis of the field of the Couette flow.

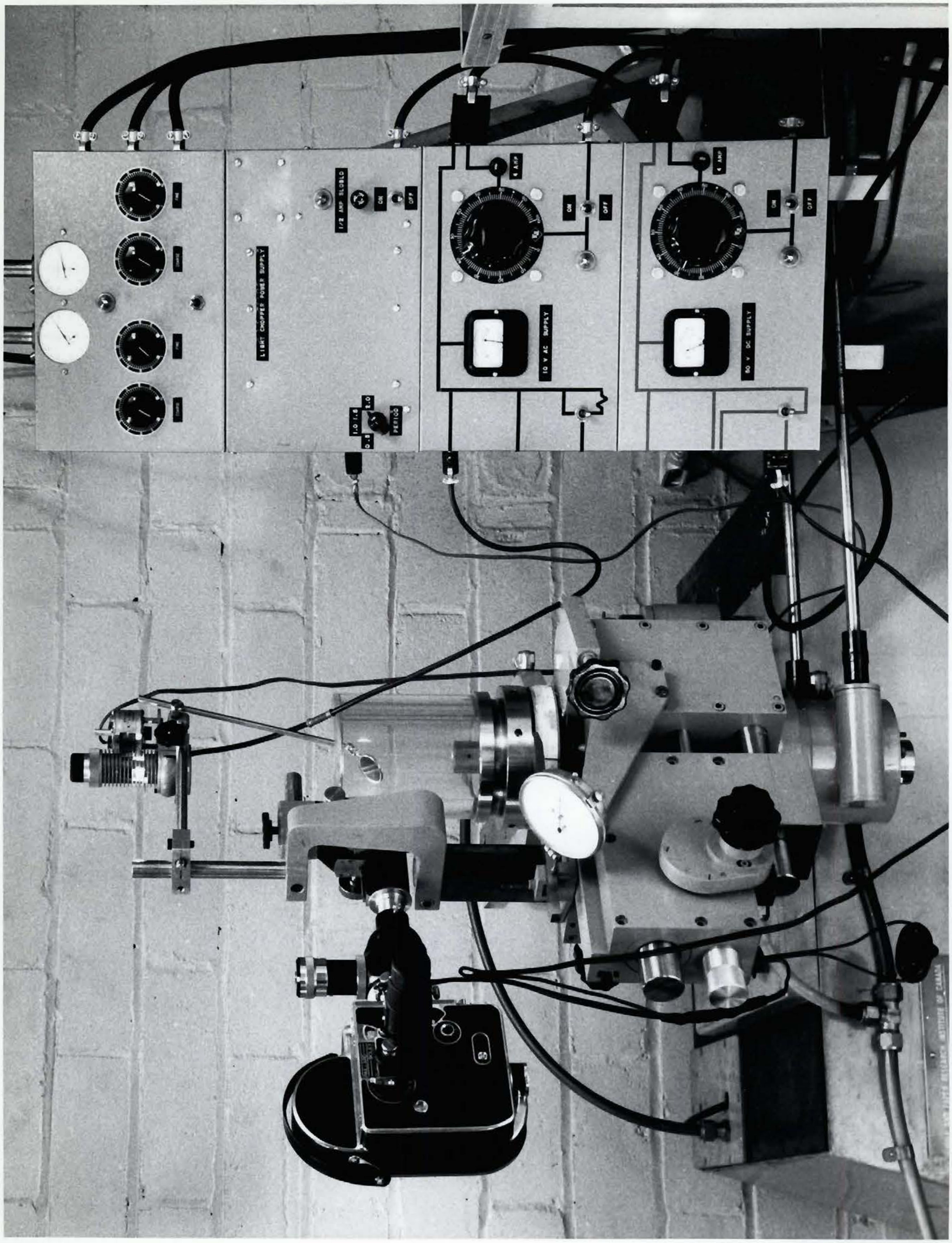
LIGHT CHOPPER POWER SUPPLY
1/2 AMP SLOBLO
PERIOD
10 V AC SUPPLY
80 V DC SUPPLY
4 AMP
ON
OFF